



Nanostructured metallic surfaces of Au implemented as electrochemical glucose sensors

A thesis submitted in fulfilment of the requirements for the degree of
Doctor of Philosophy

Victoria Elizabeth Coyle

BSc. (Applied Chemistry) (Honours), RMIT University, 2014
BSc. (Applied Science), RMIT University, 2013

School of Science
College of Science, Engineering and Health
RMIT University

August 2019

Declaration

I certify that except where due acknowledgement has been made, the work is that of the author alone; the work has not been submitted previously, in whole or in part, to qualify for any academic award; the content of this thesis is the result of work which has been carried out since the official commencement date of the approved research program; and any editorial work, paid or unpaid, carried out by a third party is acknowledged.

I acknowledge the support I have received for my research through the provision of an Australian Government Research Training Program Scholarship.

Victoria E. Coyle

30 August 2019

Acknowledgements

Undertaking any form of research is never due to one person but is a task undertaken by multiple contributors be that via support, knowledge, guidance and wisdom. Throughout my pursuit to complete this thesis many people aided me on my journey and I would like to take this opportunity to thank them.

Firstly, I cannot thank my supervisors enough for the ongoing support they provided me with throughout this entire endeavour. Dr. Ahmad Kandjani and Dr. Ylias Sabri, without you two I know I would not have achieved as much as I have and your enjoyment and excitement about science has been a major driving force in me undertaking the challenge of this work. I would like to further thank you two for enduring the constant mood changes and erratic behaviour I exhibited throughout this time, which I know from friends and family can be of the hardest undertakings a person can experience.

To Professor Suresh Bhargava, you took a massive chance on me when I walked into your office fresh out of my honours year. Although I did not have the best grades or experience for this field, you took a chance on me and for that I will be forever grateful. Your support and guidance has pushed me to be become the scientist I am today.

To Professor Miao Chen, you are what I strive to be. An extremely intelligent and successful woman in science and working with you throughout this time has been the greatest example I could have seen pushing me to be a better scientist and enhancing my range of skills and knowledge.

I would like to extend my gratitude to Dr. Matthew Field in the RMMF department of RMIT. I think I harassed you almost as much as my supervisors throughout my journey. Your guidance and lessons in sample characterization were among some of the greatest skills and knowledge I could have got access to across my candidature and for that I will be forever grateful.

To my collaborators Dr. Rahul Ram, Dr. Mohibul Kabir, Dr. Jampaiah Deshetti, Mr. Beбето Lay, Dr. Daniel Oppedisano, Dr. Lathe Jones, Dr. Mamad Amin, Dr. Sarvesh Soni and Dr. Aaron Elbourne, the opportunity to work with each one of you has drastically impacted my view of science in the most positive way and I thank you for allowing me to collaborate with each and every one of you.

To my friends and family who provided me with the emotional support I needed to get through these years I will forever be grateful for your continued acceptance of me as a person and the ability to endure me. Mom and dad, you will continue to be my role models and give me endless love and support regardless of my mistakes. James, Kristina, Tiffany and Sophea,

you will always be the people I come to with my crazy ideas and to lighten up my days, especially my two beautiful nieces Bella and Ariana. And finally, to my friends Ally, Isabel, Jess, Nebeal and Sam, without you guys I wouldn't be able to put aside my thesis and just enjoy life throughout this time.

To everyone who has helped me through this journey, you are irreplaceable to me and there is no way I could have finished this without you.

This thesis is dedicated to:

Any person that has failed but has refused to give up on their dreams

"She is like a phoenix rising from the ashes into something more fabulous"

- James Brian Coyle

Journal Publications included in Thesis

1. **Coyle, V. E.;** Kandjani, A. E.; Sabri, Y. M.; Bhargava, S. K., Au Nanospikes as a Non-enzymatic Glucose Sensor: Exploring Morphological Changes with the Elaborated Chronoamperometric Method. *Electroanalysis* 2017, 29 (1), 294-304. (**Chapter 3**)
2. **Coyle, V. E.;** Oppedisano, D. K.; Jones, L. A.; Kandjani, A. E.; Sabri, Y. M.; Bhargava, S. K., Hydrogen Bubble Templated Growth of Honeycomb-Like Au-Pt Alloy Films for Non-Enzymatic Glucose Sensing. *J. Electrochem. Soc.* 2016, 163 (14), B689-B695. (**Chapter 4**)
3. Lay, B.; **Coyle, V. E.;** Kandjani, A. E.; Amin, M. H.; Sabri, Y. M.; Bhargava, S. K., Nickel–gold bimetallic monolayer colloidal crystals fabricated via galvanic replacement as a highly sensitive electrochemical sensor. *J. Mater. Chem. B* 2017, 5 (27), 5441-5449. (**Chapter 5**)
4. **Coyle, V. E.;** Kandjani, A. E.; Field, M. R.; Hartley, P.; Chen, M.; Sabri, Y. M.; Bhargava, S. K., Co₃O₄ needles on Au honeycomb as a non-invasive electrochemical biosensor for glucose in saliva. *Biosens. Bioelectron.* 2019, 141, 111479. (**Chapter 6**)

Additional relevant Publications

5. Jampaiah, D.; Reddy, T. S.; Kandjani, A. E.; Selvakannan, P.; Sabri, Y. M.; **Coyle, V. E.;** Shukla, R.; Bhargava, S. K., Fe-doped CeO₂ nanorods for enhanced peroxidase-like activity and their application towards glucose detection. *J. Mater. Chem. B* 2016, 4 (22), 3874-3885.

6. Jampaiah, D.; Venkataswamy, P.; **Coyle, V. E.**; Reddy, B. M.; Bhargava, S. K., Low-temperature CO oxidation over manganese, cobalt, and nickel doped CeO₂ nanorods. RSC Adv. 2016, 6 (84), 80541-80548.
7. Jampaiah, D.; Reddy, T. S.; **Coyle, V. E.**; Nafady, A.; Bhargava, S. K., Co₃O₄@ CeO₂ hybrid flower-like microspheres: a strong synergistic peroxidase-mimicking artificial enzyme with high sensitivity for glucose detection. J. Mater. Chem. B 2017, 5 (4), 720-730.
8. Jampaiah, D.; Velisoju, V. K.; Venkataswamy, P.; **Coyle, V. E.**; Nafady, A.; Reddy, B. M.; Bhargava, S. K., Nanowire morphology of mono-and bidoped α -MnO₂ catalysts for remarkable enhancement in soot oxidation. ACS Appl. Mater. Interfaces 2017, 9 (38), 32652-32666.
9. Kandjani, A. E.; Sabri, Y. M.; Field, M. R.; **Coyle, V. E.**; Smith, R.; Bhargava, S. K., Candle-soot derived photoactive and superamphiphobic fractal titania electrode. Chem. Mater. 2016, 28 (21), 7919-7927.
10. Kabir, K. M.; Sabri, Y. M.; Myers, L.; Harrison, I.; Boom, E.; **Coyle, V. E.**; Ippolito, S. J.; Bhargava, S. K., Investigating the cross-interference effects of alumina refinery process gas species on a SAW based mercury vapor sensor. Hydrometallurgy 2017, 170, 51-57.
11. Griffin, M. J.; Kabir, K. M.; **Coyle, V. E.**; Kandjani, A. E.; Sabri, Y. M.; Ippolito, S. J.; Bhargava, S. K., A nanoengineered conductometric device for accurate analysis of elemental mercury vapor. Environmental science & technology 2015, 50 (3), 1384-1392.
12. Elbourne, A.; **Coyle, V. E.**; Truong, V. K.; Sabri, Y. M.; Kandjani, A. E.; Bhargava, S. K.; Ivanova, E. P.; Crawford, R. J., Multi-directional electrodeposited gold nanospikes for antibacterial surface applications. Nanoscale Advances 2019, 1 (1), 203-212.
13. Jampaiah, D.; Velisoju, V. K.; Devaiah, D.; Singh, M.; Mayes, E. L.; **Coyle, V. E.**; Reddy, B. M.; Bansal, V.; Bhargava, S. K., Flower-like Mn₃O₄/CeO₂ microspheres as an efficient

catalyst for diesel soot and CO oxidation: Synergistic effects for enhanced catalytic performance. *Appl. Surf. Sci.* 2019, 473, 209-221.

14. Soni, S. K.; Kabir, K. M.; Babarao, R.; **Coyle, V. E.**; Sarkar, S.; Sabri, Y. M.; Bhargava, S. K., A QCM-based 'on-off' mechanistic study of gas adsorption by plasmid DNA and DNA-[Bmim][PF 6] construct. *RSC Adv.* 2016, 6 (84), 81318-81329.

Research outcomes

Journal articles under preparation

- ❖ **Victoria E. Coyle**, Ylias M. Sabri, Ahmad E. Kandjani and Suresh K. Bhargava. 'TiO₂ soot on Au honeycomb for photoelectrochemical glucose sensing in synthetic saliva.'
- ❖ **Victoria E. Coyle**, Ylias M. Sabri, Ahmad E. Kandjani and Suresh K. Bhargava. 'Co₃O₄ on Ni honeycomb electrode for high-performance supercapacitor analysis.'
- ❖ Ahmad E. Kandjani, **Victoria E. Coyle**, Dilek, Ylias M. Sabri and Suresh K. Bhargava. 'Au pineapples for long range ordered crystals for efficient recyclable SERS.'
- ❖ **Victoria E. Coyle**, Ahmad E. Kadjani, Ylias M. Sabri and Suresh K. Bhargava. 'Porous Au atop PDMS sponge for sweat detection of glucose.'
- ❖ **Victoria E. Coyle**, Rahul Ram, Lathe Jones, Miao Chen and Suresh K. Bhargava. 'The influence of pH, Eh and temperature in controlling Chalcopyrite (CuFeS₂) leaching; a Scanning Electro-Chemical Microscopy (SECM) study.'

Conferences

- ❖ Coyle, V¹, Kandjani, A¹, Chen, M^{1,2} and Sabri, Y¹. 'Hydrogen bubble templated Au/Co₃O₄ biosensors for electrochemical non-enzymatic glucose sensing', Chemeca, 2017, poster presentation

Journal Cover page

- ❖ *Environmental Science and Technology*, 2016, Volume 50, Issue 3



Relevant awards and Scholarships

- ❖ Won the Royal society of Victoria's (RSV) Young Scientist prize for 2018 in Physical Science
- ❖ Second place in the RMMF SEM image competition 2017
- ❖ CSIRO research scholarship (2016 - 2019)

Media publications

- ❖ Featured Scientist article for my PhD research and SEM imaging entitled "Golden Glucose Sensor" Newsletter: AMMRF Profile 2015 (Annual Newsletter)

Abstract

Diabetes is one of the most prevalent chronic diseases growing globally with 450 million people currently being diagnosed with the disease. With this number dramatically increasing every year the need for highly sensitive and selective glucose sensors are of great importance. Along with this, the comfort of the patient when analysing their glucose concentrations has come to the forefront of research with the push towards non-invasive sensing devices becoming the major focus in this research. The aim of this research was to develop Au-based nanostructures and study their effectiveness in detecting ultra-low concentrations ($<100\ \mu\text{M}$) of glucose. Au has shown excellent biocompatibility as well as its ability to be moulded for shape, size and density which can be tailored specifically to get enhanced glucose electrooxidation. Following a thorough literature review, the materials that were developed and investigated were pure mono-metallic Au structures, Au-Pt alloy and Au-Ni particles as well as Au- Co_3O_4 composites.

Initially, a pure nanostructure of Au was studied in the form of Au nanospikes where the impact of HAuCl_4 concentration, Pb acetate concentration (growth agent for shape), electrodeposition time and electrodeposition potential were studied. From these studies the optimal conditions to produce Au nanospikes for optimal glucose sensing were found to have a HAuCl_4 concentration of 13.6 mM, a Pb acetate concentration of 1 mM, an electrodeposition time of 12 mins and an applied electrodeposition potential of +0.05 V. Analysis of this optimal pure Au sensor was performed with calculated sensitivity of $91.8\ \mu\text{A}\cdot\text{mM}^{-1}\cdot\text{cm}^{-2}$ with no interference from common physiological contaminants making this sensor sensitive and highly selective. Further study of the Au-based sensors pushed the study to use Au in conjunction with Pt in an alloyed form. Using the hydrogen bubble template technique with varying concentrations of Pt were used to form a sensor with a very large electrochemical surface area (ECSA). In this study various concentrations of Pt were added to the electrodeposition solution with 0.5 mM of Pt showing the largest overall surface area and the highest sensitivity in the presence of glucose. Electrochemical glucose sensing analysis was performed on the Au-Pt alloyed sensor producing a high sensitivity of $109.3\ \mu\text{A}\cdot\text{mM}^{-1}\cdot\text{cm}^{-2}$ showing the alloyed material produced a higher sensitivity than that of the monometallic Au sensor. With the addition of Pt, a higher sensitivity was obtained whilst the large presence of

Au allowed for the sensor to have excellent selectivity in the presence of common physiological contaminants which has previously hindered the use of Pt in glucose sensing nanostructures.

To reduce Au content yet increase sensitivity, highly active Au nanoparticles on a Ni platform were employed. It is well known that Au nanoparticles grown by galvanic replacement are highly active however a uniform formation is a major challenge due to the mechanism by which a galvanic replacement reaction occurs. From this knowledge, Ni colloidal crystals were employed to attempt to overcome this issue. Multiple concentrations of Au were used to determine the optimal concentration of Au which was found to be 0.1 mM of HAuCl₄. Analysis of this formed sensor was performed and a very large sensitivity of 506 $\mu\text{A}\cdot\text{mM}^{-1}\cdot\text{cm}^{-2}$ showing a much larger enhancement of sensitivity compared to both the pure Au and Au-Pt alloyed sensors. The Ni-Au colloidal sensor showed minimal effect from common physiological contaminants due to the presence of Au in the structure. Finally, a study of the effect of an additional material was studied in the presence of the metal oxide Co₃O₄ due to its excellent biocompatibility and excellent sensitivity in the presence of glucose. The hydrogen bubble templated technique was used to form a pure Au lattice structure which was then coated in pure Co₃O₄ nanowires using the hydrothermal technique. The formed structure had a completely cohesive structure where Co₃O₄ moulded over the Au allowing for synchronized sensing between the Au and Co₃O₄ components to occur. The electrochemical sensing analysis of the Au-Co₃O₄ structure showed a huge sensitivity of 2014 $\mu\text{A}\cdot\text{mM}^{-1}\cdot\text{cm}^{-2}$ within the glucose concentration range between 0.02 and 1 mM. This large sensitivity in the low region of glucose concentrations showed the possibility of the sensor performing successfully within the glucose concentration range of saliva (20 – 1000 μM). Further analysis of the sensor was performed in the presence of synthetic saliva showing an excellent linearity of glucose additions and minimal to no effect from common physiological contaminants found in saliva. These findings showed the feasibility of the developed electrochemical glucose sensor to be employed for non-invasive diabetes monitoring and diagnostic applications.

Table of contents

Declaration	ii
Acknowledgements	iii
Journal publications included in thesis	vi
Additional relevant publications	vi
Research outcomes	viii
Thesis with Publications Declaration	x
Chapter I: Introduction	3
1.1 Introduction	4
1.2 Motivation	4
1.3 Objectives	5
1.4 Thesis outline	6
Chapter II: Literature review	9
2.1 Diabetes and its global impact	10
2.1.1 Diabetes	10
2.2 Glucose biosensors	11
2.2.1 Glucose biosensors- general theory	11
2.2.2 Glucose biosensors- general enzyme mechanism	12
2.3 Enzymatic glucose sensors	13
2.4 Non-enzymatic glucose sensors	15
2.5 Gold as a non-enzymatic glucose sensor	19
2.6 Metal composites	22
2.7 Alloys	22
2.8 Metal-oxides	26
2.9 Other types of glucose sensors	30
2.10 Non-invasive glucose detection	33
Chapter III: Au Nanospikes as a Non-enzymatic Glucose Sensor: Exploring Morphological Changes with the Elaborated Chronoamperometric Method	48
3.1 Published Manuscript	49

3.2	Supplementary Information	61
	Chapter IV: Hydrogen Bubble Templated Growth of Honeycomb-Like Au-Pt Alloy	72
	Films for Non-Enzymatic Glucose Sensing	
4.1	Published Manuscript	73
4.2	Supplementary Information	80
	Chapter V: Nickel–gold bimetallic monolayer colloidal crystals fabricated via galvanic replacement as a highly sensitive electrochemical sensor	87
5.1	Published Manuscript	88
5.2	Supplementary Information	97
	Chapter VI: Co₃O₄ needles on Au honeycomb as a non-invasive electrochemical biosensor for glucose in saliva	102
6.1	Published Manuscript	103
6.2	Supplementary Information	110
	Chapter VII: Conclusions and Future work	118
7.1	Summary of key Findings	119
7.2	Future Work	121
	Bibliography	122
	Appendix	132
	A. Abbreviations	133
	B. Co-Author statements for the publications representing chapters III-VI	135

CHAPTER I:

Introduction

This chapter provides an overview of the thesis, including the motivations and key objectives of the study. A concise thesis outline is provided

1.1 Introduction

This section addresses the motivations for this thesis and the objectives implemented to address the direction of the research. The author's achievements throughout the duration of this work have been outlined and the organisation of the thesis is explained.

1.2 Motivation

Diabetes is a global epidemic effecting the lives of both the people struggling with the chronic disease as well as the people aiding in their treatment. Diabetes is a chronic disease which effects the production of insulin via over-production (hyperglycaemia) or under-production (hypoglycaemia). Currently there are 4 types of diabetes that are recognised by the world health organization known as Type 1 (insulin dependent), Type 2 (adult-onset), gestational and pre-diabetes.¹ In 2015, 415 million people were estimated to have diabetes globally with that number expected to increase to 642 million by the year 2024. In 2015 the International Diabetes Federation (IDF) estimated there were 5 million deaths per year due to the effects of diabetes, which is included as one of the 3 major killers in the world along with ischaemic heart disease and cerebrovascular disease.² As the number of people being diagnosed with this chronic disease increases, the need for patients to easily manage and assess the state of their health is ever increasing. The criteria for a person to be diagnosed with diabetes is mainly attributed to their fasting plasma glucose (FPG) threshold which has currently been recorded as 7.0 mmolL^{-1} and above.³ The necessity for a person managing their symptoms to be able to easily and comfortably determine their glucose concentrations without the need for medical assistance is of the greatest importance. The idea of a blood glucose sensor was initiated by Clarke and Lyons in 1962⁴ using glucose oxidase in conjunction with an oxygen electrode which was classified as an enzymatic glucose sensor. As glucose sensing research has improved over the years the push for non-enzymatic glucose sensors; sensors where the main sensing component is made of metal-based materials, has increased. This push towards non-enzymatic sensors is due to the poor reproducibility, chemical instability and high cost of enzymatic sensors that have been developed.⁵⁻⁶ As research continued with non-enzymatic glucose sensors, higher sensitivities,⁷ better reproducibility and selectivity in common physiological contaminants were encountered compared to the enzyme-based counterparts.⁸

As breakthroughs are being reported in developing relatively more sensitive glucose detection techniques, the desire for patients to no longer use blood as their main measurement tool has pushed towards developing non-invasive glucose sensors. Research has steadily increased in this area predominantly via optical-based sensing methods⁹⁻¹⁰ however electrochemical sensors have the ability of producing higher selectivity's with limited to no interference with physiological contaminants compared to optical counterparts. Research in this area has started to target other bodily fluids easily obtained with little to no invasive sampling from the patient compared to blood, such as the detection of glucose in tears, sweat, saliva and breath.¹¹ Pure metal-based sensors have a good selectivity (Au has shown the least amount of surface poisoning from research) however their sensitivities are not high enough for low concentration range suitability. Additional materials such as alloys (specifically Au-Pt) and metal oxides (Co_3O_4) have improved sensitivities depending on their morphology and cohesion with all components. Each of these materials have been shown to be effective in-situ with minimal success in real-life blood and non-invasive media analysis. In this thesis steps were taken to fully understand and analyse the most effective structure morphology and additional component to achieve a large sensitivity with good selectivity which would then be effective in non-invasive media. For all developments the method of detection was to be via electrochemical sensing which has shown to be impacted minimally by physiological interferences, having the greatest success for real-life sensor development in the future.

1.3 Objectives

In this research the aim is to investigate the development of Au-based nanostructures in different forms which have been tailored towards specific glucose sensor properties. Sensor reproducibility and selectivity in the presence of common physiological contaminants, high sensitivities with all components being bio-compatible was the focus of the project. As the development of various nanostructures continued, the size, shape and density of the nanostructures were altered to fully understand the role of Au in the sensing of glucose before introducing additional materials with their specific roles to develop functional composite materials. The effect of combining material components (different

metals/additional materials) which exhibited all the necessary characteristics needed for a possible non-invasive glucose sensor were also investigated. To develop a sensor which met these goals the following objectives were followed:

- To develop Au-based nanostructured materials which are tailored specifically for the desired usage as an electrochemical glucose sensor
- To determine the best size, shape and morphology of pure nanostructured Au surfaces which are the most active when undergoing electrochemical-based glucose electro-oxidation
- To study and analyze the sensing performance of Au-based materials in an alloyed form with carrying amounts of Pt added. To study and analyze the effect of Au as an additional material (scattered Au nanoparticles) to an overall nanostructured material and how this enhances the electrochemical glucose sensing of the composite material
- To study and analyze the effect of an additional material (Co_3O_4) to a Au nanostructured material and how this new structure is enhanced for the electrochemical glucose sensing of the composite material

1.4 Thesis Outline

This thesis has been structured to tell a story of the development and application of Au in different forms and how each form effects the glucose sensing capabilities of Au based materials. Varying concentrations of additional materials were studied via their morphology, surface area and electrochemical glucose sensing performance. Each chapter underwent similar processes through material development, material characterization and finally sensing capabilities. To communicate the investigation, one literature review chapter and 4 major results chapters have been presented each with their own supporting information which have all been peer-reviewed and published in reputable journals. Each chapter is detailed as follows:

The initial chapter (**Chapter 1**) outlines the overall motivation, objectives and thesis organization of this work which acts as an introduction to the overall thesis.

Chapter 2 is a full review of the past and current literature of glucose sensing. In assessing the pros/cons of different materials/techniques studied and reported in literature or glucose

sensing applications, the author concentrated on Au nanostructures for detecting glucose via electrochemical technique with a view of reaching detection limits and sensitivities that enable the use of the materials and techniques for non-invasive glucose detection applications in the future.

Chapter 3 begins with the aim of developing a pure Au nanostructured sensor in the form of nanospikes. The nanospikes growth conditions were varied by using different HAuCl_4 concentration, Pb acetate concentration (used as additive), growth time variation and electrochemical deposition potential variation. Each of these parameters were studied in the presence of glucose thus enabling the determination of the optimal nanospikes growth conditions for glucose sensing performance. The optimum spike structure showed a larger current response in the presence of glucose compared to pure Au with the sample exhibiting the greatest response undergoing electrochemical glucose sensing measurements to determine its sensing performance.

In **chapter 4** the author furthered the development of Au by developing Au-Pt alloys. A constant concentration of HAuCl_4 was used with varying Pt concentrations added for optimal morphology and glucose sensing performance. This nanostructure was formed using the hydrogen bubble template technique drastically increasing the surface area of the sensor compared to chapter 3. The optimal Au-Pt alloy sample then underwent electrochemical glucose sensing measurements to determine its sensing capabilities.

Chapter 5 continues the analysis of implementing Au by utilizing Au as an additional material. As even morphology was found to be a contributing factor in sensing performance from chapters 3 and 4, a sensing material composing of Ni colloids was developed with varying concentrations of galvanically replaced Au atop the Ni colloids. The even structure of the Ni colloids across the surface of the substrate presented a seamless yet highly active surface for our base structure. The addition of Au nanoparticles was evenly distributed by galvanic replacement after varying the HAuCl_4 concentration to the optimal concentration. As with the previous sensors electrochemical glucose sensing measurements were performed determining its sensing capabilities.

In **chapter 6** the studies of chapters 3-5 showed the importance of large surface area and seamless surface structure, thus a hydrogen bubble templated Au base structure was analysed with the addition of a metal oxide in the form of Co_3O_4 nanowires. The addition of Co_3O_4 was chosen due to its cohesion with Au which has been shown to drastically increase

sensitivity whilst allowing the good selectivity of Au to be maintained. The concentration of CoCl_2 salt was varied for optimal performance in glucose. The optimal Au/ Co_3O_4 sensor then underwent electrochemical glucose sensing presenting an exceptional sensitivity. From this high sensitivity the capabilities of the sensor in the presence of synthetic saliva were then performed using electrochemical sensing techniques in the form of a non-invasive electrochemical glucose sensor.

The summation of the thesis is outlined in **chapter 7** where the conclusions of the thesis are extrapolated upon and future research direction is outlined.

References

1. Zimmet, P. Z.; Magliano, D. J.; Herman, W. H.; Shaw, J. E., *The lancet Diabetes & endocrinology* **2014**, 2 (1), 56-64.
2. Atlas, D., International Diabetes Federation. IDF Diabetes Atlas, 7th edn. Brussels, Belgium: International Diabetes Federation, 2015.
3. Alberti, K. G. M. M.; Zimmet, P. f., *Diabetic medicine* **1998**, 15 (7), 539-553.
4. Clark Jr, L. C.; Lyons, C., *Ann. N.Y. Acad. Sci.* **1962**, 102 (1), 29-45.
5. Kang, X.; Mai, Z.; Zou, X.; Cai, P.; Mo, J., *Anal. Biochem.* **2007**, 369 (1), 71-79.
6. Li, X.; Zhu, Q.; Tong, S.; Wang, W.; Song, W., *Sens. Actuator B-Chem.* **2009**, 136 (2), 444-450.
7. Ernst, S.; Heitbaum, J.; Hamann, C., *J. Electroanal. Chem. Interfacial Electrochem.* **1979**, 100 (1), 173-183.
8. Vassilyev, Y. B.; Khazova, O.; Nikolaeva, N., *J. Electroanal. Chem. Interfacial Electrochem.* **1985**, 196 (1), 105-125.
9. Heise, H.; Marbach, R.; Koschinsky, T.; Gries, F., *Artificial Organs* **1994**, 18 (6), 439-447.
10. Coté, G. L.; Fox, M. D.; Northrop, R. B., *IEEE Transactions on biomedical engineering* **1992**, 39 (7), 752-756.
11. Srinivasan, V.; Pamula, V. K.; Pollack, M. G.; Fair, R. B. In *Clinical diagnostics on human whole blood, plasma, serum, urine, saliva, sweat, and tears on a digital microfluidic platform*, Proc. MicroTAS, 2003; pp 1287-1290.

CHAPTER II:

Literature Review

This chapter covers the literature related to this research thesis. The many developments in glucose biosensor research will also be discussed. How the biosensor has changed over time and the different types of glucose biosensors available. The recent developments in glucose biosensor research are also explained.

2.1 Diabetes and its global impact

This subsection explains what diabetes is, who it effects and the global impact of diabetes.

2.1.1 Diabetes

Diabetes is one of the most prevalent diseases effecting the world today. Approximately 422 million adults are currently living with the disease, a number that has quadrupled from 108 million since the year 1980.¹ Diabetes is a chronic disease which effects the production of insulin, a hormone that normalizes blood glucose levels. For many years the classification for diabetes was separated into 3 distinct categories, referred to as type 1, type 2 or gestational diabetes. Type 1 diabetes effects the pancreas causing an inability to produce enough insulin to maintain normal glucose levels and is most commonly developed due to genetic markers. Type 2 diabetes is due to a reduction in insulin production where the produced insulin does not work effectively. Type 2 represents 85-90% of all cases and is most commonly developed due to an unhealthy lifestyle and genetic markers. Gestational diabetes occurs in women who are pregnant at around the 24-28 week mark in their pregnancies and blood glucose levels commonly return to normal levels after childbirth.² A new study conducted by Dennis et. al.³ showed 5 distinct forms of diabetes named as 'clusters'. Cluster 1 is in the form of the traditional type 1 diabetes definition, with cluster 2 causing severe insulin deficiency in children, cluster 3 being a severe case of insulin-resistance leading to a higher risk of kidney disease, cluster 4 being a mild form of type 2 diabetes where obese patients develop the disease and cluster 5 which is the development of a mild form of diabetes in elderly patients.³ Along with patients being effected by diabetes, the families and support networks of the people struggling with this disease are also effected. More work needs to be done for managing the disease which would reduce the impact on the carers of the patients living with diabetes. With such a large number of people in the world living with diabetes (costing \$825 billion annually for treatment⁴) the ability for sufferers to self-monitor their glucose levels is of great need. This self-monitoring would allow for a patient to check their glucose levels in real-time that is both consistent and accurate in their response, without the need for a medical professional. This development would reduce ongoing costs for the patient as well as reducing the in-face contact time between patient and doctor. Previous efforts in research to solve this problem focused on invasive-type sensors which required the patient to puncture their skin and use a blood sample to measure their blood glucose level. Due to the discomfort

exhibited by the patient for this highly invasive technique, non-invasive forms of analysis are being developed for self-monitoring devices. A full understanding of the history of glucose biosensor development will be discussed to examine the progression of research to date in this exciting area.

2.2 Glucose biosensors

2.2.1 Glucose biosensors-general theory

A biosensor can be defined as a 'compact analytical device or unit incorporating a biological or biologically derived recognition element integrated or associated with a physio-chemical transducer'.⁵ The main components of a biosensor (**Figure 1**) consist of a recognition element which differentiates between the desired molecule and common interfering species, a transducer element which converts the target being analysed into a measurable signal and a processing system converting the signal into a form that is easily read and analysed.⁶⁻⁸ In

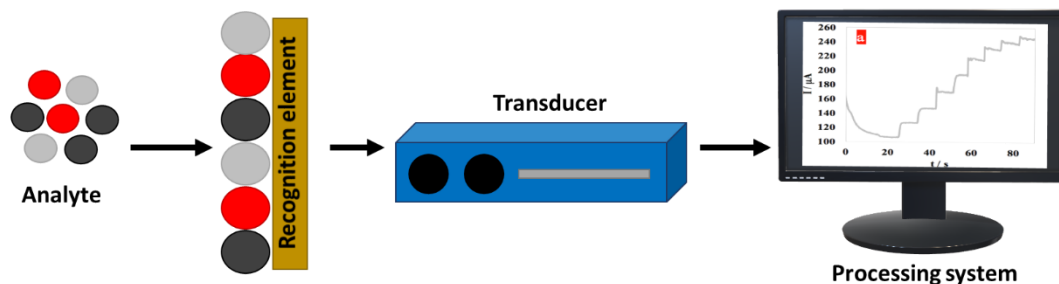


Figure 1 Schematic of a common biosensor

general the 3 main types of electrochemical sensors are potentiometric, amperometric and conductometric.⁹⁻¹¹ Potentiometric sensors are small, portable, produce low-oxygen consumption and are cheap to develop.¹² Amperometric sensors can be categorised into two generations and are the most commonly used for glucose sensors. The first (**Figure 2A**) consisting of an electroactive specie which is produced or consumed as the sensor substrate interacts with the attached enzyme. The downfall of using amperometric sensors is their inability to be utilized at high potential regions due to the oxidation of most physiological components, thus poisoning the system.¹³ The second generation of amperometric based biosensors (**Figure 2B**) involves a co-reactant and the auxiliary enzyme being integrated to the biosensor's biological layer for lower on-set potentials which reduces the poisoning of its surface.¹⁴ Conductometric sensors have the advantage of not using a reference electrode and

can be miniaturized quite successfully, however this type of sensor is relatively sensitive to light causing issues in everyday usage.¹⁵

2.2.2 Glucose biosensors- general enzyme mechanism

The main glucose interactions which produce the signal analysed by the enzyme-based biosensor come from the interaction between glucose and either glucose oxidase (GOx) or glucose-1-dehydrogenase (GDH) formed on the sensors surface.¹⁶⁻¹⁷ The main mechanism for enzyme-electrodes (equation 1) involves glucose oxidase catalysing glucose via oxidation forming gluconic acid and hydrogen peroxide.¹⁸

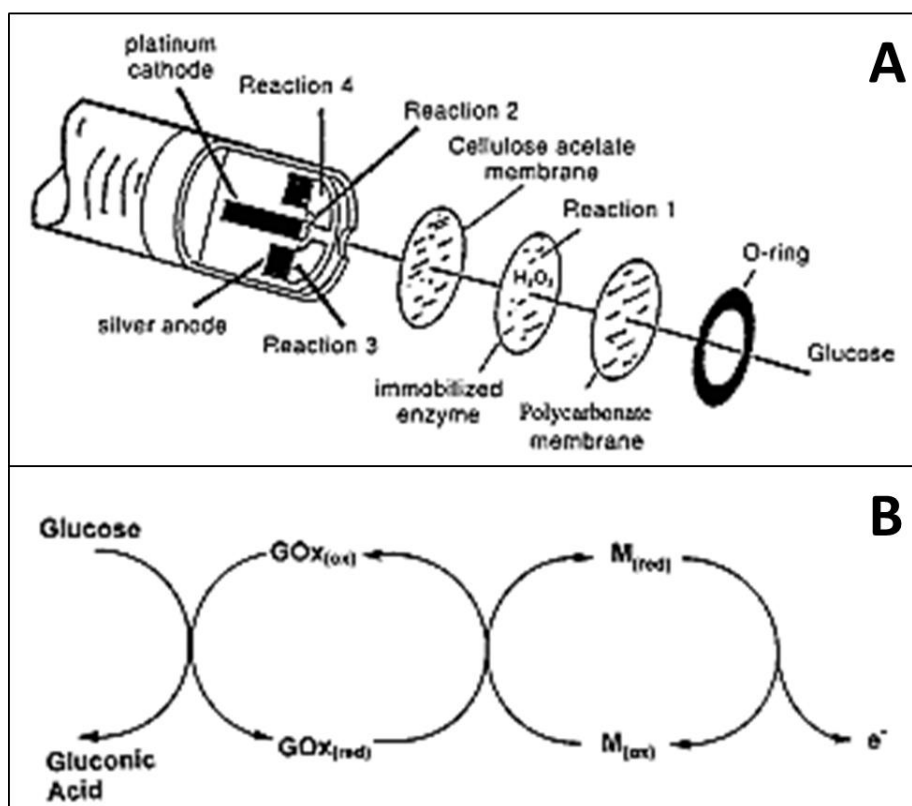


Figure 2 (A) Schematic of a first-generation glucose biosensor (based on a probe manufactured by YSI Inc.) and (B) second-generation glucose sensor mediated system (reprinted with permission from Ref. 20)



Along with this reaction, the attached glucose oxidase (which has formed on the surface) (equation 2) can bond with the metal surface via a reaction with oxygen leading to the formation of hydrogen peroxides (equation 3a), followed by the oxidization of the produced hydrogen peroxide on the surface (equation 3b). By conversion into an electrochemical signal,

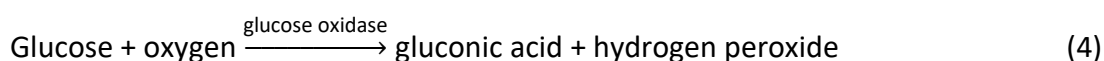
the number of electron transfers allows for the number of glucose molecules present in the blood to be determined.¹⁹⁻²⁰



From this mechanism glucose sensors have been produced across the years developed from utilizing the enzyme glucose oxidase (GOx) which is an enzyme produced when oxygen and glucose are present. This enzyme was originally utilized as the active species for early generation glucose sensors with further sensor development utilizing pure metals, metal composites, alloyed materials and metal oxides to achieve higher sensitivities and selectivity against common interfering species which could hinder the sensors response. The progression and development of each of these sensors will be discussed in the next sections.

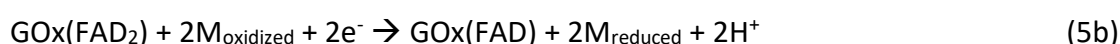
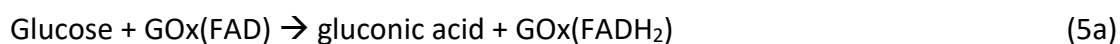
2.3 Enzymatic glucose sensors

Clarke and Lyons proposed the first glucose oxidase (GOx) based glucose sensor in 1962⁶ which consisted of GOx placed over an electrode which monitored the oxygen consumption, denoted by the equation:



From this initial glucose sensor, the modification and improvement history for glucose sensor development has taken many strides in not only the analysis technique (invasive/non-invasive) but also the type of electrode being used. The initial success of the enzyme-based electrode predominantly relied on the use of oxygen as the physiological electron acceptor. Unfortunately the use of oxygen caused numerous limitations for the functionality of the electrode most commonly due to the glucose/oxygen ration being too large which can cause peroxide causing the signal and the glucose concentration to be lost.²¹ Due to the major limitations in functionality, second-generation glucose biosensors began to be researched. The second-generation biosensors mainly involved electron transfer between GOx and electrode surfaces,²² artificial mediators²³⁻²⁴ and the attachment of electron-transfer relays.²⁵ Second-generation glucose sensors had further limitations due to environmental conditions,

such as temperature, pH and humidity along with enzyme-poisoning molecules which effected their performance.²⁶ The mediating material (M) replaces the O₂ molecules whilst a shuffling of electrons occurs to react with the redox centre of the GOx enzyme. This is then followed by the re-oxidation of the reduced mediator generating a current which allows for interaction with the working electrode.^{23, 27} The mechanism pathway for second-generation biosensors are described in equation (5a,b and c).



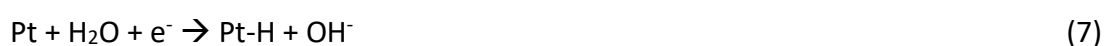
Enzyme-based glucose sensors were a necessary step in the glucose biosensing phase however as they suffer poor reproducibility, thermal and chemical instability and are expensive to produce.³⁸⁻³⁹ Different enzyme-based sensors and their characteristics are presented in **Table 1**. Metal-based additions (nanoparticles, metal oxides) to enzymatic glucose sensors have been able to increase sensitivities whilst keeping detection limits quite low in the μM region. The addition of the metal component has also improved selectivity of the sensors allowing for less surface poisoning due to interfering species. Further detail of the effect of individual metals and additions against glucose are discussed in the ongoing chapters.

Material	Applied potential/ scan rate	Sensitivity ($\mu\text{A}\cdot\text{mM}^{-1}\cdot\text{cm}^{-2}$)	Detection Limit (μM)	Linear range (mM)	Ref.
GR-CNT-ZnO-GOx	-	5.36	4.5	0.5-6	28
ERGO-MWCNT/GOx/Nf	+0.35 V	7.95	4.7	0.01-6.5	29
Gelatin-MWCNT-GOx	-0.44 V	2.47	-	6.3-20.1	30
GOx/NdPO ₄ NPs/CHIT	+0.4 V	1.92	0.08	0.15-10	31
GOD-GR-chitosan NC	100 mVs ⁻¹	37.93	0.02	0.08-12	32
Nafion-GOx-SWCNHs	+0.3 V	1.06	6	0-6	33
Silica sol-gel- Gox-CNTs	+0.3 V	0.196	150	-	34
GOD/CdS-PGE	200 mVs ⁻¹	7	0.05	0.5-11.1	35
Nafion-CdTe-GOD/GC	50 mVs ⁻¹	1.018	-	0-1	36
MWCNT-Nafion-GOD-NBC	+0.7 V	0.33	4	0.025-2	37

Table 1 Comparison table of enzymatic electrochemical glucose sensors

2.4 Non-enzymatic glucose sensors

Much success in the form of electrochemical devices incorporating structured materials have been exhibited due to better sensitivities, good reproduction of results and can withstand effects from interfering species whilst being cheaper to develop compared to their enzyme-based counterpart. Non-enzymatic glucose sensors differ from enzyme-based glucose sensors through the lack of using an enzyme as the working electrode and implementing a metal structure in its place. The electrode therefore relies on the surface formation of gluconolactone without producing peroxide (unlike enzyme-based sensors) which reduces the effect of physiological contaminants and low sensitivities. Non-enzymatic glucose sensors include individual metals, alloys, bimetallics, carbon-based materials, heterogeneous metal-metal oxide nanocomposites etc. The main functionality of non-enzymatic glucose sensors involves the process of electrocatalysis via the adsorption of the analyte to the electrode surface allowing for a suitable bond with the absorbate.⁴⁰ Metals that have shown great success as non-enzymatic glucose sensors include Pt,⁴¹⁻⁴⁴ Au,⁴⁵⁻⁴⁷ Ni,⁴⁸⁻⁵⁰ Cu,⁵¹⁻⁵⁴ Pd⁵⁵⁻⁵⁷ and Ag.⁵⁸⁻⁶⁰ Pt electrodes were highly popular in initial tests due to the great chemical electrooxidation of glucose atop Pt surfaces having similar response values in acidic, neutral or alkali buffer solutions. Very high sensitivities and excellent electrocatalytic activity are commonly exhibited for Pt electrodes towards glucose,⁶¹ however they are easily affected by the chemisorption of Cl⁻ ions on the electrode surface impeding glucose, hydrogen and hydrous oxides from being detected on the surface.⁶² Hoa et. al.⁴¹ formed a Pt/GOH/HPT glucose biosensor shown in **Figure 3A** and **B**. This sensor was highly sensitive (137.4 $\mu\text{A}\cdot\text{mM}^{-1}\cdot\text{cm}^{-2}$) showing large amounts of Pt particles caused agglomerates on the surface reducing the electrocatalytic surface area.⁴¹ Unlike many other metals which experience hydrogen adsorption on the surface, Pt experiences chemisorption on its bare surface known as a 'dehydration step'. Further oxidation of the adsorbed dehydrated intermediate then occurs forming weakly adsorbed gluconate. At high potentials the adsorbed dehydrogenated intermediate gets oxidized forming glucono- δ -lactone then eventually desorbs back to gluconate.⁶³ These reactions are exhibited in equations (6) and (7)



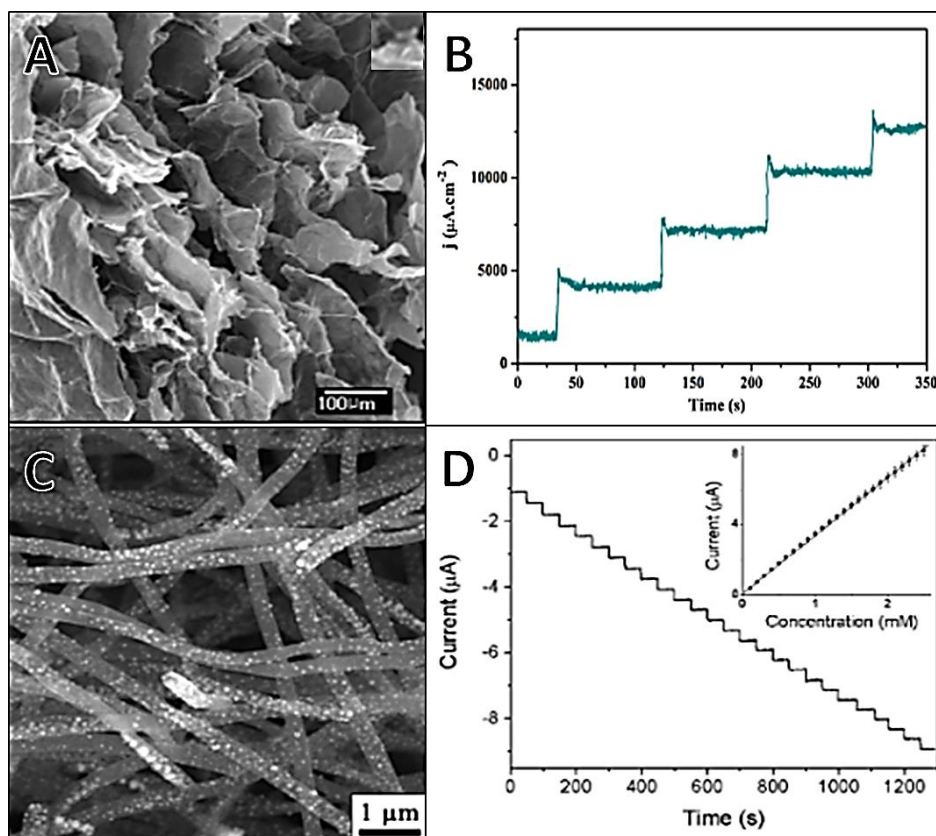


Figure 3 (A) SEM image of Pt/GOH/HPT glucose biosensor and (B) its corresponding amperometric I-V graph in glucose at +0.1 V (Reprinted with permission with Ref. 43). (C) SEM image of NiCF nanocomposite and (D) its corresponding amperometric response when undergoing glucose additions at +0.6 V (Reprinted with permission with Ref. 72).

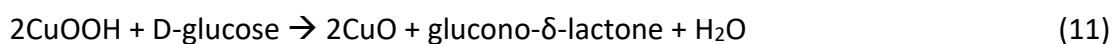
The extremely high cost of Pt was a major deterrent for further application as a glucose biosensor. Au has been widely used as a non-enzymatic glucose sensor due to its high electroactivity towards glucose, excellent biocompatibility, stability in the presence of common physiological contaminants (due to low-on-set potentials) and a high activity in the presence of neutral or alkali electrolytes.⁶⁴⁻⁶⁵ However, similar to Pt, Au suffers from poisoning by chloride ions in neutral electrolytes due to the absorbance of amino acids on the Au surface.⁶⁶ The electrochemical glucose sensing mechanism for Au will be discussed in detail in the next section as opposed to the mentioned metal reactions, the mechanism for Au remains relatively unknown.

Ni has been widely explored in alkaline medias for glucose sensing applications. The well-established mechanism of Ni in the presence of glucose involves Ni(III) oxyhydroxide partnering with a hydroxyl group to form Ni(OH)₂ or NiO(OH) as a redox couple. This coupling then finalizes with oxidation of glucose to gluconolactone which is catalyzed by the Ni(III)/(II) redox couple.⁶⁷ This mechanism is denoted by the equations (8) and (9).^{48, 68}



Due to this highly effective mechanism Ni displays a much higher sensitivity compared to Au and Pt. However, Ni is a challenge to be used in neutral and acidic solutions due to the high dependence on OH⁻ anions in the reaction mechanism that catalysis the electrooxidation of glucose.⁶⁹ Liu et. al.⁷⁰ formed a Ni nanoparticle-loaded carbon nanofiber paste electrode (**Figure 3C**) exhibiting a very low detection limit of 1 μM with a wide linear range between 2 and 2.5 mM and shown by the amperometric analysis in **Figure 3D**.

Cu is most commonly used in research as it is cheaper than the previous metals mentioned (Pt, Ni and Au) making it more economical as the electrode sensitive layer in glucose biosensor development. It displays sufficient sensitivity and selectivity in physiological contaminants however has similar pitfalls to Pt such as the adsorption of chloride ions on the surface. Luo et. al.⁵⁴ formed Cu nanoparticles on graphene sheets (**Figure 4A**) which exhibited a very low detection limit of 0.5 μM with a large linear range up to 4.5 mM in the presence of glucose (**Figure 4B**). The electrochemical oxidation of glucose via Cu involves the transition of Cu(II) to Cu (III) with a clear indication of Cu(III) occurring at a high on-set potential very similar to the redox reactions occurring for Pt in the presence of glucose.⁷¹⁻⁷² This process involves a 2 step mechanism where the CuO layer on the surface of the electrode is oxidized to the active Cu(III) species. Glucose is then oxidized to glucono-δ-lactone due to the Cu(III) radical. This mechanism is denoted by equations (10) and (11).⁷³⁻⁷⁶



Palladium is growing in its use as a non-enzymatic glucose sensor, most commonly paired with carbon-based nanomaterials (graphene⁷⁷ or carbon nanotubes⁷⁸). The effect of this pairing between Pd and its carbon-counterpart produces good electrocatalytic activity in the presence of glucose.⁷⁹ Yi et. al.⁵⁵ formed a nanoporous Pd-modified TiO₂ electrode (**Figure 4C and D**) with a linear range in glucose solution between 7 and 35 mM. Similar to Cu, Pd is oxidized to form PdOH which then interacts with glucose forming gluconolactone. The mechanism is described in equations (12) and (13).

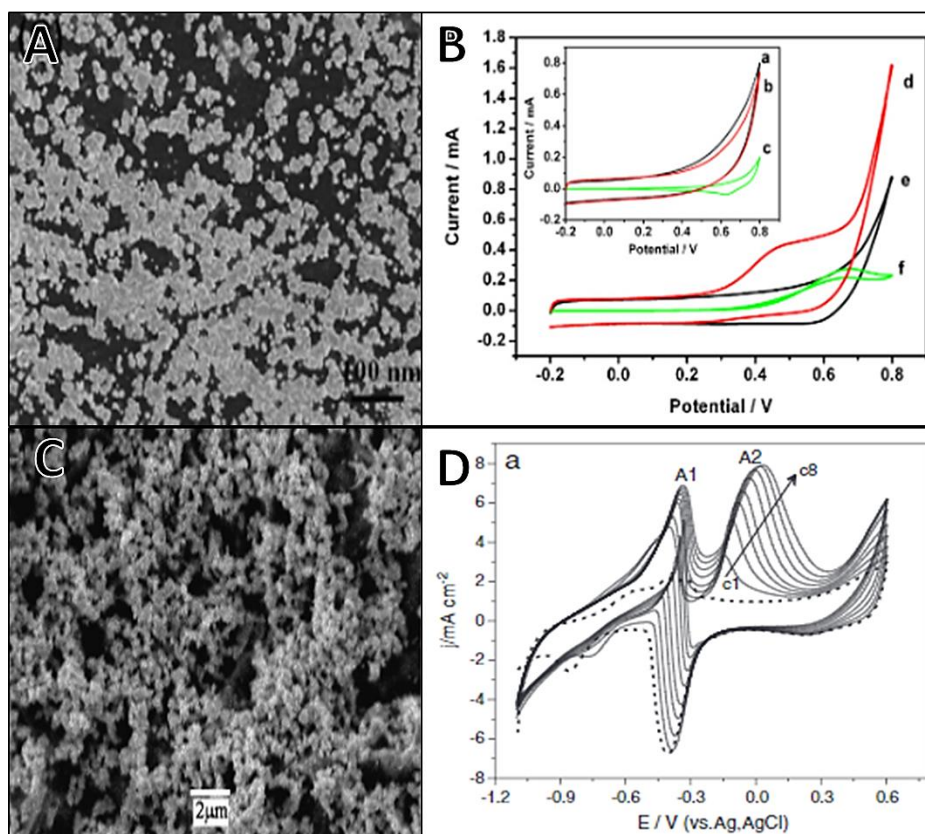


Figure 4 (A) SEM image of Cu-graphene sheet with (B) the corresponding cyclic voltammograms in 2 mM glucose solution at 100 mVs⁻¹ (Reprinted with permission from Ref. 56). (C) SEM image of Pd modified TiO₂ electrode and (D) the corresponding cyclic voltammograms in glucose at 20mVs⁻¹ (Reprinted with permission from Ref. 57).



Ag based glucose biosensors have received much attention as a quality noble metal with further enhancement compared to others due to their biocompatibility, great catalytic activity and low toxicity.⁸⁰ However, the structure, size and shape greatly affect their sensitivity and selectivity in the presence of glucose making them difficult to be used. Much like Pd, Ag has shown greater success when paired with carbon-based materials such as carbon nanotubes⁶⁰ and graphene⁵⁸ showing improved linear ranges and lower detection limits. A comparison table of various mono-metallic non-enzymatic glucose sensors are shown in **Table 2**. From this table it is observed that Cu based sensors required higher applied potentials where Pt showed the lowest applied potentials which can aid in reducing the effect of common physiological contaminants. Metals which combined with carbon-based materials such as Pt-MWCNT's-Nafion showed the greatest linear ranges compared to pure metal

materials.

Material	Applied potential (V)	Sensitivity ($\mu\text{A}\cdot\text{mM}^{-1}\cdot\text{cm}^{-2}$)	Detection Limit (μM)	Linear range (mM)	Ref.
Pt-MWCNTs-Nafion	0.0	-	-	1-11.7	81
Pt-MCs	+0.1	8.52	3	0-7	82
Ni CFP	+0.6	3.3	1	0.002-2.5	70
Ni NWAs	+0.55	1043	0.01	0.05-7	48
Cu-graphene	+0.5	-	0.5	0.0005-4.5	54
Cu nanocluster/MWCNT/GC	+0.65	17.76	0.21	0.0021-3.5	83
Pd nanoparticles	+0.18	-	-	1-20	84
Pd NP -CNT	+0.4	11.4	-	0-46	85
Ag MWCNT NC	+0.7	-	0.0003	0.001-3.5	60
AgNPs-graphene	-0.5	-	100	-	58

Table 2 Comparison table of non-enzymatic monometallic electrochemical glucose

2.5 Gold as a non-enzymatic glucose sensor

Among the metals tested to date, gold has been shown to be easily modified, both in their structure and functionality as desired for a particular application. These properties mainly come from the high chemical stability of gold and fairly uncomplicated synthesis and modification procedures.⁸⁶ Controlling the size, shape and morphology of Au,⁸⁷ adjustment for the application can improve the chemical sensors sensitivity and selectivity by functionalizing the particle surface designing application-specific functional groups. For the specific application of glucose sensors, studies into the use of Au have shown that the main catalytic component of Au is AuOH forming on the electrode's surface. This product (AuOH) is due to the chemisorption of hydroxide anions in alkaline environments.^{64,88} Although much work has been done for the application of Au as a non-enzymatic glucose sensor, the exact mechanism in the presence of glucose is still unknown. Some of the proposed mechanisms involving the reaction between Au and glucose are as follows:

Nikolaeva et. al.⁸⁹ proposed glucose electrooxidation occurred at high on-set potentials where gold oxide is formed along the surface of the Au which causes a large catalytic effect.⁸⁹ This mechanism is denoted by equation (14):



Makavos and Liu⁹⁰ showed a positive current peak via the cathodic sweep in cyclic voltammetry (CV) analysis which exhibited a highly linear dependence via the maximum current values and the glucose concentration in a large potential range. This reaction was highly dependent on the electrolyte composition, where a new mechanism was proposed for the peak composition. In this mechanism they proposed that the previous mechanism proposed by Nikolaeva et. al.,⁸⁹ did not allow for the continuation of the reaction when the potential favoured the partial reduction of gold oxides.⁹⁰



From this proposed mechanism they concluded that gold oxide can be utilized as a catalyst for glucose oxidation in glucose biosensor due to proper separation of inhibitors present such as chlorides, amino acids and human albumin.⁹¹ From the proposed mechanisms, the overall reaction of gold via glucose electrooxidation is explained. Step (1) shows the glucose molecule

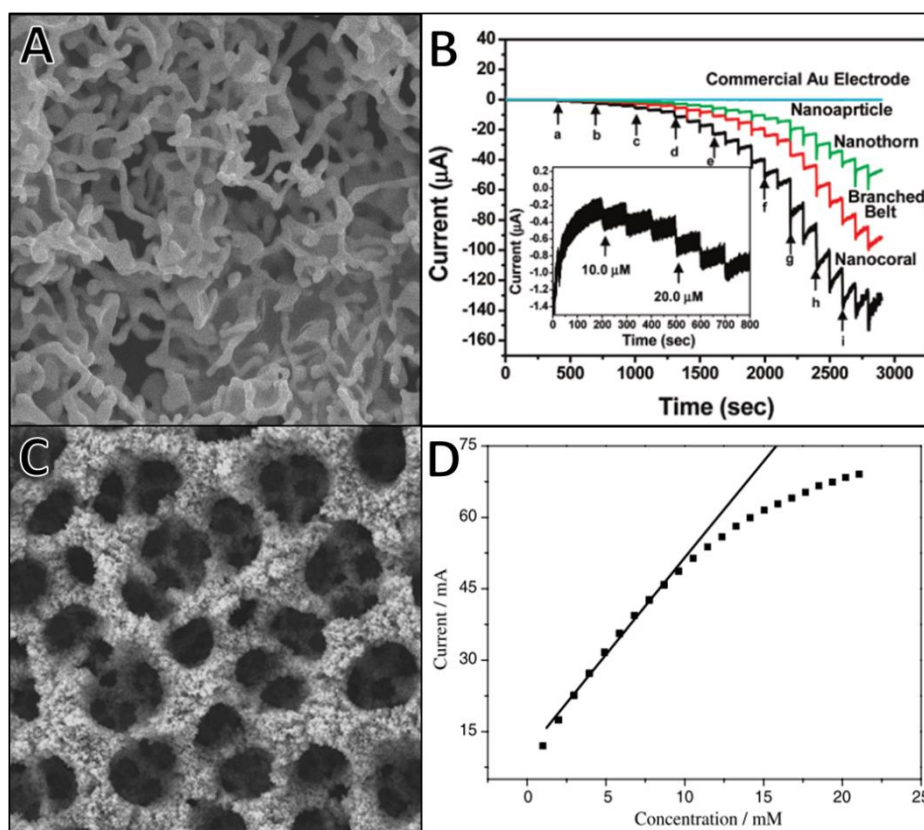


Figure 6 SEM image of (A) nanocoral Au and (B) the corresponding chronoamperometric additions analysis of glucose (Reprinted with permission from Ref. 47). SEM images of (C) porous Au and (D) its corresponding amperometric linear response in the presence of glucose (Reprinted with permission from Ref. 103).

electrochemically adsorbing on the electrode surface due to dehydrogenation. Step (2) occurs directly after this dehydrogenation, which involves the dehydrogenated molecule being converted to gluconate via direct oxidation involving the production of a hydroxide ion and the elimination of a hydrogen ion (H⁺). Step (3) proposes a secondary reaction path involving the oxidation of the dehydrogenated glucose to δ -gluconolactone. This δ -gluconolactone then reacts with a hydroxide ion forming gluconate.⁹² An overall mechanism for the glucose electrooxidation of glucose is described in equation (16).⁹³



Further to the mechanism of gold in the presence of glucose, improvement on the functionality of the gold as a successful glucose sensor occurred via the development of modified shapes and morphologies of the gold structures forming the gold electrode surface. Cheng et. al.⁴⁵ formed a coral-like pure gold structure (**Figure 6A and B**) displaying a quasi-one-dimensional structure which displayed a very high sensitivity in the presence of glucose. From this study comparing numerous formations of gold-based nanostructures they concluded that the overall surface area that was exposed to glucose effected the amount of gold oxides formed via glucose electrooxidation. Li et. al.⁹⁴ proposed the porosity of the gold material (**Figure 6C and D**) could dramatically enhance the glucose electrooxidation on the electrode surface via the hydrogen bubbling templating technique.⁹⁴ Comparison of various Au-based electrochemical glucose sensors are shown in **Table 3** where the type of structure effected the applied potential with sensitivities relatively similar in most cases.

Material	Applied potential (V)	Sensitivity ($\mu\text{A}\cdot\text{mM}^{-1}\cdot\text{cm}^{-2}$)	Detection limit (μM)	Ref.
AuNPs/C/chitosan	-0.2	0.55	180	95
Au NT array	+0.25	1.13	10	96
Au nanorods	+0.3	15.17	-	97
Au nanoplates	+0.65	49.5	200	98
Au nanodendrite	+1	46.76	7	99
Au nanocorals	+0.2	22.6	10	45
Au polycrystalline	+0.25	32	6	100
Nanostructured Au	-0.55	-	0.32	101
Porous Au	+0.35	11.8	5	94
Au film/GCE	-0.05	153	50	102

Table 3 Comparison table of non-enzymatic pure Au electrochemical glucose sensors

2.6 Metal composites

Along with monometallic non-enzymatic glucose sensors, combinations of metals and metal oxides have been highly successful. The use of a combination of materials has been shown to enhance sensor performance such as excellent sensitivity, low detection limits and larger linear ranges; while reducing poisoning on the surface to enhance selectivity toward glucose. Common metal composites are presented in **Table 4** with combinations with metal oxides producing the highest sensitivities and lowest detection limits with metal combinations (Pt-Au and Pt-Ni) showing the lowest applied potentials which enhances the sensors selectivity.

Material	Applied potential (V)	Sensitivity ($\mu\text{A}\cdot\text{mM}^{-1}\cdot\text{cm}^{-2}$)	Detection limit (μM)	Ref.
Cu-NiO composite/GCE	+0.4	171.8	0.5	103
Pt-Pd nanoparticles/mesoporous carbon/Nafion/GCE	-0.02	0.11	120	104
Cu-Cu ₂ O microspheres/GCE	+0.45	33.63	0.05	105
PtNi nanoparticles/graphene	-0.35	20.42	10	106
MnO ₂ /MWNRs composite	+0.3	33.19	-	107
Au-Ni nanorods	+0.4	778.2	5.5	108
NiO/Pt/ERGO	+0.6	668.2	0.2	109
CuO-Ag ₂ O NPs	+0.45	3130	0.098	110
NiO-GR/GCE	+0.35	158	5	111
PtAu nanoporous	+0.6	22.77	0.5	112

Table 4 Comparison table of metal-composite non-enzymatic electrochemical glucose

2.7 Alloys

As discussed in the previous section (*section 2.7 and 2.8*), the individual metals used for non-enzymatic glucose sensors display benefits and pitfalls when used regardless of structure and size. By combining two different metals as alloyed materials or bimetallic composites the glucose sensing capabilities of the individual components can be enhanced and reduction of surface poisoning and pitfalls can be reduced. Most commonly Pt,¹¹³ Pb,¹¹⁴ Au,³⁸ Ag,¹¹⁵ Pd,¹¹⁶ Co,¹¹⁷ Cu¹¹⁸ and Ni¹¹⁹ are used for these conjunctive formations,¹²⁰ with common alloy pairs being Ag-Ni,¹²¹ Pt-Pb,¹²² Cu-Co,¹²³ Ni-Cu,¹²⁴ Ni-Co,¹²⁵ Pt-Au¹²⁶ and Pd-Cu.¹²⁷⁻¹²⁸ Kang et. al.³⁸ proposed that by forming an Au-Pt alloy (**Figure 7A and B**) improvement in the electrocatalytic properties occurs compared to their monometallic counterparts, increasing the overall electroactive surface area as well as allowing for lower applied potentials during the

electrooxidation of glucose. The lower applied potentials can drastically improve the selectivity of the glucose sensor.³⁸ Ranjani et. al.¹²⁵ showed the formation of a Ni-Co alloyed nanostructure which was proposed due to Ni and Co displaying a similar crystal structure allowing for an enhancement in electrochemical and structural stability of the formed materials.¹²⁵ Sun et. al.¹¹⁹ proposed a Pt-Ni alloy nanotube electrode (**Figure 7C and D**) which displayed an enhanced sensitivity compared to their individual components. They also observed that the conjunction of these two components (Pt and Ni) offered a much lower working potential reducing the effect of common interfering species which had previously hindered the electrooxidation capabilities of Pt and Ni when used individually.¹¹⁹ For Ni-Ag, Ni exhibits poor electric conductivity¹²⁹ impeding their performance as a good glucose biosensor. To counteract this phenomenon the addition of Ag was used by Miao et. al.¹³⁰ due to silvers excellent activity towards the electrocatalytic oxidation of glucose molecules.¹³⁰ In the case of Pt-Pb, Pt can be easily poisoned by adsorbed chloride ions and intermediates which then block the electroactive surface of the electrode impeding its response. Along with

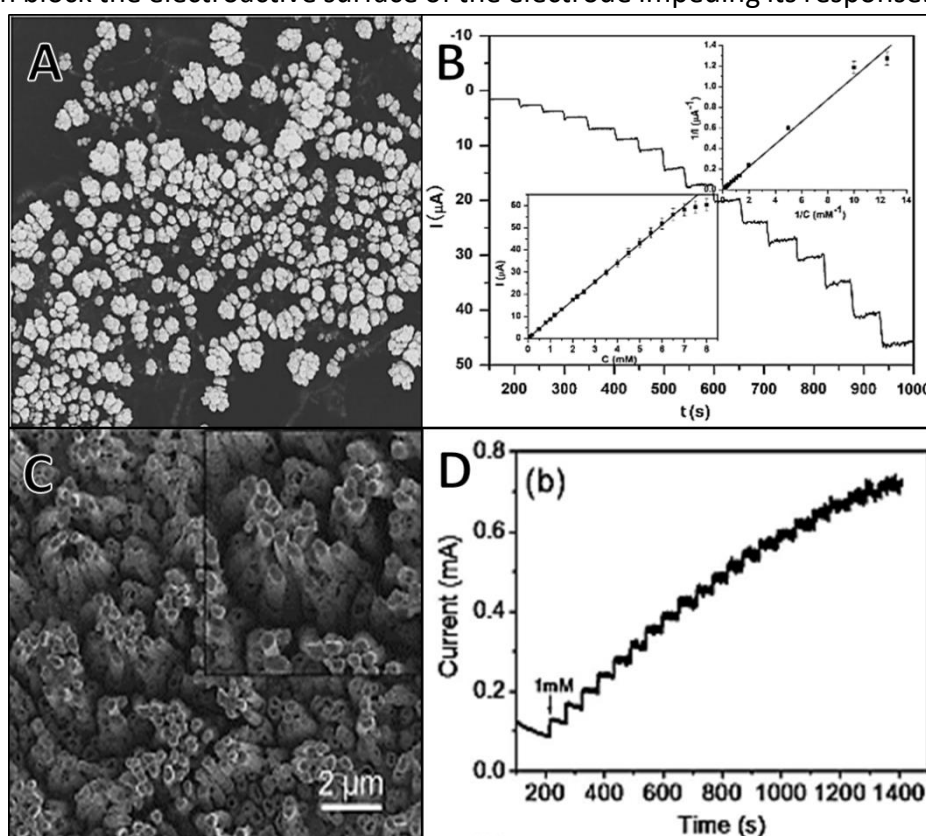


Figure 7 (A) SEM image of Au-Pt alloy NP's on CNTs/CS modified GC and (B) its corresponding amperometric response when undergoing glucose additions at +0.1 V (Reprinted with permission from Ref. 38) (C) SEM image of Pt replaced Ni nanowires and (D) its corresponding amperometric response when undergoing glucose additions at -0.35 V (Reprinted with permission from Ref. 121).

this surface poisoning, slow response to faradaic currents and selectivity in the presence of ascorbic acid (AA), Uric acid (UA) and other problematic interfering species is poor causing surface poisoning.^{62-63, 131} By pairing Pt with an element such as Pb the authors were able to reduce the applied potential of the reaction further negative reducing the effect of physiological contaminants that could possibly poison the sensitive layer. Although selectivity is improved, poisoning by chloride ions still occurs so larger surface areas when using this alloy are of great importance, as the larger the active surface area the better the glucose electro-oxidation of the sensor.^{114, 132} Noh et. al.¹²³ (**Figure 8A and B**) studied the alloy combination of Cu-Co for glucose electrooxidation with Cu as the main metal constituent as it is not effected by chemisorbed intermediates like Pt and Ni commonly exhibit. Their structure produced an excellent dynamic range in the presence of glucose ranging between 0.5 and 14 mM, well within the physiological range of blood glucose concentrations.¹²³ Commonly Ni-Cu has been used for corrosion protection and reduction in sensitivity from poisoning materials¹³³ and the conjunction of the two elements takes advantage of the high

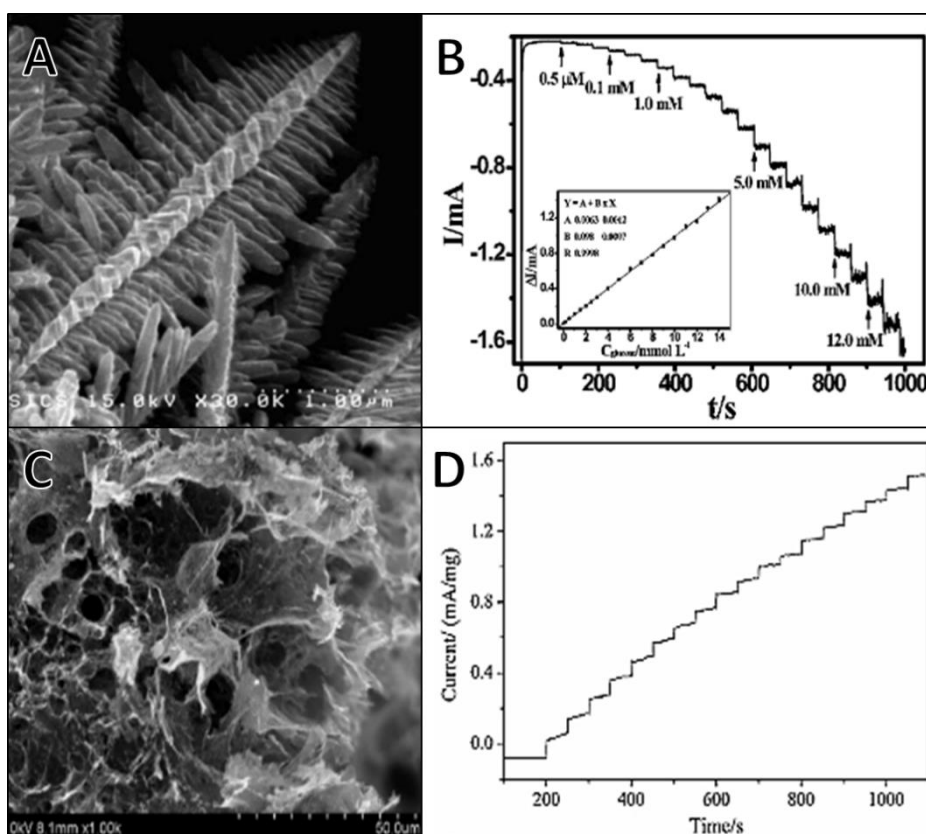


Figure 8 (A) SEM image of Cu-Co alloy dendrite and (B) its corresponding amperometric response when undergoing glucose additions at +0.65 V (Reprinted with permission from Ref. 125). (C) SEM image of Pd₆₆Cu₃₄/GCE hydrogel and (D) its corresponding amperometric response when undergoing glucose additions at -0.4 V (Reprinted with permission from Ref. 129)

sensitivities commonly exhibited with the capabilities of Cu to inhibit surface poisoning.¹³⁴⁻¹³⁵ Pd-Cu compared to many other alloy combinations is eco-friendly and cheaper to be used as catalysts for electrooxidation of glucose.¹³⁶ Pd-Cu's compatibility makes them a great combination of metallic materials for forming nanocomposites and nanocrystals.¹³⁷ Yuan et. al.¹²⁷ combined Pd and Cu (**Figure 8C and D**) forming alloyed nanoparticles where the onset potential was drastically reduced to -0.4 V improving selectivity of the sensor with a very wide linear range between 0 and 18 mM. Each of the aforementioned alloy combinations demonstrate the possibilities alloy materials pose for enhancement in sensing materials. By combining two materials with differing optimal properties in the presence of glucose; such as good selectivity, low detection limit or high sensitivity, there is the possibility that this will minimize the pitfalls of each material (surface poisoning, poor selectivity or low sensitivity) Through research many of the alloy combinations involved the addition of the oxide-form of the metal alloy component. This shifts the focus to further enhancement of materials to composite metal-oxide materials for glucose sensor enhancement. Common alloy-based non-enzymatic glucose sensors and their properties are shown in **Table 5**. From the table it can be seen that a Pt-Cu alloy has the lowest applied potential which reduces surface poisoning by interfering species with the Co-CuNP/TDNT producing the largest sensitivity. The combination of Cu-Co showed the lowest detection limits with Pt-Pd showing the largest detection limit but having the lowest applied potential.

Material	Applied potential (V)	Sensitivity ($\mu\text{A}\cdot\text{mM}^{-1}\cdot\text{cm}^{-2}$)	Detection limit (μM)	Ref.
Ag-Ni alloy/GCE	+0.45	6.48	0.49	120
Cu-Co alloy	+0.65	-	0.1	123
Pt-Cu nanochains	-0.01	135	2.5	138
Au-Cu/CNTs/C	+0.34	22	4	139
Pt ₃ Ru ₁ Ns	+0.05	31.3	0.3	140
PtPbNP/MWCNT	+0.3	17.8	7	141
Co-CuNP/TDNT	+0.6	2581.7	0.6	142
NP-PdCr	+0.35	0.75	1.8	143
NP-PdCu	+0.35	1.6	1.9	128
Pt-Pd nanoflakes	-0.3	48	20.6	144

Table 5 Comparison table of non-enzymatic alloy-based electrochemical glucose sensors

2.8 Metal-oxides

Metal oxides are fast becoming a key-area of modification for glucose biosensors. Metal-oxide biosensors have shown to be highly sensitive, relatively inexpensive and have rapid response when developed into specific nanostructure forms including nanowires, nanorods, nanotubes, nanospheres, nanoparticles and nanofibers.¹⁴⁵ The most common metal-oxides that have shown the greatest improvement in glucose biosensing development include ZnO,¹⁴⁶⁻¹⁴⁷ CuO,¹⁴⁸ NiO,¹⁴⁹ TiO₂,¹⁵⁰ CeO₂,¹⁵¹ SiO₂,¹⁵² ZrO₂¹⁵³ and Co₃O₄.¹⁵⁴ ZnO displays excellent biocompatibility, chemical stability, electrochemical activity and rapid electron transfer rate whilst displaying a large surface-to-volume ratio of nanostructured ZnO allowing for the immobilization of GOx, improving the electrical contact between the surface and GOx.¹⁵⁵⁻¹⁵⁶ Marie et. al.¹⁵⁷ formed an electrochemical sensor using zinc oxide nanorods (**Figure 9A and B**) displaying fast amperometric response of 3s and an excellent sensitivity of 10.911 mA·mM⁻¹·cm⁻². This increase in electrical contact can further be explained via GOx being immobilized

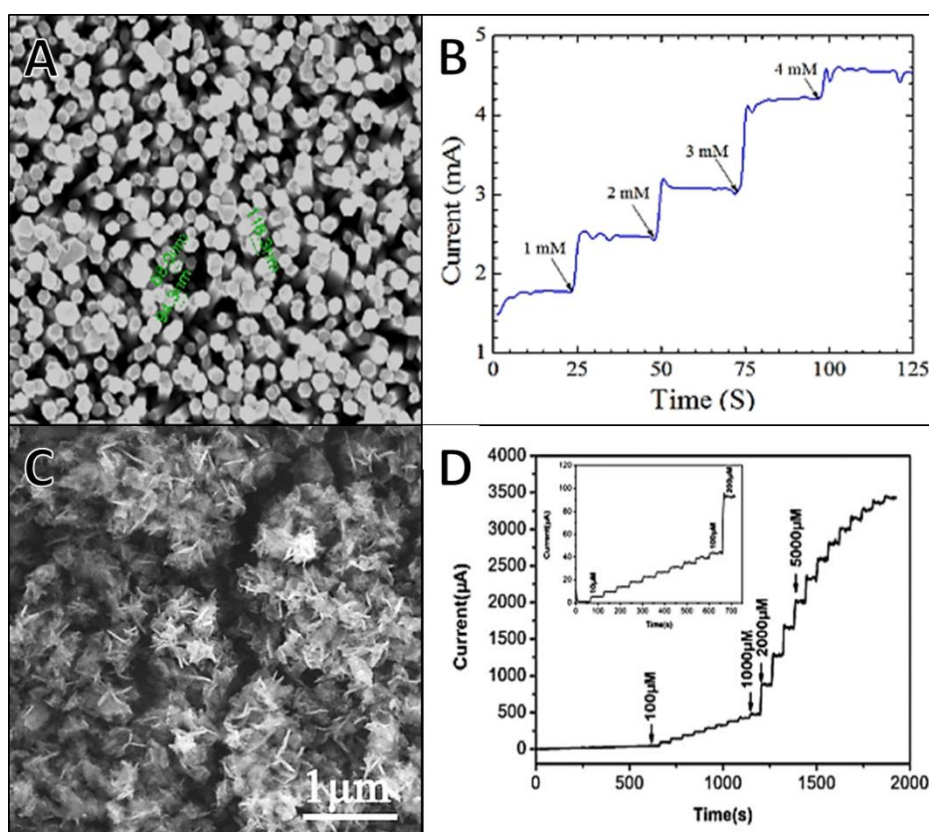


Figure 9 (A) SEM image of ZnO nanorods and (B) its corresponding amperometric response when undergoing glucose additions (Reprinted with permission from Ref. 159). (C) FESEM image of CuO nanoflowers and (D) its corresponding amperometric response when undergoing glucose additions at +0.5 V (Reprinted with permission from Ref. 165).

on the surface of the ZnO surface due to the D-glucose being hydrolyzed producing D-gluconic acid and hydrogen peroxide, as shown in equation (17).¹⁵⁸



CuO and NiO are able to oxidize sugars whilst avoiding the poisoning of their electrode surface.¹⁵⁹ As opposed to their Cu and Ni counterparts, their oxide forms are relatively stable in air and solutions,¹⁶⁰ as well as having a low development cost whilst exhibiting good catalytic and electrochemical performance.¹⁶¹⁻¹⁶² Cu in particular shows a very high specific surface area (reactive area), good electrochemical activity and the ability to have a large electron-transfer rate at lower potentials. Sun et. al.¹⁶³ formed CuO nanoflowers (**Figure 9C and D**) displaying an excellent sensitivity of $2657 \mu\text{A}\cdot\text{mM}^{-1}\cdot\text{cm}^{-2}$ with a very good linear range between 0 and 6000 μM at a low on-set potential of +0.5 V in alkaline media. The good sensing qualities of copper are enhanced when added to a carbon-based backbone material such as CNT or carbon nanofibers. These backbone materials allow for the charge transfer of the CuO-carbon structure to increase, hence improving sensing performance.¹⁶⁴⁻¹⁶⁵ The mechanism for CuO consists of an oxidation reaction forming due to the deprotonation of glucose isomerization to CuOOH. This reaction is followed by the adsorption of glucose onto the surface via the oxidation of Cu(II) and Cu(III). This mechanism is shown in equation (18).¹⁶³



Although NiO exhibits excellent sensitivities, NiO is unable to electrocatalyze in low or neutral solutions due to the electrocatalysis dependence of NiOOH to its hydroxyl anion.¹⁶⁶ Guo et. al.¹⁶⁷ formed a 3D nickel oxide electrode on Ni foam (**Figure 10A and B**) showing excellent electrocatalytic activity towards glucose ($6657.5 \mu\text{A}\cdot\text{mM}^{-1}\cdot\text{cm}^{-2}$) in NaOH with a very low detection limit of 0.46 μM . The glucose mechanism for NiO consists of Ni^{2+} being oxidized to Ni^{3+} due to the presence of glucose. This NiOOH composite (Ni^{3+}) oxidizes glucose by reducing itself into peroxide and gluconolactone reforming the Ni^{2+} species. These reactions are dictated in equation (19).¹⁶⁸



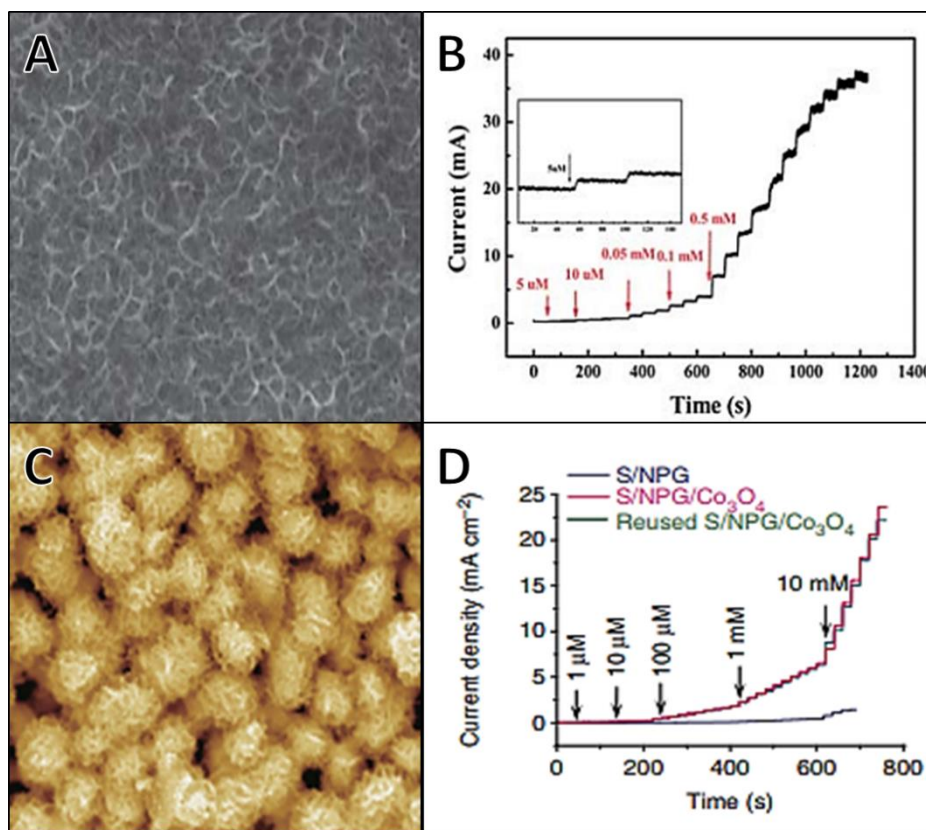


Figure 10 (A) SEM image of NiO/NF and (B) its corresponding amperometric response when undergoing glucose additions (Reprinted with permission from Ref. 169). (C) SEM image of S/NPG/Co₃O₄ hybrid and (D) its corresponding amperometric response when undergoing glucose additions at +0.26 V (Reprinted with permission from Ref. 177).



TiO₂ has received considerable attention due to its minimal cost, ability to be formed to a variety of morphologies, shows an excellent biocompatibility, is non-toxic and has good chemical/thermal stability.¹⁶⁹⁻¹⁷¹

CeO₂ possessing interesting properties as it is chemically inert, nontoxic, biocompatible, possesses high specific surface areas, has good electrical conductivity and possess good electron transfer features.¹⁵¹ Due to these properties CeO₂ can demonstrate low detection limited and with excellent linear ranges in the presence of glucose.¹⁷² The mechanism for CeO₂ consists of enzymatically H₂O₂ being generated due to the oxidation of glucose which can then decompose to react with CeO₂, shown in equation (20).



Co₃O₄ has shown excellent enhancement when used as a glucose biosensor due to its excellent biocompatibility, high electrocatalytic activity and adsorption capacity,¹⁷³⁻¹⁷⁴ particularly when used in conjunction with a secondary material such as Au,¹⁷⁵ TiO₂,¹⁷⁶ graphene,¹⁷⁷ NiO,¹⁷⁸ or PbO₂.¹⁷⁹ Lang et. al.¹⁷⁵ proposed a glucose biosensor consisting of hierarchical gold formations via the alloying/dealloying technique forming a large Au base with a large surface area (**Figure 10C and D**). Co₃O₄ was then hydrothermally placed upon the surface of the gold coating the gold electrode surface. This conjunction between the Au and metal oxide allowed for an exceedingly large sensitivity when compared to previously produced electrochemical sensors along with having minimal effect from physiological contaminants due to the combination of Au forming large amounts of AuOH and CoOOH. The formation of these intermediates on the internal surface of the electrode is due to the partial discharge of OH⁻, which in turn catalyzed the oxidation of intermediates and allowed for the direct oxidation of glucose due to the conversion of Au → AuOH and CoOOH → Co₃O₄.¹⁷⁵ The general mechanism for Co₃O₄ in the presence of glucose involves the reversible transition between Co₃O₄ and CoOOH followed by the further conversion of CoOOH to CoO₂. This formed Co product then reacts with the glucose present which catalyzes the Co₃O₄ structure producing CoOOH and gluconolactone.^{154, 180-181}



A comparison table of the discussed metal oxides are shown in **Table 6** showing the variable properties of the comparative glucose biosensors. Co₃O₄ showed the highest sensitivities in the presence of glucose with very low detection limits. For all metal-oxide sensors the applied potentials were shown to be much higher than the previous types of sensors studied with most having an applied potential < +0.2 V which can cause more surface poisoning and affecting their selectivity against common interfering species. As the progression of glucose biosensors continues these proposed materials have been successful when applied to blood glucose measurements. As metal-oxide materials possess high sensitivities, their application for non-invasive glucose sensing is where research has been directed.

Material	Applied potential (V)	Sensitivity ($\mu\text{A}\cdot\text{mM}^{-1}\cdot\text{cm}^{-2}$)	Detection limit (μM)	Ref.
CuO nanoflowers	+0.5	2657	1.71	163
NiO microfiber/FTO	+0.5	1785	0.033	167
Co ₃ O ₄ NPs	+0.59	521	0.00013	182
Cu ₂ O/GNs NC	+0.6	0.285	3.3	183
AuNi-Ni(OH) ₂	+0.16	707	1	184
ZnO nanowires	+0.8	10911	0.22	157
NiO-Au nanobelt	+0.6	48.35	1.32	149
Nano NiO	+0.7	66	0.16	185
3D graphene/Co ₃ O ₄	+0.58	3390	0.025	177
Au/Co ₃ O ₄ wire	+0.26	12500	0.005	175

Table 6 Comparison table of non-enzymatic metal oxide electrochemical glucose

2.9 Other types of glucose sensors

Further to electrochemical enzymatic and non-enzymatic glucose sensors, much work is being done for other methods of glucose detection. Optical and photoelectrochemical glucose detection has gained much popularity as non-invasive detection of glucose becomes more prevalent. Optical glucose sensors are finding their footing in glucose analysis as they utilize nonionizing radiation to interrogate the sample, do not require consumable reagents (such as saliva, tears, blood) and take fast measurements. Areas of analysis include Infrared¹⁸⁶/near-infrared spectroscopy,¹⁸⁶ raman spectroscopy,¹⁸⁷ polarimetry¹⁸⁸ and fluorescence spectroscopy.¹⁸⁹ The approach towards optical sensing has been slow due to the downfalls such as a lack in good sensitivities appropriate for real-life usage and interfering species have similar response features in optical analysis making selectivity and specificity an ever-present issue with optical sensors.¹⁹⁰ Mid-infrared (MIR) and near-infrared (NIR) are the most common optical absorption spectroscopy used for glucose quantification, represented in **Figure 11**.¹⁹⁰ Rosenthal et. al.¹⁹¹ proposed the use of NIR transmission spectroscopy within a wavelength region of 700-1300 nm via the fingertip.¹⁹¹⁻¹⁹² Danzer et. al.¹⁹³ employed diffuse reflectance spectroscopy in a similar region showing that spectral peaks are difficult to analyze in this wavelength region due to low physiological concentrations.¹⁹³ Low signal-to-noise measurements are exhibited for glucose absorption for NIR analysis and are highly impacted by pH, temperature and scattering hindering response accountability. A very

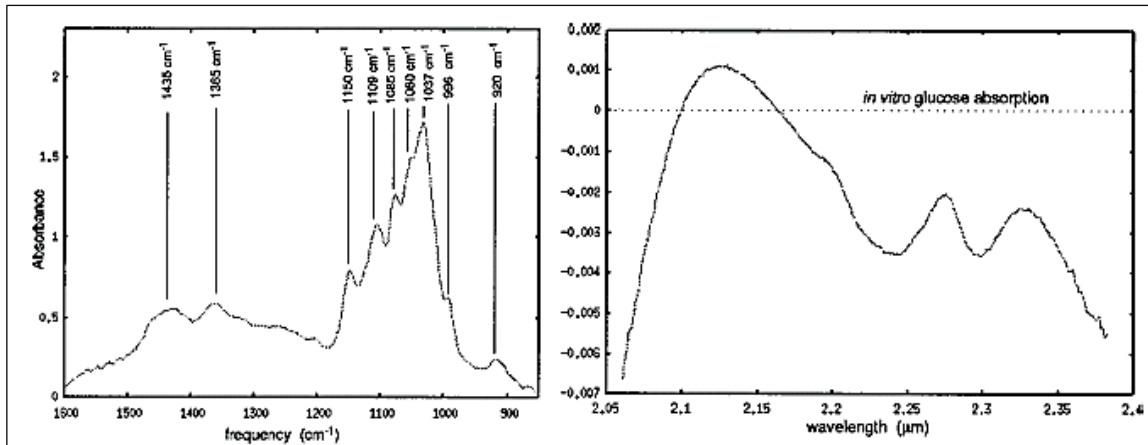


Figure 11 (left) MIR spectra showing absorption peak assignment for glucose and (right) NIR spectra for in-vitro adsorption of glucose (Reprinted with permission from Ref. 192).

important downfall for NIR spectroscopy is from the similar spectral peaks of glucose to other common physiological sugars such as fructose and sucrose which can cause issues when employing this type of analysis.¹⁹⁴ Polarimetry analysis of glucose is based off of optical rotary dispersion (ORD) which occurs when a chiral molecule in the aqueous state, will rotate the plane of linearly polarized light which passes through the analysed solution due to refraction indices differences.¹⁹⁵ The advantages of using polarimetry for glucose sensing applications are its ability to use substantial path lengths in aqueous solutions and the ability for sensor miniaturization for the components needed. The main disadvantage for using polarimetry for non-invasive analysis is mainly contributed to the depolarization of the optical source due to skin tissue. Skin tissue easily scatters the signal producing a large loss in signal-noise ratio for the sensor.¹⁹⁶ Coté et. al.¹⁸⁸ (**Figure 12A**) showed the linearity of the phase change vs applied current coefficient allowing for the measurement of optical rotatory effects as a true phase shift. Raman spectroscopy exhibits specific bands which are highly dependent on concentration making the spectra simpler and quite weak. The main drawback of raman spectroscopy for glucose sensing is its scattering and reabsorption in the presence of biological tissues interfering with the raman shifts of physiological concentration ranges. Eye-based sensing has become increasingly popular for this reason however the risk for the patient developing cancerous cells is a main drawback.¹⁹⁷⁻¹⁹⁸ Fluorescent techniques involve either a glucose-oxidase based sensor or an affinity-binding sensor.¹⁸⁹ The GOx sensor generates an optically detected glucose signal where the oxidation of glucose and oxygen forms gluconolactone and hydrogen peroxide. Using this type of chemical reaction, a fluorophore can be incorporated to the reaction which is highly sensitive to present oxygen

concentrations allow for the quantification of glucose concentration as is exhibited quantitatively by Evans et. al.¹⁸⁹ in **Figure 12B**. The main drawback for these forms of sensors is from the dependence on local oxygen tension as well as glucose, making the response system more complicated than straightforward sensing techniques.¹⁹⁹⁻²⁰⁰ Raman spectroscopy exhibits higher spectral resolution and reduced interference with water compared to other optical forms of analysis; mainly IR and raman spectroscopy. Due to these drawbacks focus on surface-enhanced raman spectroscopy (SERS) is very promising for glucose sensing due to the intensified local electromagnetic field due to nanostructured surfaces enhancing the raman response by $10^6 - 10^8$.²⁰¹⁻²⁰² Common SERS response for a nanostructured surface in the presence of glucose is shown by Lyandres et. al.¹⁸⁷ in **Figure 12C**. Transdermal sensing devices such as the fluorescence affinity nanospheres sensor formed by Ballerstadt et. al.²⁰³ (**Figure 12D**) have shown similar progress to optical sensors where a wearable device can be used by using reverse iontophoresis (removal of molecules from within the body for detection). However these types of sensors tend to suffer from

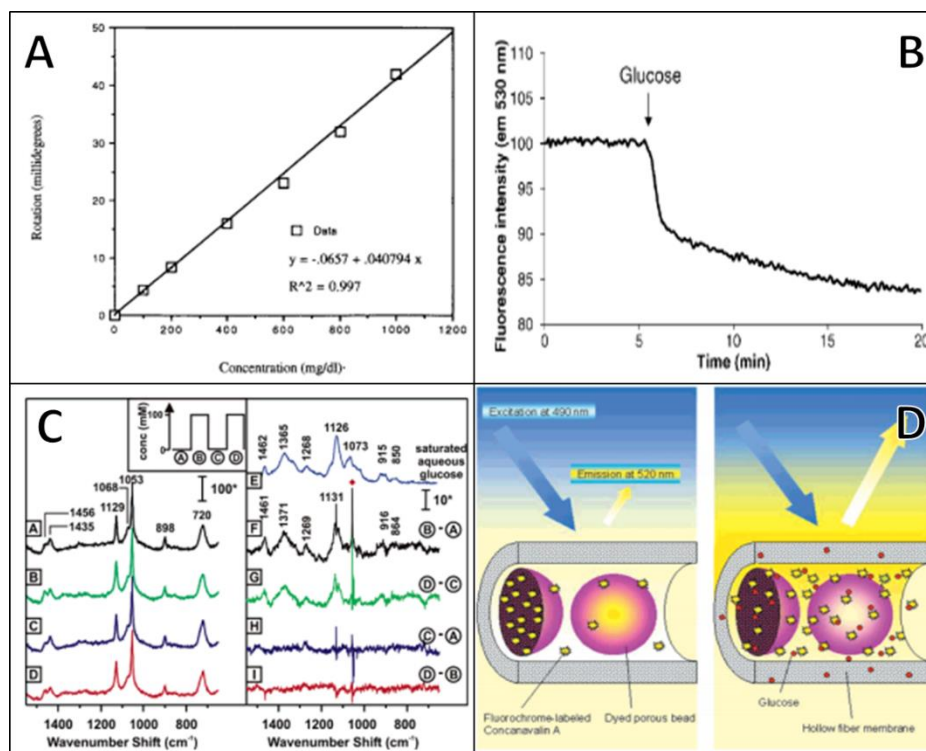


Figure 12 (A) *In-vitro* glucose levels vs polarization rotation using the true test phase approach (Reprinted with permission from Ref. 190). (B) glucose induced quenching of the fluorescence of fibroblasts in culture (Reprinted with permission from Ref. 191). (C) SERS spectra of AgFON in the presence of glucose (Reprinted with permission from Ref. 189). (D) Schematic of a fluorescence affinity hollow fiber sensor used for transdermal glucose analysis (Reprinted with permission from Ref. 205).

severe pitfalls such as a long warm-up time, inaccuracy, skin irritation and excessive sweating.²⁰⁴ Photoelectrochemical (PEC) sensing techniques of glucose are steadily entering the realm of analysis as this technique incorporates the benefits of optical sensing and electrochemical sensing. A normal electrochemical set-up is used whilst being exposed to light with the sensing material typically being a semi-conducting material such as TiO_2 ,²⁰⁵ ZnO ,²⁰⁶ SiO_2 ²⁰⁷ and CuO .²⁰⁸ Zheng et. al.²⁰⁵ showed the effectiveness of TiO_2 (**Figure 13A and B**) in the form of a nanocomposite with excellent glucose addition linearity for photocurrent vs time over a range of 1-8 mM. A Au nanoparticle photoelectrochemical sensor was presented by Cao et. al.²⁰⁷ (**Figure 13 C and D**) displaying a linear range between 1 μM and 1 mM with a very low detection limit of 0.46 μM . PEC sensing has attracted wide attention as it is cost-effective, produced quick responses, are simple and easy to use.²⁰⁷

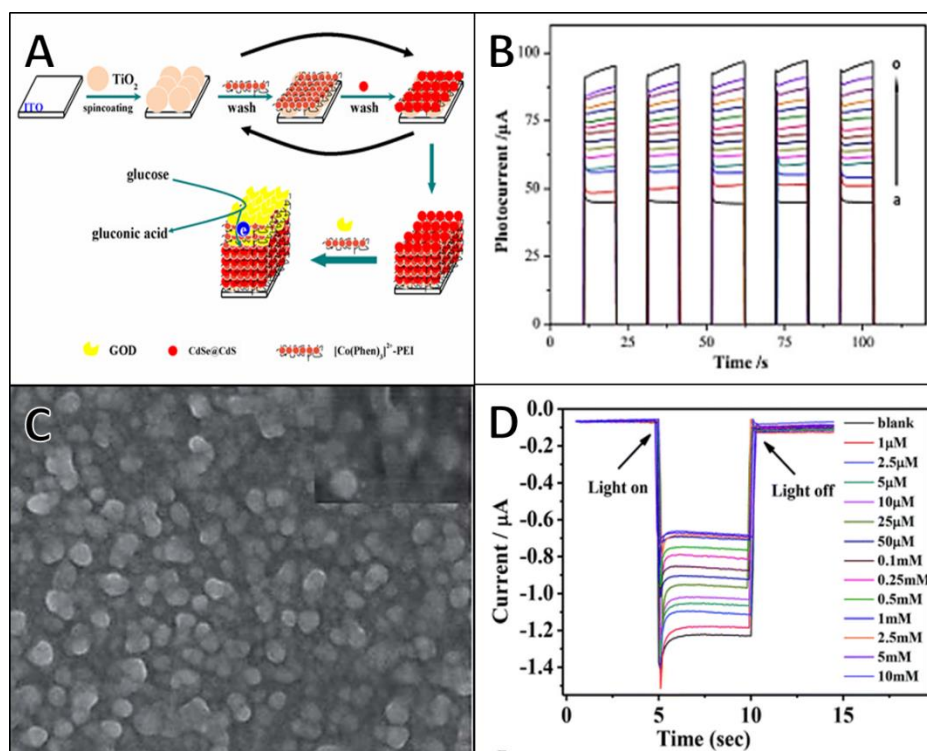


Figure 13 (A) Schematic of $\text{TiO}_2/\text{CdSe@CdS}$ NC and (B) its corresponding photoelectrochemical analysis in the presence of glucose (Reprinted with permission from Ref. 207). (C) SEM image of $\text{ITO}/\text{PbS}/\text{SiO}_2/\text{AuNPs}$ electrode and (D) the corresponding photoelectrochemical analysis in the presence of glucose (Reprinted with permission from Ref. 209)

2.10 Non-invasive glucose detection

As the development of glucose biosensors becomes oversaturated with blood-glucose devices the push for non-invasive methods of glucose analysis are of much excitement. Not only would it be less irritating and painful for the person suffering from diabetes, but it allows

for continuous and repeated use due to less poisoning by common interfering biological species present. Possible methods of analysis would be through the detection of glucose through excreted biological fluids such as urine, saliva, sweat, tears or breath.²⁰⁹⁻²¹⁰ Current non-invasive detection methods are most commonly optical-based sensors which suffer from insufficient sensitivities and selectiveness. These drawbacks have caused a push for the alteration and development of invasive electrochemical sensors (due to their high performance, portability, simplicity and low cost²¹¹) to develop electrochemical sensors which are tapered to be effective in a non-invasive form. Invasive methods have become a key problem as more neonatal, elderly and hemophobic patients have been diagnosed with diabetes making monitoring of their blood sugars an onerous task. A few key challenges for non-invasive electrochemical sensors occur which need to be addressed as research continues in this area including: obtaining sensor responses in low analyte concentrations, small sample volumes are used, mechanical resilience, biofouling and biocompatibility.²¹² Current electrochemical non-invasive sensors need much improvement however many advances have been made. Modes of analysis have been varied and creative to create the best and most accurate form of detection. For Saliva analysis multiple wearable devices are beginning to be developed using already existing mouth-based accessories to make the useability more realistic for the wearer of the device. Graf et. al.²¹³ formed a potentiometric denture using a glass membrane and Kim et. al.²¹⁴ created a wearable mouthguard (**Figure 14A and B**) based off of an amperometric enzymatic biosensor utilizing an immobilized lactate oxidase. Tear analysis has had much success using contact lenses with imbedded sensing materials, however due to the sensitive nature of the human eye, sample collection continues to be an issue. Yao et. al.²¹⁵ developed an amperometric contact lens (**Figure 14 C and D**) which contained imbedded wireless electronics for data transmission. Their first generation contact lens sensor using a biofunctionalized PET-based contact lens with a glucose oxidase enzyme in a Ti sol-gel matrix which slowly developed to their secondary generation contact lens, which incorporated a dual sensor of activated and deactivated glucose oxidase which would minimize interfering species.²¹⁵⁻²¹⁷ Sweat-based electrochemical glucose sensors can be grouped into fabric/flexible plastic-type sensors or epidermal-type sensors. Textiles present a good base for a sensing material due to the large surface area which is in constant contact with the skin. Wool, nylon and cotton are highly attractive starting materials as they possess excellent capabilities for incorporating chemical sensors. Yang et. al.²²⁵ created an

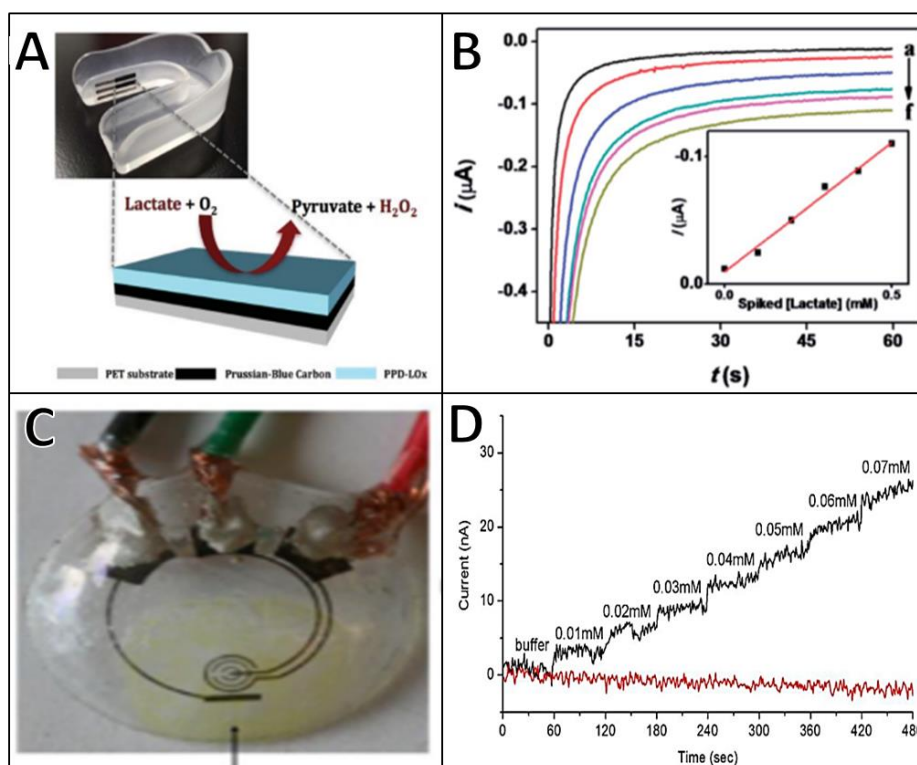


Figure 14 (A) Mouthguard biosensor used for saliva-based glucose sensing and (B) its corresponding chronoamperometric additions analysis in the presence of glucose (Reprinted with permission from Ref. 216). (C) Contact lens sensor pre-treated with GOD/titania/Nafion and (D) the corresponding amperometric additions analysis in the presence of glucose in tears (Reprinted with permission from Ref. 217)

amperometric sensor using screen printed bare carbon onto undergarments within a small range of 0-3mM with reasonable response.²²⁵ Epidermal sensors are slightly more attractive for sweat analysis as textile sensors restrict the analysis regions to very intimate regions. New work is being done using temporary tattoos predominantly consisting of carbon fibres. Amperometric and Potentiometric tattoos have been created using numerous activation elements including lactate oxidase,²²⁶ ammonium ionophore²²⁷ and sodium ionophore.²²⁸ Non-invasive electrochemical sensors have gained much popularity as they have higher sensitivities and can monitor glucose concentrations over larger ranges compared to their optical predecessors. Electrochemical non-invasive devices are described in **Table 7** referencing the non-invasive fluid the device is used to detect. From the table the linear range for all the sensors is quite small however sweat sensors produce the largest linear ranges. Saliva-based sensors produced the greatest sensitivities with tear-based sensors having lower

detection limits. Electrochemical glucose sensor research has been varied throughout research however as the knowledge of different material types (metal/non-metal/enzyme) is studied the ongoing progression towards non-invasive glucose sensors continues to be studied. As the push towards non-invasive glucose sensing research continues the previous studies have aided others to combine knowledge from various studies to produce a highly effect, sensitive and selective glucose sensor and implement it into everyday use.

Material	Media	Sensitivity ($\mu\text{A}\cdot\text{mM}^{-1}\cdot\text{cm}^{-2}$)	Detection limit (μM)	Linear range (mM)	Ref.
Telecommunicated contact lens	Tears	-	-	0-2	217
Contact lens/ polymer substrate	Tears	0.18		0.05-1	218
Contact lens/Ti sol-gel-GOx-Nafion	tears	240	<0.01	0.1-0.6	215
Pt/Ag-AgCl-GOx	saliva	-	-	0.05-1	219
PAA/SWNT/(CS/GNp/GOx) ₃	saliva	26.6	11.1	0.017-1.11	220
PAA/SWNT/(CS/GNp/GOx) ₃ on Pt electrode	saliva	69.9	16.7	0.027-0.56	221
AuNS/CNT with CoWO ₄ /CNT NC	sweat	10.89	1.3	0-0.3	222
Au/rGO/AuPtNP/GOx/nafion)	sweat	48	5	0-2.4	223
v-Au NW-based stretchable electrode	sweat	27.32	10	0-1.15	224

Table 7 Comparison table of non-invasive electrochemical glucose sensors

References

1. Organization, W. H., *Global report on diabetes*. World Health Organization: 2016.
2. Australia, D., *Diabetes Australia*. [cited November 1, 2015]. <https://www.diabetesaustralia.com.au/diabetes-globally> **2015**.
3. Dennis, J. M.; Shields, B. M.; Henley, W. E.; Jones, A. G.; Hattersley, A. T., *The Lancet Diabetes & Endocrinology* **2019**, 7 (6), 442-451.
4. Collaboration, N. R. F., *The Lancet* **2016**, 387 (10027), 1513-1530.
5. Turner, A. P., *Science* **2000**, 290 (5495), 1315-1317.
6. Clark Jr, L. C.; Lyons, C., *Ann. N.Y. Acad. Sci.* **1962**, 102 (1), 29-45.
7. Updike, S.; Hicks, G., *Nature* **1967**, 214 (5092), 986.
8. Hiratsuka, A.; Fujisawa, K.; Muguruma, H., *Anal. Sci.* **2008**, 24 (4), 483-486.
9. Habermüller, K.; Mosbach, M.; Schuhmann, W., *Fresenius' journal of analytical chemistry* **2000**, 366 (6-7), 560-568.

10. Pearson, J.; Gill, A.; Vadgama, P., *Ann. Clin. Biochem.* **2000**, *37* (2), 119-145.
11. Thevenot, D. R.; Toth, K.; Durst, R. A.; Wilson, G. S., *Pure Appl. Chem.* **1999**, *71* (12), 2333-2348.
12. Bobacka, J.; Ivaska, A.; Lewenstam, A., *Chem. Rev.* **2008**, *108* (2), 329-351.
13. Basu, S.; Debnath, A. K., Chapter V - Special Instrument. In *Power Plant Instrumentation and Control Handbook*, Basu, S.; Debnath, A. K., Eds. Academic Press: Boston, 2015; pp 297-386.
14. Scheller, F. W.; Schubert, F.; Neumann, B.; Pfeiffer, D.; Hintsche, R.; Dransfeld, I.; Wollenberger, U.; Renneberg, R.; Warsinke, A.; Johansson, G.; Skoog, M.; Yang, X.; Bogdanovskaya, V.; Bückmann, A.; Zaitsev, S. Y., *Biosens. Bioelectron.* **1991**, *6* (3), 245-253.
15. Dzyadevych, S.; Jaffrezic-Renault, N., 6 - Conductometric biosensors. In *Biological Identification*, Schaudies, R. P., Ed. Woodhead Publishing: 2014; pp 153-193.
16. Price, C. P., *Clinical chemistry and laboratory medicine* **2003**, *41* (9), 1213-1219.
17. D'costa, E.; Higgins, I.; Turner, A., *Biosensors* **1986**, *2* (2), 71-87.
18. Foulds, N.; Frew, J.; Green, M., *Biosensors—A Practical Approach*. IRL Press—Oxford University Press, Oxford **1990**, 97-124.
19. Guilbault, G.; Lubrano, G., *Anal. Chim. Acta* **1973**, *64* (3), 439-455.
20. Wang, J., *Chem. Rev.* **2008**, *108* (2), 814-825.
21. Armour, J. C.; Lucisano, J. Y.; McKean, B. D.; Gough, D. A., *Diabetes* **1990**, *39* (12), 1519-1526.
22. Marcus, R. A.; Sutin, N., *Biochimica et Biophysica Acta (BBA)-Reviews on Bioenergetics* **1985**, *811* (3), 265-322.
23. Cass, A. E.; Davis, G.; Francis, G. D.; Hill, H. A. O.; Aston, W. J.; Higgins, I. J.; Plotkin, E. V.; Scott, L. D.; Turner, A. P., *Anal. Chem.* **1984**, *56* (4), 667-671.
24. Frew, J. E.; Hill, H. A. O., *Anal. Chem.* **1987**, *59* (15), 933A-944A.
25. Ohara, T. J.; Rajagopalan, R.; Heller, A., *Anal. Chem.* **1994**, *66* (15), 2451-2457.
26. Wilson, R.; Turner, A., *Biosens. Bioelectron.* **1992**, *7* (3), 165-185.
27. Hale, P. D.; Inagaki, T.; Karan, H. I.; Okamoto, Y.; Skotheim, T. A., *J. Am. Chem. Soc.* **1989**, *111* (9), 3482-3484.
28. Hwa, K.-Y.; Subramani, B., *Biosens. Bioelectron.* **2014**, *62*, 127-133.
29. Mani, V.; Devadas, B.; Chen, S.-M., *Biosens. Bioelectron.* **2013**, *41*, 309-315.

30. Periasamy, A. P.; Chang, Y.-J.; Chen, S.-M., *Bioelectrochemistry* **2011**, *80* (2), 114-120.
31. Sheng, Q.; Luo, K.; Li, L.; Zheng, J., *Bioelectrochemistry* **2009**, *74* (2), 246-253.
32. Kang, X.; Wang, J.; Wu, H.; Aksay, I. A.; Liu, J.; Lin, Y., *Biosens. Bioelectron.* **2009**, *25* (4), 901-905.
33. Liu, X.; Shi, L.; Niu, W.; Li, H.; Xu, G., *Biosens. Bioelectron.* **2008**, *23* (12), 1887-1890.
34. Salimi, A.; Compton, R. G.; Hallaj, R., *Anal. Biochem.* **2004**, *333* (1), 49-56.
35. Huang, Y.; Zhang, W.; Xiao, H.; Li, G., *Biosens. Bioelectron.* **2005**, *21* (5), 817-821.
36. Liu, Q.; Lu, X.; Li, J.; Yao, X.; Li, J., *Biosens. Bioelectron.* **2007**, *22* (12), 3203-3209.
37. Tsai, Y.-C.; Li, S.-C.; Chen, J.-M., *Langmuir* **2005**, *21* (8), 3653-3658.
38. Kang, X.; Mai, Z.; Zou, X.; Cai, P.; Mo, J., *Anal. Biochem.* **2007**, *369* (1), 71-79.
39. Li, X.; Zhu, Q.; Tong, S.; Wang, W.; Song, W., *Sens. Actuator B-Chem.* **2009**, *136* (2), 444-450.
40. Pletcher, D., *J. Appl. Electrochem.* **1984**, *14* (4), 403-415.
41. Hoa, L. T.; Sun, K. G.; Hur, S. H., *Sens. Actuator B-Chem.* **2015**, *210*, 618-623.
42. Shen, Q.; Jiang, L.; Zhang, H.; Min, Q.; Hou, W.; Zhu, J.-J., *J. Phys. Chem. C* **2008**, *112* (42), 16385-16392.
43. Guo, M.; Hong, H.; Tang, X.; Fang, H.; Xu, X., *Electrochim. Acta* **2012**, *63*, 1-8.
44. Joo, S.; Park, S.; Chung, T. D.; Kim, H. C., *Anal. Sci.* **2007**, *23* (3), 277-281.
45. Cheng, T.-M.; Huang, T.-K.; Lin, H.-K.; Tung, S.-P.; Chen, Y.-L.; Lee, C.-Y.; Chiu, H.-T., *ACS Appl. Mater. Interfaces* **2010**, *2* (10), 2773-2780.
46. Bai, Y.; Yang, W.; Sun, Y.; Sun, C., *Sens. Actuator B-Chem.* **2008**, *134* (2), 471-476.
47. Li, J.; Yuan, R.; Chai, Y.; Che, X.; Li, W.; Zhong, X., *Microchim. Acta* **2011**, *172* (1-2), 163-169.
48. Lu, L.-M.; Zhang, L.; Qu, F.-L.; Lu, H.-X.; Zhang, X.-B.; Wu, Z.-S.; Huan, S.-Y.; Wang, Q.-A.; Shen, G.-L.; Yu, R.-Q., *Biosens. Bioelectron.* **2009**, *25* (1), 218-223.
49. Cataldi, T. R.; Desimoni, E.; Ricciardi, G.; Lelj, F., *Electroanalysis* **1995**, *7* (5), 435-441.
50. Salimi, A.; Roushani, M., *Electrochem. Commun.* **2005**, *7* (9), 879-887.
51. Huang, T.-K.; Lin, K.-W.; Tung, S.-P.; Cheng, T.-M.; Chang, I.-C.; Hsieh, Y.-Z.; Lee, C.-Y.; Chiu, H.-T., *J. Electroanal. Chem.* **2009**, *636* (1-2), 123-127.
52. Chen, Z.-L.; Hibbert, D., *J. Chromatogr. A* **1997**, *766* (1-2), 27-33.
53. Chen, D.-J.; Lu, Y.-H.; Wang, A.-J.; Feng, J.-J.; Huo, T.-T.; Dong, W.-J., *J. Solid State Electrochem.* **2012**, *16* (4), 1313-1321.

54. Luo, J.; Jiang, S.; Zhang, H.; Jiang, J.; Liu, X., *Anal. Chim. Acta* **2012**, *709*, 47-53.
55. Yi, Q.; Niu, F.; Yu, W., *Thin Solid Films* **2011**, *519* (10), 3155-3161.
56. Ye, J.-S.; Chen, C.-W.; Lee, C.-L., *Sens. Actuator B-Chem.* **2015**, *208*, 569-574.
57. Han, M.; Liu, S.; Bao, J.; Dai, Z., *Biosens. Bioelectron.* **2012**, *31* (1), 151-156.
58. Zhang, Y.; Liu, S.; Wang, L.; Qin, X.; Tian, J.; Lu, W.; Chang, G.; Sun, X., *RSC Adv.* **2012**, *2* (2), 538-545.
59. Lu, W.; Luo, Y.; Chang, G.; Sun, X., *Biosens. Bioelectron.* **2011**, *26* (12), 4791-4797.
60. Baghayeri, M.; Amiri, A.; Farhadi, S., *Sens. Actuator B-Chem.* **2016**, *225*, 354-362.
61. Ernst, S.; Heitbaum, J.; Hamann, C., *J. Electroanal. Chem. Interfacial Electrochem.* **1979**, *100* (1), 173-183.
62. Vassilyev, Y. B.; Khazova, O.; Nikolaeva, N., *J. Electroanal. Chem. Interfacial Electrochem.* **1985**, *196* (1), 105-125.
63. Beden, B.; Largeaud, F.; Kokoh, K.; Lamy, C., *Electrochim. Acta* **1996**, *41* (5), 701-709.
64. Vassilyev, Y. B.; Khazova, O.; Nikolaeva, N., *J. Electroanal. Chem. Interfacial Electrochem.* **1985**, *196* (1), 127-144.
65. Adzic, R.; Hsiao, M.; Yeager, E., *J. Electroanal. Chem. Interfacial Electrochem.* **1989**, *260* (2), 475-485.
66. Bond, G. C., *Molecules* **2012**, *17* (2), 1716-1743.
67. Zhao, C.; Shao, C.; Li, M.; Jiao, K., *Talanta* **2007**, *71* (4), 1769-1773.
68. Yu, S.; Peng, X.; Cao, G.; Zhou, M.; Qiao, L.; Yao, J.; He, H., *Electrochim. Acta* **2012**, *76*, 512-517.
69. Luo, Z.; Yin, S.; Wang, K.; Li, H.; Wang, L.; Xu, H.; Xia, J., *Mater. Chem. Phys.* **2012**, *132* (2-3), 387-394.
70. Liu, Y.; Teng, H.; Hou, H.; You, T., *Biosens. Bioelectron.* **2009**, *24* (11), 3329-3334.
71. Fleischmann, M.; Korinek, K.; Pletcher, D., *Journal of the Chemical Society, Perkin Transactions 2* **1972**, (10), 1396-1403.
72. Miller, B., *J. Electrochem. Soc.* **1969**, *116* (12), 1675-1680.
73. Li, C.; Kurniawan, M.; Sun, D.; Tabata, H.; Delaunay, J.-J., *Nanotechnology* **2014**, *26* (1), 015503.
74. Marioli, J. M.; Kuwana, T., *Electrochim. Acta* **1992**, *37* (7), 1187-1197.
75. Sun, S.; Zhang, X.; Sun, Y.; Yang, S.; Song, X.; Yang, Z., *ACS Appl. Mater. Interfaces* **2013**, *5* (10), 4429-4437.

76. Song, J.; Xu, L.; Zhou, C.; Xing, R.; Dai, Q.; Liu, D.; Song, H., *ACS Appl. Mater. Interfaces* **2013**, *5* (24), 12928-12934.
77. Wang, Q.; Cui, X.; Chen, J.; Zheng, X.; Liu, C.; Xue, T.; Wang, H.; Jin, Z.; Qiao, L.; Zheng, W., *RSC Adv.* **2012**, *2* (15), 6245-6249.
78. Meng, L.; Jin, J.; Yang, G.; Lu, T.; Zhang, H.; Cai, C., *Anal. Chem.* **2009**, *81* (17), 7271-7280.
79. Lu, L.-M.; Li, H.-B.; Qu, F.; Zhang, X.-B.; Shen, G.-L.; Yu, R.-Q., *Biosens. Bioelectron.* **2011**, *26* (8), 3500-3504.
80. Han, Y.; Zheng, J.; Dong, S., *Electrochim. Acta* **2013**, *90*, 35-43.
81. Rong, L.-Q.; Yang, C.; Qian, Q.-Y.; Xia, X.-H., *Talanta* **2007**, *72* (2), 819-824.
82. Su, C.; Zhang, C.; Lu, G.; Ma, C., *Electroanalysis* **2010**, *22* (16), 1901-1905.
83. Kang, X.; Mai, Z.; Zou, X.; Cai, P.; Mo, J., *Anal. Biochem.* **2007**, *363* (1), 143-150.
84. Gutés, A.; Carraro, C.; Maboudian, R., *Electrochim. Acta* **2011**, *56* (17), 5855-5859.
85. Chen, X.-m.; Lin, Z.-j.; Chen, D.-J.; Jia, T.-t.; Cai, Z.-m.; Wang, X.-r.; Chen, X.; Chen, G.-n.; Oyama, M., *Biosens. Bioelectron.* **2010**, *25* (7), 1803-1808.
86. Tokonami, S.; Yamamoto, Y.; Shiigi, H.; Nagaoka, T., *Anal. Chim. Acta* **2012**, *716*, 76-91.
87. Saha, K.; Agasti, S. S.; Kim, C.; Li, X.; Rotello, V. M., *Chemical reviews* **2012**, *112* (5), 2739-2779.
88. Burke, L., *Electrochim. Acta* **1994**, *39* (11-12), 1841-1848.
89. Nikolaeva, N.; Khazova, O.; Vasil'ev, Y. B., *Elektrokhimiya* **1983**, *19*, 1042-1048.
90. Makovos, E.; Liu, C., *Bioelectrochem. Bioenerg.* **1986**, *15* (2), 157-165.
91. LaCourse, W. R.; Johnson, D. C., *Anal. Chem.* **1993**, *65* (1), 50-55.
92. Pasta, M.; La Mantia, F.; Cui, Y., *Electrochim. Acta* **2010**, *55* (20), 5561-5568.
93. Han, L.; Zhang, S.; Han, L.; Yang, D.-P.; Hou, C.; Liu, A., *Electrochim. Acta* **2014**, *138*, 109-114.
94. Li, Y.; Song, Y.-Y.; Yang, C.; Xia, X.-H., *Electrochem. Commun.* **2007**, *9* (5), 981-988.
95. Shan, C.; Yang, H.; Han, D.; Zhang, Q.; Ivaska, A.; Niu, L., *Biosens. Bioelectron.* **2010**, *25* (5), 1070-1074.
96. Zhou, Y.-G.; Yang, S.; Qian, Q.-Y.; Xia, X.-H., *Electrochem. Commun.* **2009**, *11* (1), 216-219.
97. Li, Y.; Wang, X.; Dong, X.; He, Z.; Zhang, H., *Rare Metals* **2010**, *29* (3), 238-242.

98. Zhang, Y.; Chang, G.; Liu, S.; Lu, W.; Tian, J.; Sun, X., *Biosens. Bioelectron.* **2011**, *28* (1), 344-348.
99. Liu, H.-C.; Tsai, C.-C.; Wang, G.-J., *Nanotechnology* **2013**, *24* (21), 215101.
100. Cho, S.; Kang, C., *Electroanalysis* **2007**, *19* (22), 2315-2320.
101. Qiu, C.; Wang, X.; Liu, X.; Hou, S.; Ma, H., *Electrochim. Acta* **2012**, *67*, 140-146.
102. Xie, F.; Huang, Z.; Chen, C.; Xie, Q.; Huang, Y.; Qin, C.; Liu, Y.; Su, Z.; Yao, S., *Electrochem. Commun.* **2012**, *18*, 108-111.
103. Zhang, X.; Gu, A.; Wang, G.; Huang, Y.; Ji, H.; Fang, B., *Analyst* **2011**, *136* (24), 5175-5180.
104. Bo, X.; Bai, J.; Yang, L.; Guo, L., *Sens. Actuator B-Chem.* **2011**, *157* (2), 662-668.
105. Wang, A.-J.; Feng, J.-J.; Li, Z.-H.; Liao, Q.-C.; Wang, Z.-Z.; Chen, J.-R., *CrystEngComm* **2012**, *14* (4), 1289-1295.
106. Gao, H.; Xiao, F.; Ching, C. B.; Duan, H., *ACS Appl. Mater. Interfaces* **2011**, *3* (8), 3049-3057.
107. Chen, J.; Zhang, W.-D.; Ye, J.-S., *Electrochem. Commun.* **2008**, *10* (9), 1268-1271.
108. Hsu, C.-W.; Wang, G.-J., *Biosens. Bioelectron.* **2014**, *56*, 204-209.
109. Li, M.; Bo, X.; Mu, Z.; Zhang, Y.; Guo, L., *Sens. Actuator B-Chem.* **2014**, *192*, 261-268.
110. Jin, Z.; Li, P.; Zheng, B.; Yuan, H.; Xiao, D., *Analytical Methods* **2014**, *6* (7), 2215-2220.
111. Zhu, X.; Jiao, Q.; Zhang, C.; Zuo, X.; Xiao, X.; Liang, Y.; Nan, J., *Microchim. Acta* **2013**, *180* (5-6), 477-483.
112. Wang, J.; Gao, H.; Sun, F.; Xu, C., *Sens. Actuator B-Chem.* **2014**, *191*, 612-618.
113. Zhao, A.; Zhang, Z.; Zhang, P.; Xiao, S.; Wang, L.; Dong, Y.; Yuan, H.; Li, P.; Sun, Y.; Jiang, X., *Anal. Chim. Acta* **2016**, *938*, 63-71.
114. Cui, H.-F.; Ye, J.-S.; Liu, X.; Zhang, W.-D.; Sheu, F.-S., *Nanotechnology* **2006**, *17* (9), 2334.
115. Tominaga, M.; Shimazoe, T.; Nagashima, M.; Kusuda, H.; Kubo, A.; Kuwahara, Y.; Taniguchi, I., *J. Electroanal. Chem.* **2006**, *590* (1), 37-46.
116. Xiao, F.; Zhao, F.; Mei, D.; Mo, Z.; Zeng, B., *Biosens. Bioelectron.* **2009**, *24* (12), 3481-3486.
117. Liu, L.; Pippel, E.; Scholz, R.; Gösele, U., *Nano Lett.* **2009**, *9* (12), 4352-4358.
118. Jafarian, M.; Forouzandeh, F.; Danaee, I.; Gobal, F.; Mahjani, M., *J. Solid State Electrochem.* **2009**, *13* (8), 1171-1179.

119. Sun, Y.; Yang, H.; Yu, X.; Meng, H.; Xu, X., *RSC Adv.* **2015**, *5* (86), 70387-70394.
120. Tian, K.; Prestgard, M.; Tiwari, A., *Materials Science and Engineering: C* **2014**, *41*, 100-118.
121. Miao, Y.; Wu, J.; Zhou, S.; Yang, Z.; Ouyang, R., *J. Electrochem. Soc.* **2013**, *160* (4), B47-B53.
122. Bai, Y.; Sun, Y.; Sun, C., *Biosens. Bioelectron.* **2008**, *24* (4), 579-585.
123. Noh, H.-B.; Lee, K.-S.; Chandra, P.; Won, M.-S.; Shim, Y.-B., *Electrochim. Acta* **2012**, *61*, 36-43.
124. Li, X.; Yao, J.; Liu, F.; He, H.; Zhou, M.; Mao, N.; Xiao, P.; Zhang, Y., *Sens. Actuator B-Chem.* **2013**, *181*, 501-508.
125. Ranjani, M.; Sathishkumar, Y.; Lee, Y. S.; Yoo, D. J.; Kim, A. R., *RSC Adv.* **2015**, *5* (71), 57804-57814.
126. Ryu, J.; Kim, K.; Kim, H.-S.; Hahn, H. T.; Lashmore, D., *Biosens. Bioelectron.* **2010**, *26* (2), 602-607.
127. Yuan, M.; Liu, A.; Zhao, M.; Dong, W.; Zhao, T.; Wang, J.; Tang, W., *Sens. Actuator B-Chem.* **2014**, *190*, 707-714.
128. Yang, H.; Wang, Z.; Li, C.; Xu, C., *J. Colloid Interface Sci.* **2017**, *491*, 321-328.
129. Jia, D.; Ren, Q.; Sheng, L.; Li, F.; Xie, G.; Miao, Y., *Sens. Actuator B-Chem.* **2011**, *160* (1), 168-173.
130. Quan, H.; Park, S.-U.; Park, J., *Electrochim. Acta* **2010**, *55* (7), 2232-2237.
131. Bae, I.; Yeager, E.; Xing, X.; Liu, C., *J. Electroanal. Chem. Interfacial Electrochem.* **1991**, *309* (1-2), 131-145.
132. Zhang, L.; Wang, Z.; Xia, D., *J. Alloys Compd.* **2006**, *426* (1-2), 268-271.
133. Yan, W.; Wang, D.; Botte, G. G., *Electrochim. Acta* **2012**, *61*, 25-30.
134. Ding, R.; Liu, J.; Jiang, J.; Wu, F.; Zhu, J.; Huang, X., *Catalysis Science & Technology* **2011**, *1* (8), 1406-1411.
135. Tong, S.; Xu, Y.; Zhang, Z.; Song, W., *J. Phys. Chem. C* **2010**, *114* (49), 20925-20931.
136. Wang, W.; Li, Z.; Zheng, W.; Yang, J.; Zhang, H.; Wang, C., *Electrochem. Commun.* **2009**, *11* (9), 1811-1814.
137. Jin, M.; Zhang, H.; Wang, J.; Zhong, X.; Lu, N.; Li, Z.; Xie, Z.; Kim, M. J.; Xia, Y., *ACS nano* **2012**, *6* (3), 2566-2573.
138. Cao, X.; Wang, N.; Jia, S.; Shao, Y., *Anal. Chem.* **2013**, *85* (10), 5040-5046.

139. Liu, D.; Luo, Q.; Zhou, F., *Synth. Met.* **2010**, *160* (15-16), 1745-1748.
140. Yang, J.; Liang, X.; Cui, L.; Liu, H.; Xie, J.; Liu, W., *Biosens. Bioelectron.* **2016**, *80*, 171-174.
141. Cui, H.-F.; Ye, J.-S.; Zhang, W.-D.; Li, C.-M.; Luong, J. H.; Sheu, F.-S., *Anal. Chim. Acta* **2007**, *594* (2), 175-183.
142. Suneesh, P.; Vargis, V. S.; Ramachandran, T.; Nair, B. G.; Babu, T. S., *Sens. Actuator B-Chem.* **2015**, *215*, 337-344.
143. Zhao, D.; Wang, Z.; Wang, J.; Xu, C., *J. Mater. Chem. B* **2014**, *2* (32), 5195-5201.
144. Niu, X.; Lan, M.; Chen, C.; Zhao, H., *Talanta* **2012**, *99*, 1062-1067.
145. Rahman, M.; Ahammad, A.; Jin, J.-H.; Ahn, S. J.; Lee, J.-J., *Sensors* **2010**, *10* (5), 4855-4886.
146. Kavitha, T.; Gopalan, A. I.; Lee, K.-P.; Park, S.-Y., *Carbon* **2012**, *50* (8), 2994-3000.
147. Ahmad, R.; Tripathy, N.; Kim, J. H.; Hahn, Y.-B., *Sens. Actuator B-Chem.* **2012**, *174*, 195-201.
148. Cherevko, S.; Chung, C.-H., *Talanta* **2010**, *80* (3), 1371-1377.
149. Ding, Y.; Liu, Y.; Parisi, J.; Zhang, L.; Lei, Y., *Biosens. Bioelectron.* **2011**, *28* (1), 393-398.
150. Bao, S. J.; Li, C. M.; Zang, J. F.; Cui, X. Q.; Qiao, Y.; Guo, J., *Adv. Funct. Mater.* **2008**, *18* (4), 591-599.
151. Patil, D.; Dung, N. Q.; Jung, H.; Ahn, S. Y.; Jang, D. M.; Kim, D., *Biosens. Bioelectron.* **2012**, *31* (1), 176-181.
152. Luo, X.-L.; Xu, J.-J.; Zhao, W.; Chen, H.-Y., *Sens. Actuator B-Chem.* **2004**, *97* (2-3), 249-255.
153. Yang, Y.; Yang, H.; Yang, M.; Shen, G.; Yu, R., *Anal. Chim. Acta* **2004**, *525* (2), 213-220.
154. Ding, Y.; Wang, Y.; Su, L.; Bellagamba, M.; Zhang, H.; Lei, Y., *Biosens. Bioelectron.* **2010**, *26* (2), 542-548.
155. Rodriguez, J. A.; Jirsak, T.; Dvorak, J.; Sambasivan, S.; Fischer, D., *The Journal of Physical Chemistry B* **2000**, *104* (2), 319-328.
156. Tian, Z. R.; Voigt, J. A.; Liu, J.; Mckenzie, B.; Mcdermott, M. J., *J. Am. Chem. Soc.* **2002**, *124* (44), 12954-12955.
157. Marie, M.; Mandal, S.; Manasreh, O., *Sensors* **2015**, *15* (8), 18714-18723.
158. Aini, B. N.; Siddiquee, S.; Ampon, K.; Rodrigues, K. F.; Suryani, S., *Sensing and Bio-Sensing Research* **2015**, *4*, 46-56.

159. Jiang, X.; Herricks, T.; Xia, Y., *Nano Lett.* **2002**, *2* (12), 1333-1338.
160. Wang, D.; Song, C.; Hu, Z.; Fu, X., *The Journal of Physical Chemistry B* **2005**, *109* (3), 1125-1129.
161. Gao, X.; Bao, J.; Pan, G.; Zhu, H.; Huang, P.; Wu, F.; Song, D., *The Journal of Physical Chemistry B* **2004**, *108* (18), 5547-5551.
162. Zhang, J.; Liu, J.; Peng, Q.; Wang, X.; Li, Y., *Chem. Mater.* **2006**, *18* (4), 867-871.
163. Sun, S.; Zhang, X.; Sun, Y.; Yang, S.; Song, X.; Yang, Z., *Phys. Chem. Chem. Phys.* **2013**, *15* (26), 10904-10913.
164. Ahmad, R.; Vaseem, M.; Tripathy, N.; Hahn, Y.-B., *Anal. Chem.* **2013**, *85* (21), 10448-10454.
165. Yang, J.; Jiang, L.-C.; Zhang, W.-D.; Gunasekaran, S., *Talanta* **2010**, *82* (1), 25-33.
166. Toghill, K. E.; Compton, R. G., *Int. J. Electrochem. Sci* **2010**, *5* (9), 1246-1301.
167. Guo, C.; Wang, Y.; Zhao, Y.; Xu, C., *Analytical Methods* **2013**, *5* (7), 1644-1647.
168. Mishra, S.; Yogi, P.; Sagdeo, P.; Kumar, R., *Nanoscale Res. Lett.* **2018**, *13* (1), 16.
169. Yu, J.; Ju, H., *Anal. Chem.* **2002**, *74* (14), 3579-3583.
170. Zhang, T.; Tian, B.; Kong, J.; Yang, P.; Liu, B., *Anal. Chim. Acta* **2003**, *489* (2), 199-206.
171. Zheng, W.; Zheng, Y.; Jin, K.; Wang, N., *Talanta* **2008**, *74* (5), 1414-1419.
172. Ansari, A. A.; Kaushik, A.; Solanki, P.; Malhotra, B., *Electrochem. Commun.* **2008**, *10* (9), 1246-1249.
173. Solanki, P. R.; Kaushik, A.; Agrawal, V. V.; Malhotra, B. D., *NPG Asia Mater.* **2011**, *3* (1), 17.
174. Kimmel, D. W.; LeBlanc, G.; Meschievitz, M. E.; Cliffel, D. E., *Anal. Chem.* **2011**, *84* (2), 685-707.
175. Lang, X.-Y.; Fu, H.-Y.; Hou, C.; Han, G.-F.; Yang, P.; Liu, Y.-B.; Jiang, Q., *Nat. Commun.* **2013**, *4*, 2169.
176. Gao, Z.; Zhang, L.; Ma, C.; Zhou, Q.; Tang, Y.; Tu, Z.; Yang, W.; Cui, L.; Li, Y., *Biosens. Bioelectron.* **2016**, *80*, 511-518.
177. Dong, X.-C.; Xu, H.; Wang, X.-W.; Huang, Y.-X.; Chan-Park, M. B.; Zhang, H.; Wang, L.-H.; Huang, W.; Chen, P., *ACS nano* **2012**, *6* (4), 3206-3213.
178. Ramasamy, R.; Ramachandran, K.; Philip, G. G.; Ramachandran, R.; Therese, H. A.; Gnana kumar, G., *RSC Adv.* **2015**, *5* (93), 76538-76547.

179. Chen, T.; Li, X.; Qiu, C.; Zhu, W.; Ma, H.; Chen, S.; Meng, O., *Biosens. Bioelectron.* **2014**, *53* (0), 200-206.
180. Casella, I. G.; Gatta, M., *J. Electroanal. Chem.* **2002**, *534* (1), 31-38.
181. Park, S.; Boo, H.; Chung, T. D., *Anal. Chim. Acta* **2006**, *556* (1), 46-57.
182. Hou, C.; Xu, Q.; Yin, L.; Hu, X., *Analyst* **2012**, *137* (24), 5803-5808.
183. Liu, M.; Liu, R.; Chen, W., *Biosens. Bioelectron.* **2013**, *45*, 206-212.
184. Han, G.-F.; Xiao, B.-B.; Lang, X.-Y.; Wen, Z.; Zhu, Y.-F.; Zhao, M.; Li, J.-C.; Jiang, Q., *ACS Appl. Mater. Interfaces* **2014**, *6* (19), 16966-16973.
185. Mu, Y.; Jia, D.; He, Y.; Miao, Y.; Wu, H.-L., *Biosens. Bioelectron.* **2011**, *26* (6), 2948-2952.
186. Heise, H.; Marbach, R.; Koschinsky, T.; Gries, F., *Artificial Organs* **1994**, *18* (6), 439-447.
187. Lyandres, O.; Shah, N. C.; Yonzon, C. R.; Walsh, J. T.; Glucksberg, M. R.; Van Duyne, R. P., *Anal. Chem.* **2005**, *77* (19), 6134-6139.
188. Coté, G. L.; Fox, M. D.; Northrop, R. B., *IEEE Transactions on biomedical engineering* **1992**, *39* (7), 752-756.
189. Evans, N. D.; Gnudi, L.; Rolinski, O. J.; Birch, D. J.; Pickup, J. C., *Diabetes Technol. Ther.* **2003**, *5* (5), 807-816.
190. McNichols, R. J.; Cote, G. L., *Journal of Biomedical Optics* **2000**, *5* (1), 5-17.
191. Rosenthal, R. D.; Paynter, L. N.; Mackie, L. H., Non-invasive measurement of blood glucose. Google Patents: 1991.
192. Amato, I., *Science* **1992**, *258* (5084), 892-894.
193. Danzer, K., *LEOS Newslett.* **1998**, *12*, 9-11.
194. Lanza, E.; Li, B., *J. Food Sci.* **1984**, *49* (4), 995-998.
195. Browne, C. A. *Physical and chemical methods of sugar analysis; a practical and descriptive treatise for use in research, technical, and control laboratories*; 1912.
196. Coté, G. L., *Journal of Clinical Engineering* **1997**, *22* (4), 253.
197. Wicksted, J. P.; Erckens, R. J.; Motamedi, M.; March, W. F. In *Monitoring of aqueous humor metabolites using Raman spectroscopy*, Advances in Laser and Light Spectroscopy to Diagnose Cancer and Other Diseases, International Society for Optics and Photonics: 1994; pp 264-274.
198. Tarr, R. V.; Steffes, P. G., Non-invasive blood glucose measurement system and method using stimulated Raman spectroscopy. Google Patents: 1993.

199. Rosenzweig, Z.; Kopelman, R., *Anal. Chem.* **1996**, *68* (8), 1408-1413.
200. Schaffar, B. P.; Wolfbeif, O. S., *Biosens. Bioelectron.* **1990**, *5* (2), 137-148.
201. Haynes, C. L.; Van Duyne, R. P., *The Journal of Physical Chemistry B* **2003**, *107* (30), 7426-7433.
202. McFarland, A. D.; Young, M. A.; Dieringer, J. A.; Van Duyne, R. P., *The Journal of Physical Chemistry B* **2005**, *109* (22), 11279-11285.
203. Ballerstadt, R.; Schultz, J. S., *Anal. Chem.* **2000**, *72* (17), 4185-4192.
204. Rabinovitch, B.; March, W.; Adams, R. L., *Diab. Care* **1982**, *5* (3), 254-258.
205. Zheng, M.; Cui, Y.; Li, X.; Liu, S.; Tang, Z., *J. Electroanal. Chem.* **2011**, *656* (1-2), 167-173.
206. Lee, C.-T.; Chiu, Y.-S.; Ho, S.-C.; Lee, Y.-J., *Sensors* **2011**, *11* (5), 4648-4655.
207. Cao, L.; Wang, P.; Chen, L.; Wu, Y.; Di, J., *RSC Adv.* **2019**, *9* (27), 15307-15313.
208. Xia, L.; Xu, L.; Song, J.; Xu, R.; Liu, D.; Dong, B.; Song, H., *Sci. Rep.* **2015**, *5*, 10838.
209. Srinivasan, V.; Pamula, V. K.; Pollack, M. G.; Fair, R. B. In *Clinical diagnostics on human whole blood, plasma, serum, urine, saliva, sweat, and tears on a digital microfluidic platform*, Proc. MicroTAS, 2003; pp 1287-1290.
210. Park, H. D.; Lee, K. J.; Yoon, H. R.; Nam, H. H., *Computers in biology and medicine* **2005**, *35* (4), 275-286.
211. Ronkainen, N. J.; Halsall, H. B.; Heineman, W. R., *Chem. Soc. Rev.* **2010**, *39* (5), 1747-1763.
212. Windmiller, J. R.; Wang, J., *Electroanalysis* **2013**, *25* (1), 29-46.
213. Graf, H., *Helv. odont. Acta* **1966**, *10*, 94-101.
214. Kim, J.; Valdés-Ramírez, G.; Bandodkar, A. J.; Jia, W.; Martinez, A. G.; Ramírez, J.; Mercier, P.; Wang, J., *Analyst* **2014**, *139* (7), 1632-1636.
215. Yao, H.; Shum, A. J.; Cowan, M.; Lähdesmäki, I.; Parviz, B. A., *Biosens. Bioelectron.* **2011**, *26* (7), 3290-3296.
216. Liao, Y.-T.; Yao, H.; Lingley, A.; Parviz, B.; Otis, B. P., *IEEE Journal of Solid-State Circuits* **2012**, *47* (1), 335-344.
217. Yao, H.; Liao, Y.; Lingley, A.; Afanasiev, A.; Lähdesmäki, I.; Otis, B.; Parviz, B., *Journal of Micromechanics and Microengineering* **2012**, *22* (7), 075007.
218. Liao, Y.-T.; Yao, H.; Lingley, A.; Parviz, B.; Otis, B. P., *IEEE Journal of Solid-State Circuits* **2011**, *47* (1), 335-344.

219. Arakawa, T.; Kuroki, Y.; Nitta, H.; Chouhan, P.; Toma, K.; Sawada, S.-i.; Takeuchi, S.; Sekita, T.; Akiyoshi, K.; Minakuchi, S., *Biosens. Bioelectron.* **2016**, *84*, 106-111.
220. Zhang, W.; Du, Y.; Wang, M. L., *Sensing and Bio-Sensing Research* **2015**, *4*, 23-29.
221. Zhang, W.; Du, Y.; Wang, M. L., *Sensing and Bio-Sensing Research* **2015**, *4*, 96-102.
222. Oh, S. Y.; Hong, S. Y.; Jeong, Y. R.; Yun, J.; Park, H.; Jin, S. W.; Lee, G.; Oh, J. H.; Lee, H.; Lee, S.-S., *ACS Appl. Mater. Interfaces* **2018**, *10* (16), 13729-13740.
223. Xuan, X.; Yoon, H. S.; Park, J. Y., *Biosens. Bioelectron.* **2018**, *109*, 75-82.
224. Zhai, Q.; Gong, S.; Wang, Y.; Lyu, Q.; Liu, Y.; Ling, Y.; Wang, J.; Simon, G. P.; Cheng, W., *ACS Appl. Mater. Interfaces* **2019**.
225. Yang, Y.-L.; Chuang, M.-C.; Lou, S.-L.; Wang, J., *Analyst* **2010**, *135* (6), 1230-1234.
226. Jia, W.; Bandodkar, A. J.; Valdés-Ramírez, G.; Windmiller, J. R.; Yang, Z.; Ramírez, J.; Chan, G.; Wang, J., *Anal. Chem.* **2013**, *85* (14), 6553-6560.
227. Guinovart, T.; Bandodkar, A. J.; Windmiller, J. R.; Andrade, F. J.; Wang, J., *Analyst* **2013**, *138* (22), 7031-7038.
228. Bandodkar, A. J.; Molinnus, D.; Mirza, O.; Guinovart, T.; Windmiller, J. R.; Valdés-Ramírez, G.; Andrade, F. J.; Schöning, M. J.; Wang, J., *Biosens. Bioelectron.* **2014**, *54*, 603-609.

CHAPTER III:

Au nanospikes as a non-enzymatic glucose sensor: exploring morphological changes with the elaborated chronoamperometric method

There is a continuous increasing demand for more sensitive and selective non-enzymatic glucose sensor applications ranging from medical diagnostics to food quality assurance. In this chapter, gold nanostructures (referred to as Au nanospikes) were deposited on Au thin-film substrates under different electrodeposition conditions in order to determine the optimal growth parameters to obtain an enhanced glucose sensor. A modified chronoamperometric technique was employed to determine the glucose electrooxidation and sensing capabilities of the developed Au nanospikes toward 20 μM – 10 mM glucose concentrations. The sensing method used here allowed for accurate determination of glucose concentrations whilst providing reproducible and stable response profiles. The sensor produced a low detection limit of 20 μM , a very high sensitivity of 201 $\mu\text{A}\cdot\text{mM}^{-1}\cdot\text{cm}^{-2}$ compared to 16.19 $\mu\text{A}\cdot\text{mM}^{-1}\cdot\text{cm}^{-2}$ for the unmodified Au substrate. The sensor also showed good selectivity when analysed against common physiological contaminants that usually interfere with conventional sensors.

Au Nanospikes as a Non-enzymatic Glucose Sensor: Exploring Morphological Changes with the Elaborated Chronoamperometric Method

Victoria E. Coyle,^[a] Ahmad Esmailzadeh Kandjani,^[a] Ylias M. Sabri,^{*[a]} and Suresh K. Bhargava^{*[a]}

Abstract: There is a continuous increasing demand for more sensitive and selective non-enzymatic glucose sensor applications ranging from medical diagnostics to food quality assurance. Here, we deposited gold nanostructures (referred to as Au nanospikes) on Au thin-film substrates under different electrodeposition conditions in order to determine the optimal growth parameters to obtain an enhanced glucose sensor. A modified chronoamperometric technique was employed to determine the glucose electrooxidation and sensing capabilities of

the developed Au nanospikes toward 20 μM –10 mM glucose concentrations. The sensing method used here allowed for accurate determination of glucose concentrations whilst providing reproducible and stable response profiles. The sensor produced a low detection limit of 20 μM , a very high sensitivity of 201 $\mu\text{A mM}^{-1}\cdot\text{cm}^{-2}$ compared to 16.19 $\mu\text{A mM}^{-1}\cdot\text{cm}^{-2}$ for the unmodified Au substrate. The sensor also showed good selectivity when analysed against common physiological contaminants that usually interfere with conventional sensors.

Keywords: Non-enzymatic glucose sensor • glucose sensing • Au nanospike • electrochemical sensing • elaborated chronoamperometry

1 Introduction

Over the past decade diabetes has become a keen research area for scientists as 387 million people around the world suffer from the condition [1]. As the number of people living with diabetes continues to grow; estimated to reach 592 million by 2035, the need for more accurate glucose sensors with fast response times are becoming increasingly important [1,2]. Along with increased glucose levels and insulin deficiency [3,4], more severe health risks associated with diabetes include increased risk of heart attack and stroke, damaged blood vessels in the retina resulting in blindness, renal failure and in specialized cases lower-limb amputation where 60% of all amputation cases are due to patients having diabetes [5].

Since Clark and Lyons [6] reported the first amperometric enzyme-based glucose sensor in 1962, glucose sensing has become one of the key fields of interest in materials science research. Enzyme-based glucose sensors pose quite a few issues as they have insufficient stability, low reproducibility and are limited by the requirement of an oxygen source [7]. These limitations [8] have turned the focus to creating non-enzyme based sensors as they do not suffer from these downfalls, as well as omitting the temperature control requirements associated with enzyme based sensors. Non-enzymatic glucose sensors require high overpotentials for glucose oxidation to occur which makes them less selective when other common biomolecules are present [8]. To overcome this issue, researchers are focusing on developing novel materials that function at low on-set potentials [9], show high sensitivities and have good selectivity among common biomolecules that interfere with conventional glucose sensors.

Noble metal based nanosensors (eg. Pt [10–12], Au [13–15], Ni [16,17], Cu [18,19] and Ag [20]) have shown great potential as non-enzymatic based glucose sensors. Among these noble metals, gold (Au) has shown particular promise due to its excellent biocompatibility, stability in the presence of physiological contaminants and high activity in neutral and alkali electrolytes with modified surfaces displaying enhanced functionality upon these benefits [21,22]. Furthermore relatively low positive potentials than other noble metals are required for the commencement of glucose electrooxidation on gold surfaces, thus developing Au nanostructures is an attractive method to obtaining enhanced glucose sensing [21]. Au nanostructure based sensors have shown more promising sensing efficiencies [23,24] compared to their bulk counterparts, due to the relatively increased surface-volume ratio of the nanostructures and the ability to control the shape, size and sensing active site density during the synthesis procedure [25]. A common issue when producing non-enzymatic sensing structures is the lack in consistent structure formation over the entirety of the electrodes surface. Au nanostructures are well researched with numerous methods reported [24,26] in developing uniform structure over the entire surface. Furthermore, Au nano-

[a] V. E. Coyle, A. E. Kandjani, Y. M. Sabri, S. K. Bhargava
Centre for Advanced Materials and Industrial Chemistry
(CAMIC), School of Science, RMIT University, GPO Box
2476 V, Melbourne, Victoria 3001, Australia
Phone: +61 3 99252330
*e-mail: ylias.sabri@rmit.edu.au
suresh.bhargava@rmit.edu.au

Supporting information for this article is available on the
WWW under <http://dx.doi.org/10.1002/elan.201600138>.

structures are considered very good catalysts for enzyme-free glucose sensing [27–29] due to their large electrochemical surface areas and varied morphologies as they have already shown to reduce the onset potential for glucose electro-oxidation and be highly active substrates for other applications. Recently Au nanostructures that have been deposited directly on thin-film substrates have shown good performance in applications such as electrochemical catalysis, gas sensing and SERS based biosensing [30–32]. Generally the activity of the Au nanostructures are reported to be highly dependent on their size, surface morphology and surface defect density which can all be varied according to the final application during the synthesis procedure.

In this paper we investigate the above mentioned parameters when depositing Au nanostructures (referred to as Au-nanospikes) on their glucose sensing performance relative to a control Au thin-film deposited on a silicon substrate. The glucose sensing technique generally used in literature is based on continuously monitoring the step-wise current increase following each glucose addition step [33,34]. Although a well-accepted method, the response time of the sensor is restricted to their stabilization times providing one reading per concentration and in most cases following long waiting periods of several minutes. The chronoamperometric stabilization procedure used in this study allows for stable responses to be reached following each glucose addition with the advantage of obtaining multiple confirmation readings during the stabilization procedure at various times (1–300 seconds). The results showed that the developed Au nanostructured substrates can be a promising alternative for non-enzymatic glucose sensing applications.

2 Experimental Section

2.1 Chemicals

All chemicals used in this work were purchased from Sigma-Aldrich and used as received. The solutions were prepared using ultra-pure (Milli-Q) water. The electrolyte solution for the electrodeposition [35,36] of Au nanospikes consisted of tetrachloroaurate (III) tri-hydrate ($\text{HAuCl}_4 \cdot 3\text{H}_2\text{O}$) and lead (II) acetate tri-hydrate ($\text{Pb}(\text{CH}_3\text{CO}_2)_2 \cdot 3\text{H}_2\text{O}$). The electrolyte for the chronoamperometric detection of glucose consisted of potassium hydroxide (KOH) and D-(+)-Glucose ($\text{C}_6\text{H}_{12}\text{O}_6$).

2.2 Fabrication of Au Nanospike Substrates

The Au thin-film substrates were prepared by e-beam evaporation (Balzer-BAK600) of a 10 nm Ti adhesion layer followed by 100 nm Au on the top side of a silicon wafer. The wafer was diced to individual rectangular dimensions of 8 mm × 18 mm. Each substrate was then covered with kapton tape revealing an uncovered circular Au surface ($\phi = 5.5$ mm) of the substrate. The electrodeposition experiments were performed on the revealed area

using a CH instruments (CHI760C) electrochemical analyser in an electrochemical cell that allowed reproducible positioning's of the working (Au substrate), auxiliary (graphite rod) and reference (Ag/AgCl 3 M KCl) electrodes while enabling the implementation of a nitrogen gas inlet tube. The deposition electrolyte solution contained hydrogen tetrachloroaurate (III) tri-hydrate (HAuCl_4) and lead (II) acetate tri-hydrate ($\text{Pb}(\text{CH}_3\text{CO}_2)_2$). The deposition potential was kept constant at 0.05 V (based on cyclic voltammetry (CV) of the electrolyte) throughout the deposition periods used. To determine the optimal conditions of the Au nanospikes growth for the implementation of a non-enzymatic glucose sensor the effects of synthesis variables (i.e. HAuCl_4 and $\text{Pb}(\text{CH}_3\text{CO}_2)_2$ concentrations as well as electrodeposition time) on their sensitivity toward glucose were thoroughly investigated. For each electrodeposition process, a new Au substrate was employed. Each substrate was thoroughly washed with MilliQ water and dried using N_2 gas following the electrodeposition process. The synthesis condition variables are listed in Supporting Information, Table S1.

2.3 Characterisation

Scanning Electron Microscopy (SEM) analysis was performed using a Verios-SEM instrument operated at an accelerating voltage of 5 kV and a beam current of 50 pA. X-Ray Diffraction (XRD) measurements were performed using a Bruker D8 Discover micro diffraction system with general area diffraction detector system (GADDS) operating at a voltage of 40 kV and a current of 40 mA employing Cu $K\alpha$ radiation. The electrochemical measurements were also performed with a CH instruments (CHI760C) electrochemical analyser using a three-electrode cell set-up, implementing the electrodeposited Au nanospike substrates as the working electrodes, a Pt foil as the auxiliary electrode and an Ag/AgCl electrode as the reference electrode. Nitrogen gas was bubbled through each electrolyte solution for 10 minutes before each experiment. The electrochemical surface area (ECSA) of each substrate was determined by first obtaining their CV at a sweep rate of 100 mV s^{-1} in a 1 M H_2SO_4 solution [37,38].

2.4 Glucose Sensing

To determine the Au nanospikes growth conditions that produced optimal glucose sensing performance, CV analysis was performed on each substrate electrode in a solution containing 0.5 M KOH with/without 10 mM glucose while operating at a constant sweep rate of 20 mV s^{-1} . Amperometric responses of the Au nanospikes substrate for glucose sensing were recorded using steady-state conditions at a potential of 0.26 V (versus Ag/AgCl), implementing glucose addition concentrations ranging between 20 μM and 10 mM within the biological range of glucose presence which is between 3 and 8 mM. After each addition a 300 s amperometric response curve was obtained to

ensure steady response profiles were achieved for each addition step.

3 Results and Discussion

3.1 Characterization of Au Nanospikes Nanostructures

3.1.1 Effect of HAuCl_4 Concentration

The effect of a gold precursor control on the growth of Au nanospikes was investigated considering four different concentrations: 3.4, 6.8, 13.6 and 27.2 mM as listed in Table S1 (Samples: Au_Spikes_1–4). The concentration of the $\text{Pb}(\text{CH}_3\text{CO}_2)_2$ and the deposition time were fixed at 1 mM and 12 mins, respectively.

The deposition time of 12 mins was chosen in order for the Au nanospikes to develop to a mature enough size and shape so as to easily compared and determine the effect each deposition parameter have on their morphology. The large size nanospikes are also favoured for accurately analysing the glucose sensing capabilities during chronoamperometric experiments. The initial $\text{Pb}(\text{CH}_3\text{CO}_2)_2$ concentration of 1 mM was chosen to

ensure the concentration was lower than gold yet considerable enough to act as a directional growth agent. SEM analysis was performed on each of the substrates to observe any visible morphology changes between the different concentrations of the HAuCl_4 . Figure 1a shows the growth of Au nanospikes at a Au concentration of 3.4 mM. It can be observed that the small amount of Au^{3+} ions in the solution have not allowed for mature nanospike growth. The SEM images shown in Figure 1a–d demonstrate that by increasing the concentration of HAuCl_4 , the length and base thickness of the Au nanospikes is increased. The higher magnification SEM images (see Supporting Information, Figure S1) showed that Au nanospikes can be formed evenly throughout the substrate area with all gold concentrations tested. It can also be observed that the dimensions (length \times base thickness) are changed from 200 nm \times 80 nm for Au_spikes_1, to 1.52 μm \times 560 nm for Au_spikes_4. The cyclic voltammograms (CVs) used for the electrochemical surface area (ECSA) measurements of a flat Au thin film and Au_Spikes_1–4 are shown in Figure 2a. In Figure 2b the reduction peaks from the CVs are shown. These peaks were integrated to determine the charge and therefore surface area for each of the developed Au nanospikes based substrates as well as the plain Au-substrate. (It should be noted that the geometric surface area of each substrate was 0.238 cm^2). The ECSA of the electrodes are calculated based on previous studies [36] where the integral of the reduction peak formed during CV in H_2SO_4 . This integral is used to determine the area of the peak which is equivalent to the overall charge. Using the reported charge for an Au oxide monolayer (386 μCcm^{-2}) [39] the electrochemical surface area is calculated ($\text{ECSA} (\text{cm}^{-2}) = [\text{Q}_{\text{CVcurve}}] / [\text{Q}_{\text{reported}}]$). For all the Au nanospike substrates formed the overall surface areas were higher when compared to the plain Au-substrate. Interestingly, among all the HAuCl_4 concentrations tested, Au_Spikes_1 and Au_Spikes_4 gave the lowest surface areas of 2.92 cm^2 and 3.7 cm^2 , respectively. The Au_Spikes_2 and Au_Spikes_3 showed the highest surface areas of 3.94 cm^2

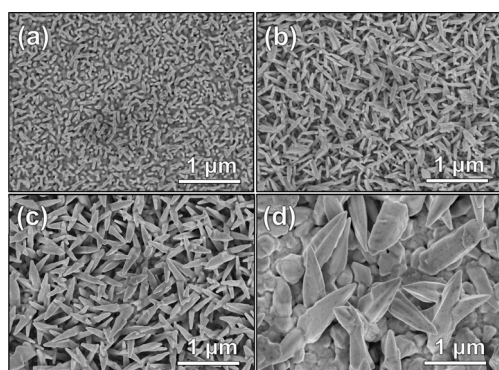


Fig. 1. SEM images of developed Au nanospikes grown with 1 mM $\text{Pb}(\text{CH}_3\text{CO}_2)_2$ and (a) 3.4 mM (b) 6.8 mM (c) 13.6 mM and (d) 27.2 mM HAuCl_4 deposited for a period of 12 mins.

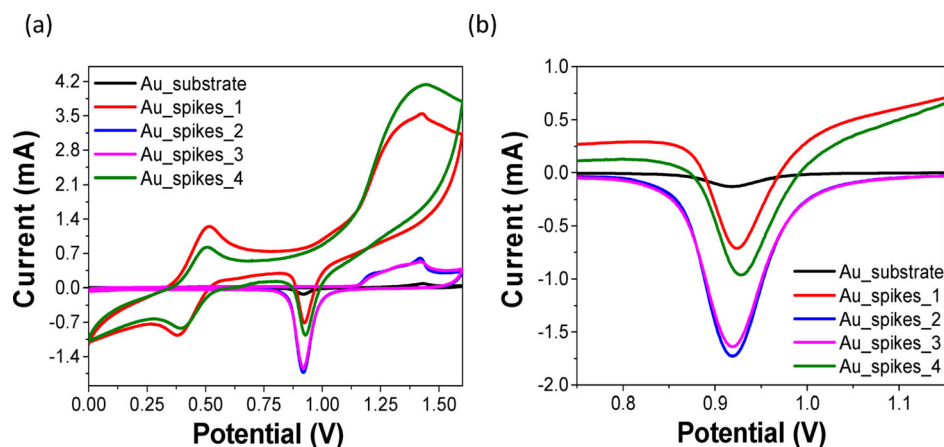


Fig. 2. (a) Electrochemical surface area (ECSA) analysis of Au nanospikes with varying HAuCl_4 concentrations and (b) 0.75–1.15 V peak analysis curves for Au nanoparticles grown with different Au concentrations in the electrolyte.

and 3.81 cm^2 , respectively which are above 13.5 times the surface area of the Au substrate.

3.1.2 Effect of $\text{Pb}(\text{CH}_3\text{CO}_2)_2$ Concentration

For one dimensional growth of nanostructures, direction growth agents [31] have a significant role in controlling their formation, alignment and coverage on the substrate. As the role of $\text{Pb}(\text{CH}_3\text{CO}_2)_2$ is a direction growth agent, the concentration of this compound can drastically change the morphology of the formed Au nanospikes. In order to investigate the effect of $\text{Pb}(\text{CH}_3\text{CO}_2)_2$ as a directional growth agent in Au nanospike formation, concentrations of 0.25, 0.5, 1 and 2 mM were tested. SEM analysis of the Au nanospikes formed using different $\text{Pb}(\text{CH}_3\text{CO}_2)_2$ concentrations clearly show changes in the morphology of the Au nanospikes (Figure 3). For 0.25 mM (Au_spikes_5) and 0.5 mM (Au_spikes_6) the Au nanospikes appear sharper and slightly longer, however the coverage of the nanospikes is not as cohesive as 1 mM (Au_spikes_3) and 2 mM (Au_spikes_7) samples. The low magnification SEM images (Figure S2a,c,e,g) of each sample shows cohesive coverage over the whole substrate, with the higher concentrations of $\text{Pb}(\text{CH}_3\text{CO}_2)_2$ showing a more seamless coverage over the surface. In addition, high magnification SEM images (Figure S2b,d,f,h) showed that Au nanospikes with different morphologies were formed for both 0.25 and 0.5 mM $\text{Pb}(\text{CH}_3\text{CO}_2)_2$ concentrations. The 0.5 mM was found to produce larger, well defined nanospikes when compared to the 0.25 mM $\text{Pb}(\text{CH}_3\text{CO}_2)_2$ concentration. On the other hand, for the larger concentrations of 1 mM and 2 mM, uniform growths of well-defined Au nanospikes are observed along the entire surface. From the ECSA analysis (see Figure S3) the Au nanospike samples had an average ECSA of 3.5 cm^2 . Interestingly, the Au_spikes_3 and Au_spikes_6 samples were found to have an almost identical ECSA of 3.8 cm^2 . The on-set potential of the reduction peak for Au_spikes_3 is further to the right compared to other samples, indicating the formation of more active sites on the surface. Similarly electrochemical sur-

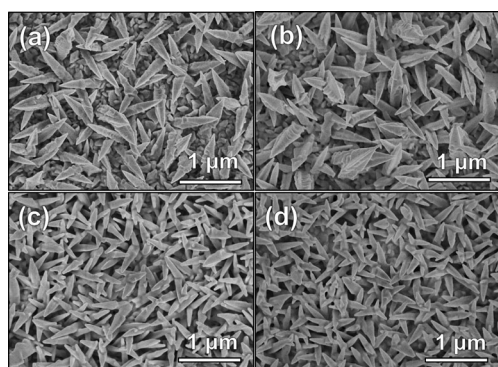


Fig. 3. SEM images of Au nanospikes synthesized with 13.6 mM HAuCl_4 and electrodeposition time of 12 mins with (a) 0.25 mM (b) 0.5 mM (c) 1 mM and (d) 2 mM $\text{Pb}(\text{CH}_3\text{CO}_2)_2$.

face areas of 3.82, 3.39, 3.73 and 3.09 cm^2 for Au_spikes_3,6,7 and 8 were observed respectively, where Au-spikes_3 showed an increase in surface area of 16.1 times to that of the plain thin-film Au substrate's geometrical surface area (0.281 cm^2).

3.1.3 Effect of Electrodeposition Time

To study the morphological changes that occur when changing the electrodeposition times, Au nanospikes were grown for 6, 12, 24, 36 and 48 mins before being analysed under SEM (Figure 4). In Figure 4a the plain Au thin-film substrate on which the Au nanospikes were grown, is shown. It can be seen that the substrate is made up of small grains (size $\sim 50\text{--}200 \text{ nm}$ width), most of which may act as the seeds for nanospike structures' growth. Figure 4b displays the initial Au nanostructures that have been formed following 6 minutes of electrodeposition (also see Figures S4a and S4b). The images indicate that the time needed for Au nanospikes to be formed must be greater than 6 minutes when employing a HAuCl_4 concentration of 13.6 mM and a $\text{Pb}(\text{CH}_3\text{CO}_2)_2$ concentration of 1 mM. Therefore the Au_spikes_8 sample was rejected for further characterization studies due to a lack of sufficient growth of the nanospike structures. Increasing the electrodeposition time to 12 or 24 minutes produces uniform nanospikes across the surface as shown in Figures 4c and 4d (high magnification), respectively. The SEM images demonstrating the surface coverage (low magnification) as well as the finer surface details are shown in Figure S5c to S5f. A further increase in the electrodeposition time to 36 mins and 48 mins (see Figure 4e and 4f, respectively) produces a build-up of much larger Au nanospikes being formed on top of smaller nanospike-

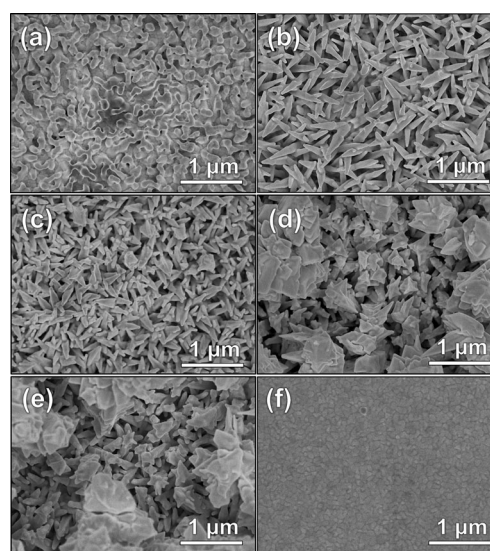


Fig. 4. SEM images of Au nanospikes with 13.6 mM HAuCl_4 and 1 mM $\text{Pb}(\text{CH}_3\text{CO}_2)_2$ for (a) plain Au substrate with no modification (b) 6 mins (c) 12 mins (d) 24 mins (e) 36 mins and (f) 48 mins.

like structures deposited across the surface. The SEM images containing the finer surface details and coverage of the formed nanostructures are shown in Figure S5g to S5j. The images clearly demonstrate the growth of uneven nanopike growth across the surface, with both the larger and smaller nanopikes growing in arbitrary positions over the exposed surface. It can be observed that the shape of the nanostructures formed are no longer 'nanopike-like' in shape, but are in fact overgrown nanostructures which have multiple peak-like points (see Figure S5h and S5j). Due to the inconsistent growth pattern at larger deposition times these substrates were deemed unviable surfaces for glucose sensing. The CV analysis to determine ECSA for different electrodeposition times are shown in Figure S4. It was found that the larger the electrodeposition time, the more active the Au nanopikes formed given that the on-set potential in the reduction peaks are shifted further to the right with increasing electrodeposition times (see Figure S4b). For electrodeposition times of 12, 24, 36 and 48 mins, the ECSAs were calculated to be 3.82, 3.93, 4.71 and 6.78 cm², respectively. The overgrowth observed in samples Au_spikes_10 and Au_spikes_11 is thought to be responsible for their drastic increase in their surface area. A summary of the substrate's ECSAs are shown in Figure S7. It can be observed that the Au_spikes_10 and 11 have the highest ECSAs among all synthesized samples.

3.1.4 Effect of Electrodeposition Potential

To study the effect of electrodeposition potential on the growth of Au nanopikes, electrodepositions were performed at -0.1 , 0.05 , 0.3 and 0.6 V and the resulting morphologies were analysed under SEM (Figure 5). Figure 5a (and Figure S6a and S6b) shows the low potential sample Au_spikes_12 forming small star-shaped nanostructures with varying sizes across the surface of the substrate. Increasing the on-set potential to 0.05 V (Au_spikes_3) allowed for the salt in the electrolyte solution to interact and form the Au nanopike structures (Figure 5b and Figure S6c and S6d). Further increase in on-set potential to

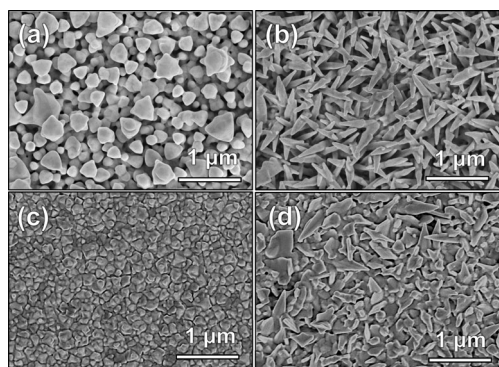


Fig. 5. SEM images of Au nanopikes with 13.6 mM HAuCl₄ and 1 mM Pb(CH₃CO₂)₂ for 12 mins run at (a) -0.1 V (b) 0.05 V (c) 0.3 V and (d) 0.6 V.

0.3 V for Au_spikes_13 (Figure 5c and Figure S6e and f) displayed little-to-no structure growth across the surface of the substrate and 0.6 V for Au_spikes_14 (Figure 5d and Figure S6g and h) exhibited very little Au structures forming on the surface with the low magnification images (Figure S6g) continuing that surface coherency has not been achieved. As the on-set potentials of -0.1 , 0.3 and 0.6 V did not form consistent nanopike-type structures, samples Au_spikes_12, 13 and 14, were rejected from any further characterization and analysis.

The purity of the Au nanopikes was confirmed by utilizing EDX and XRD characterisation techniques. The EDX spectral analysis of Au_spikes_3 (see Figure S8) showed 2 major peaks at ~ 2.2 keV and ~ 9.7 keV which can be assigned to pure Au peaks [43]. The sharp peak at ~ 1.7 keV was assigned to silicon given that silicon substrates were used for the synthesis of all surfaces in this study. No Pb²⁺ peaks were observed in the EDX spectra indicating that Pb(CH₃CO₂)₂ only functioned as the directional growth agent and was not electrodeposited as part of the gold nanostructures formed. The XRD (see Figure S9) analysis confirmed the purity of the Au nanostructures with each spectral peak successfully being assigned to pure gold. There were no peaks present which could be assigned to Pb(CH₃CO₂)₂ or lead related crystals, which was expected given that the samples were thoroughly cleaned post-deposition. Overall, XRD analysis showed that a crystalline-form of gold had been deposited on the Au thin-film substrates and each peak can be assigned to a gold component found in a face-centred-cubic arrangement [24].

3.2 Electrochemical Glucose Sensing

3.2.1 Cyclic Voltammetric Studies

The process of glucose electrooxidation on a gold surface involves the chemisorption of dehydrogenated intermediates followed by their electrocatalytic oxidation once Au hydroxides are formed at certain potentials [21,41]. However unlike acidic solutions, gold hydroxide formation readily occurs in alkaline medium through the chemisorption of OH⁻ ions on the Au surface [42,43] by $\text{Au} + \text{OH}^- \rightarrow \text{AuOH}^{(1-\lambda)} + \lambda e^-$. As KOH is a strong base, it allows for unimpeded $-\text{OH}$ reactions between the Au surface and deprotonated glucose molecules. For this reason the sensor performance was tested in an alkaline (0.5 M KOH) solution.

To investigate the electrocatalytic activities of the developed nanopikes, the samples were analysed using CV analysis in a solution of 0.5 M KOH and 10 mM glucose, the data of which is shown in Figure 6a–c. The glucose sensing performances of each substrate were ranked according to the magnitude of their peak heights which appear at 0.13 V in the forward scan of the CV profile. The potential of 0.13 V was chosen as the analysis of the CVs indicated that glucose oxidation (sensing mechanism) is most predominant at this potential. CV analysis comparing Au nanopikes and an unmodified Au sub-

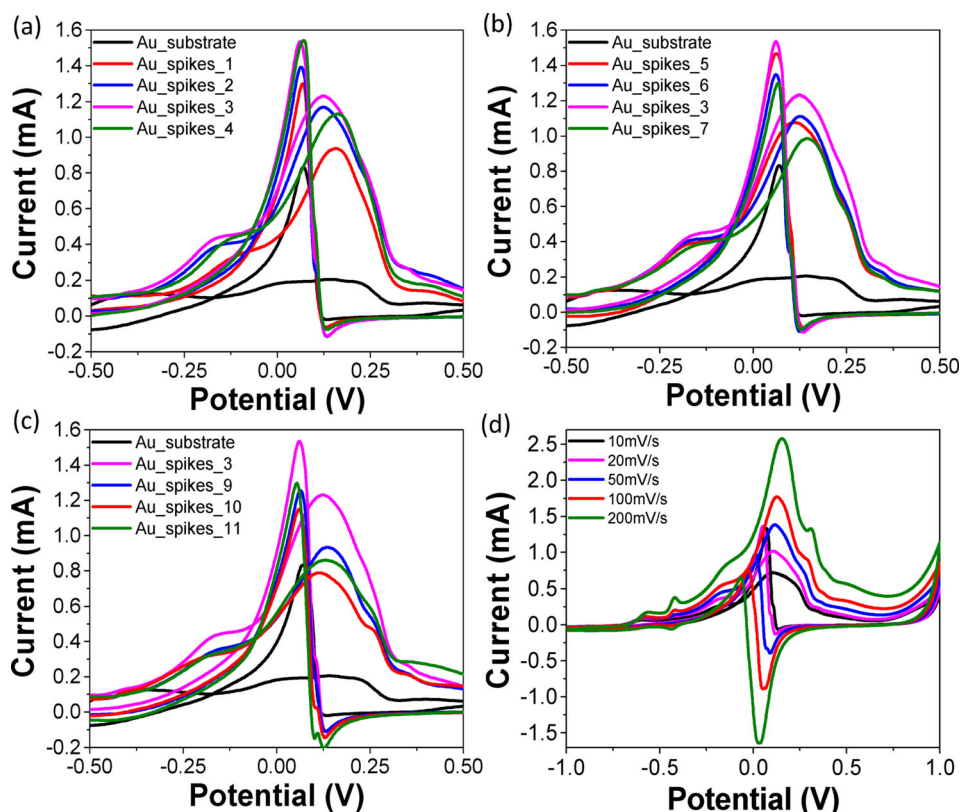


Fig. 6. CV analysis with a scan rate of 20 mV s^{-1} in 0.5 M KOH and 10 mM glucose comparing Au_substrate against the developed Au nanospike substrates. The panels refer to changes in (a) $\text{H[AuCl}_4\text{]}$ concentration, (b) $\text{Pb(CH}_3\text{CO}_2\text{)}_2$ concentration and (c) electrodeposition time. (d) shows CV analysis of 10 mM glucose with different scan rates of $10, 20, 50, 100$ and 200 mV s^{-1} for Au_Spikes_3.

strate in a solution with and without 10 mM glucose is shown in Figure S10. The exact electrooxidation mechanism during glucose sensing is not well understood although some studies [44,45] report gold oxides inhibit direct glucose electrooxidation where others [22,46] report that these inhibiting species in fact promote the reaction. It is generally accepted that the first current peak observed during the forward scan in the CV is most likely due to glucose undergoing electrosorption on the gold surface to form adsorbed intermediates, with each glucose molecule releasing one proton. As the intermediates accumulate on the active sites of the nanomaterials, they inhibit glucose oxidation to occur directly at the gold surface [37]. As the potential is increased to more positive values toward 0.13 V , hydroxide ions are partially discharged at the Au surface, which can catalyse the oxidation of the accumulated intermediates thus freeing up the active sites for glucose oxidation to occur directly on the Au surface. This decrease in current observed beyond the 0.13 V peak is postulated in most studies to be due to gold oxide formation [47]. The large sharp peak in the reverse scan at $\sim 0.1 \text{ V}$ can therefore be attributed to the reduction of the surface Au oxide thus making available the active sites for the direct electrooxidation of glucose to occur [47]. As the potential is scanned toward a more negative potential, the accumulation of intermediates on the electrode surface occur once again and the cycle con-

tinues. When a CV of the Au substrate was performed in 10 mM glucose , it produced a peak maximum of only 0.21 mA at 0.13 V . For every modified substrate, a relatively increased glucose sensing performance was evident due to their higher peak current maximums at 0.13 V when compared to the control substrate. Therefore, the optimal growth conditions of the Au nanospikes for glucose sensing were based on their CV analysis (shown in Figure 6a–c) and their peak at 0.13 V in the forward CV scan.

As previously discussed in section 3.1, the concentration of $\text{H[AuCl}_4\text{]}$ controls the aspect ratio of the nanospikes. Although Au_spikes_4 has the largest surface area among the Au concentrations, the CV analysis in 10 mM glucose solution showed a lower peak current than Au_spikes_2 and 3 (see Figure 6a). On the other hand the sample with the smallest $\text{H[AuCl}_4\text{]}$ concentration of 3.4 mM (Au_spikes_1), showed the lowest amount of glucose electrooxidation on the gold surface with a maximum peak of 0.9 mA . Figure 6b illustrates the effect of $\text{Pb(CH}_3\text{CO}_2\text{)}_2$ concentration during nanospike formation on the electrooxidation of glucose. It can be observed that Au_spikes_5 and Au_spikes_6 have relatively lower glucose oxidation performance than Au_spikes_3, presumably due to the lack in cohesive coverage. Although the glucose oxidation performance of Au_spikes_5–7 was better than that of the Au substrate, their lack of surface coherency during

deposition procedure resulted in the Au_spikes_3 (with 1 mM Pb) having the highest glucose oxidation peak (i.e. 1.25 mA which is 6 times the plain Au thin-film substrate). This is attributed to its cohesive and seamless nanopike deposition over the entirety of the deposited surface. In Figure 6c it can clearly be observed that the low electrodeposition time of 12 minutes produced the highest glucose oxidation peak and therefore glucose electrooxidation performance. As was shown earlier the ECSAs of the deposited nanopikes drastically increased increases with increasing deposition time. Although sensors developed in the past [18,24] show a correlation between increased ECSA and enhancement of glucose sensing performance, in the case of nanopikes, the ECSA did not accurately reflect the glucose sensing performance of the substrate and thereby was ruled out as a distinguishing parameter for improving glucose sensing performance. Overall the optimal Au nanopike growth conditions needed to grow an Au nanopike substrate with high activity toward non-enzymatic glucose sensing are: 13.6 mM HAuCl₄, 1 mM Pb(CH₃CO₂)₂ and 12 mins electrodeposition time, hence Au_Spike_3. Therefore all further experiments involving glucose sensing were performed using Au_spikes_3 sample.

From Figure 6d it can be observed that the electrocatalytic behaviour of Au nanopike substrates relies heavily on the scan rate. Slower scan rates (10 and 20 mVs⁻¹) produce much more electrooxidation of glucose as evidenced by the sharp and thin oxidation peaks in both the forward and reverse scans. The peak maximum at 0.13 V increases at faster scan rates as does the broadness of the peak. This phenomenon is known to reflect a surface-controlled electrochemical process [24]. In the reverse scan of the larger sweep rates (>50 mVs⁻¹) the reduction peak formed is relatively more apparent and is due to the re-activation of the Au surface for direct electrooxidation of glucose [45,48].

3.2.2 Amperometric Glucose Detection

Currently a successive addition method is predominantly employed for glucose sensing [49–51,58–60]. The method involves applying a constant potential (or current depending on the method) and reading off the current (or potential) change after each successive addition of glucose concentration. The disadvantage however is that the direct electrooxidation reaction of glucose is diffusion limited. Therefore any successive addition causes large sharp peaks in the I/V vs t profile immediately after injection, thereby drastically decreasing the final response magnitude and therefore sensitivity. These abrupt changes in the current output prior to the stabilization can also produce inconsistent results. The method employed in this study produces high current output following glucose addition before reducing to a constant value. Although the current stabilization is also a result of the diffusion limited process of glucose electrooxidation, the initial current outputs can actually be analysed and used to accurately

determine glucose concentrations with a very fast response time [34,51]. The main advantage of using this method over concurrent methods is the ability to repeat runs due to irregularities in the system and the ability to observe different current responses at numerous times along the stabilization period. To determine the optimal potential for the most sensitive and selective glucose sensing material, a thorough comparison of various testing potentials was performed using the chronoamperometry method. Each potential was chosen based on the important regions in the CVs shown in Figure 6 where a relevant peak of interest was observed. In the forward oxidation sweep it was observed that the glucose electrooxidation begins at -0.13 V and the peak maximum occurred at 0.13 V. The glucose electrooxidation current begins to deplete to half its value at the potential of ~0.26 V and completely depletes at ~0.39 V. Each of these mentioned potentials were tested (data presented in Figure 7a) with chronoamperometric additions experiments using a 10 mM glucose solution and a stabilization period of 300 s. It can be observed that the two most sensitive potentials were 0.13 V and 0.26 V with the latter producing a slightly lower response magnitude toward glucose. Selectivity analysis in the presence of physiological contaminants, were then performed at the two potentials with the highest sensitivities in order to determine the best potential for enhanced sensing performance (sensitivity and selectivity in Figure S11). It is found that although 0.13 V produces higher response magnitudes, a better selectivity is achieved at the working potential of 0.26 V as opposed to 0.13 V when tested against sucrose, fructose, acetic acid (AA) and uric acid (UA) which is further discussed later in the article. Although there was a 'trade-off' between the selectivity and sensitivity performance when choosing the working potential, the small loss in sensitivity was outweighed by the better selectivity performance of the sensor toward glucose at 0.26 V. The Au nanopike sensor (Au_spikes_3) was then used to undergo successive glucose additions using the elaborated chronoamperometric method [34] at the working potential of 0.26 V. The method results in obtaining multi-current-time curves for the glucose concentrations ranging between 20 μM and 10 mM as shown in Figure 7b. Following each addition, an increase in amperometric response was observed where such increase was more dramatic for the higher concentrations relevant to the physiological glucose levels. Figure 7c shows the comparison in current output for each glucose addition (calibration curves) for both the Au spikes and unmodified Au substrate. The current output experienced by the Au nanopikes is clearly superior with a very large enhancement in sensitivity and the calibration curves having an average R² value of 0.992 compared to R² value for the unmodified substrate of 0.857. The change in R² values shows the additions for Au spikes have a steadily linear increase in amperometric response, compared to the Au substrate which exhibited much lower amperometric responses and non-linearity for many of the additions. This comparison clearly em-

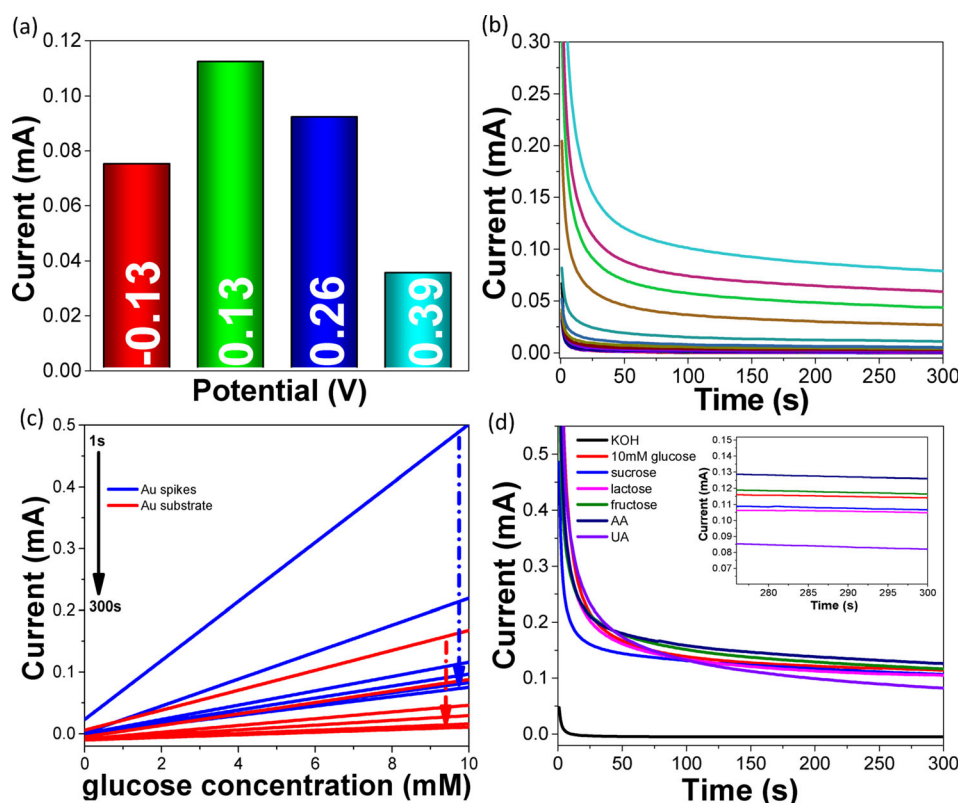


Fig. 7. (a) Bar graph analysis comparing sensitivity of different potentials in 10 mM glucose, amperometric response curves of (b) successive glucose additions (0 mM–10 mM), (c) Comparative calibration curves between the Au spikes and Au substrate additions and (d) Successive additions of 0.1 mM contaminants with inset showing the range of analysis times; 200–250 s of contaminants.

phasises the improved sensing capabilities of Au nanoparticles compared to a flat Au surface used as the control sample. Furthermore, the highest current responses were observed from the lowest stabilization times (or response times used), with the 1 s stabilization period producing the highest current output for each glucose concentration tested. As the stabilization time is increased, a steady and constant current output is produced for each glucose concentration where > 50 s show a smaller, yet constant response magnitude. This method therefore allows for the response magnitude obtained from lower response times (i.e. 1 s) to be confirmed by those of longer response times (i.e. 50 s). The calculated current density of Au nanoparticles for each glucose concentration at different stabilization times are presented in Figure S12a and the graphs were used to estimate the sensitivity of the developed Au nanoparticles towards glucose. At 1 s the sensitivity was estimated at $201 \mu\text{A mM}^{-1} \cdot \text{cm}^{-2}$. This is 12.4 times higher than the control Au substrate ($16.2 \mu\text{A mM}^{-1} \cdot \text{cm}^{-2}$). As the chronoamperometric stabilization time increased the sensitivity of the sensor dramatically decreased however producing a better stability and reliability of the current output. At 10 s the sensitivity was less than halved at $91.8 \mu\text{A mM}^{-1} \cdot \text{cm}^{-2}$ while at 50 s a sensitivity of $48.8 \mu\text{A mM}^{-1} \cdot \text{cm}^{-2}$ was calculated, although still quite impressive. The calibration curves produced from the stabilization periods ranging from 50 to

300 s can be better observed in Figure S12b. Interestingly at 100 s the sensitivity dropped by only a small margin to $40.9 \mu\text{A mM}^{-1} \cdot \text{cm}^{-2}$ relative to the 50 s stabilization time. The same trend continued for both 200 s and 300 s where the sensitivities were calculated to be $35.2 \mu\text{A mM}^{-1} \cdot \text{cm}^{-2}$ and $32 \mu\text{A mM}^{-1} \cdot \text{cm}^{-2}$ respectively. The lowest glucose concentration tested ($20 \mu\text{M}$) is shown in Figure S13 showing a good dynamic range between the preceding and proceeding concentrations. A comparison of the sensing performance comparing Au nanoparticles and existing literature is listed in Table 1. It can be seen that the Au nanoparticles have a far more superior sensitivity when compared to other pure Au based nanostructures in the presence of glucose. A much high detection limit is quoted for the Au nanoparticles, however is well below the necessary human biological range of 3–8 mM. In comparison to Au surfaces with additional components (Co_3O_4 or Ti) the detection limits compared to the pure Au nanoparticles are much lower and should be further investigated.

The selectivity performance of Au nanoparticles, in the presence of physiological contaminants is shown in Figure 7d. An aqueous solution of 0.5 M KOH [61–63] was used as the electrolyte solution, followed by the addition of 10 mM glucose. Thereon, successive additions of contaminants including 0.1 mM sucrose, lactose, fructose, AA and 0.02 mM UA followed. These contaminants have been selected as they can interfere with the conventional

Table 1. Comparison table of Au-based glucose sensors from literature.

Electrode material	Sensitivity ($\mu\text{A} \cdot \text{mM}^{-1} \cdot \text{cm}^{-2}$)	LOD (μM)	Operation potential (V)	Reference
Au nanocorals	22.6	10	+0.25 vs Ag/AgCl	[24]
Au polycrystalline	32	6	+0.22 V vs SHE	[53]
Porous Au	11.8	5	+0.35 V vs SCE	[41]
Au nanocorals on SPEs	0.5	n/a	+0.45 V vs Ag/AgCl	[54]
Nanostructured Au thin-films	n/a	0.32	-0.55 V vs SCE	[55]
NP Au/Co ₃ O ₄	1250	0.005	+0.26 vs Ag/AgCl	[26]
Macroporous Au-Pt 3D	39.53	0.025	+0.4 V vs Ag/AgCl	[56]
Au nano/Ti	140	0.0148	-0.55 V vs Ag/AgCl	[57]
Au nanopikes	201	20	+0.26 vs Ag/AgCl	*This work

electrochemical glucose sensors. As our applied potential is 0.26 V and the fact that the developed nanopikes were synthesised for optimal glucose sensing performance, the interference of the common biological contaminants is greatly reduced relative to higher positive potentials, showing great selectivity towards glucose. Sucrose, lactose and fructose showed very small change in current (0.01 mA) indicating that the Au nanopikes are unaffected by biological sugars. Ascorbic acid showed minor change in the current response, increasing by only 0.01 mA indicating it does not significantly interfere with the sensor. Similar to other studies using Au based surfaces [24] UA showed a decrease in current output, which can be explained by the interfering capping of Au active surface sites on the Au nanopikes surface, reducing the sensors ability to effectively undergo direct electrooxidation of glucose [24]. This phenomenon only causes minimal interference and does not impede the sensors ability to detect physiological glucose levels given that the monolayer capping formation can only occur as a singular event and the related current change is relatively small as evidenced from the CV profiles obtained from a 10 mM glucose solution. The sensing capabilities (sensitivity and selectivity) in the presence of UA could be improved with the introduction of an additional metal forming an Au nanopike alloy [14,64–66] or introducing secondary oxide components such as Co₃O₄ or ZnO [56,67,68].

8 successive repeat chronoamperometric runs were performed in 10 mM glucose solution to determine the effect in current response for reproducibility analysis (Figure S14). From the figure we can see a good level of signal reproducibility across all 8 runs. The CoV (coefficient of variance) was calculated using equations (1) and (2), respectively [69], where Δf_i is the final current response for each run.

$$\Delta f_{I(\text{avg.})} = \frac{\sum^A f_i}{n} \quad (1)$$

$$\sigma = \sqrt{\frac{\sum (\Delta f_i - \Delta f_{I(\text{avg.})})^2}{n - 1}} \quad (2)$$

The calculated CoV for Au_spikes_3 in 10 mM glucose was calculated to be 7.2% which is equivalent to 93%.

Overall the sensitivity, selectivity and repeatability data presented indicates that among the Au nanopikes developed, Au_spikes_3 has the best glucose performance in terms of both sensitivity and selectivity and shows excellent sensitivity when in the presence of glucose

4 Conclusions

In this study we have developed Au nanostructures (referred to as nanopikes) for enhanced electrochemical based non-enzymatic glucose sensing applications. Au nanopikes with different morphologies were fabricated and tested for their glucose sensing performances. The effects of HAuCl₄ and directional growth agent concentration as well as electrodeposition time on the glucose sensing performance of Au nanopikes were investigated and optimal conditions were determined. The study shows that the resultant morphology of the Au nanopikes directly affected the sensing capabilities of the sensor with thinner, sharper nanopikes being more sensitive towards glucose. The optimal Au nanopike glucose sensor was electrodeposited with 13.6 mM of HAuCl₄ as gold source, 1 mM of Pb(CH₃CO₂)₂ as directional growth agent and an electrodeposition period of 12 mins (Au_spikes_3). From amperometric analysis the sensitivity of this sensor was determined to be 201 $\mu\text{A} \cdot \text{mM}^{-1} \cdot \text{cm}^{-2}$ (12.4 $\mu\text{A} \cdot \text{mM}^{-1} \cdot \text{cm}^{-2}$ higher than the control Au substrate) after 1s of stabilization time when a 0.26 V potential was applied. The limit of detection (lowest concentration actually tested) was determined to be 20 μM with minimal cross-sensitivity and functionality loss when tested against physiological contaminants such as UA, AA and various sugars at levels found in the body. The results suggest that Au nanopikes are promising substrates for non-enzymatic glucose sensing applications as they are highly reproducible and show great sensitivity towards glucose.

Acknowledgements

The authors acknowledge RMIT Microscopy and Microanalysis Facility (RMMF) for the help received from their technical staff and for allowing the use of their comprehensive facilities and services. The technical staff (Mr

Yuxun Cao and Mr Paul Jones) at the Microelectronics Materials and Technology Centre is also acknowledged for the chemical vapour deposition of Au on Si substrates.

References

- [1] G. Danaei, M. M. Finucane, Y. Lu, G. M. Singh, M. J. Cowan, C. J. Paciorek, J. K. Lin, F. Farzadfar, Y.-H. Khang, G. A. Stevens, M. Rao, M. K. Ali, L. M. Riley, C. A. Robinson, M. Ezzati, *The Lancet* **378**, 31.
- [2] A. Alwan, W. H. Organization, Global status report on non-communicable diseases **2010**, World Health Organization **2011**.
- [3] S. P. Nichols, A. Koh, W. L. Storm, J. H. Shin, M. H. Schoenfish, *Chem. Rev.* **2013**, *113*, 2528.
- [4] K. M. Shaw, M. H. Cummings, Diabetes and the eye, Third ed., John Wiley & Sons, Diabetes chronic complications **2012**.
- [5] A. H. Mokdad, E. S. Ford, B. A. Bowman, W. H. Dietz, F. Vinicor, V. S. Bales, J. S. Marks, *Jama* **2003**, *289*, 76.
- [6] L. C. Clark, C. Lyons, *Ann. N. Y. Acad. Sci.* **1962**, *102*, 29.
- [7] G. Wang, X. He, L. Wang, A. Gu, Y. Huang, B. Fang, B. Geng, X. Zhang, *Mikrochim. Acta* **2013**, *180*, 161.
- [8] S. Ernst, J. Heitbaum, C. Hamann, *J. Electroanal. Chem. Interfacial. Electrochem.* **1979**, *100*, 173.
- [9] K. E. Toghill, R. G. Compton, *Int. J. Electrochem. Sci.* **2010**, *5*, 1246.
- [10] Y. Bai, Y. Sun, C. Sun, *Biosens. Bioelectron.* **2008**, *24*, 579.
- [11] J. Wang, D. F. Thomas, A. Chen, *Anal. Chem.* **2008**, *80*, 997.
- [12] L.-Q. Rong, C. Yang, Q.-Y. Qian, X.-H. Xia, *Talanta* **2007**, *72*, 819.
- [13] K. Saha, S. S. Agasti, C. Kim, X. Li, V. M. Rotello, *Chem. Rev.* **2012**, *112*, 2739.
- [14] C. Shan, H. Yang, D. Han, Q. Zhang, A. Ivaska, L. Niu, *Biosens. Bioelectron.* **2010**, *25*, 1070.
- [15] Y. Xian, Y. Hu, F. Liu, Y. Xian, H. Wang, L. Jin, *Biosens. Bioelectron.* **2006**, *21*, 1996.
- [16] H. Tian, M. Jia, M. Zhang, J. Hu, *Electrochim. Acta* **2013**, *96*, 285.
- [17] Y. Liu, H. Teng, H. Hou, T. You, *Biosens. Bioelectron.* **2009**, *24*, 3329.
- [18] Z. Zhuang, X. Su, H. Yuan, Q. Sun, D. Xiao, M. M. Choi, *Analyst* **2008**, *133*, 126.
- [19] J. Luo, S. Jiang, H. Zhang, J. Jiang, X. Liu, *Anal. Chim. Acta* **2012**, *709*, 47.
- [20] Y. Ding, Y. Wang, L. Su, H. Zhang, Y. Lei, *J. Mater. Chem.* **2010**, *20*, 9918.
- [21] Y. B. Vassilyev, O. A. Khazova, N. N. Nikolaeva, *J. Electroanal. Chem. Interfacial. Electrochem.* **1985**, *196*, 127.
- [22] R. R. Adzic, M. W. Hsiao, E. B. Yeager, *J. Electroanal. Chem. Interfacial. Electrochem.* **1989**, *260*, 475.
- [23] Y. Zhang, G. Chang, S. Liu, W. Lu, J. Tian, X. Sun, *Biosens. Bioelectron.* **2011**, *28*, 344.
- [24] T.-M. Cheng, T.-K. Huang, H.-K. Lin, S.-P. Tung, Y.-L. Chen, C.-Y. Lee, H.-T. Chiu, *ACS Appl. Mater. Interfaces* **2010**, *2*, 2773.
- [25] E. Boisselier, D. Astruc, *Chem. Soc. Rev.* **2009**, *38*, 1759.
- [26] X.-Y. Lang, H.-Y. Fu, C. Hou, G.-F. Han, P. Yang, Y.-B. Liu, Q. Jiang, *Nat. Commun.* **2013**, *4*.
- [27] G. Schmid, B. Corain, *Eur. J. Inorg. Chem.* **2003**, *2003*, 3081.
- [28] S. Biella, L. Prati, M. Rossi, *J. Catal.* **2002**, *206*, 242.
- [29] G. C. Bond, *Catal. Today* **2002**, *72*, 5.
- [30] Y. M. Sabri, S. J. Ippolito, J. Tardio, V. Bansal, A. P. O'Mullane, S. K. Bhargava, *Sci. Rep.* **2014**, *4*, 1.
- [31] B. Plowman, S. J. Ippolito, V. Bansal, Y. M. Sabri, A. P. O'Mullane, S. K. Bhargava, *Chem. Commun.* **2009**, 5039.
- [32] B. J. Plowman, S. K. Bhargava, A. P. O'Mullane, *Analyst* **2011**, *136*, 5107.
- [33] C. Radovan, F. Manea, *Electroanalysis* **2007**, *19*, 91.
- [34] C. Cofan, C. Radovan, *Sensors* **2008**, *8*, 3952.
- [35] N. German, A. Ramanavicius, A. Ramanaviciene, *Sens. Actuator B-Chem.* **2014**, *203*, 25.
- [36] J. Luo, H. Zhang, S. Jiang, J. Jiang, X. Liu, *Mikrochim. Acta* **2012**, *177*, 485.
- [37] Y. M. Sabri, A. E. Kandjani, S. J. Ippolito, S. K. Bhargava, *ACS Appl. Mater. Interfaces* **2015**, *7*, 1494.
- [38] S. Trasatti, O. Petrii, *Pure Appl. Chem.* **1991**, *63*, 711.
- [39] S. Trasatti, O. Petrii, *Pure Appl. Chem.* **1991**, *63*, 711.
- [40] K. M. Kabir, Y. M. Sabri, A. E. Kandjani, G. I. Matthews, M. Field, L. A. Jones, A. Nafady, S. J. Ippolito, S. K. Bhargava, *Langmuir* **2015**, *31*, 8519.
- [41] Y. Li, Y.-Y. Song, C. Yang, X.-H. Xia, *Electrochem. Commun.* **2007**, *9*, 981.
- [42] Y. B. Vassilyev, O. Khazova, N. Nikolaeva, *J. Electroanal. Chem. Interfacial. Electrochem.* **1985**, *196*, 127.
- [43] M. Hsiao, R. Adzic, E. Yeager, *J. Electrochem. Soc.* **1996**, *143*, 759.
- [44] M. Pasta, F. La Mantia, Y. Cui, *Electrochim. Acta* **2010**, *55*, 5561.
- [45] E. B. Makovos, C. C. Liu, *Bioelectrochem. Bioenerg.* **1986**, *15*, 157.
- [46] D. Kirk, F. Foulkes, W. Graydon, *J. Electrochem. Soc.* **1980**, *127*, 1069.
- [47] S. B. Aoun, Z. Dursun, T. Koga, G. S. Bang, T. Sotomura, I. Taniguchi, *J. Electroanal. Chem.* **2004**, *567*, 175.
- [48] L. Burke, *Electrochim. Acta* **1994**, *39*, 1841.
- [49] P. Holt-Hindle, S. Nigro, M. Asmussen, A. Chen, *Electrochem. Commun.* **2008**, *10*, 1438.
- [50] F. Xiao, F. Zhao, D. Mei, Z. Mo, B. Zeng, *Biosens. Bioelectron.* **2009**, *24*, 3481.
- [51] Z. W. Zhao, X. J. Chen, B. K. Tay, J. S. Chen, Z. J. Han, K. A. Khor, *Biosens. Bioelectron.* **2007**, *23*, 135.
- [52] T.-M. Cheng, T.-K. Huang, H.-K. Lin, S.-P. Tung, Y.-L. Chen, C.-Y. Lee, H.-T. Chiu, *ACS Appl. Mater. Interfaces* **2010**, *2*, 2773.
- [53] S. Cho, C. Kang, *Electroanalysis* **2007**, *19*, 2315.
- [54] G. Sanz , I. Taurino, R. Antiochia, L. Gorton, G. Favero, F. Mazzei, G. De Micheli, S. Carrara, Bioelectrochemistry, DOI: <http://dx.doi.org/10.1016/j.bioelechem.2016.02.012>.
- [55] C. Qiu, X. Wang, X. Liu, S. Hou, H. Ma, *Electrochim. Acta* **2012**, *67*, 140.
- [56] Y.-J. Lee, J.-Y. Park, *Sens. Actuator B-Chem.* **2011**, *155*, 134.
- [57] Q. Yi, W. Yu, *J. Electroanal. Chem.* **2009**, *633*, 159.
- [58] X. Liu, Q. Hu, Q. Wu, W. Zhang, Z. Fang, Q. Xie, *Colloids surf., B* **2009**, *74*, 154.
- [59] C. Guo, X. Zhang, H. Huo, C. Xu, X. Han, *Analyst* **2013**, *138*, 6727.
- [60] C. Radovan, D. Cinghit , F. Manea, M. Mincea, C. Cofan, V. Ostafe, *Sensors* **2008**, *8*, 4330.
- [61] M. Tominaga, T. Shimazoe, M. Nagashima, I. Taniguchi, *Electrochem. Commun.* **2005**, *7*, 189.
- [62] Y. Bai, W. Yang, Y. Sun, C. Sun, *Sens. Actuator B-Chem.* **2008**, *134*, 471.
- [63] L. Chen, T. Fujita, Y. Ding, M. Chen, *Adv. Funct. Mater.* **2010**, *20*, 2279.
- [64] A. Habrioux, E. Sibert, K. Servat, W. Vogel, K. B. Kokoh, N. Alonso-Vante, *J. Phys. Chem. B* **2007**, *111*, 10329.
- [65] X. Ren, X. Meng, F. Tang, *Sens. Actuator B-Chem.* **2005**, *110*, 358.
- [66] D. Pan, J. Chen, S. Yao, L. Nie, J. Xia, W. Tao, *Sens. Actuator B-Chem.* **2005**, *104*, 68.

- [67] X.-C. Dong, H. Xu, X.-W. Wang, Y.-X. Huang, M. B. Chan-Park, H. Zhang, L.-H. Wang, W. Huang, P. Chen, *ACS nano* **2012**, *6*, 3206.
- [68] S.-Y. Lin, S.-J. Chang, T.-J. Hsueh, *Appl. Phys. Lett.* **2014**, *104*, 193704.
- [69] K. M. Kabir, Y. M. Sabri, G. I. Matthews, L. A. Jones, S. J. Ippolito, S. K. Bhargava, *Analyst* **2015**, *140*, 5508.

Received: March 3, 2016

Accepted: July 25, 2016

Published online: ■ ■ ■ ■, 0000

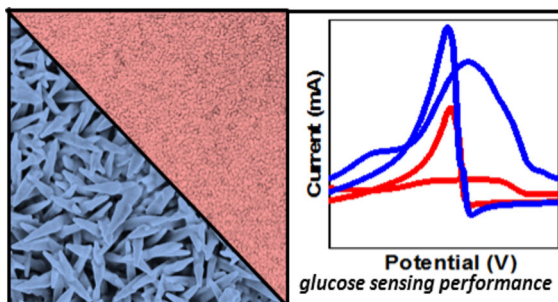
FULL PAPERS

V. E. Coyle, A. E. Kandjani,
Y. M. Sabri,* S. K. Bhargava*

■■ – ■■



**Au Nanospikes as a Non-enzymatic
Glucose Sensor: Exploring
Morphological Changes with the
Elaborated Chronoamperometric
Method**



Supporting Information

Au nanospikes as a non-enzymatic glucose sensor: Exploring morphological changes with the elaborated chronoamperometric method

Victoria E Coyle,^a Ahmad Esmailzadeh Kandjani,^a Ylias M Sabri^{a} and Suresh K. Bhargava^{a*}*

^a Centre for Advanced Materials and Industrial Chemistry (CAMIC), School of Applied Sciences, RMIT University, GPO Box 2476 V, Melbourne, Victoria 3001, Australia

*email: ylias.sabri@rmit.edu.au , suresh.bhargava@rmit.edu.au, Phone: +61 3 99252330

RECEIVED DATE (to be automatically inserted after your manuscript is accepted if required according to the journal that you are submitting your paper to)

Sample Name	H ₂ AuCl ₄ concentration (mM)	Pb(CH ₃ CO ₂) ₂ concentration (mM)	Time (min)	On-set potential (V)
Au substrate	0	0	0	0.05
Au_spikes_1	3.4	1	12	0.05
Au_spikes_2	6.8	1	12	0.05
Au_spikes_3	13.6	1	12	0.05
Au_spikes_4	27.2	1	12	0.05
Au_spikes_5	13.6	0.25	12	0.05
Au_spikes_6	13.6	0.5	12	0.05
Au_spikes_7	13.6	2	12	0.05
Au_spikes_8	13.6	1	6	0.05
Au_spikes_9	13.6	1	24	0.05
Au_spikes_10	13.6	1	36	0.05
Au_spikes_11	13.6	1	48	0.05
Au_spikes_12	13.6	1	12	-0.1
Au_spikes_13	13.6	1	12	0.3
Au_spikes_14	13.6	1	12	0.6

Table. S1 Synthesis variables for Au nanospike substrates used for glucose sensing experiments

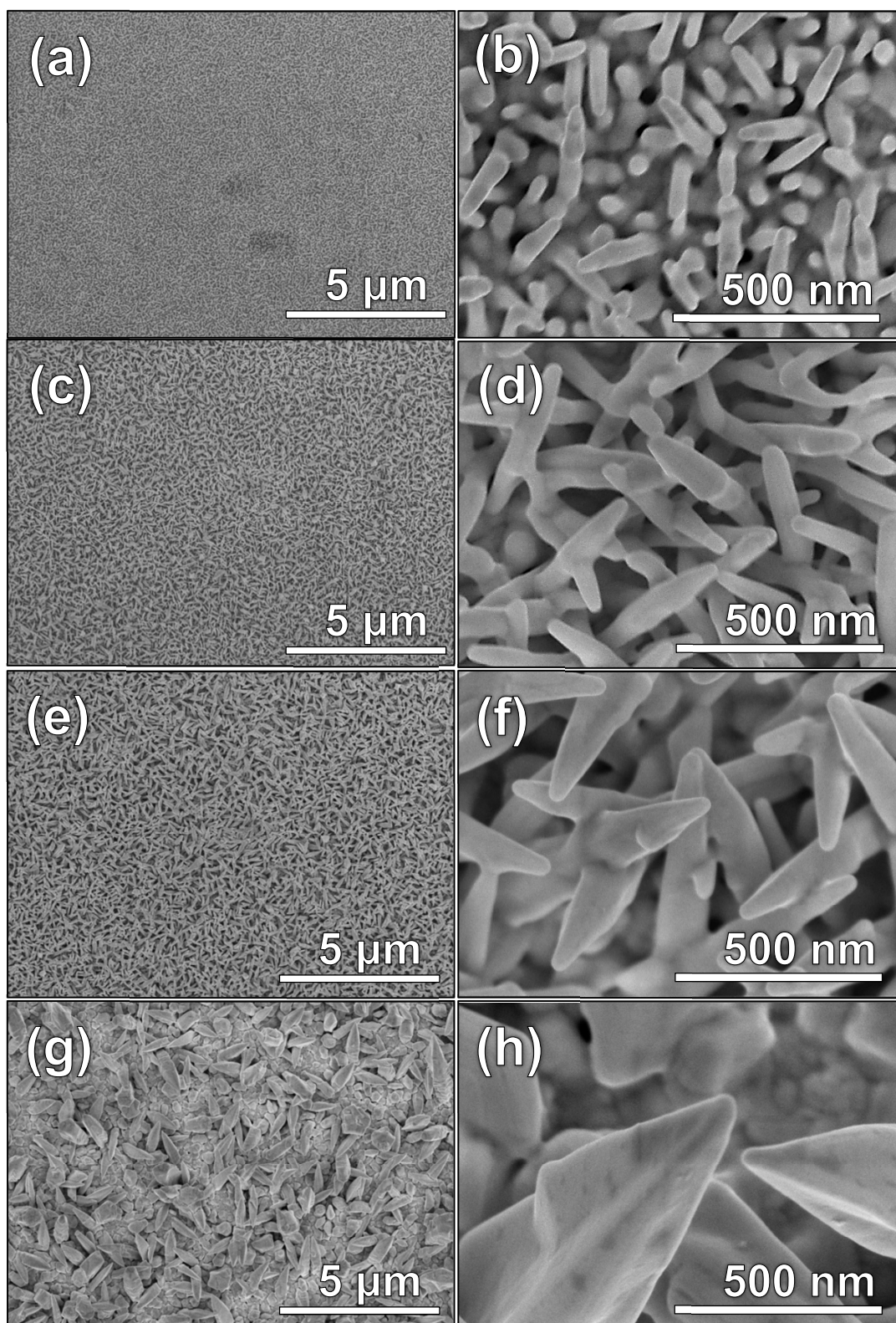


Figure. S1 low magnification (a,c,e,g) and high magnification (b,d,f,h) SEM images of Au nanopikes with 1mM $\text{Pb}(\text{CH}_3\text{CO}_2)_2$ and (a,b) 3.4 mM (c,d) 6.8 mM (e,f) 13.6 mM and (g,h) 27.2 mM HAuCl_4 deposited for 12 mins

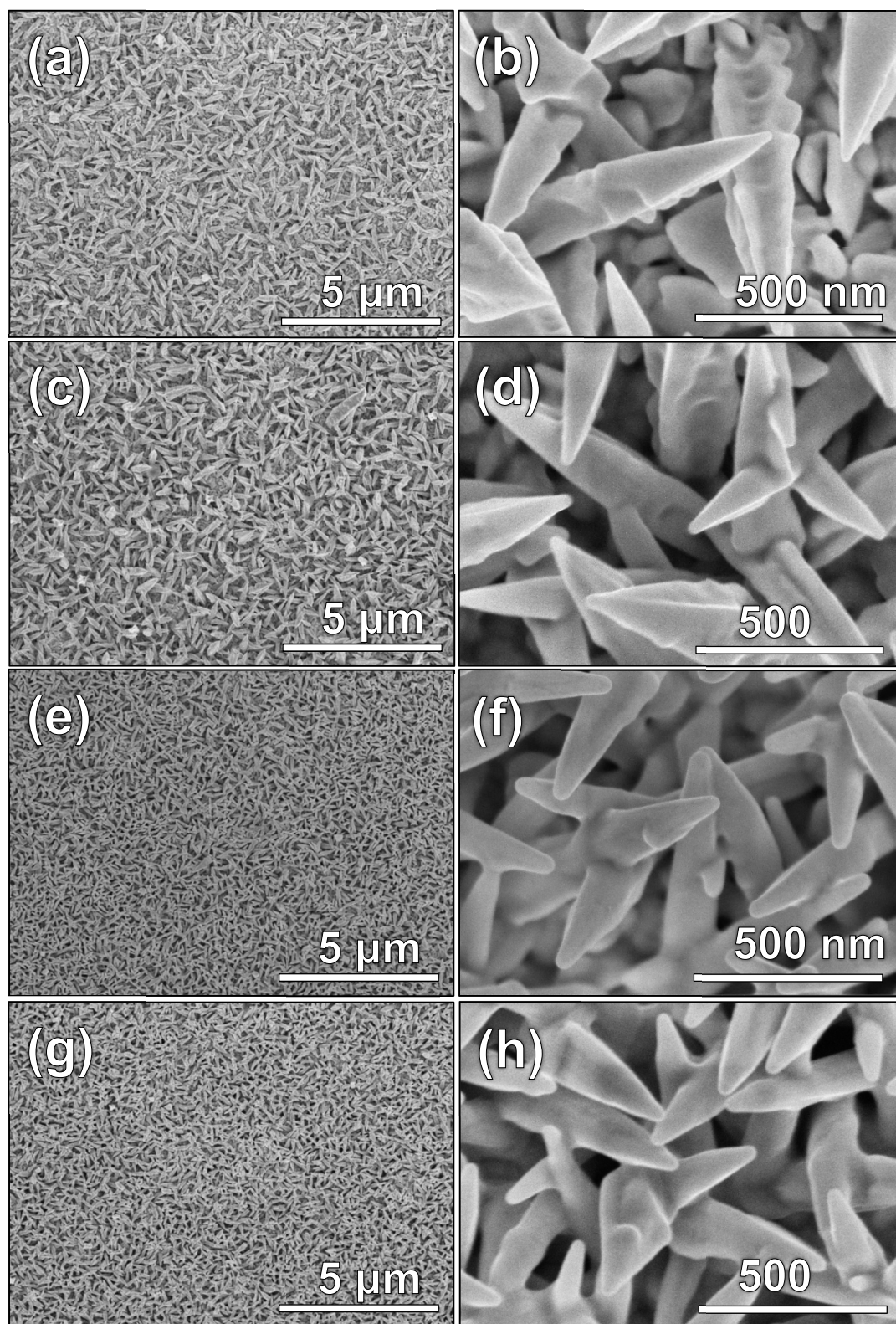


Figure. S2 low magnification (a,c,e,g) and high magnification (b,d,f,h) SEM images of Au nanospikes with 13.6 mM H₂AuCl₄ and (a,b) 0.25 mM (c,d) 0.5 mM (e,f) 1 mM and (g,h) 2 mM Pb(CH₃CO₂)₂ deposited for 12 min

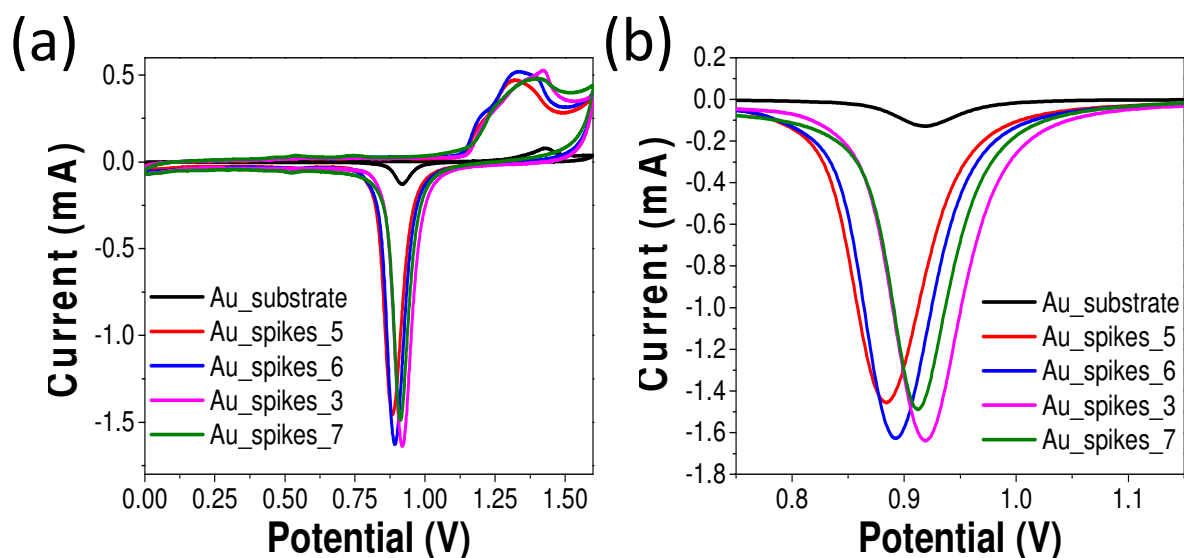


Figure. S3 ECSA analysis of Au nanospikes with varying $\text{Pb}(\text{CH}_3\text{CO}_2)_2$ concentration, (a) overall experimental ECSA analysis and (b) 0.75 V-1.15 V peak analysis curves

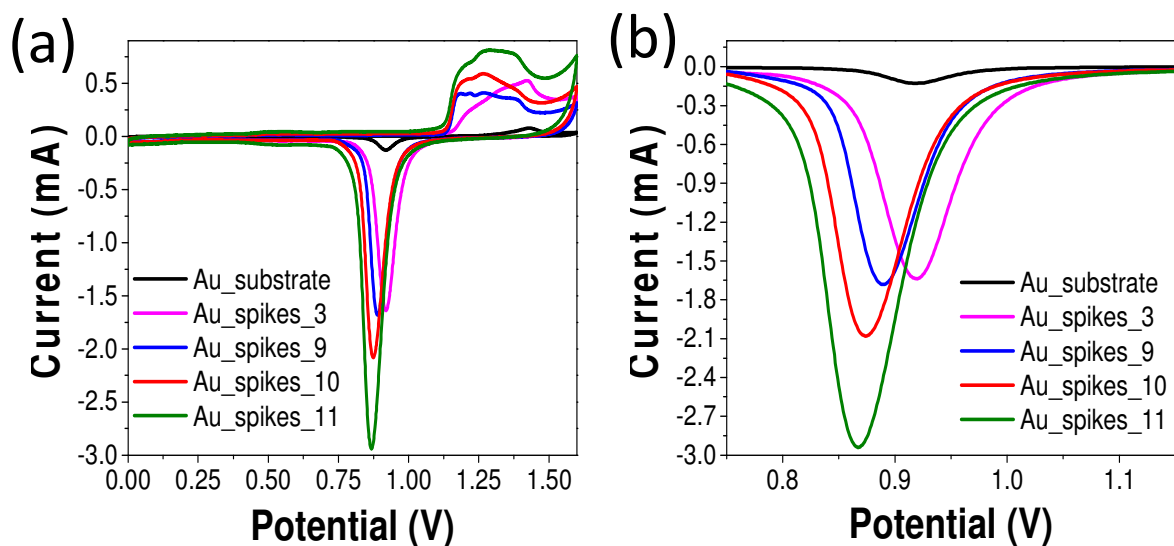


Figure. S4 ECSA analysis of Au nanospikes with varying electrodeposition times, (a) overall experimental ECSA analysis and (b) 0.75 V-1.15 V peak analysis curves

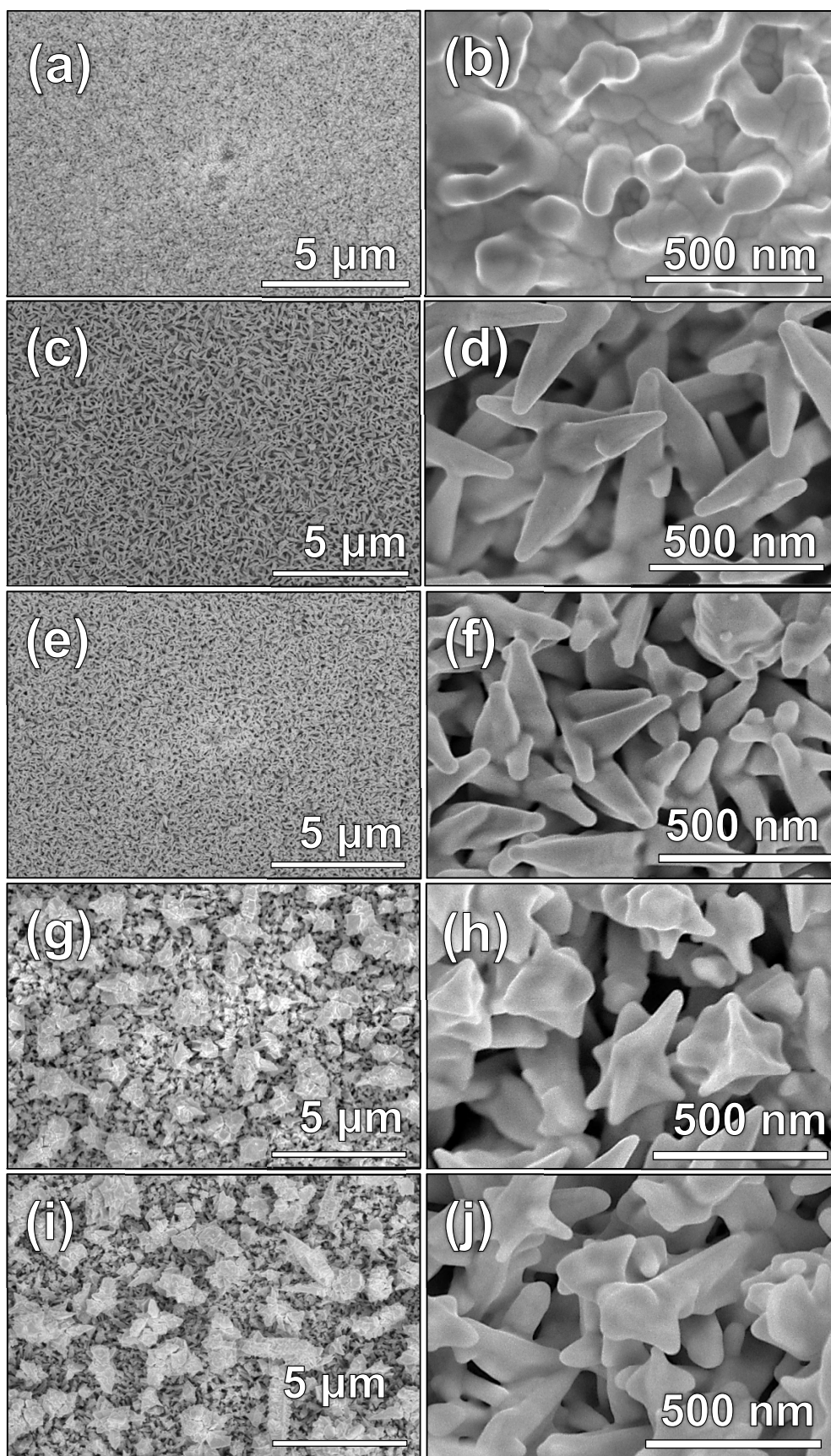


Figure. S5 low magnification (a,c,e,g,i) and high magnification (b,d,f,h,j) SEM images of Au nanopikes with 13.6 mM HAuCl_4 and 1 mM $\text{Pb}(\text{CH}_3\text{CO}_2)_2$ deposited for (a,b) 6 mins (c,d) 12 mins (e,f) 24 mins (g,h) 36 mins and (i,j) 48 mins

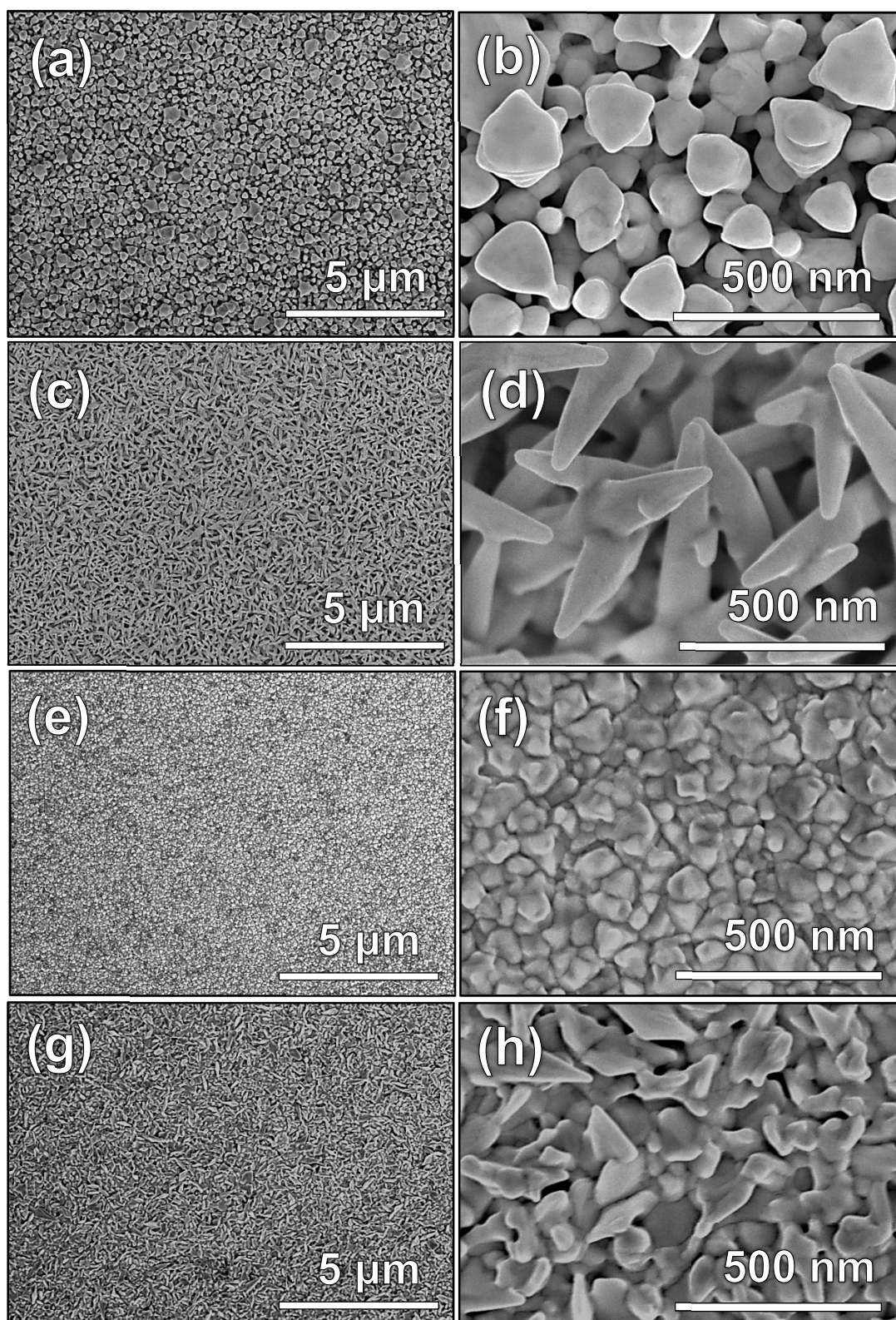


Figure. S6 low magnification (a,c,e,g,i) and high magnification (b,d,f,h,j) SEM images of Au nanospikes with 13.6 mM HAuCl₄ and 1 mM Pb(CH₃CO₂)₂ deposited for 12 mins at on-set potentials of (a,b) -0.1V (c,d) 0.05V (e,f) 0.3V and (g,h) 0.6V

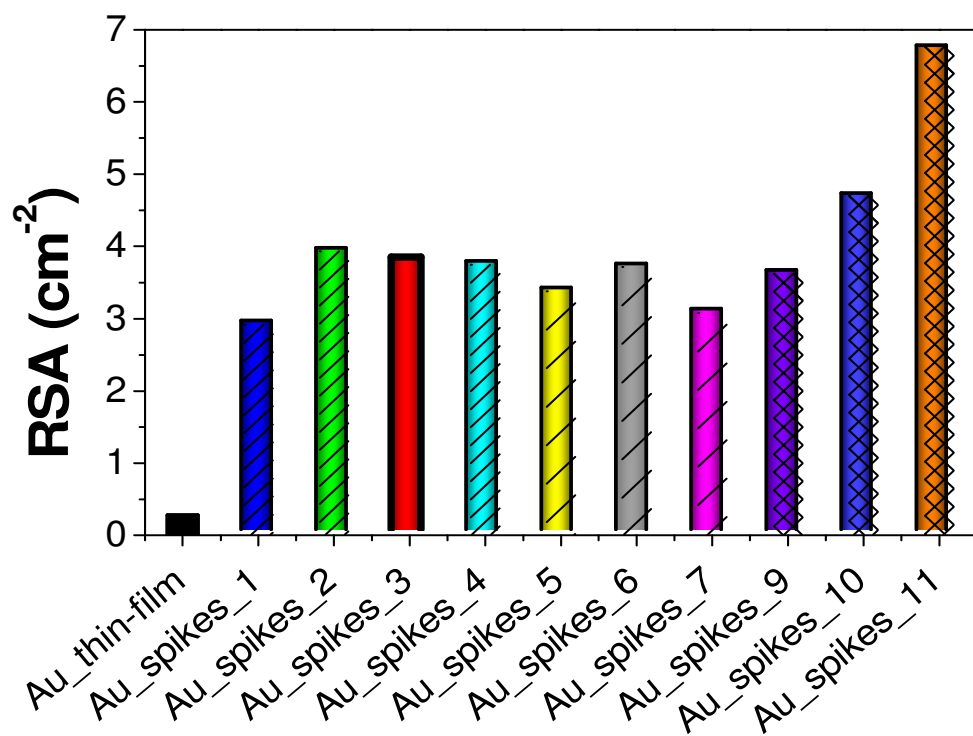


Figure. S7 RSA values of modified substrates and RSA value compared to geometric area of the plain Au-substrate (0.238 cm⁻²)

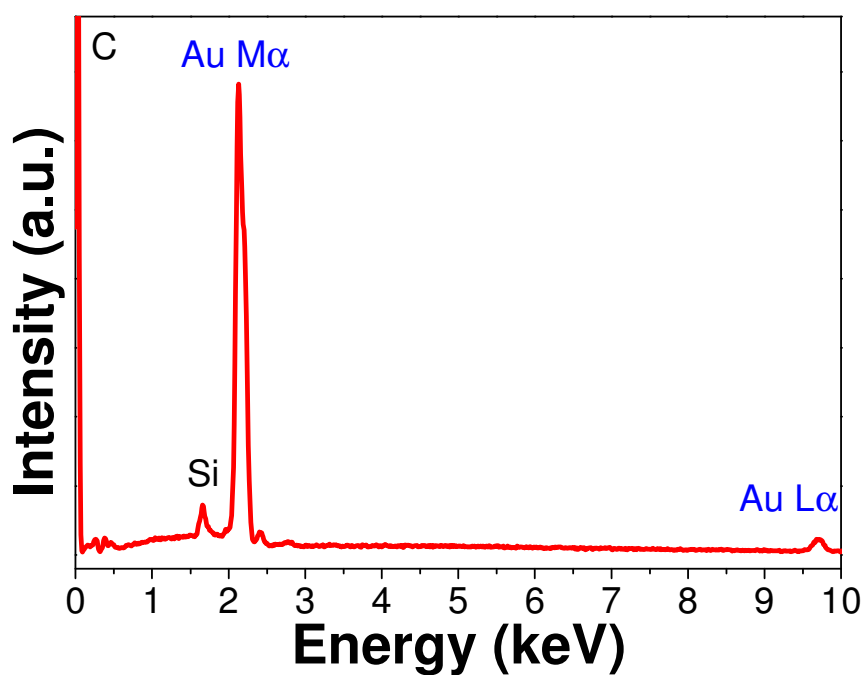


Figure. S8 EDX spectral analysis of Au nanopike substrate

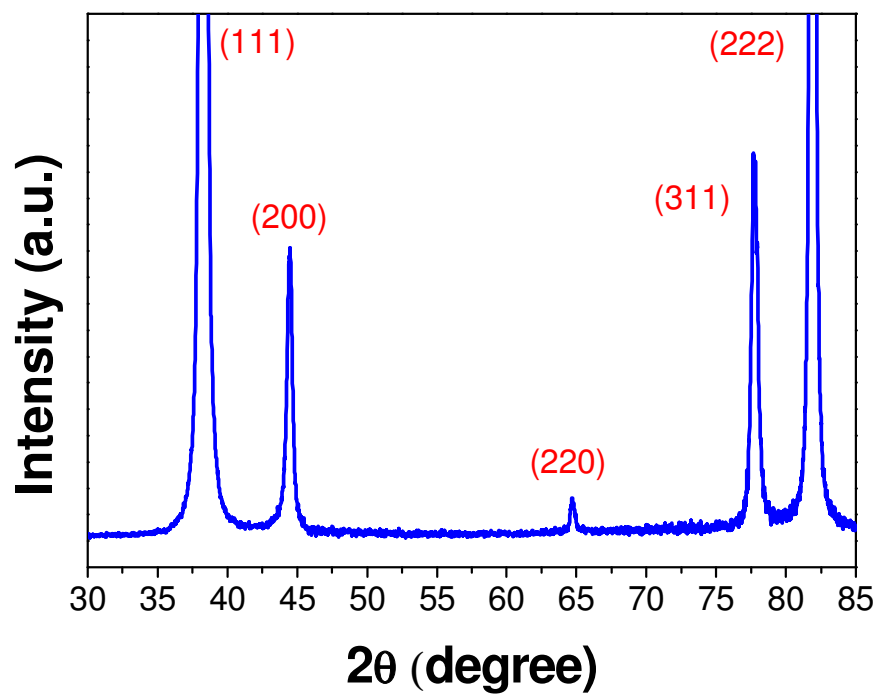


Figure. S9 XRD pattern of nanospike substrate

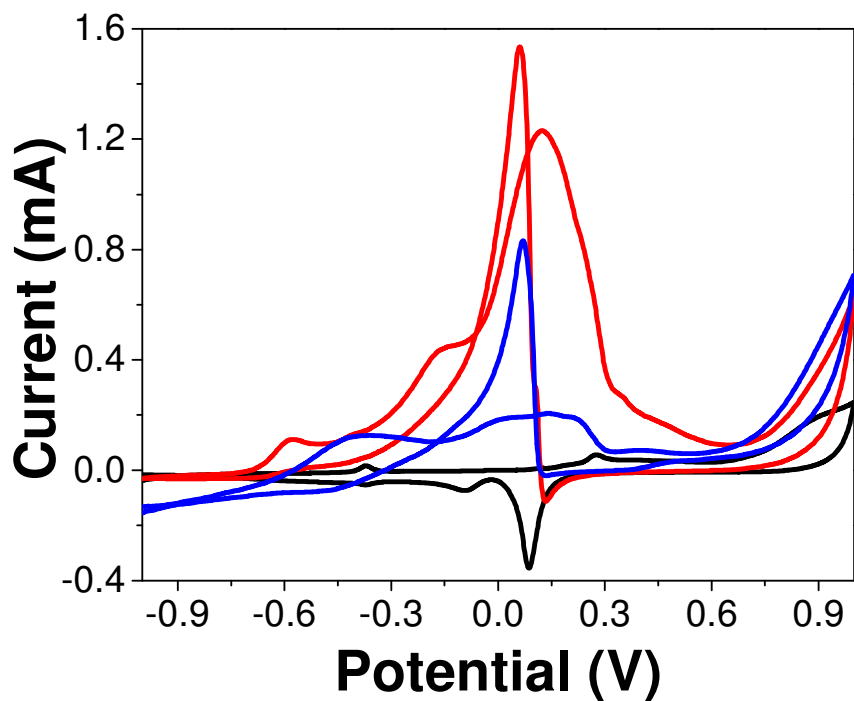


Figure. S10 CV analysis of Au nanoparticles in 0.5 M KOH solution (black) and Au_spikes_3 (red) and Au_substrate (blue) in 0.5 M KOH and 10 mM glucose solution

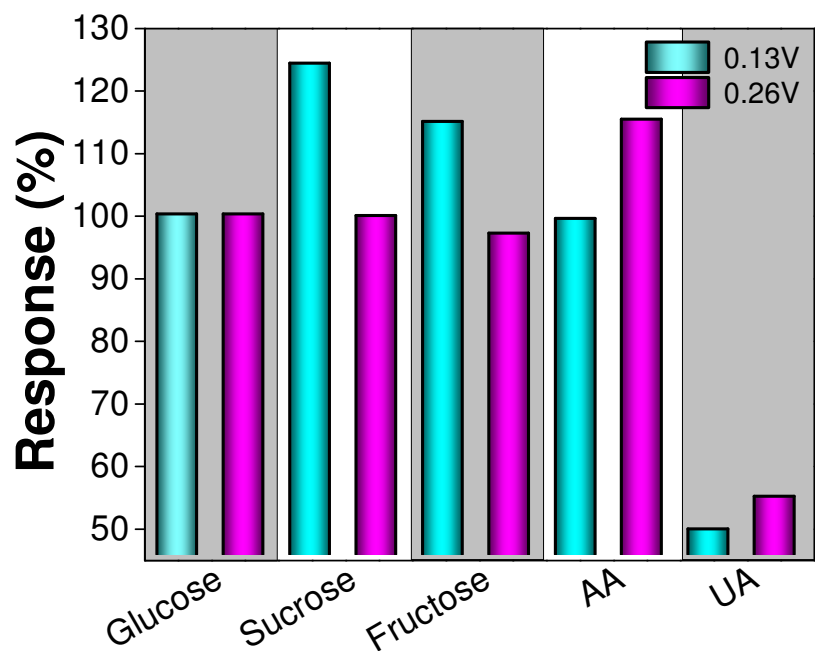


Figure. S11 Bar graph analysis comparing selectivity analysis of 0.13V and 0.26V.

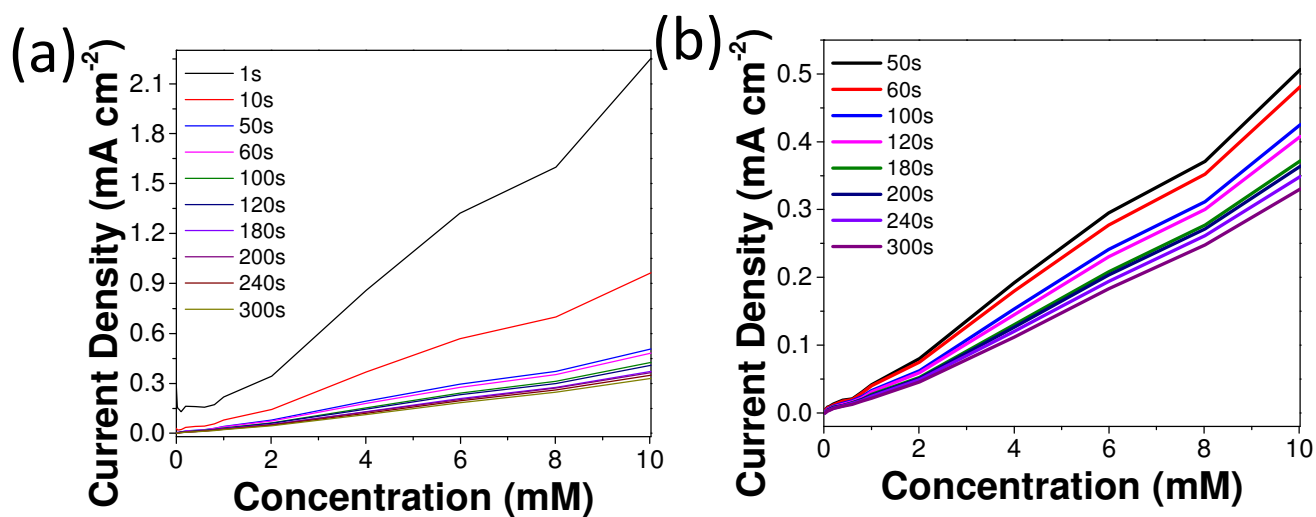


Figure. S12 Current density vs Concentration analysis (a) 1s-300s and (b) 50s – 300s

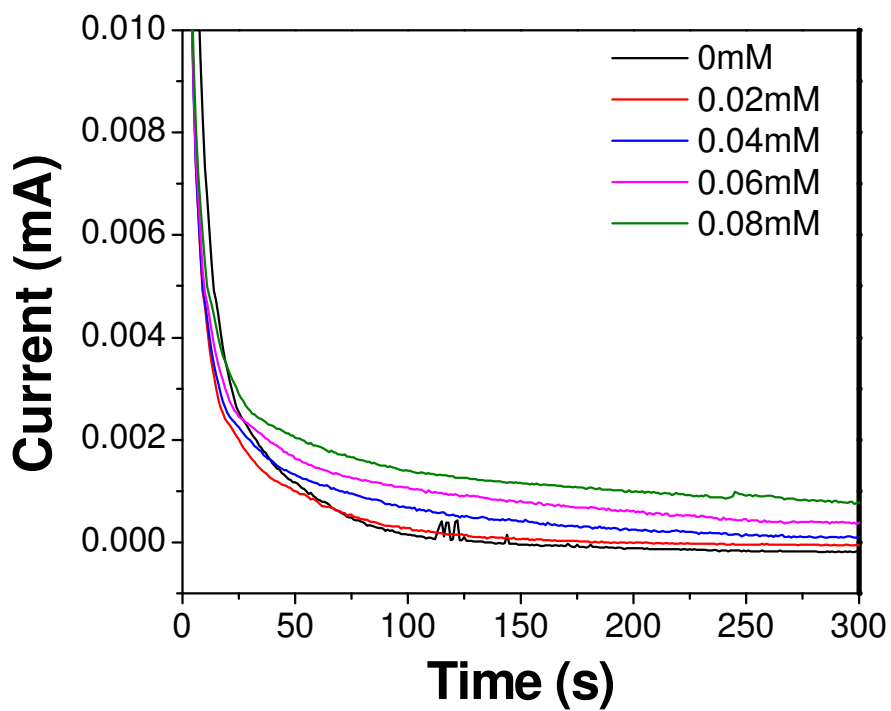


Figure. S13 Lowest concentration to be detected at 20 μ M

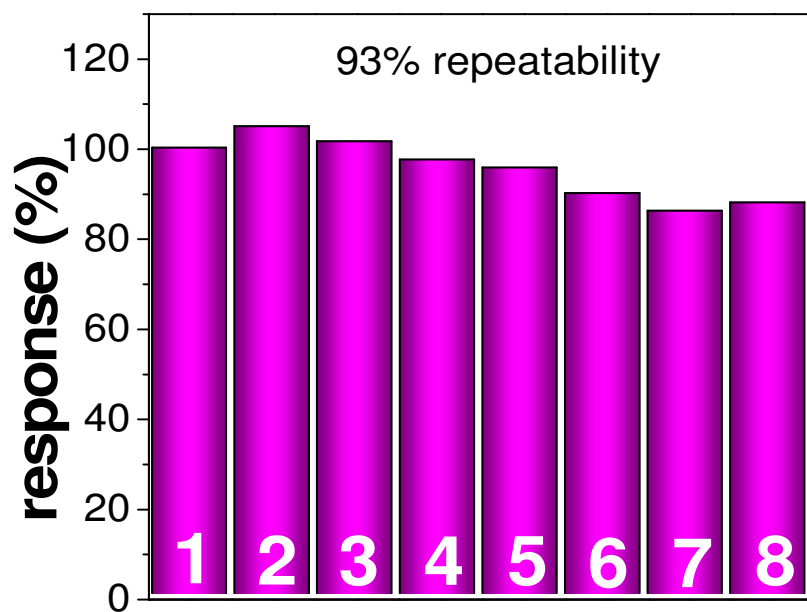


Figure. S14 repeatability in 10mM glucose at 0.13V for Au_spikes_3

CHAPTER IV:

Hydrogen bubble templated growth of honeycomb-like Au-Pt alloy films for non-enzymatic glucose sensing

Au and Pt based nanomaterials have shown great promise for non-enzymatic based electrochemical glucose sensing, however obtaining a balance between good selectivity and high sensitivity is still an ongoing challenge. In this chapter a glucose sensor was developed to unite the properties of both metals through the formation of bi-metallic Au-Pt alloy honeycomblike structures with controlled Pt content during electrodeposition. The honeycomb-like structures were formed by employing hydrogen gas bubbles developed in-situ as a dynamic template. The developed films were found to possess large surface areas with a homogeneous spread of Au and Pt throughout the surface, enabling both high sensitivity and selectivity when compared to monometallic metal nanostructures. The sensitivity and experimental detection limit of the developed glucose sensor was determined to be $109.3 \mu\text{A}\cdot\text{mM}^{-1}\cdot\text{cm}^{-2}$ (after a 10 s stabilization period) and $20 \mu\text{M}$, respectively. Selectivity studies showed minimal to no interference in the presence of Acetic Acid (AA) and Uric Acid (UA), which we have attributed to the Au component of the electrodeposited nanostructures allowing detection at a lower potential, overcoming the lack of selectivity typically experienced by Pt.



Hydrogen Bubble Templated Growth of Honeycomb-Like Au-Pt Alloy Films for Non-Enzymatic Glucose Sensing

Victoria E. Coyle, Daniel K. J. Oppedisano,* Lathe A. Jones,**
Ahmad Esmailzadeh Kandjani,^z Ylias M. Sabri, and Suresh K. Bhargava^z

Centre for Advanced Materials & Industrial Chemistry (CAMIC), School of Science, RMIT University, Melbourne, Victoria 3001, Australia

Au and Pt based nanomaterials have shown great promise for non-enzymatic based electrochemical glucose sensing, however obtaining a balance between good selectivity and high sensitivity is still an ongoing challenge. In this work we have developed glucose sensors that take advantage of the properties of both metals through the formation of bi-metallic Au-Pt alloy honeycomb-like structures with controlled Pt content during electrodeposition. The honeycomb-like structures were formed by employing hydrogen gas bubbles developed in-situ as a dynamic template. The developed films were found to possess large surface areas with a homogeneous spread of Au and Pt throughout the surface, enabling both high sensitivity and selectivity when compared to monometallic metal nanostructures. The sensitivity and experimental detection limit of the developed glucose sensor was determined to be $109.3 \mu\text{A} \cdot \text{mM}^{-1} \cdot \text{cm}^{-2}$ (after a 10 s stabilization period) and $20 \mu\text{M}$, respectively. Selectivity studies showed minimal to no interference in the presence of Acetic Acid (AA) and Uric Acid (UA), which we have attributed to the Au component of the electrodeposited nanostructures allowing detection at a lower potential, overcoming the lack of selectivity typically experienced by Pt.

© 2016 The Electrochemical Society. [DOI: 10.1149/2.0301614jes] All rights reserved.

Manuscript submitted July 22, 2016; revised manuscript received October 17, 2016. Published October 27, 2016.

Diabetes is a chronic health condition affecting 387 million people worldwide and rising,¹ causing a lack in blood glucose concentration (Hypoglycemia) or an increase in blood glucose concentration (Hyperglycemia). The normal human blood glucose concentration is between 4.4–6.6 mM,² however a person with hypoglycemia experiences blood glucose levels between 2.8–3.3 mM³ whilst a person with hyperglycemia has a blood glucose concentration between 7–11.1 mM.⁴ Due to this wide range in possible blood glucose concentrations which are exhibited, the need for more sensitive and accurate glucose sensors is becoming increasingly important. This rise in diabetic population has propagated research into the development of glucose sensors, with the number of papers reporting new developments increasing exponentially in recent years.⁵ Enzyme based glucose sensors initially reported by Clark and Lyons⁶ in 1962 were the first type of electrochemical based sensors developed, based around modified electrodes employing enzymes as the active component. Metal-based non-enzymatic glucose sensors were later shown to have greater promise due to their improved stability in varying pH media, high reproducibility and exclusion of the need for an oxygen source, as was the case to enzyme-based counterparts.⁷

As such, non-enzymatic glucose sensors have become the main focus of research and are usually based on noble-metals such as Au,⁸ Pt⁹ and Pd¹⁰ because they are simple to synthesize and are able to form nanostructures with high surface areas.¹¹ In general, metals that are chosen for the sensor need to provide low on-set potentials for glucose oxidation, high sensitivities, low detection limits and/or good selectivity when interacting with common physiological contaminants.¹² However, many pure metals display poor sensitivity for glucose in the presence of interfering contaminants and can be easily poisoned by adsorbed intermediates, affecting surface selectivity for the glucose electrooxidation. Of the aforementioned noble-metals, Au and Pt show the greatest promise^{12,13} with Au displaying low on-set potentials, good stability against physiological species and high activity in both neutral and alkali electrolytes.^{14,15} On the other hand, Pt displays very high sensitivities and excellent electrocatalytic activity toward glucose, however has poor selectivity, being easily hindered by physiological contaminants¹⁶ and a rapid loss in activity due to the accumulation of chemisorbed intermediates blocking the electrode surface.¹⁷ Each metal thus has their own advantages, where higher sensitivities are reported for Pt electrodes, but Au displays better electroactivity toward glucose oxidation than Pt.¹² Therefore the use of bimetallic

alloy materials is becoming more popular, as the secondary metal can further enhance the electrochemical glucose sensing performance of the substrate (or primary) by combining the individual properties of each metal. Previous research using alloy-based non-enzymatic glucose sensors which have proved such approach to be successful include Au-Pt,^{17,18} Ni-Co,^{19,20} Pt-Ni,^{21,22} Ni-Cu²³ and Pt-Pb.²⁴

From the numerous studies reported thus far, it has been shown that generally materials with large surface areas have relatively better glucose sensing performance. Furthermore, the alloying of Pt with Au is known to enhance the overall performance (sensitivity and selectivity) of electrochemical sensors toward glucose.^{24,25} Therefore it is proposed that by combining these two aspects of large surface area and control of the metal content while alloying, a synergistic enhancement of the surface toward non-enzymatic electrochemical sensing of glucose may be obtained, while overcoming the drawbacks of each metal. We tested our hypothesis by employing the recently developed dynamic hydrogen bubble template method²⁶ to electrochemically deposit large honeycomb-like porous Au-Pt alloy films whilst controlling the metal content in the material produced. Au was chosen as the main component of the electrolyte due to its higher electroactivity toward glucose compared to Pt and the high level of reproducibility for Au-based electrodeposition methods. The cohesive (interconnected) growth of the Au-Pt alloys displayed excellent glucose sensing performance. It is envisaged that the alloy formation method and performance enhancement concepts presented in this study could potentially be used in other chemical and biochemical sensing applications.

Experimental

All chemicals used in this work were purchased from Sigma-Aldrich and used as received. Au films deposited on Si substrates were prepared using E-beam evaporation with an adhesion layer of 10 nm Ti on a Si wafer followed by application of a 100 nm Au layer. The wafer was diced to dimensions of 8 mm × 18 mm and masked in order to expose a consistent circular surface with an area of 0.238 cm² having been used ((ϕ) of 5.5 mm) for each experiment. The electrodeposition experiments were performed using a CH instruments (CHI760C) electrochemical workstation attached to a model 680 amp booster. The electrochemical cell consisted of the working electrode (Au substrate), an auxiliary electrode (graphite rod) and a reference electrode (Ag/AgCl 3 M KCl, +0.197 V vs SHE). The Au substrate was pre-treated by electrochemically cycling between the potentials of 0 V and +1.4 V in 0.5 M sulfuric acid (H₂SO₄) at a scan rate of 100 mV · s⁻¹. The electrodeposition of the Au-Pt alloy honeycomb

*Electrochemical Society Student Member.

**Electrochemical Society Member.

^zE-mail: ahmad.kandjani@rmit.edu.au; suresh.bhargava@rmit.edu.au

Table I. Electrodeposition variables for Au-Pt alloy honeycombs and the Au:Pt ratio of contributing percentages on the materials surface.

Sample Name	HAuCl ₄ conc. (mM)	K ₂ PtCl ₄ conc. (mM)	Au:Pt XPS composition (atom %)
Au	0	0	100: 0
Au ₁₀	10	0	100: 0
Au ₁₀ Pt _{0.5}	10	0.5	92.3: 7.7
Au ₁₀ Pt ₁	10	1	86.9: 13.1
Au ₁₀ Pt _{2.5}	10	2.5	69.2: 30.8
Au ₁₀ Pt ₅	10	5	44.9: 55.1

films were performed at a constant potential of -4 V for 300s similar to the technique employed by Cherevko et al.²⁷ The electrodeposition solution consisted of 10 mM HAuCl₄ in 2 M H₂SO₄ with varying K₂PtCl₄ concentrations (0, 0.5, 1, 2.5 and 5 mM). The electrolyte salt concentration for each prepared sample of the honeycomb-like films is listed in Table I.

Surface characterization of the Au-Pt honeycomb substrates was performed using scanning electron microscopy (SEM) with high resolution (Verios 460L), energy dispersive X-ray spectroscopy (EDX) at an operating potential of 15 kV, X-ray diffraction (XRD, Bruker D8 Discover micro diffraction system with a general area diffraction detector system) which had a Cu-K α radiation source with an operating voltage of 40 kV and a current of 40 mA and X-ray photoelectron spectroscopy (XPS, Thermo K-alpha, Al K α) which operated at less than 10^{-9} Torr (data shifted according to C1 BE of 285 eV). Electrochemical surface area was determined using cyclic voltammetry in 10 mM K₃Fe(CN)₆ and 0.2 mM KCl at a scan rate of 50 mVs⁻¹ employing a 3-electrode set-up, implementing the Au-Pt honeycomb as the working electrode, a Ag/AgCl reference electrode and a graphite rod as the counter electrode.

Glucose sensing was undertaken using cyclic voltammetry at a scan rate of 20 mV · s⁻¹ in a solution of 0.5 M KOH and 10 mM glucose. Although the normal human glucose concentration range is between 4.4 and 6.6 mM,² comparison analysis (CV and chronoamperometry at various applied potentials) was performed at 10 mM which allowed for relatively better response comparisons between the synthesized sensors over a lower glucose concentration. Chronoamperometric additions analysis of the optimal synthesized sensor was performed in a solution of 0.5 M KOH with various glucose concentrations ranging between 20 μ M and 10 mM. This range covers concentrations of glucose in normal people (4.4–6.6 mM) and those with hyperglycaemia (7–11.1 mM). The concentrations lower than 4.4 mM were tested in order to show the relevance of our developed sensors for other applications such as food analysis.

Results and Discussion

The characterization of the electrochemically deposited Au-Pt honeycomb structures and their employment as electrode substrates for non-enzymatic electrochemical sensing application is presented in this section.

Au-Pt alloy honeycomb characterization.—The deposition of Au-Pt honeycomb-like structures was performed at a potential of -4 V in electrolytes containing different Au and Pt concentrations to form alloys with varying Pt contents, as detailed in Table I. The extreme negative potential was used in order to generate hydrogen gas bubbles at the working electrode in-situ during the deposition process, which acts as a dynamic template for the porous honeycomb structures. The morphological changes that occur in the Au-Pt honeycomb structure as a result of increasing Pt concentration in the electrolyte are shown in Figure 1. The preparation of these honeycomb-like structures proved to be fast (within 300 seconds) and reproducible (similar images observed when surfaces were made on several occasions). Figure 1a

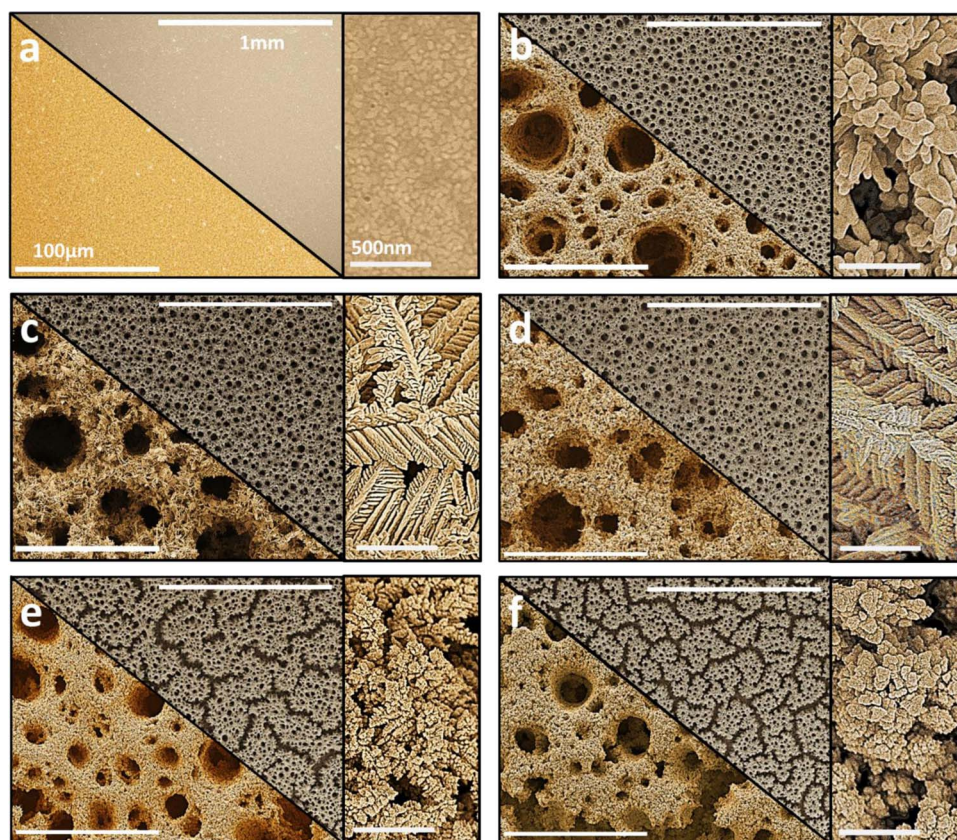


Figure 1. Low (top panel), high (bottom panel) and higher (right panel) magnification SEM images of Au-Pt honeycomb (a) Au substrate (b) Au₁₀ (c) Au₁₀Pt_{0.5} (d) Au₁₀Pt₁ (e) Au₁₀Pt_{2.5} and (f) Au₁₀Pt₅.

shows an unmodified Au substrate which was used as the control substrate (Au-Ctrl) upon which electrodeposition was performed. Figure 1b displays the pure Au honeycomb (Au₁₀) formed on the Au-Ctrl through the electrodeposition process. Large pores are seen across the surface of the film with an average diameter (ϕ) of 31.8 μm . The finer particles forming the overall structure are observed to have sizes in the range of ~ 75 nm. The introduction of 0.5 mM Pt in the electrolyte (Au₁₀Pt_{0.5}) also leads to the formation of honeycomb-like structures with large pores (average ϕ of 22.9 μm) as shown in Figure 1c, however the finer features were observed to resemble thin leaf-like shapes branching off into large structures. This change in the finer structure morphology demonstrates how the introduction of Pt into the electrolyte solution significantly changes the fine structure of the honeycomb films formed. Increasing the Pt concentration in the electrolyte to 1 mM (Au₁₀Pt₁) was found to have an influence on the pore size (an average ϕ of only 22.3 μm) of the honeycomb structures and to a lesser extent, on the leaf-like shapes making up the structures as shown in Figure 1d. We attributed the evenly dispersed pore size across the surfaces resulting from relatively low Pt concentration to the occurrence of relatively low turbulent hydrogen evolution. The SEM images of the surfaces formed by further increasing the amount of Pt present in the electrolyte to 2.5 mM (Au₁₀Pt_{2.5}) and 5 mM (Au₁₀Pt₅) are shown in Figure 1e and Figure 1f, respectively. It can be seen that cracks appear to form across the surface of the substrate, which is postulated to be due to the increased Pt concentration resulting in a vigorous evolution of smaller hydrogen bubbles thereby giving rise to an alternative macro structure.²⁸ As a result the average pore diameters have drastically reduced to 18.9 and 14.8 μm for Au₁₀Pt_{2.5} and Au₁₀Pt₅, respectively. Similar to Au₁₀, the finer structures making up the honeycombs are observed to be clumps of nanoparticles, which are thought to have reduced the active site density relative to lower Pt contents, which will be confirmed in the characterization results discussed further on. The thickness of the electrodeposited Au-Pt films were determined to be ~ 90 μm from the SEM image taken at a 90° angle and presented in Figure S1 in SI. The porous nature of the developed Au-Pt films can also be observed from the higher magnification SEM image presented in Figure S2 in SI. The larger pores observed are a result of the hydrogen bubble template that was employed during electrodeposition process. Furthermore, the mechanical adhesion of bimetallic surfaces formed by electrodeposition is a common motivation²⁶ of employing this technique to produce robust sensitive layers. The developed structures in this study were observed to maintain on the substrate throughout the characterization and experimental procedures thus demonstrating their strong adherence and robustness.

XRD analysis was performed in order to determine the crystalline nature of the structures formed, the results of which are shown in Figure 2a. The XRD patterns showed peaks in 5 major locations where Au and Pt should appear for each substrate analyzed. A pure Pt substrate was used as a reference to demonstrate the shifting in 2θ values with changing Pt concentrations. There are 4 peaks that can be assigned to both Au and Pt face-center cubic (FCC) arrangements for the (111), (200), (220) and (331) reflections^{25,29} and are labelled accordingly in the figure. The peak relating to Pt (222) is not present for the samples formed in electrolytes with relatively lower Pt contents however starts to appear for the Au₁₀Pt₅ sample, along the Au (222) reflection. This is attributed to the dominant presence of Au in most of the Au-Pt honeycomb structures. The peaks observed in the XRD spectra have increased in 2θ values with increasing amounts of Pt in the solution (see Figure 2b and Table S1 in Supporting Information (SI)) which is a clear indication that Au-Pt alloy is being formed with an increasing Pt content in the electrodeposited surfaces.³⁰

The increase in the Pt in the films is also evidenced from the EDX spectra presented in Figure 2c. A reduction in energy for the L α peak from 2.14 keV for Au₁₀ to 2.11 keV for Au₁₀Pt₅ was observed. Furthermore, each modified alloy shifted closer toward the pure Pt L α peak (Figure 2d) which lies at 2.05 keV. These results confirm that increased Pt content in the electrolyte forms Au-Pt alloy surfaces. Significantly our EDX mapping, presented in Figure S3 in SI showed that

both Au and Pt are spread evenly on the surfaces. This is advantageous from an application point of view (i.e. sensing or catalysis) where the surface property of each material formed will be homogeneous across the surface. Furthermore, the evenness of the metal content throughout the surface also confirms the alloy nature of the deposited material.

In order to confirm that both Au and Pt are present on the surface, high resolution XPS analysis was performed. The separated spectra for Au 4f and Pt 4f are shown in Figure 2e and Figure 2f, respectively. The 4f_{7/2} core level spectrum of these samples for Au was observed to have a shift to a lower binding energy as the Pt content was increased. In contrast, the Pt 4f_{7/2} core level spectrum showed an increase in the binding energy as the amount of Pt increases in the electrolyte solution. These binding energy shifts are evidence of electron shifts occurring between Au and Pt due to a bi-metallic (Au-Pt) electronic interaction between the atomic orbitals of the 2 alloy components. A summary of all XPS peak assignments are presented in Table S2 in SI. The EDX and XPS data confirm that the Au-Pt alloy is formed both in the bulk and on the surface and that the alloy is spread uniformly throughout the surface of the deposited materials.

Although there is not a precise method for accurate determination of the electrochemical surface areas (ECSA) of Au-Pt alloys, cyclic voltammetry (CV) of a ferricyanide system (Randle-Sevcik method)³¹ has been previously used to estimate the ECSA of Au-Pt structures and was thus employed in this study. In Figure 3 it can be seen that there is a dramatic increase in the ECSA of the alloy surfaces when compared to the unmodified Au substrate. Given that the peak heights (I_p) in the CV are directly proportional to ECSA at constant scan rate, the I_p (obtained at a scan rate 100 mV \cdot s⁻¹) values were used to compare the surface areas between the electrodeposited surfaces. It was found that Au₁₀Pt₁ and Au₁₀Pt_{0.5} exhibited the largest ECSA, with Au₁₀Pt_{2.5} and Au₁₀Pt₅ having a comparatively smaller ECSA. The ECSA differences are due to the finer surface morphological and structural size differences that are observed in the SEM images in Figure 1. The Au₁₀Pt₁ and Au₁₀Pt_{0.5} surfaces show branching, dendritic structures, with well-defined branches with sharp edges, leading to a higher surface area than Au₁₀Pt_{2.5} and Au₁₀Pt₅, where the branching fine structure is not observed.

Electrochemical sensing of glucose.—Cyclic Voltammetry in the presence of glucose.—The developed materials were characterized electrochemically in order to determine the Au-Pt alloy honeycomb substrate that was most active toward glucose sensing. Due to the presence of Pt in the honeycomb surfaces, KOH was employed to increase the pH of the solution, which would be easy to undertake in real-world analysis. An alkaline solution is necessary for Pt based materials as the metal can easily be poisoned by intermediate species that form during electro-oxidation of glucose, and Pt can also generate products during electrochemical analysis in neutral solutions which suppresses activity.³² The reaction mechanism between Pt and glucose involves the initial chemisorption of glucose (referred to as the ‘dehydration’ step) which is quickly followed by adsorbed dehydrate intermediates oxidizing on the surface and forming weakly adsorbed gluconate. At higher potentials these adsorbed intermediates weaken in strength allowing for the dehydrogenated intermediates to oxidize to glucono- δ -lactone. As the glucono- δ -lactone slowly desorbs, gluconate is formed as the result of hydrolysis.³³ Au readily forms gold hydroxide in alkaline solutions due to the chemisorption of OH⁻ ions on the Au surface (Au + OH⁽¹⁻⁾ + λe^-)^{34,35} which occurs in the premonolayer oxidation region of the gold surface.¹² Figure 4a shows the CVs of modified Au (Au₁₀) and Au-Pt honeycomb (Au₁₀Pt_{0.5}) in a solution of 0.5 M KOH and 10 mM glucose. The CV profiles are used to determine the difference in oxidation and reduction peaks between plain Au and the Au-Pt alloy honeycomb structure. Furthermore, the potentials at different stages of glucose electrooxidation on the Au-Pt alloy surface (i.e. formation of intermediate species) can be observed. The CV profiles in a 0.5 M KOH and 10 mM glucose solution for each alloy substrate developed are presented in Figure S4 in SI. It can be observed that the current maxima on the CV profiles are dependent on the amount of Pt that was used in the electrolyte while depositing

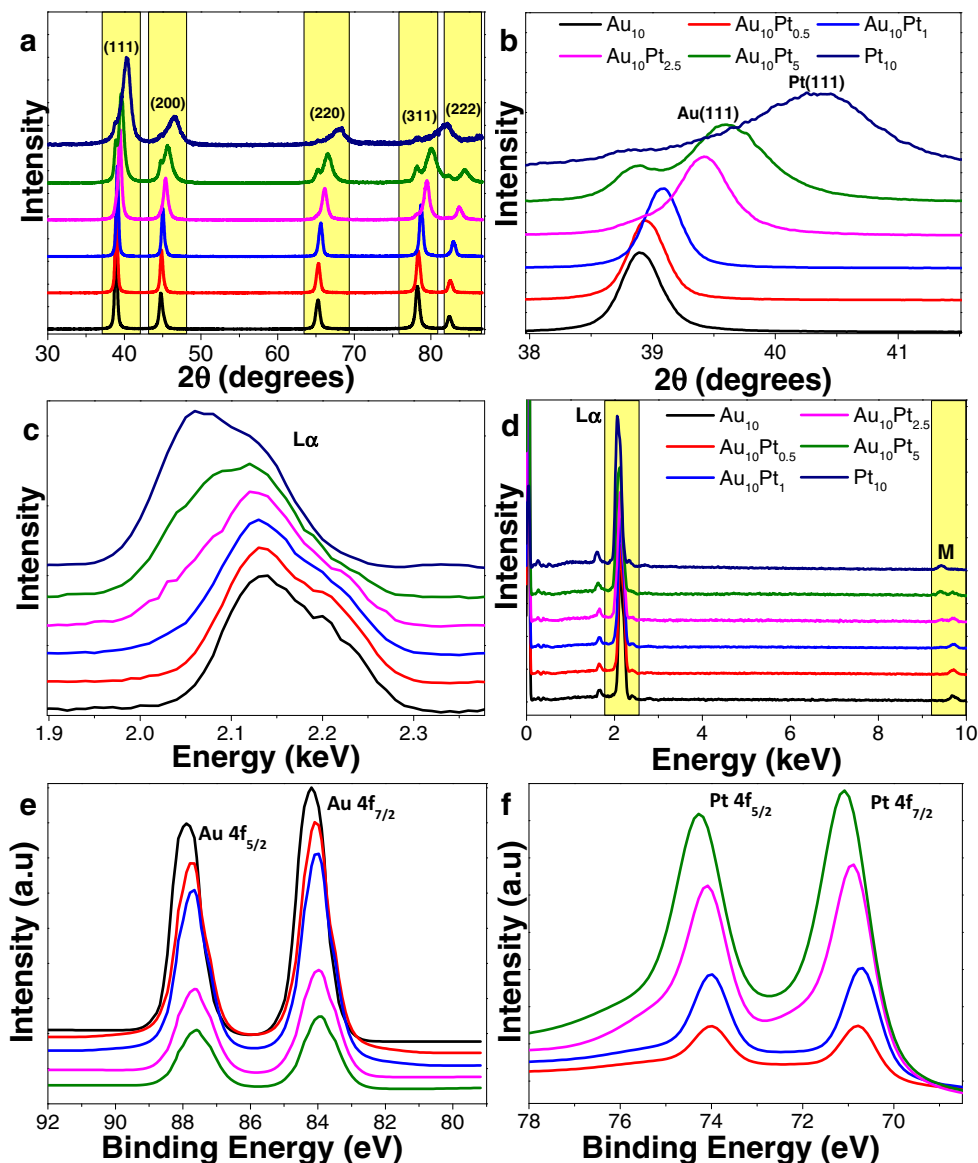


Figure 2. Characterization of Au-Pt honeycomb-like substrates (a) XRD analysis (b) magnified (111) peak of XRD pattern (c) EDX spectra (d) magnified $L\alpha$ peak at 2.15 keV of EDX spectra (e) XPS analysis of Au 4f and (f) XPS analysis of Pt 4f core levels. (Labels in XRD and EDX analysis (Figure 2a and 2c) are consistent for XPS characterization graphs).

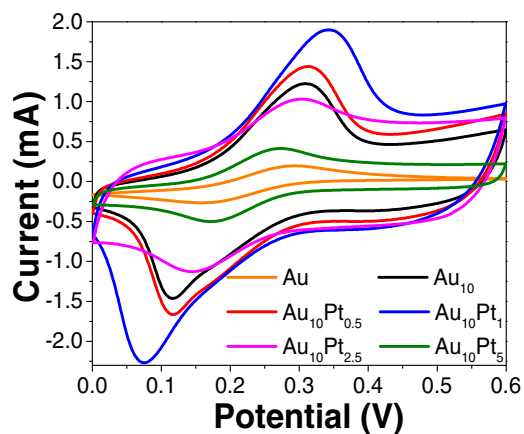


Figure 3. Cyclic voltammetry of all Au-Pt substrates in 10 mM $K_3Fe(CN)_6$ and 0.2 mM KCl at a scan rate of 50 mVs^{-1} .

the alloy structures. The Au-OH reduction peak at 0.15 V is visible for Pt concentrations of 0, 0.5, 1 and 2.5 mM however the CV for the surface prepared in the 5 mM Pt electrolyte no longer displays the Au-OH reduction peak due to the high Pt content. That is, Pt forms multiple glucose related intermediate species on the surface of the alloy which is thought to inhibit glucose from reaching the gold and undergoing surface oxide adsorption.^{18,36} Figure S5 in SI shows the CV sweep rate analysis of the optimal Au-Pt alloy ($Au_{10}Pt_1$) substrate where an increase in peak maximum was observed as the sweep rate increased. This relationship between peak height and scan rate shows that the reaction occurring between the Au-Pt alloy and glucose is a surface-controlled electrochemical process.²⁵

Chronoamperometric analysis in the presence of glucose.—The activity of the surfaces for glucose analysis was tested using chronoamperometry at various potentials (0, -0.1 and -0.2 V). These potentials were chosen based on the glucose oxidation/reduction peaks observed in the CV profiles (Figure 4a) discussed in Cyclic voltammetry in the presence of glucose section. These peaks are attributed to glucose

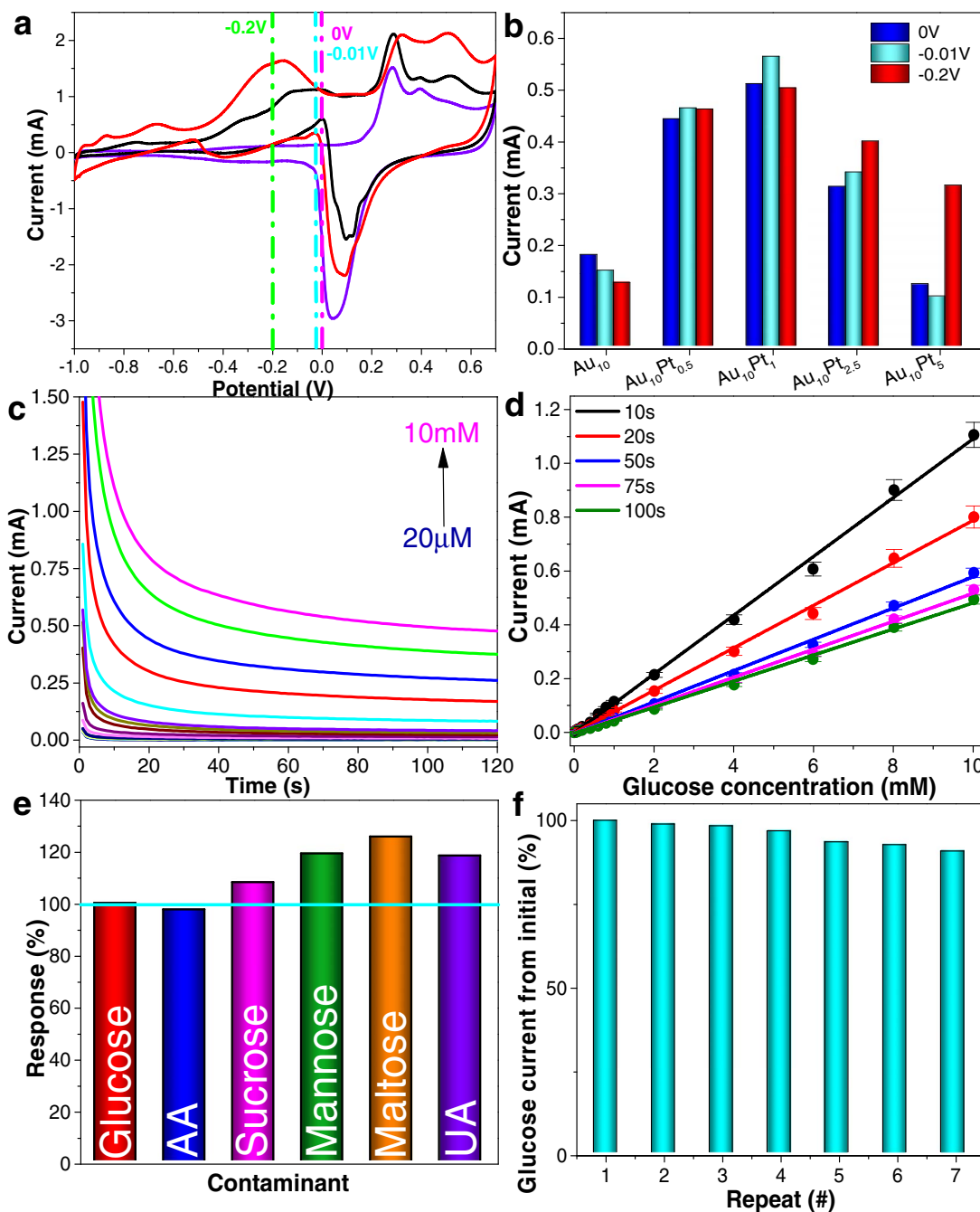


Figure 4. (a) CV analysis comparing Au₁₀ in 0.5 M KOH with 10 mM glucose (black) and Au₁₀Pt_{0.5} in 0.5 M KOH with (red) and without (purple) 10 mM glucose (b) Potential analysis of Au-Pt substrates at 0, -0.01 and -0.2 V (c) Chronoamperometric analysis of glucose additions for Au₁₀Pt₁ in 0.5 M KOH and increasing glucose concentrations (20 μ M–10 mM) with an applied potential of -0.01 V where the error bars represent 1 σ from seven separate testing events. (d) Calibration curves of additions analysis after 10, 20, 50, 75 and 100 s of stabilization (error bars are calculated due to standard deviation) (e) Selectivity analysis of Au₁₀Pt₁ after the addition of 10 mM glucose followed by 0.1 mM additions of acetic acid (AA), sucrose, mannose, maltose and 0.2 mM uric acid (UA) and (f) Current maximum from chronoamperometric responses in 10 mM glucose for 7 consecutive scans for Au₁₀Pt₁.

oxidation occurring at both active Au and Pt sites, as opposed to either the formation of Au-OH or Pt-OH at higher potentials.^{37,38} Furthermore, the adsorption of intermediates during glucose electrooxidation for Au-Pt alloys occurs at potentials more negative than pure gold alone,³⁹ therefore potentials lower than and including 0 V were selected. Figure 4b clearly demonstrates that Au₁₀Pt₁ has the highest glucose electrooxidation current compared to the other alloy samples. From the 3 potentials analyzed, -0.01 V displays the highest sensitivity when tested for a 10 mM glucose solution. The peak related to glucose oxidation occurs at 0 V, showing good sensitivity due to the

maximum peak height of Au and Pt-OH forming on the surface of the alloyed honeycombs. However when the onset potential applied sits just after the peak at -0.01 V, the sensitivity of the alloy is dramatically enhanced (Figure 4b). Furthermore, the increase in the response magnitude at -0.01 V was found to be ~3 times higher than that obtained for the control (Au₁₀) substrate. Given that only 55% increase in I_p value (shown in Figure 3) was observed for the same substrate (relative to the control (Au₁₀) substrate), the results are a clear indication that the high activity of the Au₁₀Pt₁ substrate is not solely due to the increase in ECSA but primarily due to the Au-Pt content of the alloy.

Table II. Comparison of the developed Au-Pt alloy honeycomb-like structures with recently reported materials for non-enzymatic electrochemical glucose sensing.

Electrode material	Sensitivity ($\mu\text{A} \cdot \text{mM}^{-1} \cdot \text{cm}^{-2}$)	LOD (μM)	Linear range (mM)	Operation potential (V)	Reference
Au nanocorals	22.6	10	0.05–30	+0.25 vs Ag/AgCl	25
Au nanospikes	91.8	20	0.02–10	+0.13 vs Ag/AgCl	47
Porous Au film	10.76	1	0.01–10	+0.1 V vs SCE	48
Pt nanoporous	37.5	50	0.05–30	−0.12 V vs Ag/AgCl	49
Porous Pt-Pd	20.1	n/a	0–12	−0.3 V vs Ag/AgCl	50
Au-Pt nanocorals	24.6	3.2	0.03–7.2	+0.4 V vs Ag/AgCl	51
Au-Pt-CNT	10.71	10	Up to 24.44	+0.3 V vs Ag/AgCl	39
Nanoporous PtAu	n/a	0.5	0.2–5.4	+0.6 V vs Ag/AgCl	18
Au-Pt honeycomb	109.3	12.9	0.020–10	−0.01 V vs Ag/AgCl	*This work

To examine the sensitivity and selectivity of the Au₁₀Pt₁ honeycomb alloy, chronoamperometric analysis was employed with a glucose addition concentration range of 20 μM –10 mM. The additions analysis (Figure 4c) displays excellent stability of the alloyed substrate after each addition and analysis times, where the more pronounced differences between each addition are shown in Figure S6 presented in the SI. Figure 4d shows the current vs glucose concentration calibration curves, with the current sampled at different times from chronoamperometric curves and have been analyzed for their sensitivity, limit of detection (LOD) and R² values as can be seen in Table S3 in SI. The sensitivity^{40,41} and limit of detection was calculated using the method of three standard deviation of the blank as reported in our previous sensing studies.^{42,43} From this data we can see that the sensing linearity is excellent (R² values >0.99) for all concentrations, across all analyzed time points ranging from 10 to 100 seconds. From the experimental concentrations analyzed we can determine the linear range of the Au-Pt honeycomb sensor is 20 μM –10 mM with a response time as low as 10 s. The calculated sensitivity of the Au-Pt honeycomb was determined to be 109.3 $\mu\text{A} \cdot \text{mM}^{-1} \cdot \text{cm}^{-2}$ after 10 s and 39.7 $\mu\text{A} \cdot \text{mM}^{-1} \cdot \text{cm}^{-2}$ after 100 s with a calculated LOD (limit of detection) of 12.9 μM (experimental data in Figure S7 in SI) and 9.1 μM respectively. The high sensitivity and low detection limit displayed by the Au-Pt alloy sensors can be attributed to the Pt component of the alloy as Pt displays very high sensitivity in glucose sensing.^{44–46} According to previous studies surface poisoning readily occurs on pure Pt surfaces however due to the alloying with Au, an improved selectivity of the sensor has been achieved as is demonstrated in Figure 4e. A comparison of the optimum sensor developed in this study (Au₁₀Pt₁) with that reported in literature is shown in Table II. It can be seen that the Au-Pt honeycombs displayed a similar linear concentration range to those sensors reported in previous studies, however with a much higher calculated sensitivity compared to other Au-Pt alloy based sensors. Furthermore, when comparing to the plain monoatomic Au structures, our developed sensor was able to achieve a large sensitivity at quite a low operational potential, which is also thought to be advantageous from a selectivity point of view. That is, the addition of physiological contaminants did not hinder the sensitivity of the sensors, and a good selectivity was displayed in the presence of physiological related species (see Figure 4e and dynamic response data in Figure S8 in SI). The data shows that physiological sugars such as ascorbic acid (AA), sucrose, mannose, maltose and uric acid (UA) appear to be the main component in reducing the sensors selectivity; however the main competing contaminants AA and UA appear to cause little-to-no change in the current response of the sensor in the presence of 10 mM glucose. The main contribution for this successful selectivity is the reduction in the on-set potential observed for the Au-Pt alloy. Lower applied potentials effectively improve selectivity in glucose sensors, therefore the fact our glucose sensor has improved sensitivity at such a low potential is promising for these types of materials in future glucose research.

Given the encouraging sensitivity and selectivity performance of the developed sensor, a series of 7 sensing events in a solution of 0.5 M KOH and 10 mM glucose were performed at −0.01 V for 100 s to determine the repeatability of Au₁₀Pt₁ which is shown in

Figure 4f (dynamic response data in Figure S9 in SI). The sensor was found to exhibit good reproducibility during repeated glucose sensing events with a coefficient of variance (CoV) calculated to be less than 8%, displaying 92% repeatability after 7 successive runs making this sensor highly reusable for glucose sensing applications.

Conclusions

We have presented Au-Pt honeycomb-like porous structures that can be employed as an electrode material for non-enzymatic electrochemical glucose sensing applications. The material was developed using the hydrogen bubble template method to form honeycomb nanostructures made of pure Au-Pt alloy, with both Au and Pt evenly dispersed throughout the material. A low detection limit of 12.9 μM was obtained, with a linear concentration range of 20 μM to 10 mM. Furthermore, a high sensitivity of 109.3 $\mu\text{A} \cdot \text{mM}^{-1} \cdot \text{cm}^{-2}$ after only 10 s of stabilization was also observed. The optimum material (Au₁₀Pt₁) showed good selectivity toward glucose and did not respond to other physiological species such as Ascorbic acid and biological sugars, making Au-Pt alloy honeycomb a promising non-enzymatic glucose sensor, and a versatile material well-suited to other electrocatalytic applications.

Acknowledgments

The authors acknowledge RMIT Microscopy and Microanalysis Facility (RMMF) for the help received from their technical staff and for allowing the use of their comprehensive facilities and services. The technical staff (Yuxun Cao and Paul Jones) at the Microelectronics Materials and Technology Centre is also acknowledged for the chemical vapour deposition of Au on Si substrates.

References

- S. P. Nichols, A. Koh, W. L. Storm, J. H. Shin, and M. H. Schoenfish, *Chem. Rev.*, **113**(4), 2528 (2013).
- J. Wang, *Chem. Rev.*, **108**(2), 814 (2008).
- P. Cryer, S. Davis, and H. Shamoon, *Diabetes care*, **26**(6), 1902 (2003).
- G. E. Umpierrez, S. D. Isaacs, N. Bazargan, X. You, L. M. Thaler, and A. E. Kitabchi, *J. Clin. Endocrinol. Metab.*, **87**(3), 978 (2002).
- X. Niu, L. Shi, H. Zhao, and M. Lan, *Analytical Methods*, **8**, 1755 (2016).
- L. C. Clark and C. Lyons, *Ann. N.Y. Acad. Sci.*, **102**(1), 29 (1962).
- G. Wang, X. He, L. Wang, A. Gu, Y. Huang, B. Fang, B. Geng, and X. Zhang, *Mikrochim. Acta*, **180**(3–4), 161 (2013).
- F. Xu, K. Cui, Y. Sun, C. Guo, Z. Liu, Y. Zhang, Y. Shi, and Z. Li, *Talanta*, **82**(5), 1845 (2010).
- S. Joo, S. Park, T. D. Chung, and H. C. Kim, *Anal. Sci.*, **23**(3), 277 (2007).
- H.-Y. Huang and P.-Y. Chen, *Talanta*, **83**(2), 379 (2010).
- J. Wang, *J. Pharm. Biomed. Anal.*, **19**(1–2), 47 (1999).
- K. E. Toghill and R. G. Compton, *Int. J. Electrochem. Sci.*, **5**(9), 1246 (2010).
- G. Sanz , I. Taurino, R. Antiochia, L. Gorton, G. Favero, F. Mazzei, G. De Micheli, and S. Carrara, *Bioelectrochemistry*, **112**, 125 (2016).
- Y. B. Vassilyev, O. A. Khazova, and N. N. Nikolaeva, *J. Electroanal Chem Interfacial Electrochem.*, **196**(1), 127 (1985).
- R. R. Adzic, M. W. Hsiao, and E. B. Yeager, *J. Electroanal Chem Interfacial Electrochem.*, **260**(2), 475 (1989).
- S. Ernst, J. Heitbaum, and C. H. Hamann, *J. Electroanal Chem Interfacial Electrochem.*, **100**(1), 173 (1979).
- Y. Sun, H. Buck, and T. E. Mallouk, *Anal. Chem.*, **73**(7), 1599 (2001).

18. J. Wang, H. Gao, F. Sun, and C. Xu, *Sens. Actuator B-Chem.*, **191**, 612 (2014).
19. B. Z. Zeng, S. H. Wei, F. Q. Zhao, and Q. L. Zou, *Wuhan University Journal (Natural Science Edition)*, **2**, 7 (2005).
20. M. Ranjani, Y. Sathishkumar, Y. S. Lee, D. J. Yoo, and A. R. Kim, *RSC Advances*, **5**(71), 57804 (2015).
21. Y. Sun, H. Yang, X. Yu, H. Meng, and X. Xu, *RSC Advances*, **5**(86), 70387 (2015).
22. H. Mei, W. Wu, B. Yu, H. Wu, S. Wang, X. Zhang, and Q. Xia, *Electroanalysis*, **28**, 671 (2015).
23. M. Jafarian, F. Forouzandeh, I. Danaee, F. Gobal, and M. Mahjani, *J. Solid State Electrochem.*, **13**(8), 1171 (2009).
24. J. Wang, D. F. Thomas, and A. Chen, *Anal. Chem.*, **80**(4), 997 (2008).
25. T.-M. Cheng, T.-K. Huang, H.-K. Lin, S.-P. Tung, Y.-L. Chen, C.-Y. Lee, and H.-T. Chiu, *ACS Appl. Mater. Interfaces*, **2**(10), 2773 (2010).
26. B. J. Plowman, L. A. Jones, and S. K. Bhargava, *Chem. Commun.*, **51**(21), 4331 (2015).
27. S. Cherevko and C.-H. Chung, *Electrochem. Commun.*, **13**(1), 16 (2011).
28. Y. Li, W.-Z. Jia, Y.-Y. Song, and X.-H. Xia, *Chem. Mater.*, **19**(23), 5758 (2007).
29. T.-M. Tseng, R.-H. Huang, C.-Y. Huang, K.-L. Hsueh, and F.-S. Shieu, *J. Electrochem. Soc.*, **160**(4), A690 (2013).
30. S. Zhou, G. S. Jackson, and B. Eichhorn, *Adv. Funct. Mater.*, **17**(16), 3099 (2007).
31. L. Yuan, M. Yang, F. Qu, G. Shen, and R. Yu, *Electrochim. Acta*, **53**(10), 3559 (2008).
32. S. C. Chang, L. W. H. Leung, and M. J. Weaver, *J. Phys. Chem.*, **94**(15), 6013 (1990).
33. S. Park, H. Boo, and T. D. Chung, *Anal. Chim. Acta*, **556**(1), 46 (2006).
34. M. Hsiao, R. Adžić, and E. Yeager, *J. Electrochem. Soc.*, **143**(3), 759 (1996).
35. Y. B. Vassilyev, O. Khazova, and N. Nikolaeva, *J. Electroanal. Chem. Interfacial Electrochem.*, **196**(1), 127 (1985).
36. H. Qiu and X. Huang, *J. Electroanal. Chem.*, **643**(1–2), 39 (2010).
37. A. Habrioux, E. Sibert, K. Servat, W. Vogel, K. B. Kokoh, and N. Alonso-Vante, *J. Phys. Chem. B*, **111**(34), 10329 (2007).
38. F. Xiao, F. Zhao, D. Mei, Z. Mo, and B. Zeng, *Biosens. Bioelectron.*, **24**(12), 3481 (2009).
39. J. Ryu, K. Kim, H.-S. Kim, H. T. Hahn, and D. Lashmore, *Biosens. Bioelectron.*, **26**(2), 602 (2010).
40. K. M. Kabir, Y. M. Sabri, A. E. Kandjani, G. I. Matthews, M. Field, L. A. Jones, A. Nafady, S. J. Ippolito, and S. K. Bhargava, *Langmuir*, **31**(30), 8519 (2015).
41. K. M. Kabir, Y. M. Sabri, G. I. Matthews, L. A. Jones, S. J. Ippolito, and S. K. Bhargava, *Analyst*, **140**(16), 5508 (2015).
42. Y. M. Sabri, A. E. Kandjani, S. J. Ippolito, and S. K. Bhargava, *Sci. Rep.*, **6**, (2016).
43. Y. M. Sabri, A. E. Kandjani, S. J. Ippolito, and S. K. Bhargava, *ACS Appl. Mater. Interfaces*, **7**(3), 1491 (2015).
44. H.-W. Lei, B. Wu, C.-S. Cha, and H. Kita, *J. Electroanal. Chem.*, **382**(1–2), 103 (1995).
45. L.-Q. Rong, C. Yang, Q.-Y. Qian, and X.-H. Xia, *Talanta*, **72**(2), 819 (2007).
46. V. R. Stamenkovic, B. S. Mun, M. Arenz, K. J. Mayrhofer, C. A. Lucas, G. Wang, P. N. Ross, and N. M. Markovic, *Nat. Mater.*, **6**(3), 241 (2007).
47. V. E. Coyle, A. E. Kandjani, Y. M. Sabri, and S. K. Bhargava, *Electroanalysis* (2016).
48. L. Han, S. Zhang, L. Han, D.-P. Yang, C. Hou, and A. Liu, *Electrochim. Acta*, **138**, 109 (2014).
49. Y.-J. Lee, D.-J. Park, J.-Y. Park, and Y. Kim, *Sensors*, **8**(10), 6154 (2008).
50. X. Niu, H. Zhao, C. Chen, and M. Lan, *ChemCatChem*, **5**(6), 1416 (2013).
51. Y. Liu, Y. Ding, Y. Zhang, and Y. Lei, *Sens. Actuator B-Chem.*, **171**, 954 (2012).

Supporting Information

Hydrogen bubble templated growth of Au-Pt alloy honeycomb-like films for non-enzymatic glucose sensing

Victoria E. Coyle^a, Daniel K. J. Oppedisano^a, Lathe A. Jones^a, Ahmad Esmailzadeh

Kandjani,^{a*} Ylias M. Sabri^a and Suresh K. Bhargava^{a*}

*Email: ahmad.kandjani@rmit.edu.au, suresh.bhargava@rmit.edu.au, Ph: +61 3 99252330

^a *Centre for Advanced Materials & Industrial Chemistry (CAMIC), School of Science, RMIT*

University, Melbourne, Victoria 3001, Australia

**RECEIVED DATE (to be automatically inserted after your manuscript is accepted if required
according to the journal that you are submitting your paper to)**

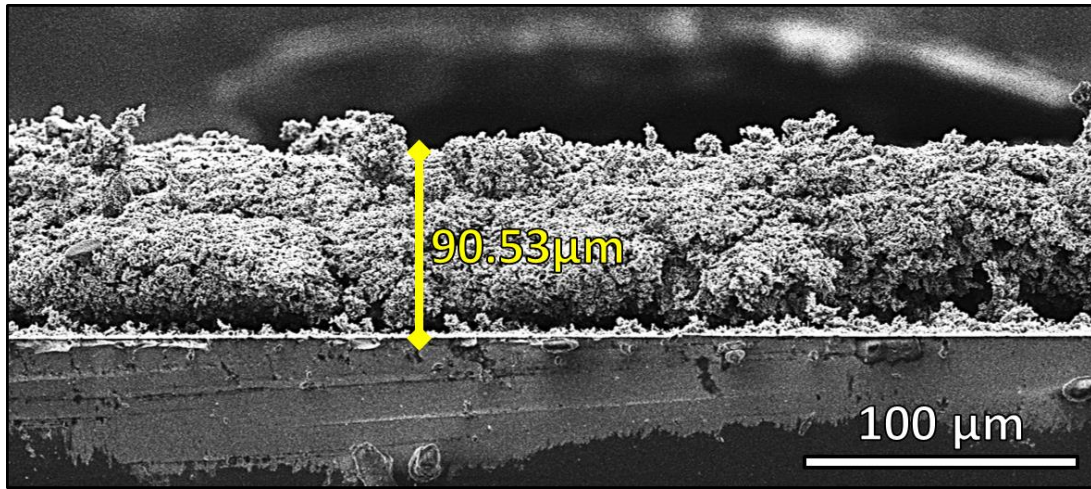


Figure S1. SEM image of Au₁₀Pt₁ at a 90° angle showing the thickness of the electrodeposited Au-Pt alloy honeycomb

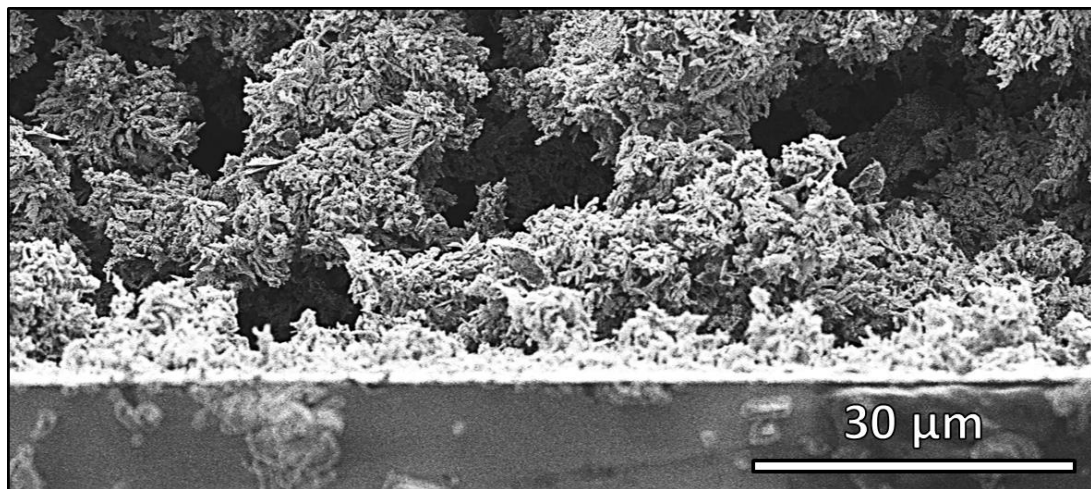


Figure S2. SEM image of Au₁₀Pt₁ at a 90° angle showing the porous structure of the Au-Pt alloy deposition to the substrate.

	XRD analysis			2 θ values	
	(111)	(200)	(220)	(311)	(222)
Au₁₀Pt	38.89	44.73	65.26	78.19	82.37
Au₁₀Pt_{0.5}	38.94	44.85	65.36	78.32	82.53
Au₁₀Pt₁	39.09	45.01	65.63	78.69	82.92
Au₁₀Pt_{2.5}	39.42	45.41	66.17	79.48	83.68
Au₁₀Pt₅	39.59	45.62	66.55	80.15	84.5
Pt₁₀	40.31	46.48	68.24	82.19	n/a

Table S1. XRD analysis 2 θ values for all analysed substrates as well as Au₀Pt₁₀ as a pure Pt reference

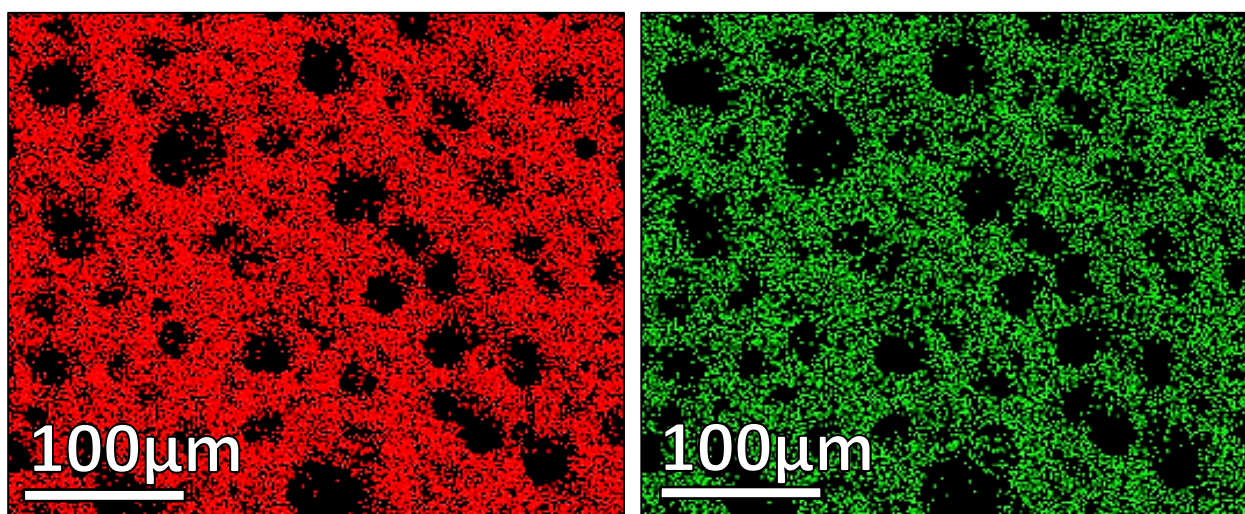


Figure S3. EDX mapping of Au₁₀Pt₁ showing Au(red) and Pt(green) present in the surface of the electrodeposited material

	XPS analysis		Binding energy (eV)	
	Au _(7/2)	Au _(5/2)	Pt _(7/2)	Pt _(5/2)
Au ₁₀	84.19	87.89	n/a	n/a
Au ₁₀ Pt _{0.5}	84.09	87.78	70.78	73.98
Au ₁₀ Pt ₁	83.97	87.66	70.80	73.98
Au ₁₀ Pt _{2.5}	83.96	87.65	70.88	74.08
Au ₁₀ Pt ₅	83.88	87.59	71.08	74.28

Table S2. XPS analysis binding energies for all analysed substrates

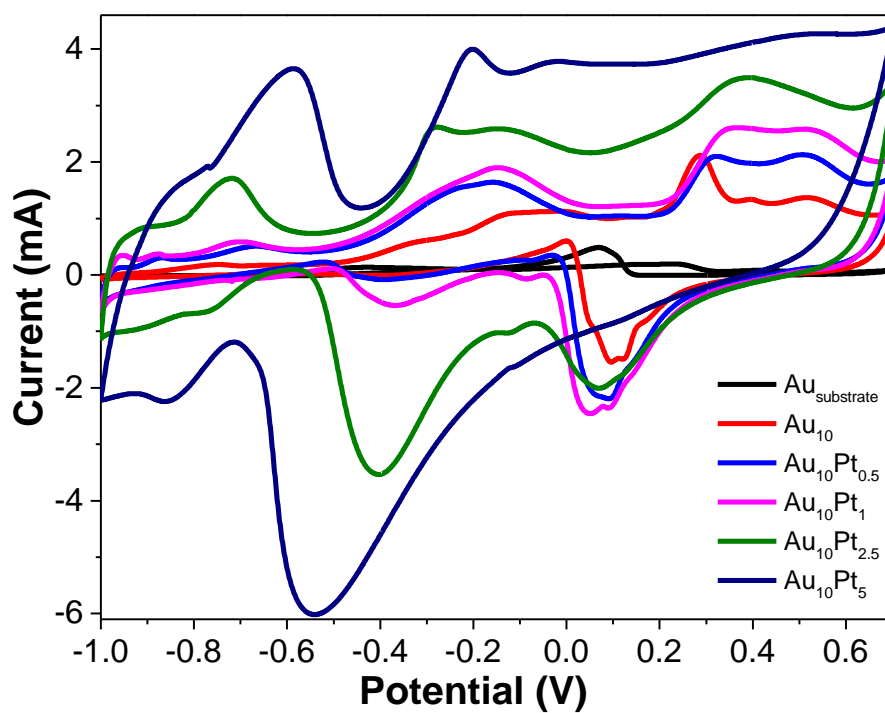


Figure S4. CV analysis of all samples in 0.5M KOH and 10mM glucose solution

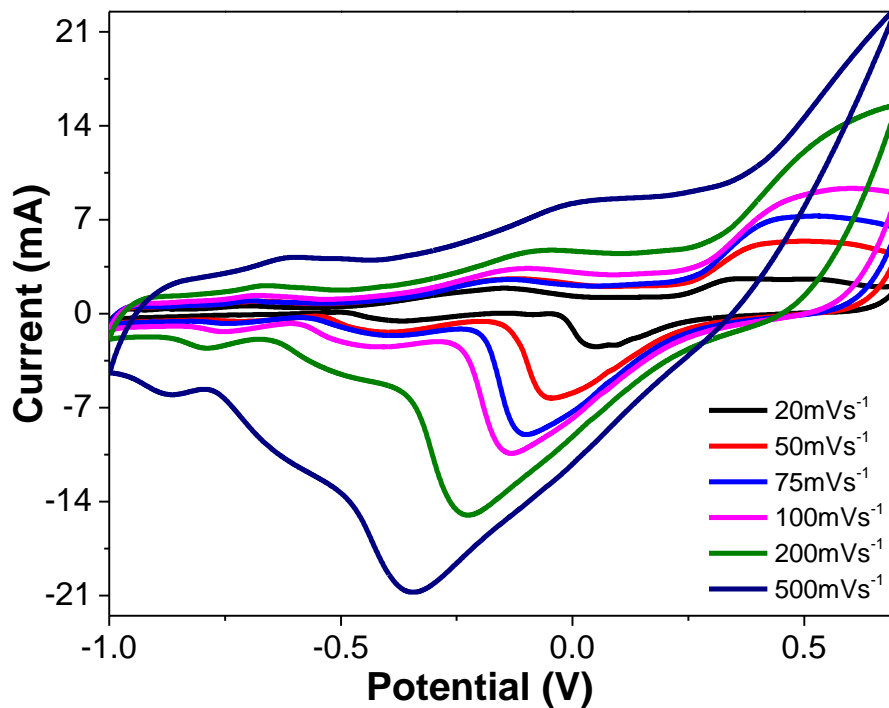


Figure S5. Cyclic Voltammetry (CV) analysis of Au₁₀Pt₁ in the presence of 0.5M KOH and 10mM glucose at sweep rate values of 20, 50, 75, 100, 200 and 500 mVs⁻¹

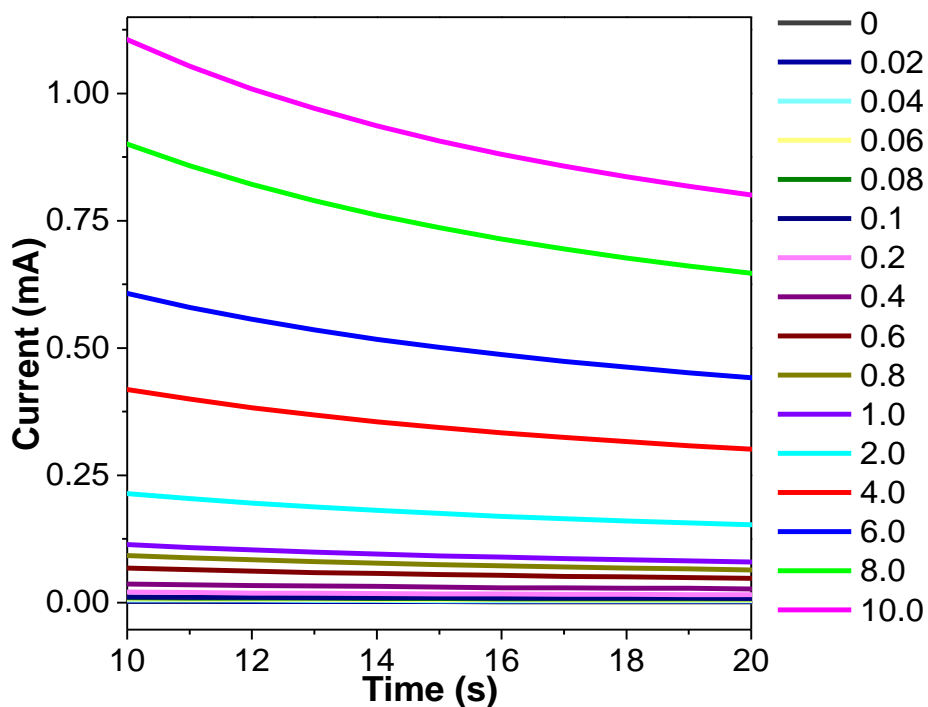


Figure S6. Chronoamperometric analysis of glucose additions in the concentration range between 20µM and 10mM. The legend details the concentration of each addition in mM.

Time (s)	Sensitivity ($\mu\text{A}\cdot\text{mM}^{-1}\cdot\text{cm}^{-2}$)	R ² (value)	LOD (calculated)
10	110	0.997	12.9
20	79	0.998	9.9
50	58	0.997	12.0
75	52	0.998	7.4
100	48	0.997	9.1

Table S3. Comparison table of glucose additions analysis and their calibration curves at difference times for sensitivity, R² value and limit of detection (LOD).

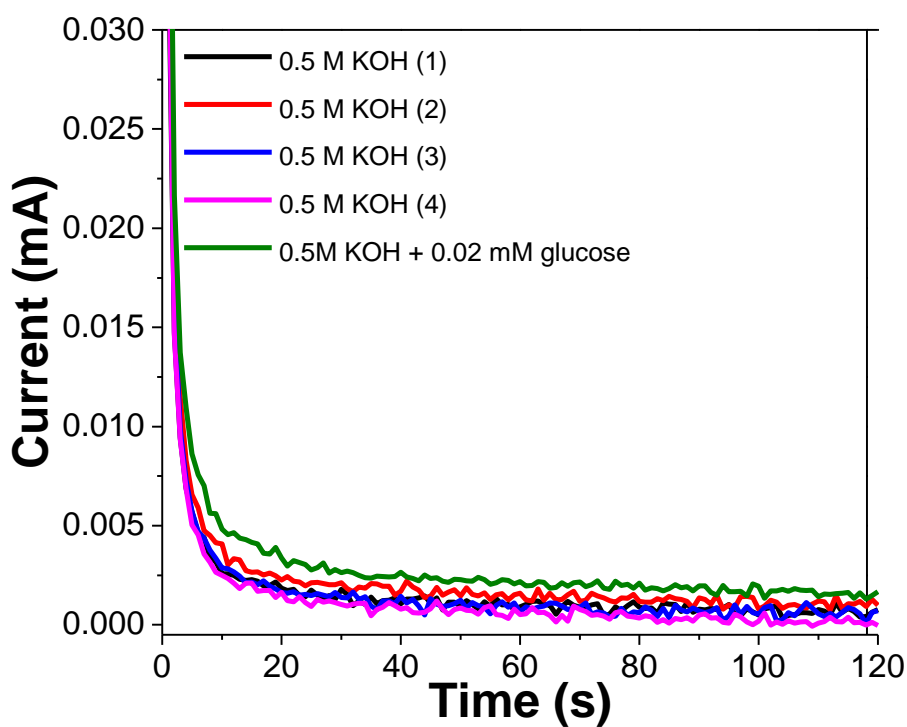


Figure S7. Experimental chronoamperometric analysis for determining the detection limit for Au₁₀Pt₁ in the presence of 0.5M KOH for 4 repetitions following by an addition of 0.02 mM glucose

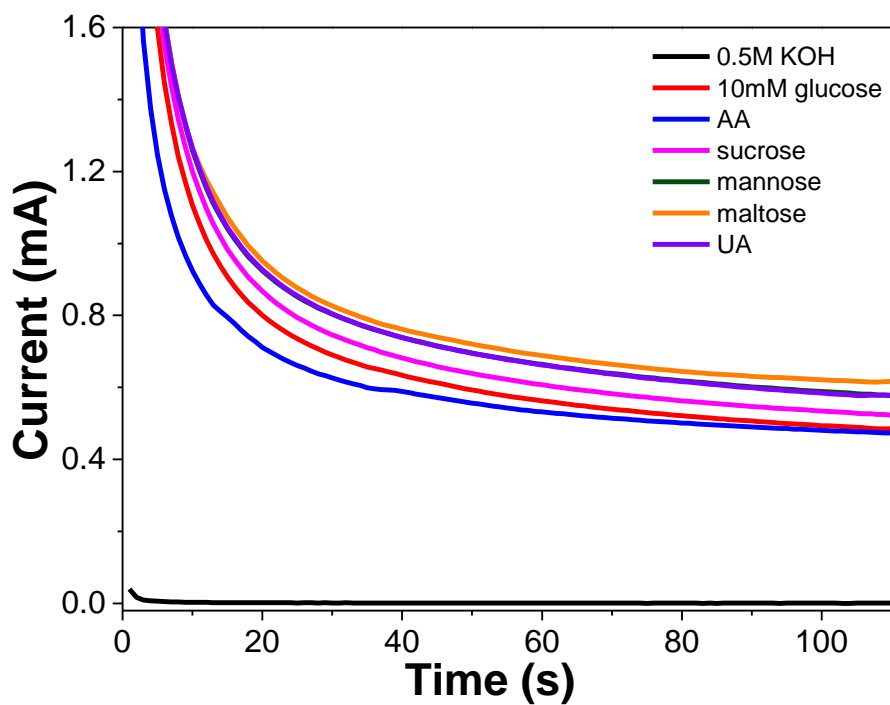


Figure S8. Experimental chronoamperometric analysis for determining selectivity of $Au_{10}Pt_1$ in the presence of glucose, acetic acid (AA), sucrose, mannose, maltose and Uric acid (UA)

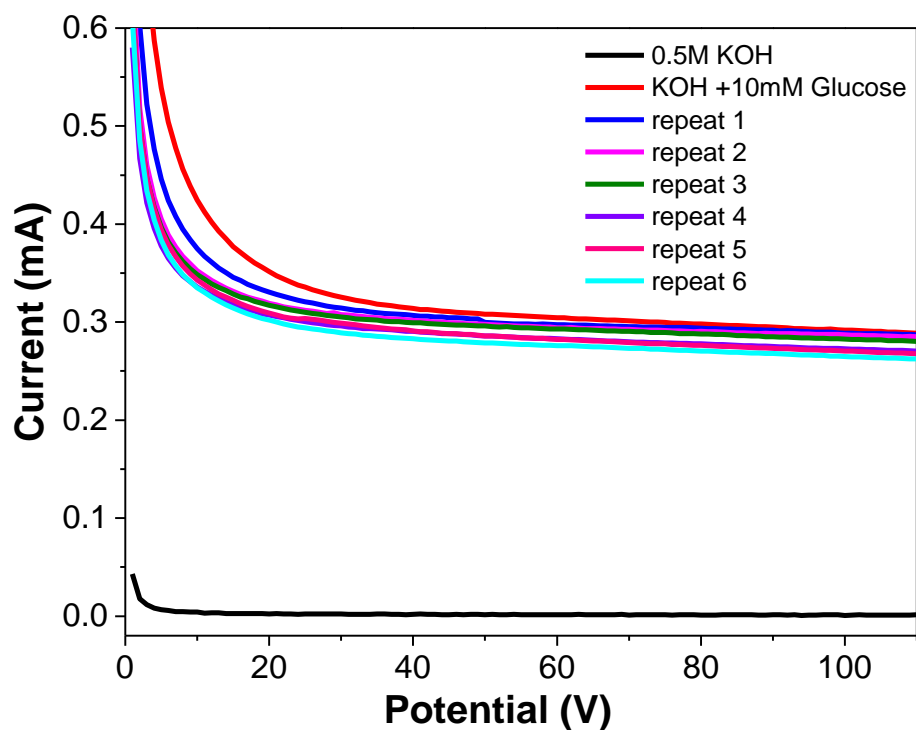


Figure S9. Experimental chronoamperometric analysis for determining repeatability for $Au_{10}Pt_1$ in the presence of 0.5M and 10mM glucose for 6 repetitions



CHAPTER V:

Nickel–gold bimetallic monolayer colloidal crystals fabricated via galvanic replacement as a highly sensitive electrochemical sensor

In this chapter bimetallic Ni–Au monolayer colloidal crystals (MCCs) were fabricated by galvanic replacement of Ni monolayers with Au salt. The influence of Au concentration used in the galvanic replacement solutions on the morphology and structure of the resulting Ni–Au surface is studied. It was found that the use of monolayer colloidal crystals, which display cohesive structure formations across the monolayer, results in the galvanic replacement reaction occurring more evenly over the surface when compared to the thin film counterpart. The fabricated devices were analyzed under alkaline conditions using chronoamperometric techniques to detect glucose concentrations ranging between 20 μM and 10 mM. The optimum Ni–Au MCC substrate was produced using 0.1 mM Au salt solution and showed a very low experimental detection limit of 14.9 μM and a calculated sensitivity of 506 $\mu\text{A}\cdot\text{mM}^{-1}\cdot\text{cm}^{-2}$, which was ~ 3 times larger than that of the plain Ni MCC substrate. The Ni–Au MCC substrate also showed minimal current response changes in the presence of common physiological contaminants, thus being a highly selective electrochemical glucose sensor.

Cite this: *J. Mater. Chem. B*, 2017,
5, 5441

Nickel–gold bimetallic monolayer colloidal crystals fabricated *via* galvanic replacement as a highly sensitive electrochemical sensor†

Bebeto Lay,‡ Victoria E. Coyle,‡ Ahmad Esmailzadeh Kandjani,*
Mohamad H. Amin,  Ylias M. Sabri and Suresh K. Bhargava 

Bimetallic Ni–Au monolayer colloidal crystals (MCCs) were fabricated by galvanic replacement of Ni monolayers with Au salt. The influence of Au concentration used in the galvanic replacement solutions on the morphology and structure of the resulting Ni–Au surface is studied. It was found that the use of monolayer colloidal crystals, which display cohesive structure formations across the monolayer, results in the galvanic replacement reaction occurring more evenly over the surface when compared to the thin film counterpart. The fabricated devices were analyzed under alkaline conditions using chronoamperometric techniques to detect glucose concentrations ranging between 20 μM and 10 mM. The optimum Ni–Au MCC substrate was produced using 0.1 mM Au salt solution and showed a very low experimental detection limit of 14.9 μM and a calculated sensitivity of 506 $\mu\text{A mM}^{-1} \text{cm}^{-2}$, which was ~ 3 times larger than that of the plain Ni MCC substrate. The Ni–Au MCC substrate also showed minimal current response changes in the presence of common physiological contaminants, thus being a highly selective electrochemical glucose sensor.

Received 24th February 2017,
Accepted 7th June 2017

DOI: 10.1039/c7tb00537g

rsc.li/materials-b

Introduction

Bimetallic materials have recently come under intense focus due to their notable electronic, optical, catalytic and sensing properties.^{1,2} Bimetallic nanomaterials are easily fabricated by utilizing a galvanic replacement (GR) reaction^{3,4} which is a facile and versatile method.⁵ As a GR reaction involves the replacement of surface atoms, hollow structures with modified surfaces are able to form, thus, bimetallic surfaces resulting from GR usually have high surface areas⁴ and an increased number of active sites, inducing higher activity toward catalysis and chemical sensing applications.⁴ As bimetallic structures can be controlled based on the types of components and percentages of each metal in the GR solution, the substrates can be tailor-designed to be selective towards specific analytes for chemical sensing applications.^{6–8} Although sensors with high sensitivity and selectivity can be made by employing a GR reaction, the reaction usually initiates at sites that possess relatively higher surface energies. That is, the reaction nucleation of alloying and bimetallic metal deposition on the surface of

the sacrificial template occurs at arbitrary sites which exhibit the highest surface energies *i.e.* defect sites, stacking faults and surface roughness.^{9,10} This phenomenon has thus far been a limitation in obtaining uniform particle decoration *via* the GR reaction due to the lack of control of the reaction sites.¹¹ To obtain a degree of uniformity in particle decoration (required for sensor substrates), it is first necessary to develop even and controlled distribution reaction site arrays on the surface before the galvanic replacement reaction. This uniformity and distribution of reaction site arrays can be obtained through the use of ordered close-packed colloidal crystals. These colloidal crystals have even curvature on their individual surface, while forming ordered arrays throughout the surface, thus providing multiple even reactions sites for an even deposition of metal through galvanic replacement reaction.

Lithography methods such as focused ion beam (FIB) and electron beam lithography (EBL) are typically used for well-ordered nanostructures; however, due to their time consuming and costly processes, they are unsuitable for the fabrication of nanostructures across large surface areas.^{12–14} The aforementioned fabrication methods have been stated to damage the formed nanostructures throughout the etching processes.¹³ As an alternative to FIB and EBL methods, colloidal lithography is a cheap, convenient and precise method of packing ordered materials with a controlled orientation and distribution of monodispersed materials.^{15,16} This type of lithography process

Centre for Advanced Materials and Industrial Chemistry (CAMIC), School of Applied Sciences, RMIT University, GPO Box 2476 V, Melbourne, Victoria 3001, Australia. E-mail: ahmad.kandjani@rmit.edu.au, suresh.bhargava@rmit.edu.au; Tel: +61 3 99252330

† Electronic supplementary information (ESI) available. See DOI: 10.1039/c7tb00537g

‡ B. L. and V. E. C. made equal contribution.

involves the self-assembly of colloids such as polystyrene (PS) nanospheres,^{17,18} a low-cost monodispersed material as a template for producing numerous closely packed and ordered structures, thereby allowing for the formation of various photonic crystals (PCs).^{19,20} Self-assembly of PS spheres can be controlled to form specific patterns that are ordered with homogeneous size, spacing and morphology²¹ across large substrate areas. The ordered structures formed have previously shown great success in applications such as photonic waveguides, optical filters and chemical sensors.^{22–26} However, such ordered structures have not yet been employed for promoting homogeneous decoration of nanoparticles on individual colloids in a PC using galvanic replacement reaction to form bimetallic structures.

In this paper, we aimed to control Au nanoparticles on a Ni film which was deposited on a PS based colloidal crystal template using the GR reaction as an enhanced non-enzymatic electrochemical glucose sensor. Both Ni^{27–29} and Au^{30–32} have previously been shown to be important elements for the development of highly selective and sensitive non-enzymatic electrochemical glucose sensors. Ni based structures are one of the most common materials employed for enhancements in glucose electrooxidation and therefore sensitivity when compared to other metal-based non-enzymatic glucose sensors.^{33–36} On the other hand, the introduction of a noble metal such as Au has been demonstrated to reduce interference from physiological contaminants and increase the selectivity of the sensor towards glucose.^{37,38} The use of Ni–Au bimetallic structures on the sensor electrode is postulated to drastically increase both the sensitivity and selectivity of electrochemical based glucose sensors. Furthermore, the developed surfaces with controlled particle size, number density and homogeneous decoration of Au nanoparticles on Ni coated PS colloids hold great promise for other chemical sensor applications.

Experimental

Chemicals

All chemicals were used as received from Sigma-Aldrich.

Synthesis of polystyrene colloids

Polystyrene colloids (PSCs) were synthesized as described in our previous work with small modifications.¹⁷ 200 mg of polyvinylpyrrolidone (PVP) was dissolved in 20 mL ethanol solution under nitrogen atmosphere, and then 2 mL of styrene was injected into the solution at 70 °C under constant stirring at 1500 rpm. A 20 mL ethanolic solution containing 28 mg of initiator (azobisisobutyronitrile (AIBN)) was then added to the reaction system which was kept at a constant temperature of 70 °C for 24 h. The produced PSCs were mono-dispersed and had a size distribution of 1300 nm. The formed colloids were washed several times and finally dispersed in 25 mL of ethanol.

Ti substrate fabrication

Silicon wafers were cleaned, followed by deposition of 300 nm Ti (Balzers, BAK 600) using e-beam evaporation. After deposition,

a thin protective layer of photoresist was spin coated on the wafer surface before being diced into rectangular substrates with dimensions of 12 mm (length) × 6.5 mm (width).

Ni–Au based electrode fabrication

The Ti based substrates (electrodes) were modified with a polystyrene monodispersed colloid monolayer (PS-MCM) using the procedure described elsewhere.¹⁷ Briefly, a suspension of polystyrene colloids (20 μL) was formed at the water/air interface in a glass Petri dish and SDS (sodium dodecyl sulfate) (20 mg mL⁻¹) was added to form a close-packed monolayer arrangement. The photoresist on the Ti electrode surfaces was removed and the close-packed monolayer was transferred from the Petri dish onto the electrode surface directly. The surfaces were then dried under N₂ gas for a period of ~20 minutes. Thereon, a 150 nm layer of Ni was deposited on the PS-MCM layer using the e-beam deposition technique. A galvanic replacement (GR) reaction was then performed on the modified electrode surfaces by placing them in 2 mL of HAuCl₄ (concentrations of 0.01 mM, 0.1 mM, 1 mM and 2 mM) for a period of 10 minutes, thereby forming a close-packed monolayer of bimetallic Ni–Au based electrochemical sensors.

Surface characterization

The morphological studies were performed by scanning electron microscopy (SEM) using an FEI Nova NanoSEM instrument. Elemental spectra and maps were collected by energy-dispersive X-ray spectroscopy (EDS) using an Oxford X-MaxN 20 EDX detector in conjunction with the FEI Nova NanoSEM. D8 Discover micro X-ray diffraction (XRD) with a general area detector diffraction system (GADDS) was used for crystal structure studies. The surface chemical state and/or species of the samples were analyzed by X-ray photoelectron spectroscopy (XPS) using a Thermo K-alpha X-ray photoelectron spectrometer at a pressure above 10⁻⁹ Torr (monochromatized Al Kα). The adventitious carbon binding energy (carbon at 285 eV) was used to align the core binding energies. High-resolution transmission electron microscopy (HR-TEM) was performed using a JEOL 2100F operating at an accelerating voltage of 200 kV. The instrument was equipped with a Gatan Orius SC1000 charge-coupled device (CCD) camera for standard imaging and an EDS spectrometer (Oxford XMax80T) which was used for elemental mapping in STEM mode.

Glucose sensing

Cyclic voltammetry (CV) analysis was performed using a CH instruments (CHI760C) electrochemical analyzer implementing a solution of 0.5 M KOH with the addition of 10 mM D-(+)-glucose at a constant sweep rate of 20 mV s⁻¹. Chronoamperometric addition analysis was performed at a constant applied potential of +0.55 V for 100 s intervals with glucose additions up to a concentration of 10 mM. The selectivity performance of the developed electrodes toward glucose were determined by adding 0.1 mM sucrose, fructose and acetic acid as well as 0.02 mM uric acid followed by the addition of 10 mM glucose in the KOH electrolyte solution.

Results and discussion

Fig. 1 shows the SEM characterization of the developed surfaces with each panel representing the images of two different magnifications of the monodisperse polystyrene monolayer which has undergone a galvanic replacement reaction with Au. The PS Ni-MCM template (referred to as Ni colloids) is shown in Fig. 1a and its corresponding fast Fourier transform (FFT) pattern is presented in Fig. 1b. It can be observed that the colloids are monodispersed with sizes of $1.3 \pm 0.02 \mu\text{m}$. The FFT pattern confirms the long-range hexagonally ordered structure with point group D6 and plane group $p6mm$, both indicative of highly close-packed ordering of the colloidal template.³⁹ After the GR reaction of the Ni colloid based substrate with Au salt at concentrations of 0 mM (no reaction, Ni colloids), 0.01 mM (Ni-Au_{0.01mM}), 0.1 mM (Ni-Au_{0.1mM}), 1 mM (Ni-Au_{1mM}) and 2 mM (Ni-Au_{2mM}) HAuCl₄ salt solution for 10 minutes, it can be observed that a small nucleation of Au nanoparticles starts to form on each of the Ni colloids in a homogenous fashion at the lower concentrations of 0.01 mM (Fig. 1c) and 0.1 mM (Fig. 1d). At a higher concentration of 1 mM (Fig. 1e), the particles are observed to have increased significantly in size; however the number density of particles appears to decrease. The deposition

of the Au nanoparticles is highly concentrated over the sphere junctions which act as active sites for the colloidal surface. Furthermore, at an Au concentration of 2 mM (Fig. 1f), the Au deposition dramatically increases with complete coverage on the outer edges of the polystyrene structures, overwhelming the Ni colloid structure. This change in deposition location during GR reaction may be due to the immiscibility between Ni and Au. At lower concentrations (0 mM, 0.01 mM and 0.1 mM), the whole Ni surface on each colloid can act as reaction sites for Au deposition, as the rate of deposition would be slow causing small particles to form across multiple reaction sites on the surface. When the concentration increases (1 mM and 2 mM), the Au nanoparticles prefer electron transfer through the formed Au nanoparticles on the surface. This interaction causes the galvanic replacement to form bigger particles with dendritic and irregular shapes whilst the growth is preferred on a pre-formed seed particle. These particles are formed on top of each other making large aggregates of Au nanoparticles atop the Ni structure as opposed to the individual particles formed at lower Au concentrations.

To determine the crystallographic nature of the deposited Au nanoparticles and to confirm the existence of the Ni-Au bimetallic microstructures, XRD analysis was performed. All the spectra were normalized to the Ni(200) peak. Fig. 2a and b show the XRD patterns of Ni-ctrl, Au-ctrl and all of the galvanically replaced samples obtained using a GAADS detector. As can be seen from Fig. 2a, after GR a peak at 39° appears which is associated with the formation of the Au(111) peak in the structure. Fig. 2b shows the Au(200)/Ni(111) peaks where a constant shift towards the Au(200) peak (for the GR structures) can be observed. As nickel and gold have limited solubility at room temperature,⁴⁰ the small shift in the XRD spectra can be

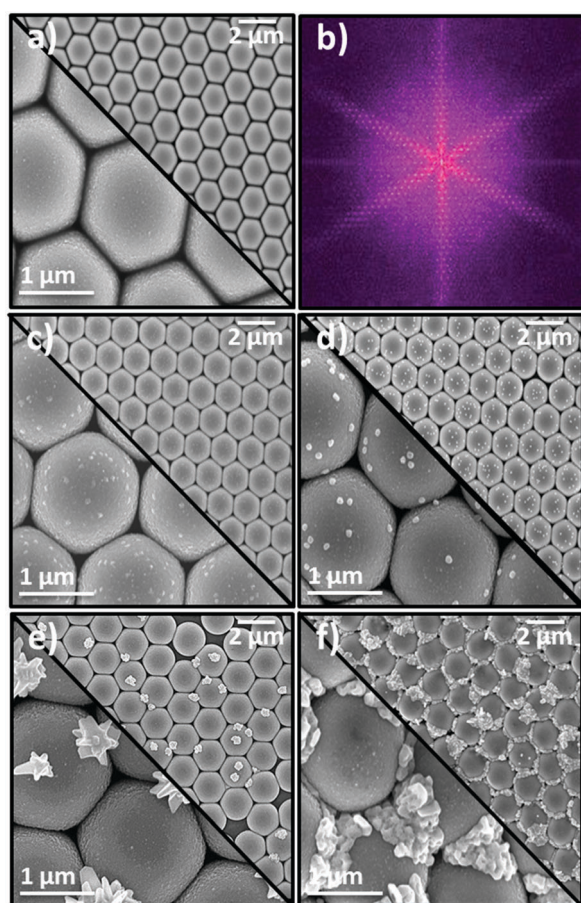


Fig. 1 (a) SEM image and (b) Fast Fourier Transform pattern (FFT) of Ni colloid surface. SEM images of Ni-Au surfaces after a 10 min GR reaction at an Au concentration of (c) 0.01 mM, (d) 0.1 mM, (e) 1 mM and (f) 2 mM.

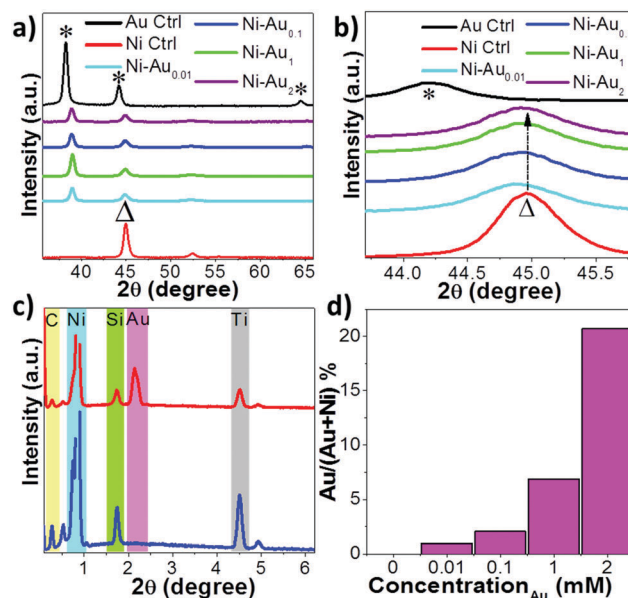


Fig. 2 XRD pattern of (a) Ni-ctrl, Au-ctrl and modified samples; (b) expanded region covering the Au(200)/Ni(111) peaks; (c) EDX spectra of Ni-ctrl (blue) and Ni-Au_{1mM} (red) bimetallic samples; (d) atomic ratio Au/(Au + Ni) vs. gold concentration used in the GR reaction: * is attributed to Au peaks and Δ is attributed to Ni peaks.

related to the formation of small amounts of alloy materials at the interface of Ni and Au structures. Thereon, Au particles are formed on the Ni colloids as the miscibility of Au and Ni is negligible in room temperature. With the increase in Au concentration, the position of the Ni peak after galvanic replacement is constant for all samples confirming that the Ni–Au bimetallic material is only available at the Ni colloid and Au particle interface.

The EDS elemental survey represented in Fig. 2c indicates the presence of nickel, gold, carbon, titanium and silicon on the surface with no peaks related to other possible contaminants which may appear during the synthesis process. In order to obtain a clear understanding of the relative increase in Au content during GR, the atomic ratio given by $Au/(Au + Ni)$ was calculated based on the EDS analysis for each of the samples (Fig. 2d). The results showed that with the increase in $HAuCl_4$ concentration, the amount of decorated Au increases on the surface of the Ni colloids. In addition, EDS mapping of Ni–Au_{1mM} indicated the formation of a uniform Ni surface across the colloidal crystal after evaporation and the gold nanoparticles have mostly formed in the intersections of the Ni colloids following GR as shown in the ESI,† Fig. S1.

To better understand the formation behavior of the Au particles on each individual PS/Ni colloid surface as a result of GR reaction, Ni–Au_{1mM} was sonicated in ethanol and then drop cast on a copper grid and characterized by TEM. Fig. 3a shows the growth of the Au nanoparticles on the outer surface of the colloid which can also be observed in Fig. 1e. An EDS overlay map of the single colloid overlaid with the TEM image is shown in Fig. 3b. The image clearly shows the coverage of each metal on the PS colloids. As explained earlier (XRD results), Au tends to grow in the active areas of the structure due to the immiscibility of both Ni and Au, leading to larger particles of Au on the Ni PS shells instead of the formation of a uniform shell. The individual maps of carbon (Fig. S2a, ESI†), nickel (Fig. S2b, ESI†) and gold (Fig. S2c, ESI†) are shown in Fig. S2, ESI.† As colloidal particles have spherical shapes, most of the nickel deposition during evaporation occurs at the top center of the PS spheres where the Ni film is thickest and begins to reduce away from the top center, to the sides due to the ‘line of site’ constraints during evaporation. The lattice fringes were recorded from two separate areas of the samples which are shown with red and yellow boxes in Fig. 3a based on the EDS mapping analysis of Ni shells and decorating Au nanoparticles. The HR-TEM studies confirm the formation of small nanoparticles of (~7 nm) NiOOH layer on the surface of the Ni layer, as shown in Fig. 3c. This can be due to the partial oxidation of the nickel layers after evaporation. A representative intensity profile was obtained for the lattice fringes covering the line scan shown within the figure and represented as an inset in Fig. 3c. The periodic dimension of 3.14 Å relates to the interplanar dimension of the [110] orthorhombic NiOOH structure. The lattice fringe study with the aid of an intensity profiler of formed Au spikes on the shown line scan indicates the formation of Au nanoparticles (Fig. 3d). The interplanar dimension of 2.36 Å is related to the [111] FCC structure of Au crystals.

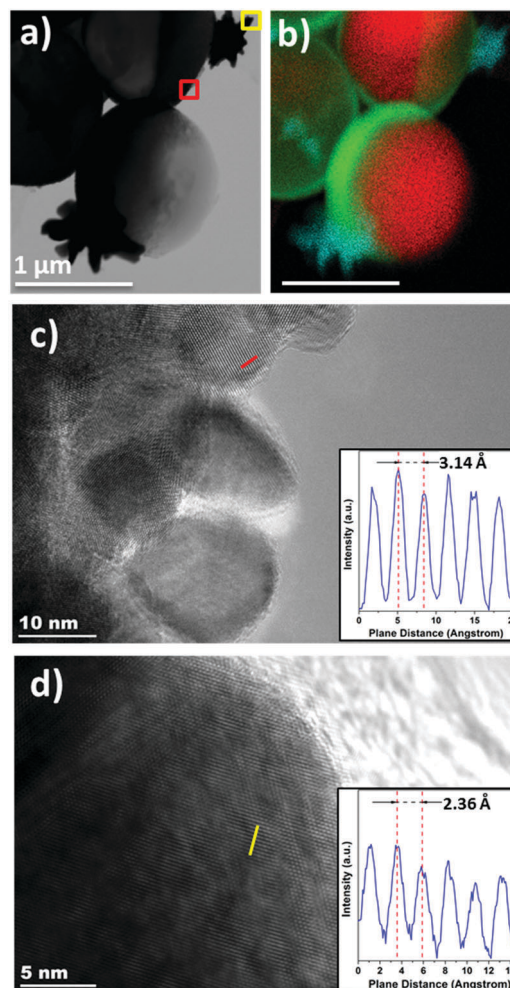


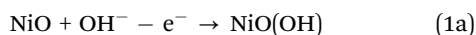
Fig. 3 TEM images of (a) Ni–Au_{1mM} shows the formation of Ni hemispherical shells and Au spikes; the red and yellow boxes relate to the corresponding places for HR-TEM presented for Ni and Au, (b) elemental EDS maps showing C (red), Ni (Green) and Au (Cyan) overlays, (c) lattice structures with the corresponding fringe distance profiles (inset) indicating the Ni shell and (d) the lattice structure indicating Au spikes. Intensity profiles for the lattice fringes covering the line scan in the HR-TEM images were obtained from the intensity contrast profile of the image across the marked lines; red in (c) and yellow in (d).

To determine the oxidation state of each of the elements, XPS spectra (Fig. S3, ESI†) has been collected from the developed Ni–Au bimetallic sensors for surfaces galvanically replaced using 1 mM solution (Ni–Au_{1mM}). The XPS survey of the electrode surface, when compared with the Ni colloid counterpart shown in Fig. S4, ESI† indicates the formation of Au on the Ni without the presence of any other contaminants. The high-resolution spectrum of Au 4f core binding energies showed two peaks at 84.18 and 87.85 eV possessing a splitting factor of 3.7 eV (Fig. S3a, ESI†) indicating the formation of Au⁰ (metallic state) on the surface.^{41,42} Au in its metallic state shows that Au has completely reduced on the Ni structures. XPS analysis of the Ni 2p_{3/2} core level spectrum (Fig. S3b, ESI†) displays five distinguished peaks at 852.54, 854.3, 856.01, 858.02 and 861.2 eV which can be attributed to Ni⁰, NiO, Ni(OH)₂, NiO(OH) and convolution of satellite peaks,

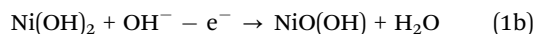
respectively.^{43,44} The presence of both Ni⁰ and different oxidation states of Ni appearing simultaneously indicates that the Ni film surface has undergone partial oxidation upon exposure to air, consistent with our HR-TEM analysis.

Determining the optimal Au concentration for glucose sensing

The glucose electrooxidation efficiency of the Ni–Au colloidal crystals with different Au concentrations was studied in 0.5 M KOH alkaline solution. Fig. 4a shows the CV analysis comparing Au-ctrl, Ni-ctrl and the Ni–Au_{0.1mM} electrode (as a comparative sample) in a solution of 0.5 M KOH with (upper graph) and without (lower graph) 10 mM glucose. The peak height of the forward scan oxidation peak in the CV analysis for the Ni–Au colloids tended to increase dramatically at *ca.* +0.5 V in the presence of glucose. The Ni–Au_{0.1mM} electrode showed the largest change in the reverse scan with the anodic peak current at +0.45 V displaying the largest improvement relative to the Ni and Au controls when glucose was added to the alkali solution. This large increase in the anodic peak is predominantly due to the presence of Au on the surface of the Ni colloids. Due to the large peak height, a good relationship between Au and Ni is clearly shown, which allows for large sensitivities in the presence of glucose media. All other samples displayed a less defined oxidation peak compared to the Ni–Au_{0.1mM} electrode with a further positive shift in peak potential. The general mechanism for Ni in the presence of glucose in alkaline solution is presented in eqn (1) and (2).⁴⁵



or



The reactants in eqn (1a) and (1b) are due to Ni(0) being oxidized to form Ni(II) in the form of NiO and Ni(OH)₂ at potentials less than +0.6 V. The Ni(II) species acts as a catalyst for the oxidation reaction between the surface of the electrode and glucose. That is, when applying a potential of 0.51 V, Ni(II) is converted to Ni(III) *via* eqn (1a) or (1b). The Ni(III) species then oxidize glucose to gluconolactone to form Ni(II) species (eqn (2)).⁴⁶ The anodic current dependence on the substrate due to glucose oxidation (*i.e.* keeping the glucose concentration constant at 10 mM) can be observed in Fig. 4a (upper panel).

Au acts in a manner similar to Ni in alkaline solutions. Au forms AuOH due to the unimpeded reactions between the OH⁻ ions in the basic electrolyte and the Au⁺ ions on the surface of the structures.³⁰ The chemisorption reaction in alkaline solution causes the dehydrogenated intermediates formed to electrocatalytically oxidize the OH⁻ group with the Au⁺ ions present on the surface of the structures followed by a reaction with deprotonated glucose molecules.^{47,48} This is explained by the reaction mechanisms in eqn (3) and (4),⁴⁹ with the overall reaction displayed in eqn (5).⁴⁷

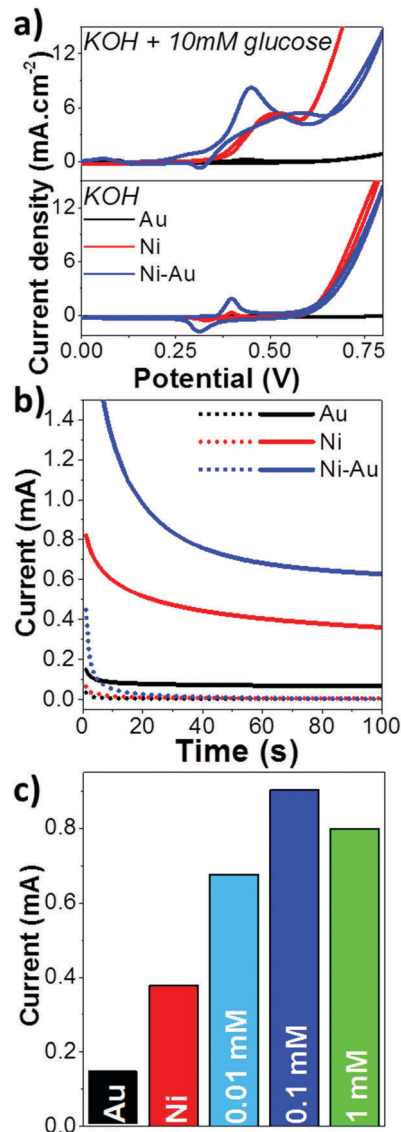
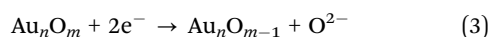
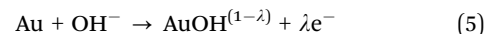
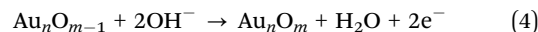


Fig. 4 (a) Cyclic voltammetry (CV) analysis comparing Au-ctrl, Ni-ctrl and Ni–Au_{0.1mM} in a solution of 0.5 M KOH with (top) and without (bottom) 10 mM glucose, (b) chronoamperometric responses of Au-ctrl (black), Ni-ctrl (red) and Ni–Au_{0.1mM} (blue) in 0.5 M KOH with (solid line) and without (dotted line) the addition of 10 mM glucose at a constant potential of +0.55 V for each analyzed substrate and (c) chronoamperometric responses of each examined substrate in 0.5 M KOH and 10 mM glucose.



Given the electrochemical glucose oxidation reaction mechanism for both Ni and Au shown above, it is clear that the reaction can be further enhanced when both metals are present concurrently on the working electrode. However, the deposition method, substrate type and metal content are all thought to play a role in enhancing the electrochemical glucose oxidation reaction.

The (anode/cathode) peak at *ca.* +0.55 V for each substrate represents the catalytic oxidation of glucose when reacting with

Ni. From the CV analysis in Fig. 4a we can see that the Ni-Au colloid displays the highest peak for glucose electrooxidation. To confirm this, we used chronoamperometric analysis at a fixed potential of +0.55 V based on previous Ni-based studies,^{29,35,36} which is shown in Fig. 4b. Au-ctrl showed minimal current response at the chosen on-set potential with Ni-ctrl showing a moderate increase in response compared to Au-ctrl. The Ni-Au colloids showed a very large enhancement in current response over the control substrates at +0.55 V, with their chronoamperometric response increased by a factor of 9.3 vs. Au-ctrl and 1.74 vs. Ni-ctrl. Chronoamperometric analysis in a solution of 0.5 M KOH and 10 mM glucose was performed by comparing both the Au and Ni control substrates with the Ni-Au PS colloid substrates (Fig. 4c). We can observe that the Ni-Au_{0.1mM} sample had the highest current output followed by Ni-Au_{1mM} and Ni-Au_{0.01mM}. As previously discussed (for Fig. 1), the Au nanoparticle formation across the surface directly affected the sensing performance results. A more uniform size, shape and spread of Au nanoparticles (as can be seen for Ni-Au_{0.1mM}) across the colloidal surface showed the largest increase in glucose oxidation current response. It is thought that the 0.1 mM substrate had a better sensing performance due to the larger number of individual Au particles evenly distributed on each individual Ni colloids. This even distribution provides a relatively larger number of active reaction sites for electrochemical glucose oxidation to occur. All sensors modified through the galvanic replacement reaction are observed to have surpassed the response magnitudes of both Au-ctrl and Ni-ctrl substrates towards glucose, clearly showing better electro-oxidation capabilities due to the use of PS colloid template and the deposition of Au nanoparticles onto the PS colloids. The data for Ni-Au_{2mM} are not shown as it could not withstand the experimental procedure (*i.e.* long testing periods and repeatability tests) due to the formation of relatively large Au particles that were poorly adhered to the Ni base as a result of the immiscibility between Au and Ni at such large Au concentrations. This is thought to be the reason for the large particles beginning to detach from the substrate surface during glucose sensing experiments. This lack of adhesion meant that the substrate was unsuitable for further analysis.

Chronoamperometric addition analysis (as is the same experimental method used previously^{30,50,51}) was then applied to Ni-Au_{0.1mM} to determine the overall sensitivity and linearity of the sensor. Fig. 5a shows the experimental data obtained with additions between 20 μ M and 10 mM of glucose in an alkaline solution of 0.5 M KOH. Each addition was run for 100 s to allow the sensor response to reach a stabilized state. By implementing this form of addition analysis, we were able to estimate the concentrations of glucose along different time points of the analysis period. The trend of increasing current with increasing glucose concentration present is constant for all time points, as displayed in Fig. 5b. It can be observed that among Au-ctrl, Ni-ctrl, Ni colloids and Ni-Au_{0.1mM}, the latter displayed a clear enhancement over all other substrates. The sensitivity of each substrate towards glucose was also calculated from their calibration curves and compared. Au-ctrl had the

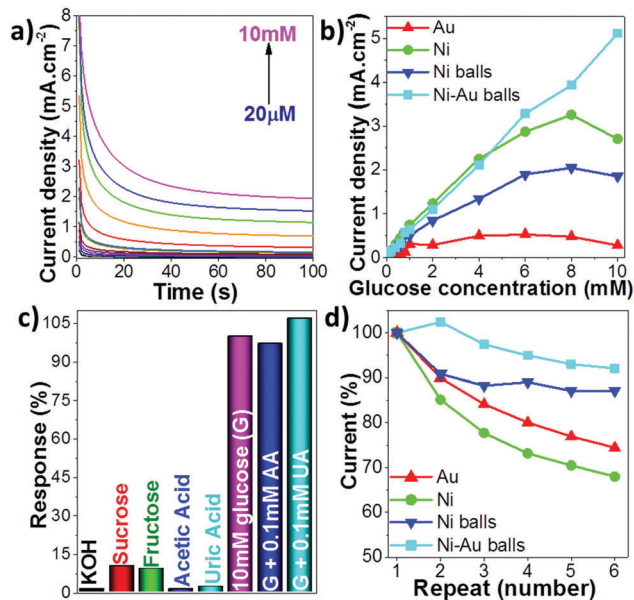


Fig. 5 (a) Chronoamperometric additions analysis on Ni-Au_{0.1mM} in a solution of 0.5 M KOH with glucose additions ranging between 20 μ M and 10 mM over a scan time of 100 s per testing event, (b) calibration curves of chronoamperometric additions analysis comparing Ni-Au_{1mM} with Ni-ctrl, Ni colloids and Au-ctrl, (c) chronoamperometric additions data analysis for selectivity when testing the presence of sucrose, fructose, acetic acid and uric acid in 0.5 M KOH and (d) repeatability comparisons of each substrate over 6 simultaneous testing events in a solution of 0.5 M KOH and 10 mM glucose.

lowest sensitivity ($46.1 \mu\text{A mM}^{-1} \text{cm}^{-2}$), followed by the plain Ni colloids ($223 \mu\text{A mM}^{-1} \text{cm}^{-2}$), Ni-ctrl ($345 \mu\text{A mM}^{-1} \text{cm}^{-2}$) and the highest sensitivity was shown by the modified Ni-Au_{0.1mM} substrate ($506 \mu\text{A mM}^{-1} \text{cm}^{-2}$). The Ni-Au colloid (Ni-Au_{0.1mM}) displayed a sensitivity ~ 11 times larger than that of Au-ctrl and 2.7 times larger than that of the plain Ni colloids. The linear fits are shown in Fig. S5, ESI[†] over a concentration range between 20 μ M and 0.2 mM. However, for Ni-Au_{0.1mM}, the sensor displayed a linear range over the whole concentration range from 20 μ M to 10 mM (shown in the inset image of Fig. S5, ESI[†]). Au-ctrl showed the lowest linear range between 20 μ M and 1 mM, plain Ni colloids between 20 μ M and 6 mM, Ni-ctrl between 20 μ M and 8 mM with Ni-Au_{0.1mM} showing the best linear range between 20 μ M and 10 mM. The experimental values analyzed were capped at 10 mM as the physiological glucose range is between 3 mM and 8 mM with hypoglycemia effects commencing at a concentration < 4 mM and hyperglycemia effects commencing at > 7 mM.^{47,52,53}

The limit of detection (LoD) for Ni-Au_{0.1mM} was calculated using 3 subsequent chronoamperometric runs at various times in a solution of 0.5 M KOH (Fig. S6, ESI[†]) followed by a single addition of 20 μ M glucose. As can be seen in the ESI[†], Table S1 the calculated LoD of Ni-Au_{0.1mM} did not vary greatly with the analysis times ranging between 1 and 100 s, where a 5 s analysis time showed a LoD of 14.9 μ M. Table 1 shows the performance of Ni-Au_{0.1mM} compared to similar sensors fabricated and reported in the literature. It can be observed that the modified

Table 1 Non-enzymatic sensors reported in the literature and comparison with the Ni–Au monolayer colloidal crystals in this work

Electrode material	Sensitivity ($\mu\text{A mM}^{-1} \text{cm}^{-2}$)	LoD (μM)	Operation potential (V)	Linear range	Medium	Ref.
Au nanocorals	22.6	10	+0.25 V vs. Ag/AgCl	50 μM –30 mM	0.1 M PBS	38
Porous Au	11.8	5	+0.35 V vs. SCE	2–10 mM	0.1 M PBS	55
Ni powder electrode	40	2	+0.4 V vs. Ag/AgCl	0.5 μM –5 mM	0.03 M NaOH	33
Ni NP CNF paste electrode	420.4	1	+0.6 V vs. Ag/AgCl	2 μM –2.5 mM	0.1 M NaOH	27
NC Ni(OH) ₂ nanoscale material	202	6	+0.55 V vs. Ag/AgCl	50 μM –23 mM	0.5 M NaOH	36
Au/Ni/Cu electrode	0.85	n/a	+0.055 V	Buffer–33 mM	0.1 M PBS	56
NiO–Au nanobelt/GCE	48.35	1.32	+0.6 V vs. Ag/AgCl	20 μM –4.55 mM	0.1 M NaOH	57
Ni–Au MCL	506	14.9	+0.55 vs. Ag/AgCl	20 μM–10 mM	0.5 M KOH	This work^a

^a NP – nanoporous; CNF – carbon nanofiber; MCL – monolayer colloidal crystal; GCE – glassy carbon electrode.

sensor developed in this study has superior sensitivity and an acceptable limit of detection (LoD) for desired application in the detection of physiological glucose concentrations.

Subsequent selectivity analysis was carried out on the Ni–Au_{0.1mM} sensor to determine the effect of physiological contaminants commonly found to hinder glucose sensors capabilities. Fig. 5c shows the percentage response (experimental data presented in the ESI,† Fig. S7) when compared to the starting electrolyte solution containing 0.5 M KOH. The sugars sucrose and fructose displayed a slight increase in response magnitude of the sensor; however, these are the most common substances which caused cross-interference in other reported sensors. Acetic acid (AA) and uric acid (UA) produced only inconsequential changes in the response signal. Subsequently addition of 10 mM glucose to the analyte solution led to a large increase in current response. With the lack of response from the previously added contaminants, we can clearly see the high selectivity of the sensor in the presence of glucose and common physiological contaminants. To further analyze the effect of physiological contaminants on the current response of glucose, a secondary addition of AA and UA was performed after the glucose addition. The results showed a slight reduction in current response in the presence of AA and a small increase in response with the addition of UA. This high level of selectivity can greatly be due to the presence of Au nanoparticles which are known for their good selectivity toward glucose in the presence of common physiological contaminants.

Repeatability analysis (Fig. 5d) was then performed on the sensor in 0.5 M KOH and 10 mM glucose; compared with Au-ctrl, Ni-ctrl and plain Ni colloids, Ni–Au_{0.1mM} showed the best repeatability over 6 consecutive cycles displaying a current response far superior to the control counterparts analyzed. The validity of the repeatability analysis was determined through calculating the coefficient of variance (CoV) (eqn (6)–(8)), where I_f is the final current response for each run and I_{avg} is the average current response.⁵⁴

$$I_{\text{avg}} = \frac{\sum I_f}{n} \quad (6)$$

$$\sigma = \sqrt{\frac{\sum (I_f - I_{\text{avg}})^2}{n - 1}} \quad (7)$$

$$\text{CoV}(\%) = \left(\frac{\sigma}{I_{\text{avg}}} \right) \times 100 \quad (8)$$

The CoV for Ni–Au_{0.1mM} was calculated to be 4.2% displaying a repeatability of 95.8% over 6 repetitive sensing events. The plain Ni colloids showed a repeatability of 94%, while Au-ctrl and Ni-ctrl had large margins in their repeatability values (88% and 85%, respectively) from the modified sensor. The high electrochemical glucose sensing performance of the modified surfaces is postulated to be due to the PS-Ni template. The outperformance of the Ni–Au_{0.1mM} electrode is due to the relatively homogeneous decoration of Au nanoparticles over each colloid when compared to other substrates modified by galvanic replacement. Given that both Au and Ni are active substrates for glucose oxidation, the electro-oxidation enhancement of Au–Ni is due to the bimetallic material at the interface of each Au nanoparticle on the Ni colloids. This is evidenced by the lack of such enhancements from the Au-ctrl and the Ni–Au electrodes modified through GR at too high or low concentrations than 0.1 mM Au salt. This clearly shows that the electrochemical activity of these colloidal bimetallic surfaces can be tuned through the choice of the GR modification parameters such as gold concentration.

Conclusions

In this paper, we have reported the synthesis of a completely monodispersed polystyrene colloid template with a sheet-layer of Ni on the surface of the colloid with scattered deposition of Au nanoparticles at different concentrations across the surface of the Ni colloids. The synthesized bimetallic Ni–Au colloidal crystals showed better control on galvanic replacement due to uniformity across the colloidal crystal of Ni. These formed substrates with differing Au concentrations were then analyzed for their glucose electrooxidation activity in an alkaline solution of 0.5 M KOH. Using cyclic voltammetry and chronoamperometry, the optimal Au concentration on the surface of the Ni colloids was determined to be 0.1 mM. Further analysis of the capabilities of the Ni–Au_{0.1mM} substrate gave a detection limit of 14.9 μM with a calculated sensitivity of 506 $\mu\text{A mM}^{-1} \text{cm}^{-2}$, which is 11 times larger than that of the control Au substrate and ~ 3 times larger than that of a PS colloid template Ni film. The overall selectivity of the Ni–Au_{0.1mM} substrate showed minimal cross-interference effect in the presence of physiological sugars, with no effect in the presence of acetic acid and uric acid, which otherwise tend to hinder many promising non-enzymatic glucose sensors. Overall, a highly sensitive and

selective non-enzymatic glucose sensor was developed; given that the modified sensor presented in the study had high electro-oxidation activity towards glucose, it is thus expected that it will be highly efficient for other chemical sensing applications.

Author contributions

All authors have contributed substantially to this work. A. E. K. and S. K. B. supervised the research. B. L., V. E. C., A. E. K. and Y. M. S. have conducted the experiments. All authors analyzed the data and reviewed the manuscript.

Acknowledgements

The authors acknowledge the RMIT microscopy and micro-analysis facility (RMMF) for allowing the use of their comprehensive facilities and services. The authors thank Mr Ciao Yuxun for his technical support.

References

- W.-Y. Yu, L. Zhang, G. M. Mullen, E. J. Evans, G. Henkelman and C. B. Mullins, *Phys. Chem. Chem. Phys.*, 2015, **17**, 20588–20596.
- W. He, X. Wu, J. Liu, X. Hu, K. Zhang, S. Hou, W. Zhou and S. Xie, *Chem. Mater.*, 2010, **22**, 2988–2994.
- P. Larki, Y. M. Sabri, K. M. Kabir, A. Nafady, A. E. Kandjani and S. K. Bhargava, *RSC Adv.*, 2015, **5**, 92303–92311.
- V. Bansal, H. Jani, J. Du Plessis, P. J. Coloe and S. K. Bhargava, *Adv. Mater.*, 2008, **20**, 717–723.
- H. Jing and H. Wang, *Chem. Mater.*, 2015, **27**, 2172–2180.
- W. Zhang, J. Yang and X. Lu, *ACS Nano*, 2012, **6**, 7397–7405.
- C.-L. Lee and C.-M. Tseng, *J. Phys. Chem. C*, 2008, **112**, 13342–13345.
- X. Lu, H.-Y. Tuan, J. Chen, Z.-Y. Li, B. A. Korgel and Y. Xia, *J. Am. Chem. Soc.*, 2007, **129**, 1733–1742.
- X. Xia, Y. Wang, A. Ruditskiy and Y. Xia, *Adv. Mater.*, 2013, **25**, 6313–6333.
- L. Fu, D. Zhu and A. Yu, *Spectrochim. Acta, Part A*, 2015, **149**, 396–401.
- B. Lay, Y. Sabri, S. Ippolito and S. Bhargava, *Phys. Chem. Chem. Phys.*, 2014, **16**, 19522–19529.
- J. Lian, L. Wang, X. Sun, Q. Yu and R. C. Ewing, *Nano Lett.*, 2006, **6**, 1047–1052.
- E. M. Hicks, S. Zou, G. C. Schatz, K. G. Spears, R. P. Van Duyne, L. Gunnarsson, T. Rindzevicius, B. Kasemo and M. Käll, *Nano Lett.*, 2005, **5**, 1065–1070.
- Z. Gan, Y. Cao, R. A. Evans and M. Gu, *Nat. Commun.*, 2013, **4**, 2061.
- M. Retsch, Z. C. Zhou, S. Rivera, M. Kappl, X. S. Zhao, U. Jonas and Q. Li, *Macromol. Chem. Phys.*, 2009, **210**, 230–241.
- A. R. Halpern and R. M. Corn, *ACS Nano*, 2013, **7**, 1755–1762.
- Y. M. Sabri, A. E. Kandjani, S. J. Ippolito and S. K. Bhargava, *ACS Appl. Mater. Interfaces*, 2015, **7**, 1494.
- Y. M. Sabri, A. E. Kandjani, S. J. Ippolito and S. K. Bhargava, *Sci. Rep.*, 2016, **6**, 24625.
- A. Manzke, N. Vogel, C. K. Weiss, U. Ziener, A. Plettl, K. Landfester and P. Ziemann, *Nanoscale*, 2011, **3**, 2523–2528.
- N. Vogel, M. Retsch, C.-A. Fustin, A. del Campo and U. Jonas, *Chem. Rev.*, 2015, **115**, 6265–6311.
- Y. M. Sabri, S. J. Ippolito, A. J. Atanacio, V. Bansal and S. K. Bhargava, *J. Mater. Chem.*, 2012, **22**, 21395–21404.
- M. Y. Tsvetkov, B. N. Khlebtsov, V. A. Khanadeev, V. N. Bagratashvili, P. S. Timashev, M. I. Samoylovich and N. G. Khlebtsov, *Nanoscale Res. Lett.*, 2013, **8**, 250.
- L. Gonzalez-Urbina, K. Baert, B. Kolaric, J. Perez-Moreno and K. Clays, *Chem. Rev.*, 2012, **112**, 2268–2285.
- A. M. Ruminski, G. Barillaro, C. Chaffin and M. J. Sailor, *Adv. Funct. Mater.*, 2011, **21**, 1511–1525.
- Y. H. Ye, T. S. Mayer, I. C. Khoo, I. B. Divliansky, N. Abrams and T. E. Mallouk, *J. Mater. Chem.*, 2002, **12**, 3637–3639.
- J. F. Galisteo-Lopez, M. Ibisate, R. Sapienza, L. S. Froufe-Perez, A. Blanco and C. Lopez, *Adv. Mater.*, 2011, **23**, 30–69.
- Y. Liu, H. Teng, H. Hou and T. You, *Biosens. Bioelectron.*, 2009, **24**, 3329–3334.
- Y. Ding, Y. Wang, L. Su, H. Zhang and Y. Lei, *J. Mater. Chem.*, 2010, **20**, 9918–9926.
- C. Y. Guo, Y. M. Wang, Y. Q. Zhao and C. L. Xu, *Anal. Methods*, 2013, **5**, 1644–1647.
- V. E. Coyle, A. E. Kandjani, Y. M. Sabri and S. K. Bhargava, *Electroanalysis*, 2017, **29**, 294–304.
- G. Sanz , I. Taurino, R. Antiochia, L. Gorton, G. Favero, F. Mazzei, G. De Micheli and S. Carrara, *Bioelectrochemistry*, 2016, **112**, 125–131.
- Y. Xia, W. Huang, J. Zheng, Z. Niu and Z. Li, *Biosens. Bioelectron.*, 2011, **26**, 3555–3561.
- T. You, O. Niwa, Z. Chen, K. Hayashi, M. Tomita and S. Hirono, *Anal. Chem.*, 2003, **75**, 5191–5196.
- X. Cheng, S. Zhang, H. Zhang, Q. Wang, P. He and Y. Fang, *Food Chem.*, 2008, **106**, 830–835.
- L.-M. Lu, L. Zhang, F.-L. Qu, H.-X. Lu, X.-B. Zhang, Z.-S. Wu, S.-Y. Huan, Q.-A. Wang, G.-L. Shen and R.-Q. Yu, *Biosens. Bioelectron.*, 2009, **25**, 218–223.
- A. Safavi, N. Maleki and E. Farjami, *Biosens. Bioelectron.*, 2009, **24**, 1655–1660.
- Y. Xian, Y. Hu, F. Liu, Y. Xian, H. Wang and L. Jin, *Biosens. Bioelectron.*, 2006, **21**, 1996–2000.
- T.-M. Cheng, T.-K. Huang, H.-K. Lin, S.-P. Tung, Y.-L. Chen, C.-Y. Lee and H.-T. Chiu, *ACS Appl. Mater. Interfaces*, 2010, **2**, 2773–2780.
- D. T. W. Toolan, S. Fujii, S. J. Ebbens, Y. Nakamura and J. R. Howse, *Soft Matter*, 2014, **10**, 8804–8812.
- A. Herz, D. Wang, T. Kups and P. Schaaf, *J. Appl. Phys.*, 2014, **116**, 044307.
- Y. Hong, X. Jing, J. Huang, D. Sun, T. Odoom-Wubah, F. Yang, M. Du and Q. Li, *ACS Sustainable Chem. Eng.*, 2014, **2**, 1752–1759.

- 42 W. Luo, M. Sankar, A. M. Beale, Q. He, C. J. Kiely, P. C. A. Bruijninx and B. M. Weckhuysen, *Nat. Commun.*, 2015, **6**, 6540.
- 43 A. P. Grosvenor, M. C. Biesinger, R. S. C. Smart and N. S. McIntyre, *Surf. Sci.*, 2006, **600**, 1771–1779.
- 44 M. C. Biesinger, B. P. Payne, A. P. Grosvenor, L. W. M. Lau, A. R. Gerson and R. S. C. Smart, *Appl. Surf. Sci.*, 2011, **257**, 2717–2730.
- 45 C. Zhao, C. Shao, M. Li and K. Jiao, *Talanta*, 2007, **71**, 1769–1773.
- 46 P. F. Luo, T. Kuwana, D. K. Paul and P. M. Sherwood, *Anal. Chem.*, 1996, **68**, 3330–3337.
- 47 Y. Vassilyev, O. Khazova and N. Nikolaeva, *J. Electroanal. Chem. Interfacial Electrochem.*, 1985, **196**, 127–144.
- 48 M. Hsiao, R. Adžić and E. Yeager, *J. Electrochem. Soc.*, 1996, **143**, 759–767.
- 49 M. Pasta, F. La Mantia and Y. Cui, *Electrochim. Acta*, 2010, **55**, 5561–5568.
- 50 V. E. Coyle, D. K. Oppedisano, L. A. Jones, A. E. Kandjani, Y. M. Sabri and S. K. Bhargava, *J. Electrochem. Soc.*, 2016, **163**, B689–B695.
- 51 C.-W. Hsu and G.-J. Wang, *Biosens. Bioelectron.*, 2014, **56**, 204–209.
- 52 S. Clement, S. S. Braithwaite, M. F. Magee, A. Ahmann, E. P. Smith, R. G. Schafer and I. B. Hirsch, *Diabetes Care*, 2004, **27**, 553–591.
- 53 J. H. Anderson, W. G. Blackard, J. Goldman and A. H. Rubenstein, *Am. J. Med.*, 1978, **64**, 868–873.
- 54 K. M. Kabir, Y. M. Sabri, G. I. Matthews, L. A. Jones, S. J. Ippolito and S. K. Bhargava, *Analyst*, 2015, **140**, 5508–5517.
- 55 Y. Li, Y.-Y. Song, C. Yang and X.-H. Xia, *Electrochem. Commun.*, 2007, **9**, 981–988.
- 56 S.-R. Lee, Y.-T. Lee, K. Sawada, H. Takao and M. Ishida, *Biosens. Bioelectron.*, 2008, **24**, 410–414.
- 57 Y. Ding, Y. Liu, J. Parisi, L. Zhang and Y. Lei, *Biosens. Bioelectron.*, 2011, **28**, 393–398.

Supporting Information

Nickel-Gold Bimetallic Monolayer Colloidal Crystal via Galvanic Replacement as a Highly Sensitive Electrochemical Sensor

Bebeto Lay[‡], Victoria E. Coyle[‡], Ahmad Esmailzadeh Kandjani^{*}, Mohamad H. Amin, Ylias M.

Sabri and Suresh K. Bhargava^{*}

Centre for Advanced Materials and Industrial Chemistry (CAMIC), School of Applied Sciences,

RMIT University, GPO Box 2476 V, Melbourne, Victoria 3001, Australia

*email: ahmad.kandjani@rmit.edu.au ; suresh.bhargava@rmit.edu.au,

Phone: +61 3 99252330

RECEIVED DATE (to be automatically inserted after your manuscript is accepted if required according to the journal that you are submitting your paper to)

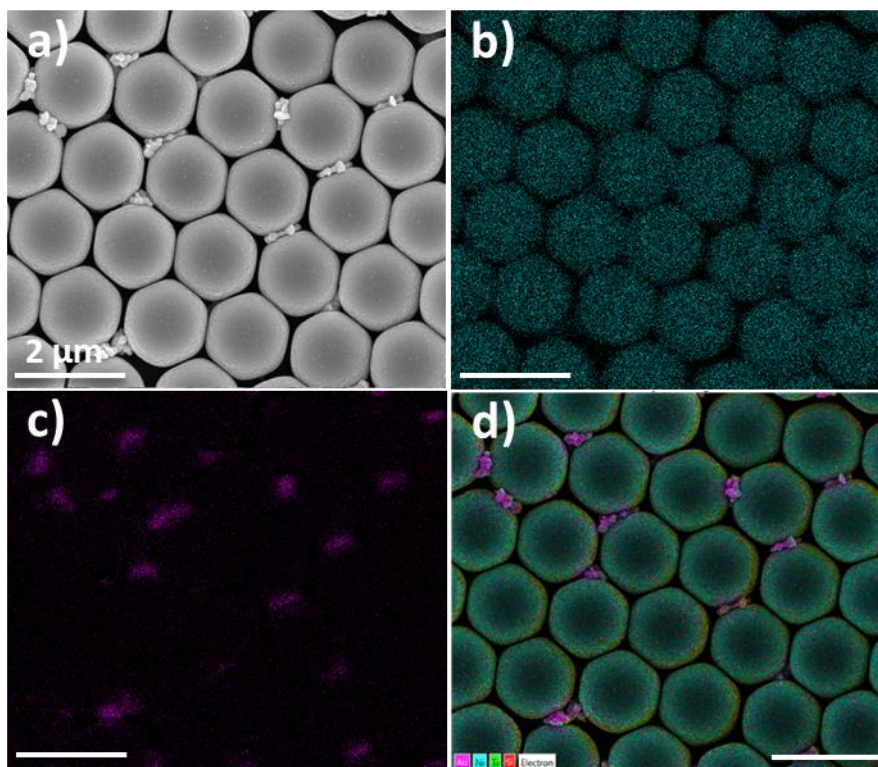


Fig. S1 SEM images of (a) Ni-Au_{1mM} monolayer and corresponding elemental map using EDS for (b) Ni (c) Au and (d) overlay of EDS maps.

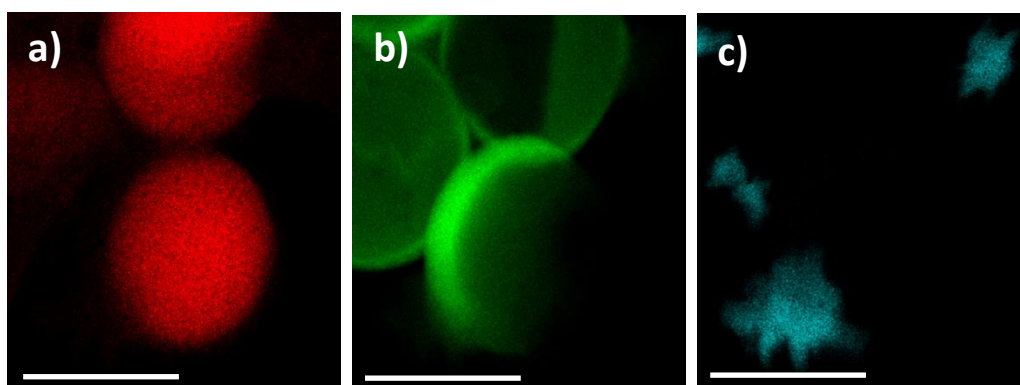


Fig. S2 TEM images of a singular PS Ni-Au monosphere with EDS elemental mapping of a) C (b) Ni and (c) Au

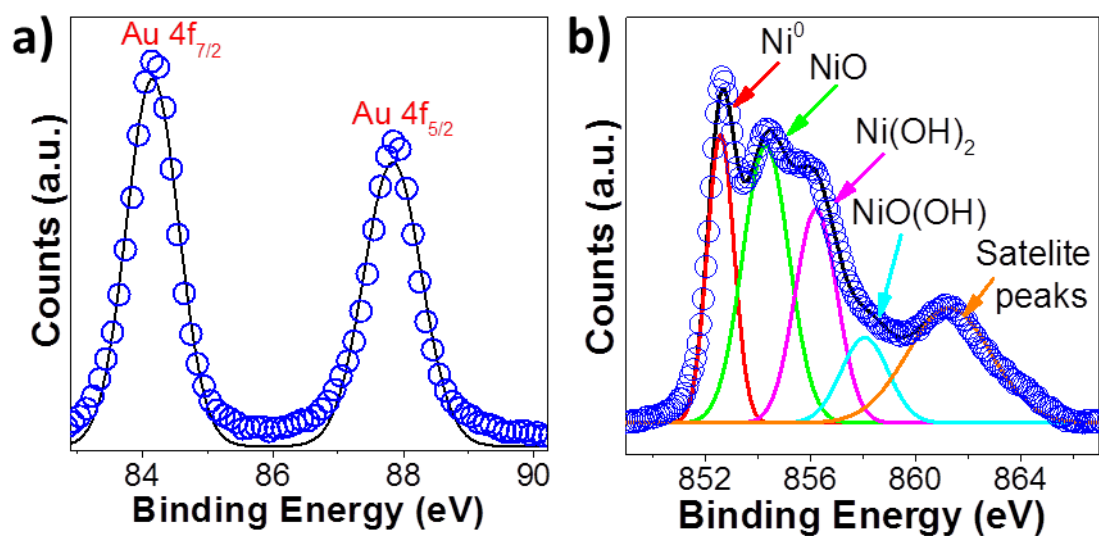


Fig. S3 XPS analysis for Ni-Au_{1mM} bimetallic systems (a) Au 4f core level and (b) Ni 2P core level spectra.

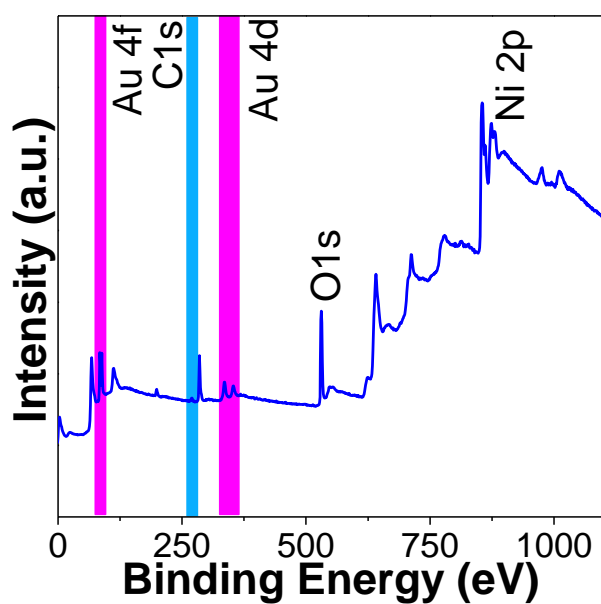


Fig. S4 XPS Survey of Ni-Au₁

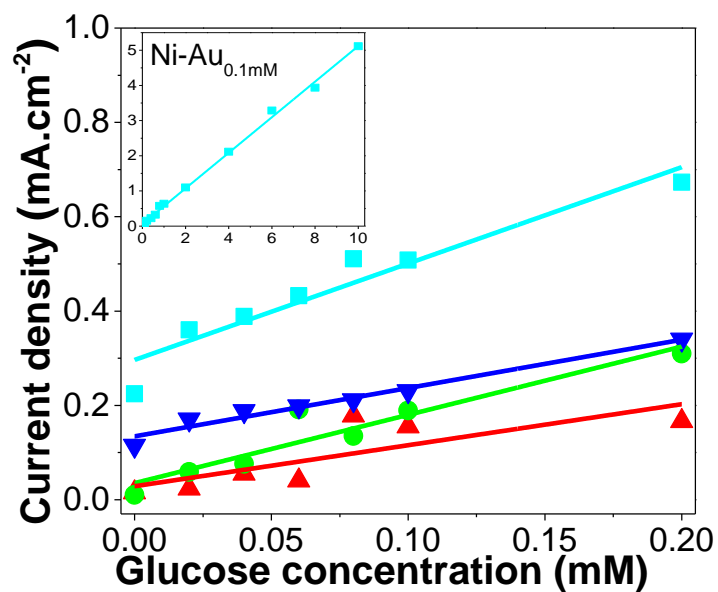


Fig. S5 Chronoamperometric analysis of Ni-Au_{0.1mM} (aqua), flat Ni (green), Ni balls (blue) and flat Au (red) in a solution of 0.5 M KOH and increasing concentrations of glucose ranging between 20 μM and 0.2 mM. (Inset image) Linear progression of Ni-Au_{0.1mM} over the glucose concentration range of 20 μM - 10 mM.

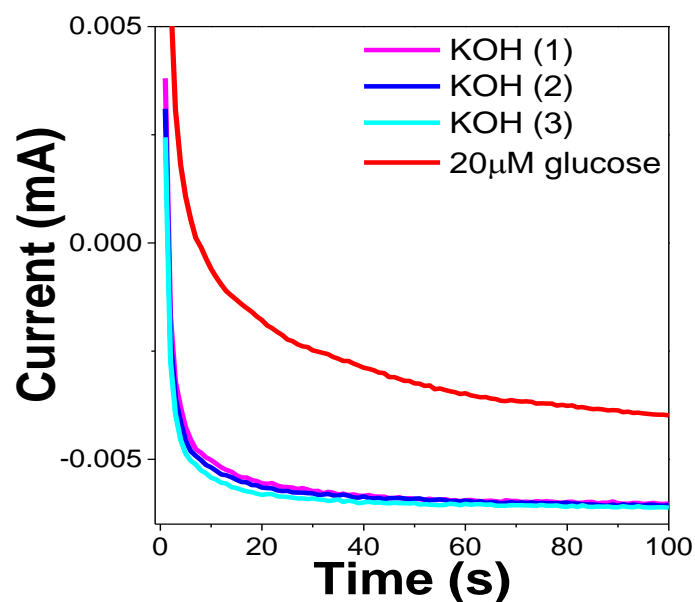


Fig. S6 Experimental chronoamperometric responses in a solution of 0.5 M KOH for a run time of 100s with 2 repeat runs followed by a single run with the addition of 20 μM glucose

Time (s)	Sensitivity ($\mu\text{A}\cdot\text{mM}^{-1}\cdot\text{cm}^{-2}$)	R^2 (value)	LOD (calculated)
1	923	0.94	14.5
5	506	0.997	14.9
10	389	0.998	14.9
50	217	0.999	15
100	179	0.998	15.1

Table S1 Comparison table of glucose additions analysis and their calibration curves at difference times for sensitivity, R^2 value and limit of detection (LOD).

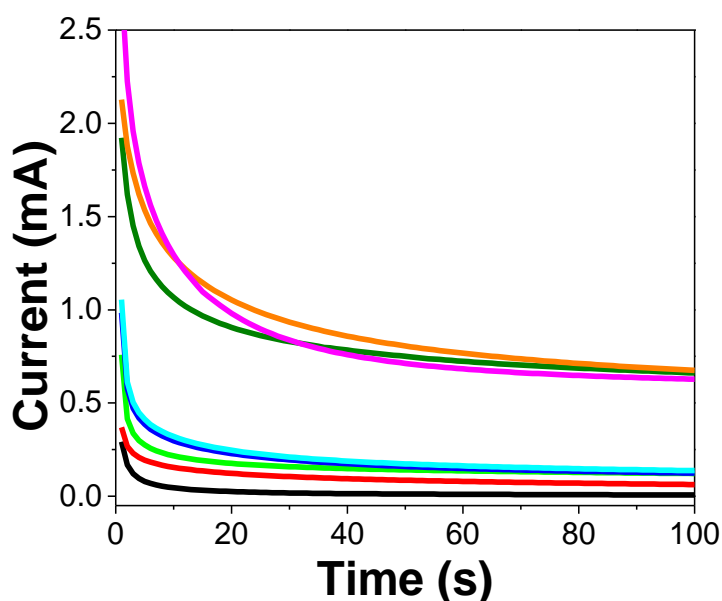


Fig. S7 Experimental chronoamperometric responses of physiological contaminants analysis in a solution of 0.5 M KOH followed by the addition of sucrose (red), fructose (green), AA (blue), UA (aqua), 10 mM glucose (magenta), 10mM glucose + AA (dark green) and 10mM glucose + UA (orange).

CHAPTER VI:

Co₃O₄ needles on Au honeycomb as a non-invasive electrochemical biosensor for glucose in saliva

While glucose monitoring technology is widely available, the continued prevalence of diabetes around the world coupled with its debilitating effects continues to grow. The significant limitations which exist in the current technology, instils the need for materials capable of non-invasive glucose detection. In this chapter a unique non-enzymatic electrochemical glucose sensor was developed, utilising a gold honeycomb-like framework upon which sharp Co₃O₄ needles are anchored. This composite nanomaterial demonstrates excellent sensing performance in glucose concentrations ranging between 20 μM and 4 mM, exceeding the range required for non-invasive glucose sensing. In conjunction with this high sensitivity (2.014 mA·mM⁻¹·cm⁻²), the material possesses excellent selectivity towards glucose for commonly interfering physiological species such as uric acid and ascorbic acid. Glucose detection in synthetic saliva was then performed showing excellent capability in the low concentration range (20 μM–1 mM) for non-invasive sensing performance. Further tests showed good selectivity of the sensor in physiological contaminants commonly found in saliva such as cortisol and dopamine. This development provides excellent scope to create next-generation non-invasive diabetes monitoring platforms, with excellent performance when detecting low glucose concentrations in complex solutions such as saliva.



Co₃O₄ needles on Au honeycomb as a non-invasive electrochemical biosensor for glucose in saliva

Victoria E. Coyle^{a,b}, Ahmad E. Kandjani^a, Matthew R. Field^c, Patrick Hartley^b, Miao Chen^{a,b}, Ylias M. Sabri^{a,**}, Suresh K. Bhargava^{a,*}

^a Centre for Advanced Materials and Industrial Chemistry (CAMIC), School of Science, RMIT University, Melbourne, Victoria, 3001, Australia

^b CSIRO, Bayview Avenue, Clayton, Victoria, 3168, Australia

^c RMIT Microscopy & Microanalysis Facility, RMIT University, Melbourne, Australia

ARTICLE INFO

Keywords:

Glucose biosensor
Electrochemical detection
Saliva
Non-invasive
Porous gold
Cobalt oxide

ABSTRACT

While glucose monitoring technology is widely available, the continued prevalence of diabetes around the world coupled with its debilitating effects continues to grow. The significant limitations which exist in the current technology, instils the need for materials capable of non-invasive glucose detection. In this study a unique non-enzymatic electrochemical glucose sensor was developed, utilising a gold honeycomb-like framework upon which sharp Co₃O₄ needles are anchored. This composite nanomaterial demonstrates excellent sensing performance in glucose concentrations ranging between 20 μM and 4 mM, exceeding the range required for non-invasive glucose sensing. In conjunction with this high sensitivity (2.014 mA mM⁻¹cm⁻²), the material possesses excellent selectivity towards glucose for commonly interfering physiological species such as uric acid and ascorbic acid. Glucose detection in synthetic saliva was then performed showing excellent capability in the low concentration range (20 μM–1 mM) for non-invasive sensing performance. Further tests showed good selectivity of the sensor in physiological contaminants commonly found in saliva such as cortisol and dopamine. This development provides excellent scope to create next-generation non-invasive diabetes monitoring platforms, with excellent performance when detecting low glucose concentrations in complex solutions such as saliva.

1. Introduction

Diabetes continues to grow as a major global health challenge with 422 million adults currently afflicted with this disease, with indicators pointing to this figure doubling by the year 2030 (Barry et al., 2017). In the United States alone, the estimated cost of diabetes in 2017 was \$327 billion (Association, 2018), highlighting the scale of the problem and the need for improved detection and treatment options. Whilst methods to monitor glucose concentrations are currently in widespread use, these detection methods are predominantly centred around blood-based detection which are non-user friendly as they involve frequent invasive and painful sampling procedures. Due to these pitfalls there is great demand for technology which will support non-invasive glucose detection for diabetes monitoring (Bandodkar and Wang, 2014). Alternative strategies to detect glucose include monitoring urine (0–0.8 mM glucose, enzymatic method) (Lankelma et al., 2012), saliva (0.03–0.08 mM glucose, non-enzymatic methods) (Raymundo-Pereira et al., 2016; Ye et al., 2013), sweat (0.02–0.6 mM glucose, non-

enzymatic method) (Anderson et al., 2017; Moyer et al., 2012), tears (0.1–0.6 mM glucose, enzymatic methods) (Kownacka et al., 2018; Yao et al., 2011) or breath (0.4–4 mM glucose, enzymatic method) (Roberts et al., 2012) based samples. The glucose concentrations for these alternative modes of detection are much lower than concentrations in blood (4.4–6.6 mM glucose) (Wang, 2008) meaning effective sensors for these non-invasive modes of analysis require a high degree of sensitivity. Moreover, their applicability is underpinned by their stability as well as their ability to selectively detect glucose in the presence of physiological contaminants such as ascorbic acid (AA) and uric acid (UA). These contaminants tend to disrupt the performance of chemical sensing results (Cheng et al., 2010; Zhang et al., 2011) by capping the active sites of electrode surfaces. While enzymatic glucose sensors have been investigated, they pose many issues such as poor stability, low reproducibility and limitations due to the need for an oxygen source (Wang et al., 2013; Zhu et al., 2016). Non-enzymatic glucose sensors are therefore an attractive option to overcome these issues, allowing for increased selectivity through low onset potentials, higher sensitivities

* Corresponding author.

** Corresponding author.

E-mail addresses: ylias.sabri@rmit.edu.au (Y.M. Sabri), suresh.bhargava@rmit.edu.au (S.K. Bhargava).

and improved stability due to the use of inorganic components in comparison to their biological counterparts (Toghill and Compton, 2010). Of the current non-enzymatic materials showing promise for glucose detection, Au has attracted much attention due to its high sensitivity but more specifically its excellent selectivity (Chakraborty et al., 2019). This excellent selectivity is attributed to its increased surface area-volume ratio, low applied onset potentials, control of structure fabrication for the nanostructures shape, size or porosity and active site density (Boisselier and Astruc, 2009; Coyle et al., 2016). Extending upon the properties of a mono-metallic structure, the addition of a metal oxide has also shown much success in non-enzymatic glucose sensing (Ding et al., 2010; Tong et al., 2012; Wang et al., 2009). Co_3O_4 in particular has excellent biocompatibility, high electrocatalytic activity and adsorption capacity for glucose making it very appealing to sensing fabrications (Kimmel et al., 2011; Solanki et al., 2011). Although Co_3O_4 shows great promise, its poor electronic conductivity limits its success to display high sensitivity, reliability and rapid response times (Ding et al., 2010; Solanki et al., 2011). A proposed method to combat these issues is to mould the Co_3O_4 to an Au scaffold structure allowing for the positive features of each material (Lang et al., 2013) to take prominence and reduce the effects of their pitfalls. The synergistic effect of the two present materials will allow for the lower sensitivities of Au and the poor selectivity of Co_3O_4 to no longer be an issue (Lay et al., 2017). In this work the fabrication of a composite nanostructure is investigated, bringing together Au and Co_3O_4 . Through the adoption of a synthesis procedure which has been previously shown to create highly porous nanomaterials, a gold scaffold is synthesised which can then be modified with Co_3O_4 in a facile manner. The potential for the use of this unique nanomaterial in non-invasive glucose sensing is then investigated using a chronoamperometric protocol.

2. Experimental

All chemicals used in this work were purchased from Sigma-Aldrich and used as received. Au films were prepared using an e-beam evaporation method utilising an adhesion layer of 150 nm Ti, followed by a 150 nm layer of Au on a Si wafer. The Si/Ti/Au wafers were then diced into 8 mm × 18 mm substrates and masked with Kapton tape to reveal an exposed region of 0.238 cm² (diameter of 5.5 mm).

2.1. Synthesis of Au honeycomb

Electrochemistry experiments were performed using a CH instrument (CHI760C) workstation with an attached amp booster (model 680). The developed substrate, a graphite rod and Ag/AgCl 3 M KCl (+0.197 V vs SHE) probe were used as the working, counter and reference electrodes, respectively. Electrodeposition of the hydrogen bubble templated Au was performed at -4 V for 300 s, in a solution of 10 mM HAuCl₄ and 2 M H₂SO₄, in accordance with our previous studies (Scheme 1A and 1B) (Coyle et al., 2016; Plowman et al. 2010, 2011).

2.2. Synthesis of Au honeycomb/ Co_3O_4 needles

Hydrothermal synthesis of cobalt hydroxide on the honeycomb-like gold surface was obtained by placing $\text{CoCl}_2 \cdot 6\text{H}_2\text{O}$ (5, 10, 25, 50 and 100 mM) and urea (60 mg) into a 6 mL capacity Teflon-lined stainless steel autoclave (Dong et al., 2012). The electrodeposited substrate was then placed into the solution standing with a 45° tilt facing the autoclave wall. The autoclave was then sealed and placed into an oven at 100 °C for 5 h. The plain Au and modified cobalt hydroxide samples were then washed with Milli-Q water, dried under N₂ gas and annealed in air at 450 °C for 2 h for the conversion of cobalt hydroxide to cobalt oxide (Scheme 1C and 1D).

2.3. Characterization

Scanning electron microscopy (SEM) was used to analyse the surface morphology by comparing the needle growth for each concentration of Co_3O_4 . SEM was performed using an FEI Verios 460L equipped with an Oxford Instruments XMax^N20 energy dispersive x-ray spectroscopy (EDX) detector. SEM imaging was performed using an accelerating voltage of 10 kV and EDX was performed at 15 kV. To view the cross section of the structures, the samples were milled using a gallium ion beam (operating at 30 kV) in an FEI Scios Dualbeam FIB. X-ray diffraction (XRD) was performed using a Bruker D8 Discover micro diffraction system with a general area diffraction detector system. A Cu-K α radiation source was used with an operating voltage of 40 kV with a current of 40 mA. X-ray photoelectron spectroscopy (XPS) was performed to determine the oxidation state of the Au, Co and O formed on the surface, using a Thermo K-alpha XPS, (Al K α = 1486.7 eV). The core level binding energies (BEs) were aligned with the adventitious C 1s binding energy of 284.8 eV.

2.4. Electrochemical glucose sensing in alkaline media

Cyclic voltammetry (CV) was employed using a scan rate 20 mV s⁻¹ in a solution of 0.5 M KOH and 10 mM glucose. Chronoamperometry was then used with a basic solution of 0.5 M KOH with glucose additions between 20 μM and 10 mM. Physiological contaminants were analysed using chronoamperometry with individual additions of 0.1 mM of sucrose, fructose, maltose and lactose and 0.02 mM of ascorbic acid and uric acid. Current density was calculated using the geometric surface area value of 0.238 cm² to enable comparison with sensors reported in literature.

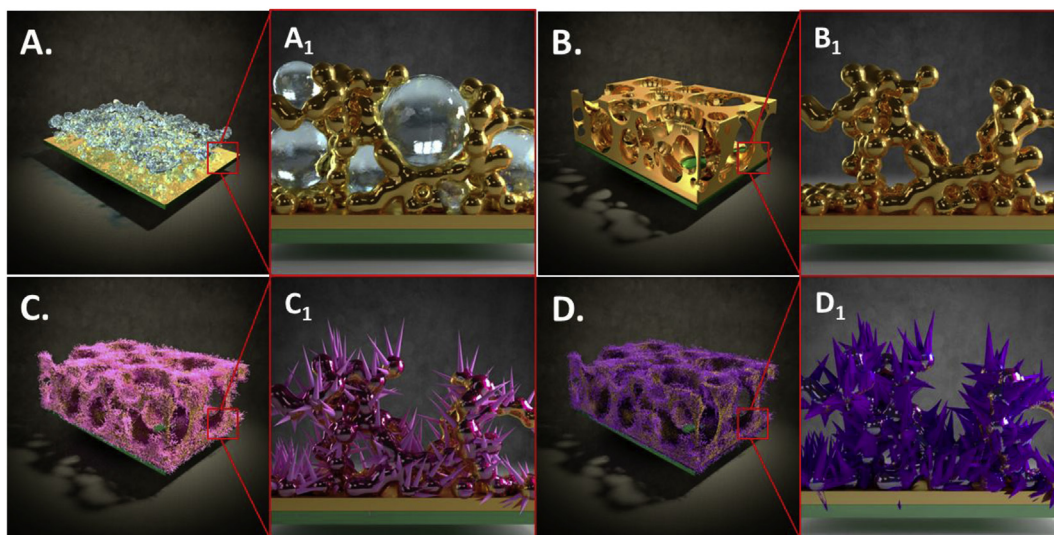
2.5. Electrochemical glucose sensing in synthetic saliva

CV analysis was employed using a scan rate of 50 mV s⁻¹ in a solution of synthetic saliva followed by the addition of 0.06 mM glucose. The synthetic saliva was prepared according to the AFNOR NF S91-141 standard which consists of Na₂HPO₄ (1 mM), KH₂PO₄ (1.5 mM), NaHCO₃ (18 mM), KSCN (3 mM), NaCl (115 mM) and KCl (16 mM) (Chaisiwamongkhon et al., 2017). Chronoamperometric additions analysis was then performed in synthetic saliva with increasing additions of glucose ranging between 0.02 mM and 1 mM. Physiological contaminants present in saliva were performed using continuous chronoamperometric additions analysis with individual additions of 2.4 μM ascorbic acid, 1.6 μM dopamine and uric acid (Raymundo-Pereira et al., 2016) followed by 0.22 μM of cortisol.

3. Results and discussion

3.1. Au honeycomb/ Co_3O_4 needle characterization

The developed hydrogen bubble templated Au honeycombs are shown in Fig. 1A displaying a highly porous large structure which formed evenly across the surface of the substrate. Fig. 1B shows the formation of the pores atop the surface of the substrate whilst retaining exposed areas of bare substrate through the porous material. The fractal formations of the hydrogen bubble templated Au which show the consistent accumulation of small Au nanostructures (~100–200 nm) are displayed in Fig. 1C–D. Smooth branched formations of Au have grown upwards from the substrate allowing for multiple active sites across the material (Coyle et al., 2017). The pure hydrogen bubble templated Au was then coated with different concentrations of CoCl_2 (5, 10, 25, 50 and 100 mM) through the hydrothermal technique mentioned above (Supplementary information S1A–F). The 5 mM surface (Supplementary information S1B) showed minimal growth of needles over the Au structures, with increasing concentrations of CoCl_2 leading to an increase in both length and spread of formations. 10 mM CoCl_2



Scheme 1. Schematic (representing low (left) and high (right) magnifications) of Au lattice formation (A) and (B) with the growth of cobalt hydroxide (C) followed by the conversion to cobalt oxide (D).

(Supplementary information S1C) and upwards, caused the needle formations to become visible at the edges of the pores. Increasing the concentration to 25 mM (Supplementary information S1D) caused a coating of needles along the top side of the structure, with the needle lengths increasing in length as the concentration was increased to 50 mM (Supplementary information S1E). The 100 mM concentration (Supplementary information S1F) appears to have completely coated the Au scaffold with obvious needle lengths increasing dramatically compared to the lower concentrations of CoCl_2 . Due to the coherent nature of the Co_3O_4 formation across the surface of the Au scaffold, all characterization and sensing studies were then focused on the 100 mM CoCl_2 sample. As is seen in Fig. 1E, the needle nanostructures have formed seamlessly across the Au scaffold whilst the pores remained unimpeded, which can be further seen in Fig. 1F. Long, sharp, needles are shown in Fig. 1G with Fig. 1H showing the needles are comprised of multiple nanoparticles forming the structure. Side imaging was performed after slicing the material using a gallium ion beam (Fig. 2A) to see how the needles formed within the Au scaffold. Backscatter imaging was then performed (Fig. 2B) where the darker regions represent Cobalt formations and the lighter regions represent Au. Analysis of high magnification images (Fig. 2C and D) showed the growth of the needles spreading throughout the Au structure. This coating (the needle-like structures) atop the Au commenced their growth both within the Au scaffold and along the top of the surface. EDX mapping of the side imaging confirms the presence of both Au (Supplementary information S2A) and Co (Supplementary information S2B) throughout the entirety of the sample, as opposed to only coating the top surface of the Au structure. Reproducibility of the sensor surfaces was performed by repeating the synthesis of the 100 mM CoCl_2 3 times (Supplementary information S3). From SEM images, repeated synthesis of the cobalt oxide rods across the surface is easily obtained via both needle length and spread across the Au scaffold. Comparison of the needle formations both pre and post annealing at 450°C were analysed using SEM imaging (Supplementary information S4A and S4B). The pre-annealed needles are observed to have a very smooth surface, whereas the needles post-annealing formed stacked particles whilst maintaining a needle-like shape (Supplementary information S4C and S4D). EDX analysis of the 100 mM CoCl_2 samples, presented in Fig. 3A shows clear peaks for Au, Co and O showing they are the three prominent materials in the sample, with calculated abundancies of Au: 44.6 wt%, Co: 23.9 wt% and O: 12.2 wt%. The appearance of Si in the EDX analysis is attributed to the Si substrate (7.4 wt%). To clarify the formed type of Co_xO_y aggregate, XRD analysis (Fig. 3B) was performed to analyse the crystalline

structure. Significant peaks in the XRD patterns appear at $2\theta = 38.4, 44.2, 64.4, 77.9$ and 81.7° which are attributed to (111), (200), (220), (311) and (222) planes of the FCC Au structure, respectively (JCPDS card no. 04-0784). Smaller and less defined peaks appear at $2\theta = 18.9, 31.3, 56.3$ and 59.4° which can be attributed to the (111), (220), (311), (422) and (511) planes of Co_3O_4 , respectively (JCPDS card no. 01-071-0816). Other peaks attributed to Co_3O_4 have been hidden by the large amount of Au in the sample, with overlapping possible between the (222), (400) and (440) peaks of Co_3O_4 and the (220), (311) and (222) planes of Au. From the XRD analysis all non-Au peaks are attributed to the common Co_3O_4 spinel phase, describing good crystalline arrays (Ibupoto et al., 2014). Further confirmation of the oxidation states of the Au, Co and O were performed using XPS analysis. The survey spectra of the formed material is shown in Fig. 3C, displaying peaks for C, Au, O and Co. Deconvolution of elemental XPS spectra for the Au (Fig. 3D), Co (Fig. 3E) and O (Fig. 3F) was used to determine the elemental states of the materials present. The main peak at 84.0 eV is attributed to the Au $4f_{7/2}$ binding energy representing the Au⁰ core level (Casaletto et al., 2006; Daima et al., 2013; Kabir et al., 2015; Pearson et al., 2011) with a corresponding doublet peak at 87.7 eV. The Co 2p spectra is consistent with previous studies comparing results obtained for different phases of cobalt species such as $\text{Co}(\text{OH})_2$, CoO and Co metal (Biesinger et al., 2011). Two main peaks lying at 780.3 and 795.4 eV represent the Co $2p_{3/2}$ and Co $2p_{1/2}$ spin-orbital lines, respectively (Liu et al., 2014; Mei et al., 2012). Upon deconvolution of the Co $2p_{3/2}$ peak it becomes apparent that both Co(II) and Co(III) oxidation states are present which is consistent with Co_3O_4 . The assurance of cobalt oxide (Co_3O_4) is further deduced from the presence of two satellite peaks (789.9 and 795.4 eV) with low intensity which have shifted to a higher binding energy, agreeing well with previous reports (Yang et al., 2010). The peak at 529.9 eV in the oxygen spectra is denoted as the O 1s peak (Nohira et al., 2002) with a satellite peak at 531.5 eV due to possible hydroxides remaining on the surface after annealing.

3.2. Au honeycomb/ Co_3O_4 needle electrochemical sensing

To analyse the applicability and on-set potential of the synthesised Au/ Co_3O_4 sensor for glucose sensing, cyclic voltammetry (CV) and chronoamperometry techniques were used. These techniques allowed for the analysis of both the surface affinity, thus rate of reaction towards glucose (e.g. sensitivity) and selectivity in the presence of common physiological contaminants. CV analysis was performed at a scan rate of 20 mVs^{-1} to examine the oxidation and reduction

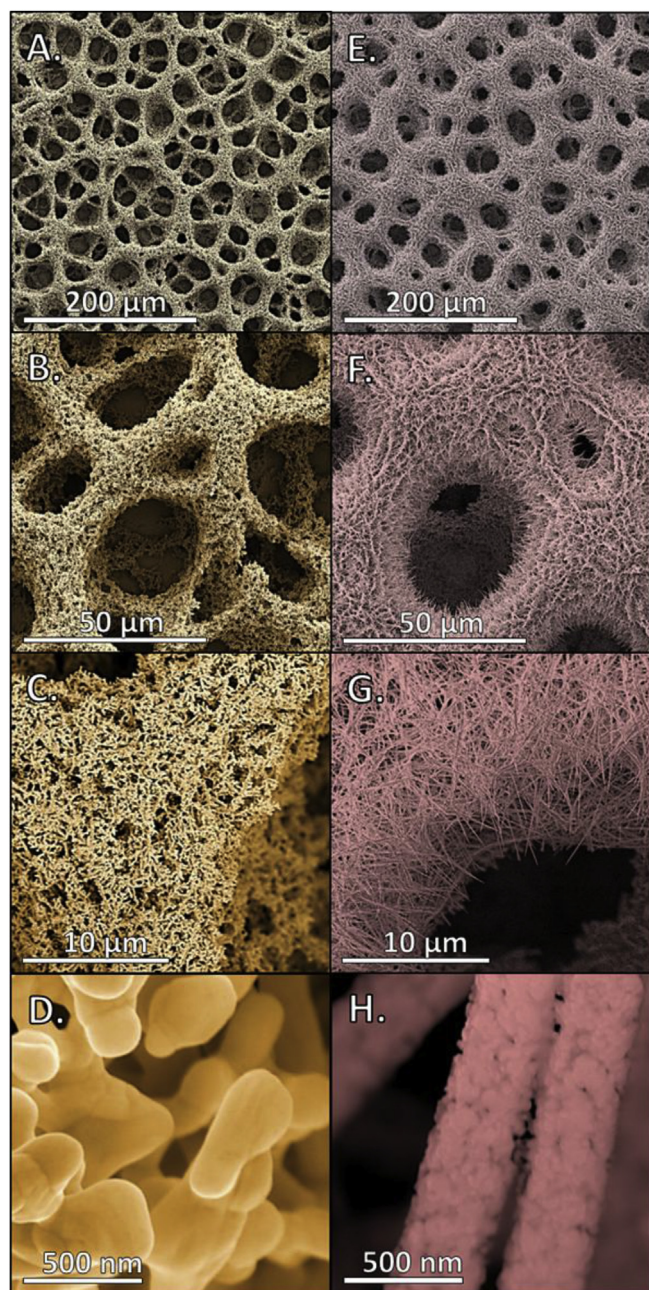
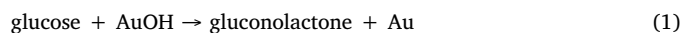


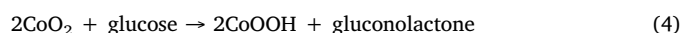
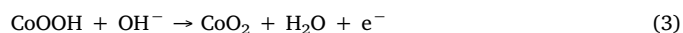
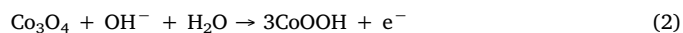
Fig. 1. SEM images (false colour) of Au honeycomb (left panel) and Au honeycomb coated with 100 mM CoCl_2 (right panel) at different magnifications (A and E) 200 μm , (B and F) 50 μm , (C and G) 10 μm and (D and H) 500 nm. (For interpretation of the references to colour in this figure legend, the reader is referred to the Web version of this article).

reactions the $\text{Au}/\text{Co}_3\text{O}_4$ undergoes in the presence of 10 mM glucose (Fig. 4A). For the continued studies 20 mV s^{-1} was chosen as the applied scan rate due to sweep rate analysis varying between 10 and 500 mV s^{-1} (Supplementary information S5) for optimal performance. From the sweep rate analysis, the increase in anodic peak height along with a shift in the peak potential as the scan rate increased was observed. The linearity of the peak increase indicates the redox process of a diffusion-controlled mechanism (Bertoncello and Ugo, 2003). This phenomenon proves the interaction between KOH, glucose and the $\text{Au}/\text{Co}_3\text{O}_4$ occurs at the electrode surface whilst maintaining electrode electroneutrality (Teixeira et al. 2004a, 2004b). From CV analysis at 20 mV s^{-1} , two large peaks were observed at +0.25 V in the forward scan and +0.1 V in the reverse scan. The large sharp peaks at each of

these points along the CV curve display a combinatory electroactivity between the Au and Co_3O_4 species in the modified $\text{Au}/\text{Co}_3\text{O}_4$ surface (Lang et al., 2013). The broad oxidation peak at +0.25 V can be attributed to the formation of gluconolactone with the conversion of Co_3O_4 to CoO_2 due to the reactions of glucose + AuOH and glucose + Co_3O_4 (Ding et al., 2010). As the potential increased above +0.3 V the formation of Au_2O_3 caused a reduction of AuOH present on the surface impeding the oxidation of glucose (Han et al., 2014). In the reverse scan the reduction of Au_2O_3 formed large amounts of AuOH and formate (Aoun et al., 2004) which allowed for a large number of active sites to be regenerated on the electrode surface. This occurrence makes way for more glucose molecules to react with the surface thus producing excellent electroactivity. The $\text{Au}/\text{Co}_3\text{O}_4$ forms a much larger anodic current for the negative scan due to the diffusion effect by the junction of Au and Co_3O_4 . As the oxide is stripped in the reverse scan, more glucose is present near the electrode surface which in turn produces a much larger enhancing the electrocatalytic activity of the sensor (Chen et al., 2010). The individual reactions are discussed below. The Au component of the surface undergoes electrosorption of glucose at low potentials which ignites the accumulation of contaminant intermediates on the electrode surface blocking the active surface sites. The formation of AuOH occurs as the potentials begin to increase which is due to the partial discharge of OH^- ions. This discharge of ions is able to catalyse glucose, forming the absorbed intermediate gluconolactone which then allows for the oxidation of Au to form AuO. This AuO formation can inhibit the electrooxidation of glucose however a further step occurs, which consists of Au being regenerated due to the AuO converting back to Au(OH) as the potentials are reduced (Ding et al., 2011). The overall reaction is described in Eqn. (1) (Han et al., 2014).



In alkaline solutions Au forms AuOH due to the reaction between OH^- ions in the basic electrolyte and the Au^+ ions on the surface structure (Coyle et al., 2017). A reversible transition between Co_3O_4 and CoOOH occurs on the surface in the presence of glucose which is represented by Eqn. (2) (Ding et al., 2010). Due to the shift in potential to the negative, a secondary reaction took place converting CoOOH to CoO_2 on the surface which is expressed by Eqn. (3) (Ramasamy et al., 2015) with the overall mechanism described in Eqn. (4) (Ding et al., 2010).



Similarly Co_3O_4 structures have been studied in the presence of glucose however due to the lack of Au in the structure, the glucose oxidation peak occurs at a much higher on-set potential (~ 0.5) (Ding et al., 2010; Kung et al., 2011) effecting the selectivity of the sensor. This desired mechanism is best observed through an alkaline electrolyte such as the KOH used in these studies, where a concentration of 0.5 M was chosen in this study as blood is slightly alkaline. As the CV peak at +0.1 V shows a high electrocatalytic activity towards glucose, chronoamperometry was performed at this onset potential to analyse its sensing capabilities in the presence of glucose. Fig. 4B shows the additions analysis of the $\text{Au}/\text{Co}_3\text{O}_4$ sensor in the presence of 0.5 M KOH with a large range of glucose concentrations (20 μM and 10 mM). The chronoamperometric additions analysis is further evidenced by the multiple linear regression lines (Supplementary information S6) showing two distinct linear ranges for the $\text{Au}/\text{Co}_3\text{O}_4$ sensor. To detail the linear regions more specifically two linear regression regions were found for the sensor giving two separate sensitivities depending on the glucose concentration. Ranging between 20 μM and 100 μM (Supplementary information S6A) a very large, sharp peak was observed

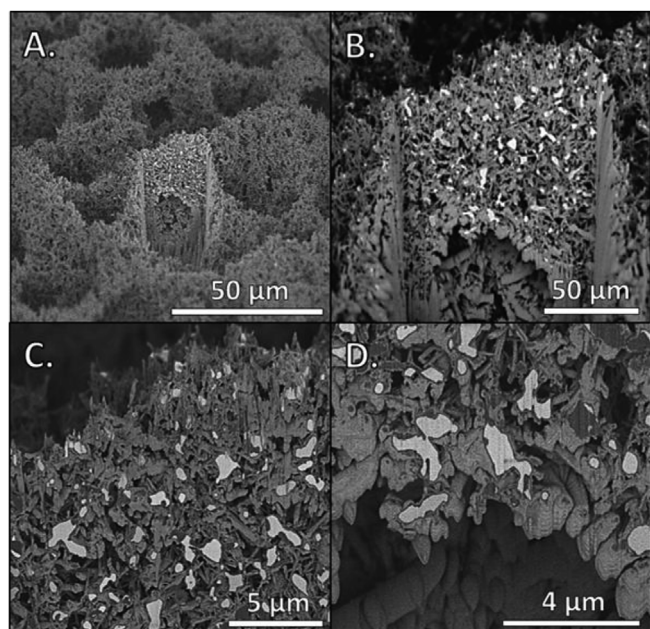


Fig. 2. (A) Low magnification side-viewing of the 100 mM sample after laser cutting followed by (B) higher magnification backscatter imaging; (C) High magnification backscatter imaging of the top and (D) bottom portions of the lattice.

equating to a calculated sensitivity of $2.014 \text{ mA mM}^{-1}\text{cm}^{-2}$. A secondary linear region ranging between 2 mM and 10 mM (Supplementary information S6B) had a calculated sensitivity of $0.011 \text{ mA mM}^{-1}\text{cm}^{-2}$, which corresponds to the blood glucose monitoring range of 3–8 mM. An experimental detection limit (Supplementary information S7) of $20 \mu\text{M}$ was observed from the initial addition of glucose to the 0.5 M KOH solution, showing the effectiveness of the sensing capabilities of the surface in the presence of very low glucose concentrations. This detection limit is much lower than common commercially available glucose sensors of recent times ($\sim 2.2 \text{ mM}$) (Lee et al., 2019). Comparatively Au honeycomb was also analysed with chronoamperometric additions analysis (Fig. 4C) showing a much lower electroactivity in the presence of glucose. A large increase in current response between the plain Au (0.146 mA cm^{-2}) and the Au/Co₃O₄ composite material (0.348 mA cm^{-2}) is observed by a factor of 2.39 showing the addition of Co₃O₄ to the surface of the Au more than doubled the glucose sensitivity. Uninterrupted chronoamperometric analysis was then performed for selectivity analysis in the presence of common physiological contaminants (Fig. 4D). The contaminants analysed were ascorbic acid, sucrose, fructose, maltose, lactose and uric acid. Little to no electrochemical signal was produced with each addition to the 0.5 M KOH solution showing the sensor is specifically catered to glucose concentrations. A subsequent glucose addition of 10 mM was introduced to the contaminants solutions showing a large current response. Due to the presence of Au in the material the on-set potential, where glucose electrooxidation is at its maximum, has been reduced to +0.1 V. Metal oxides tend to display a glucose peak with a much higher on-set potential, where common physiological contaminants display higher current responses with larger on-set potentials which can severely affect the sensors response capabilities towards glucose (Lang et al., 2013). This confirms excellent selectivity towards glucose with the further conclusion that the presence of common physiological sugars and acids do not affect the sensors performance. Repeatability analysis (Supplementary information S8) was then performed on the sensor with 5 consecutive cycles in the presence of 10 mM glucose with a slight reduction in output performance to 91%, thus showing excellent sensing performance over multiple cycles.

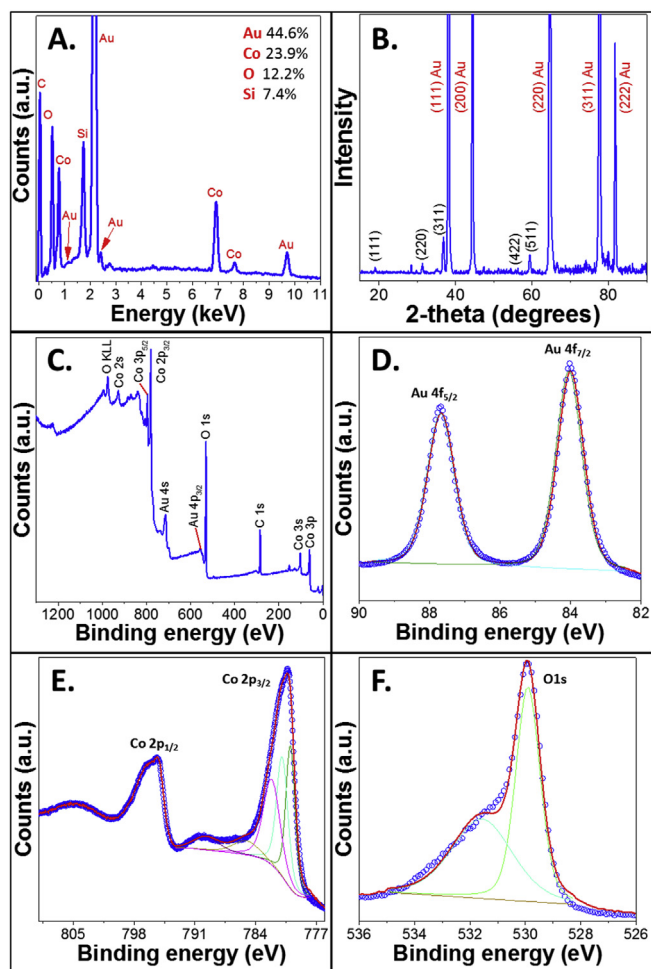


Fig. 3. Characterization of Au needles with 100 mM CoCl₂ (A) EDX spectral analysis, (B) XRD analysis (C) XPS survey spectra (D) XPS analysis of gold (E) XPS spectra of cobalt and (F) XPS spectra of oxygen. (For interpretation of the references to colour in this figure legend, the reader is referred to the Web version of this article).

3.3. Au honeycomb/Co₃O₄ needle sensing in synthetic saliva

Due to the low concentration range of glucose in saliva (0.03–0.08 mM) and the very high sensitivity of the developed sensor within this glucose concentration range ($2.014 \text{ mA mM}^{-1}\text{cm}^{-2}$), electroanalytical testing was extended to the detection of glucose in synthetic saliva. To explore this system, CV analysis was performed in the presence (80 μM) and absence of glucose (Fig. 5A) in synthetic saliva. A singular peak is formed through the oxidation of glucose ranging between +0.015 and +0.25 V with a peak maximum at +0.15 V. Based on the similar peak position in Fig. 4A, the onset potential for chronoamperometric analysis was fixed at +0.1 V. The use of +0.1 V remains consistent with our previous studies for glucose detection in the human range for blood. The chronoamperometric additions analysis (Fig. 5B) was then performed in synthetic saliva with increasing concentrations of glucose ranging between 20 μM and 1 mM (similar to common glucose concentrations in saliva) (Ye et al., 2013). The calibration curve of the additions analysis (Supplementary information S9) showed an overall sensitivity of $0.0235 \text{ mA mM}^{-1}\text{cm}^{-2}$ with an R^2 value of 0.98. Increasing current responses with incremental additions showed a good sensitivity for the low concentration range. This sensitivity demonstrates the sensor's capability to detect glucose in the synthetic saliva, showing great promise for the non-invasive detection of physiological glucose levels. Long term stability of the sensor was

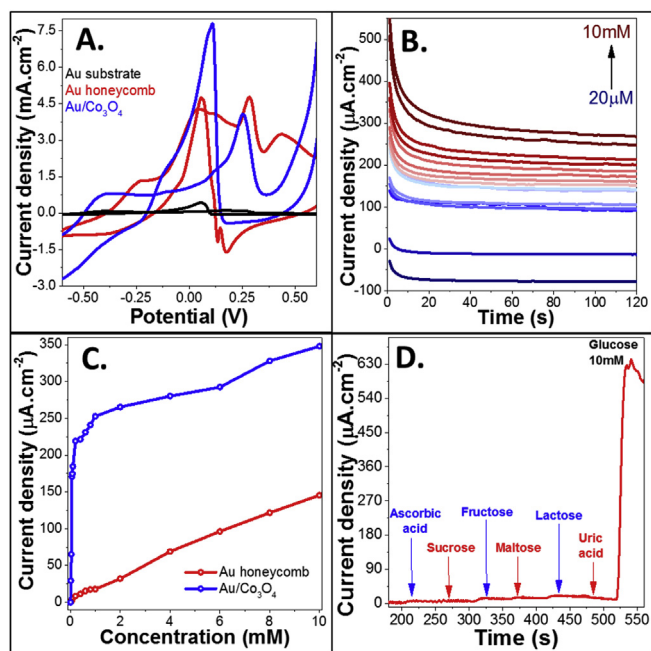


Fig. 4. (A) CV analysis of Au (black), Au honeycomb (red) and Au/Co₃O₄ (blue) in 0.5 M KOH and 10 mM glucose (B) chronoamperometric analysis of Au/Co₃O₄ with additions of glucose ranging between 20 μ M and 10 mM (C) comparison graphs of chronoamperometric additions analysis for Au honeycomb (red) and Au/Co₃O₄ and (D) chronoamperometric additions analysis of Au/Co₃O₄ in the presence of common physiological contaminants. (For interpretation of the references to colour in this figure legend, the reader is referred to the Web version of this article).

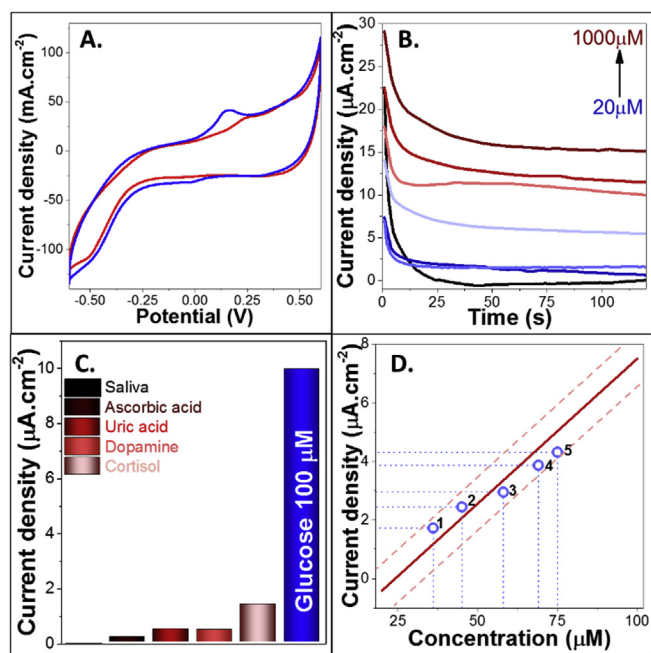


Fig. 5. (A) CV analysis of Au/Co₃O₄ in synthetic saliva with (blue) and without (red) 80 μ M glucose. (B) Chronoamperometric analysis of Au/Co₃O₄ in the presence of synthetic saliva with 20 μ M and 1 mM glucose. (C) Current density response for physiological contaminants in the presence of synthetic saliva and (D) Calibration curve (red) of current density vs concentration for glucose additions in the presence of synthetic saliva with 5 additions of unknown glucose concentrations (blue). (For interpretation of the references to colour in this figure legend, the reader is referred to the Web version of this article).

performed in synthetic saliva with glucose (Supplementary information S10) showing the current response of the sensor reducing slowly over time. The current response reduction is due to the saturation of the sensors surface due to glucose, therefore impeding the current response of the sensor over extended periods of time. Contaminants analysis was performed on the sensor (Supplementary information S11) with the additions of 2.4 μ M ascorbic acid, 1.6 μ M uric acid, 1.6 μ M dopamine and 0.22 μ M cortisol (Campos et al., 2018) followed by 100 μ M glucose. Fig. 5C displays the current response in the form of a bar graph for each addition after a stability time of 120 s was reached. From these additions ascorbic acid showed a very small response magnitude of 0.185 μ A cm⁻² (1.3% of glucose response), with uric acid showing 0.471 μ A cm⁻² (3.3% vs glucose response). Dopamine showed a miniscule decrease in current response to 0.455 μ A cm⁻² (3.2% of glucose response) while cortisol showed the largest effect to the current response, increasing to 1.384 μ A cm⁻² (9.7% of glucose response). Overall the effect of each contaminant was in the acceptable range (\pm 10%) as the current response after the addition of 100 μ M glucose was 9.98 μ A cm⁻², within a similar range to our previous glucose response analysis. The results indicate that the sensor is not only selective in KOH medium but also in synthetic saliva thus making it feasible to be used for non-invasive diagnostic applications. To test the real-life application and repeatability of the sensor, 5 unknown solutions of glucose (within the concentration range of 20–80 μ M) were tested. Initially a calibration curve was formed using the 120 s response current for each glucose addition from the additions analysis (Supplementary information S9). Using this calibration curve and the current response for the unknown additions, data points were added to the graph and analysed for their percentage change compared to the calibration line (Fig. 5D). In analysing the change in concentration between the ‘unknown’ solution and the calibration curve concentration (Supporting information Table S3), an average percentage change of 9.7% with the variance of results ranging between a percentage range of 7.8 and 13.3%. The unknown solutions analysis and excellent selectivity in the presence of common physiological contaminants in both blood and saliva shows very promising capabilities for glucose biosensor which can be used for non-invasive diagnosis applications.

4. Conclusions

In this study we have presented an easily synthesised porous Au structure with Co₃O₄ needles cohesively and seamless coating the Au surface whilst retaining its porosity and macro-structure. XRD and XPS analysis showed the clear representation of Au and Co₃O₄ on the surface, with the combination of the two components observed in cyclic voltammetry analysis in the presence of glucose. Excellent electrochemical sensing performance of the structure was observed in the presence of glucose with a calculated sensitivity of 2.014 mA mM⁻¹cm⁻² within the range of 0–0.1 mM and 0.011 mA mM⁻¹cm⁻² within 2–10 mM glucose. A very low experimental detection limit of 20 μ M makes this sensor very attractive for applications involving saliva, sweat and tear based electrochemical glucose sensors. Little or no cross-interference was observed in the presence of common physiological contaminants such as AA and UA and common biological sugars. Further to this, glucose detection in synthetic saliva showed excellent calculated sensitivity of 0.0235 mA mM⁻¹cm⁻² with minimal effect by interfering species commonly found in saliva such as cortisol and dopamine. These results showed that the fabricated sensor is highly capable for non-invasive diagnostic applications.

Declaration of interests

The authors declare that they have no known competing financial interests or personal relationships that could have appeared to influence the work reported in this paper.

CRedit authorship contribution statement

Victoria E. Coyle: Conceptualization, Investigation, Visualization, Formal analysis, Writing - original draft, Writing - review & editing. **Ahmad E. Kandjani:** Conceptualization, Investigation, Visualization, Formal analysis, Writing - review & editing. **Matthew R. Field:** Formal analysis, Writing - review & editing. **Patrick Hartley:** Investigation, Funding acquisition, Writing - review & editing. **Miao Chen:** Investigation, Funding acquisition, Writing - review & editing. **Ylias M. Sabri:** Supervision, Conceptualization, Investigation, Formal analysis, Writing - original draft, Writing - review & editing. **Suresh K. Bhargava:** Supervision, Project administration, Funding acquisition, Investigation, Formal analysis, Writing - review & editing.

Acknowledgements

The authors acknowledge the RMIT Microscopy and Microanalysis Facility (RMMF) for allowing the use of their comprehensive facilities and services. The authors thank Mr Cio Yuxun for his technical support. The authors thank CSIRO Mineral Resources for the PhD scholarship support. A.E.K. thanks RMIT University for a Vice Chancellor's Postdoctoral Fellowship.

Appendix A. Supplementary data

Supplementary data to this article can be found online at <https://doi.org/10.1016/j.bios.2019.111479>.

References

- Anderson, K., Poulter, B., Dudgeon, J., Li, S.-E., Ma, X., 2017. *Sensors* 17 (8), 1807.
- Aoun, S.B., Dursun, Z., Koga, T., Bang, G.S., Sotomura, T., Taniguchi, I., 2004. *J. Electroanal. Chem.* 567 (2), 175–183.
- Association, A.D., 2018. *Diabetes Care* 41 (5), 917.
- Bandodkar, A.J., Wang, J., 2014. *Trends Biotechnol.* 32 (7), 363–371.
- Barry, E., Roberts, S., Oke, J., Vijayaraghavan, S., Normansell, R., Greenhalgh, T., 2017. *BMJ* 356, i6538.
- Bertoncello, P., Ugo, P., 2003. *J. Braz. Chem. Soc.* 14 (4), 517–522.
- Biesinger, M.C., Payne, B.P., Grosvenor, A.P., Lau, L.W.M., Gerson, A.R., Smart, R.S.C., 2011. *Appl. Surf. Sci.* 257 (7), 2717–2730.
- Boisselier, E., Astruc, D., 2009. *Chem. Soc. Rev.* 38 (6), 1759–1782.
- Campos, A.M., Raymundo-Pereira, P.A., Mendonça, C.D., Calegari, M.L., Machado, S.A., Oliveira Jr., O.N., 2018. *ACS Appl. Nano Mater.* 1 (2), 654–661.
- Casaleto, M., Longo, A., Martorana, A., Prestianni, A., Venezia, A., 2006. *Surf. Interface Anal.* 38 (4), 215–218.
- Chaisiwamongkhon, K., Batchelor-McAuley, C., Compton, R.G., 2017. *Analyst* 142 (15), 2828–2835.
- Chakraborty, P., Dhar, S., Debnath, K., Majumder, T., Mondal, S.P., 2019. *Sensor. Actuator. B Chem.* 283, 776–785.
- Chen, L., Fujita, T., Ding, Y., Chen, M., 2010. *Adv. Funct. Mater.* 20 (14), 2279–2285.
- Cheng, T.-M., Huang, T.-K., Lin, H.-K., Tung, S.-P., Chen, Y.-L., Lee, C.-Y., Chiu, H.-T., 2010. *ACS Appl. Mater. Interfaces* 2 (10), 2773–2780.
- Coyle, V.E., Kandjani, A.E., Sabri, Y.M., Bhargava, S.K., 2017. *Electroanalysis* 29 (1), 294–304.
- Coyle, V.E., Oppedisano, D.K., Jones, L.A., Kandjani, A.E., Sabri, Y.M., Bhargava, S.K., 2016. *J. Electrochem. Soc.* 163 (14), B689–B695.
- Daima, H.K., Selvakannan, P., Shukla, R., Bhargava, S.K., Bansal, V., 2013. *PLoS One* 8 (10), e79676.
- Ding, Y., Liu, Y., Parisi, J., Zhang, L., Lei, Y., 2011. *Biosens. Bioelectron.* 28 (1), 393–398.
- Ding, Y., Wang, Y., Su, L., Bellagamba, M., Zhang, H., Lei, Y., 2010. *Biosens. Bioelectron.* 26 (2), 542–548.
- Dong, X.-C., Xu, H., Wang, X.-W., Huang, Y.-X., Chan-Park, M.B., Zhang, H., Wang, L.-H., Huang, W., Chen, P., 2012. *ACS Nano* 6 (4), 3206–3213.
- Han, L., Zhang, S., Han, L., Yang, D.-P., Hou, C., Liu, A., 2014. *Electrochim. Acta* 138, 109–114.
- Ibupoto, Z.H., Elhag, S., AlSalhi, M., Nur, O., Willander, M., 2014. *Electroanalysis* 26 (8), 1773–1781.
- Kabir, K.M., Sabri, Y.M., Kandjani, A.E., Matthews, G.I., Field, M., Jones, L.A., Nafady, A., Ippolito, S.J., Bhargava, S.K., 2015. *Langmuir* 31 (30), 8519–8529.
- Kimmel, D.W., LeBlanc, G., Meschievitz, M.E., Cliffl, D.E., 2011. *Anal. Chem.* 84 (2), 685–707.
- Kownacka, A.E., Vegelyte, D., Joosse, M., Anton, N., Toebes, B.J., Lauko, J., Buzzacchera, I., Lipinska, K., Wilson, D.A., Geelhoed-Duijvestijn, N., 2018. *Biomacromolecules* 19 (11), 4504–4511.
- Kung, C.-W., Lin, C.-Y., Lai, Y.-H., Vittal, R., Ho, K.-C., 2011. *Biosens. Bioelectron.* 27 (1), 125–131.
- Lang, X.-Y., Fu, H.-Y., Hou, C., Han, G.-F., Yang, P., Liu, Y.-B., Jiang, Q., 2013. *Nat. Commun.* 4, 2169.
- Lankelma, J., Nie, Z., Carrilho, E., Whitesides, G.M., 2012. *Anal. Chem.* 84 (9), 4147–4152.
- Lay, B., Coyle, V.E., Kandjani, A.E., Amin, M.H., Sabri, Y.M., Bhargava, S.K., 2017. *J. Mater. Chem. B* 5 (5), 5441–5449.
- Lee, I., Loew, N., Tsugawa, W., Ikebukuro, K., Sode, K., 2019. *Biosens. Bioelectron.* 124–125, 216–223.
- Liu, X., Chang, Z., Luo, L., Xu, T., Lei, X., Liu, J., Sun, X., 2014. *Chem. Mater.* 26 (5), 1889–1895.
- Mei, W., Huang, J., Zhu, L., Ye, Z., Mai, Y., Tu, J., 2012. *J. Mater. Chem.* 22 (18), 9315–9321.
- Moyer, J., Wilson, D., Finkelshtein, I., Wong, B., Potts, R., 2012. *Diabetes Technol. Ther.* 14 (5), 398–402.
- Nohira, H., Tsai, W., Besling, W., Young, E., Petry, J., Conard, T., Vandervorst, W., De Gendt, S., Heyns, M., Maes, J., Tuominen, M., 2002. *J. Non-Cryst. Solids* 303 (1), 83–87.
- Pearson, A., O'Mullane, A.P., Bansal, V., Bhargava, S.K., 2011. *Inorg. Chem.* 50 (5), 1705–1712.
- Plowman, B.J., O'Mullane, A.P., Bhargava, S.K., 2011. *Faraday Discuss* 152, 43–62.
- Plowman, B.J., O'Mullane, A.P., Selvakannan, P., Bhargava, S.K., 2010. *Chem. Commun.* 46 (48), 9182–9184.
- Ramasamy, R., Ramachandran, K., Philip, G.G., Ramachandran, R., Therese, H.A., Gnana Kumar, G., 2015. *RSC Adv.* 5 (93), 76538–76547.
- Raymundo-Pereira, P.A., Shimizu, F.M., Coelho, D., Piazzetta, M.H., Gobbi, A.L., Machado, S.A., Oliveira Jr., O.N., 2016. *Biosens. Bioelectron.* 86, 369–376.
- Roberts, K., Jaffe, A., Verge, C., Thomas, P.S., 2012. *J. Diabetes Sci. Technol.* 6 (3), 659–664.
- Solanki, P.R., Kaushik, A., Agrawal, V.V., Malhotra, B.D., 2011. *NPG Asia Mater.* 3 (1), 17.
- Teixeira, M.F., Bergamini, M.F., Marques, C.M., Bocchi, N., 2004a. *Talanta* 63 (4), 1083–1088.
- Teixeira, M.F., Marcolino-Júnior, L.H., Fatibello-Filho, O., Dockal, E.R., Cavalheiro, É.T., 2004b. *J. Braz. Chem. Soc.* 15 (6), 803–808.
- Toghill, K.E., Compton, R.G., 2010. *Int. J. Electrochem. Sci.* 5 (9), 1246–1301.
- Tong, G.-X., Liu, F.-T., Wu, W.-H., Shen, J.-P., Hu, X., Liang, Y., 2012. *CrystEngComm* 14 (18), 5963–5973.
- Wang, G., He, X., Wang, L., Gu, A., Huang, Y., Fang, B., Geng, B., Zhang, X., 2013. *Microchim. Acta* 180 (3–4), 161–186.
- Wang, J., 2008. *Chem. Rev.* 108 (2), 814–825.
- Wang, W., Li, Z., Liu, L., Zhang, H., Zheng, W., Wang, Y., Huang, H., Wang, Z., Wang, C., 2009. *Sensor. Actuator. B Chem.* 141 (2), 404–409.
- Yang, J., Liu, H., Martens, W.N., Frost, R.L., 2010. *J. Phys. Chem. C* 114 (1), 111–119.
- Yao, H., Shum, A.J., Cowan, M., Lähdesmäki, I., Parviz, B.A., 2011. *Biosens. Bioelectron.* 26 (7), 3290–3296.
- Ye, D., Liang, G., Li, H., Luo, J., Zhang, S., Chen, H., Kong, J., 2013. *Talanta* 116, 223–230.
- Zhang, Y., Chang, G., Liu, S., Lu, W., Tian, J., Sun, X., 2011. *Biosens. Bioelectron.* 28 (1), 344–348.
- Zhu, H., Li, L., Zhou, W., Shao, Z., Chen, X., 2016. *J. Mater. Chem. B* 4 (46), 7333–7349.

Supporting Information

Co₃O₄ needles on Au honeycomb as a non-invasive electrochemical biosensor in saliva

Victoria E. Coyle^{a,b}, Ahmad E. Kandjani^a, Matthew R. Field^c, Patrick Hartley^b, Miao Chen^{a,b}, Ylias M. Sabri^{a*} and Suresh K. Bhargava^{a*}

*Email: suresh.bhargava@rmit.edu.au; ylias.sabri@rmit.edu.au, Ph: +61 3 9925 2330

^a *Centre for Advanced Materials and Industrial Chemistry (CAMIC), School of Science, RMIT University, Melbourne, Victoria 3001, Australia*

^b *CSIRO, Bayview Avenue, Clayton, Victoria 3168, Australia*

^c *RMIT Microscopy & Microanalysis Facility, RMIT University, Melbourne*

**RECEIVED DATE (to be automatically inserted after your manuscript is accepted if required
according to the journal that you are submitting your paper to)**

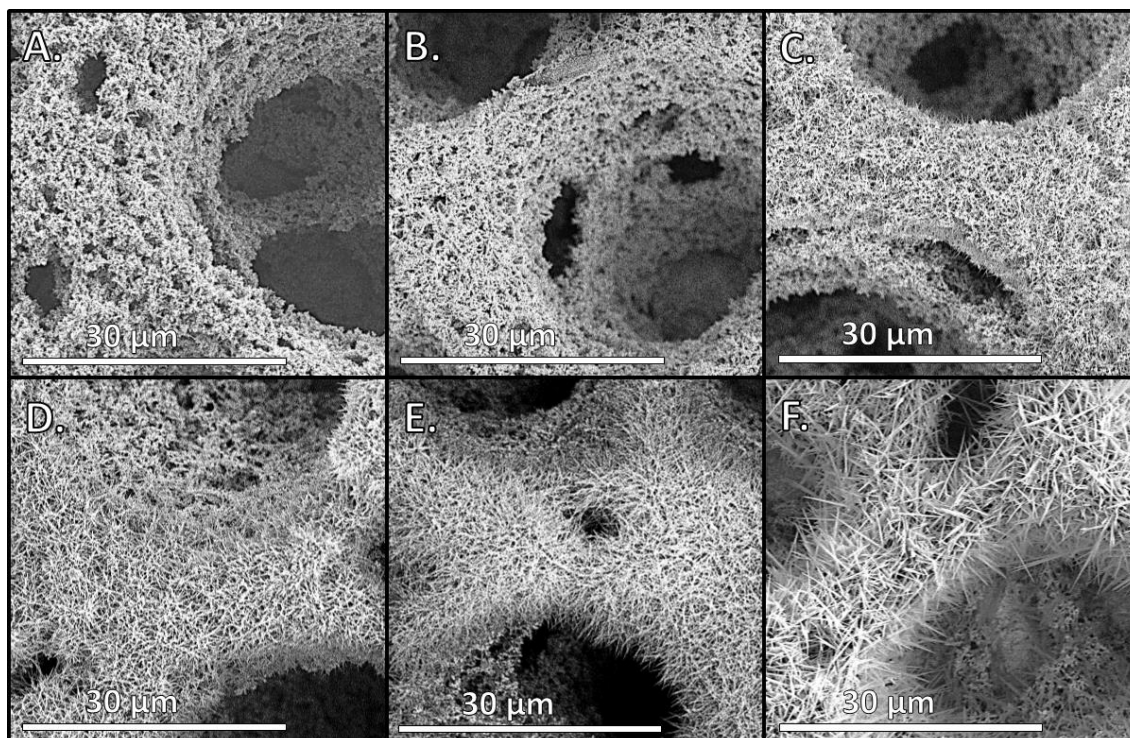


Figure S1 SEM images of Au honeycomb with differing CoCl_2 concentrations (A) 0 mM (B) 5 mM (C) 10 mM (D) 25 mM (E) 50 mM and (F) 100 mM

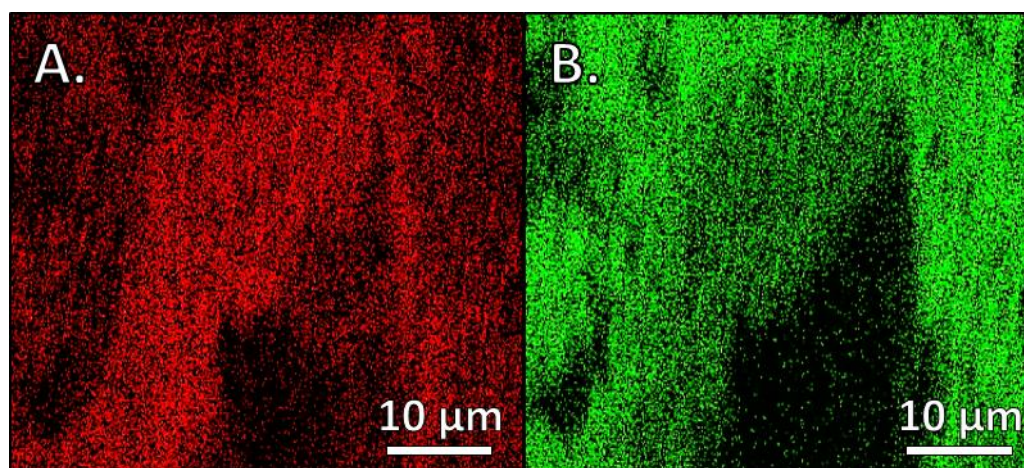


Figure S2 EDX mapping analysis of the Au with 100 mM CoCl_2 analysing for (a) Au and (b) Co

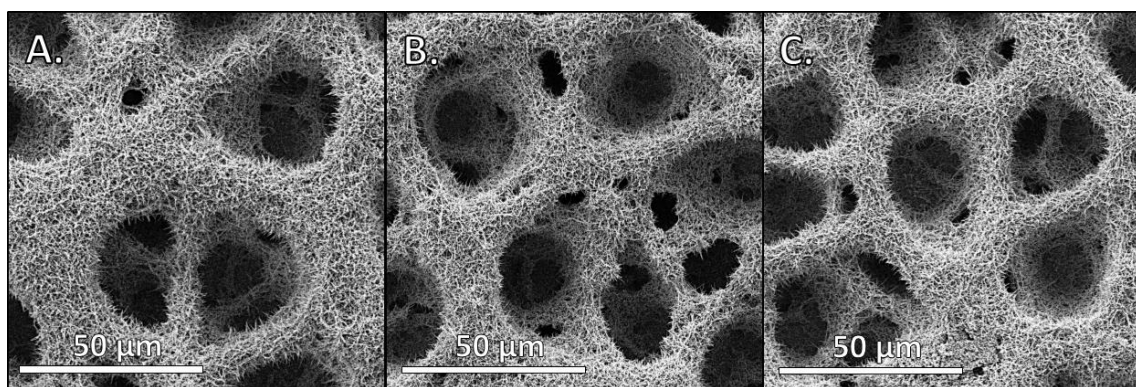


Figure S3 SEM images of Au honeycomb synthesised with 100 mM CoCl_2 reproduced 3 times

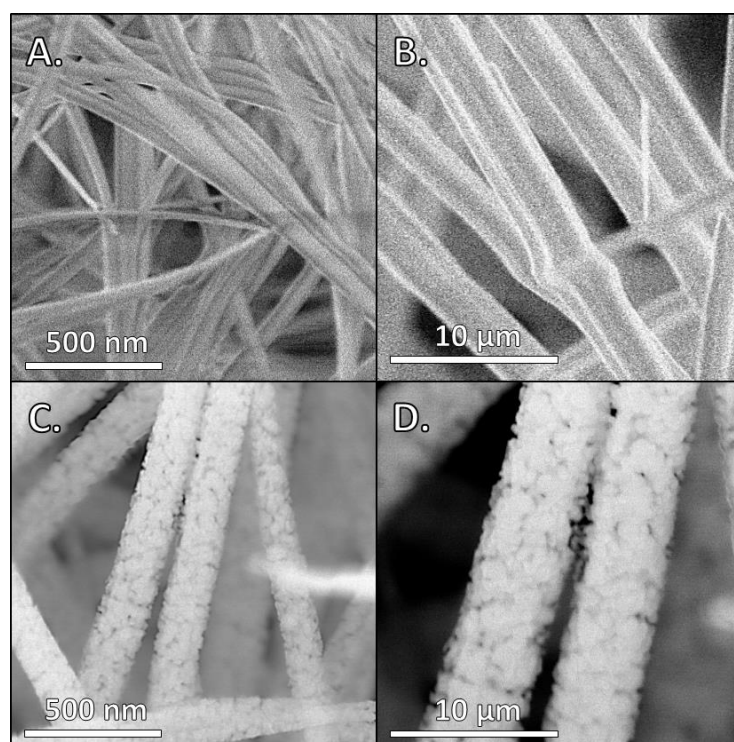


Figure S4 SEM images of needles made of 100 mM CoCl_2 unannealed (A and B) and annealed (C and D)

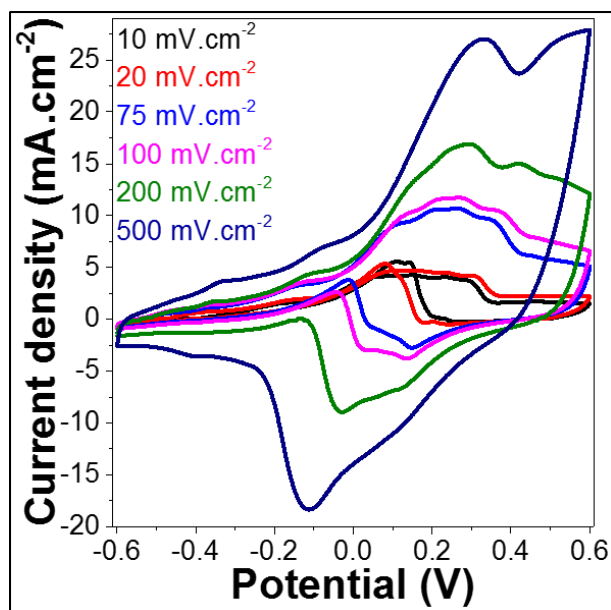


Figure S5 Cyclic voltammetry of Au/Co₃O₄ in 0.5 M KOH and 10 mM glucose solution at varying sweep rates between 10 and 500 mVs⁻¹

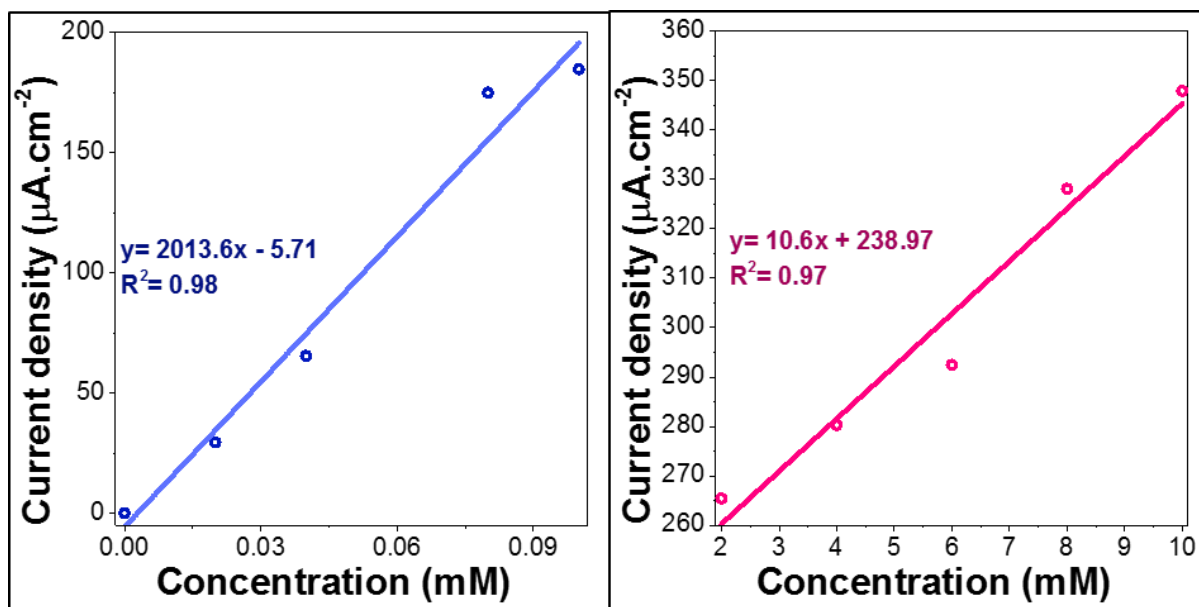


Figure S6 Linear regression graphs between concentrations of (A) 0 μM and 100 μM glucose and (B) 2 mM and 10 mM glucose in a 0.5 M KOH basic solution

Glucose addition (mM)	Current density at 5s ($\mu\text{A}\cdot\text{cm}^{-2}$)	Current density at 10s ($\mu\text{A}\cdot\text{cm}^{-2}$)	Current density at 50s ($\mu\text{A}\cdot\text{cm}^{-2}$)	Current density at 120s ($\mu\text{A}\cdot\text{cm}^{-2}$)
0.02	-14.47	-16.5	-18.24	-18.61
0.04	-0.019	-1.44	-2.85	-3.14
0.06	28.11	27.08	25.17	21.8
0.08	29.46	27.24	23.45	22.72
0.1	32.09	29.24	25.85	25.09
0.2	43.71	39.5	34.67	33.08
0.4	46.24	41.24	34.71	33.83
0.6	46.13	41.92	37.07	36.13
0.8	48.95	44.66	39.67	38.38
1	53.16	48.2	42.39	41.25
2	60.26	54.14	46.37	44.05
4	65.11	58.38	50.05	47.86
6	70.82	63.37	54.07	50.76
8	87.98	77.29	63.58	59.04
10	96.06	84.5	68.87	63.91

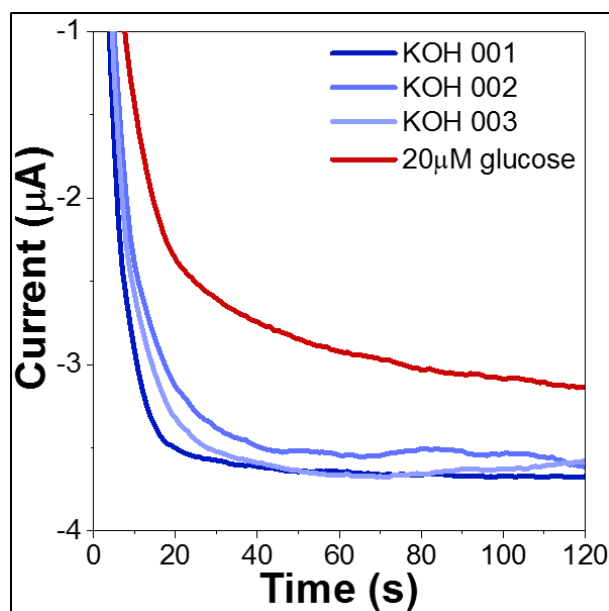
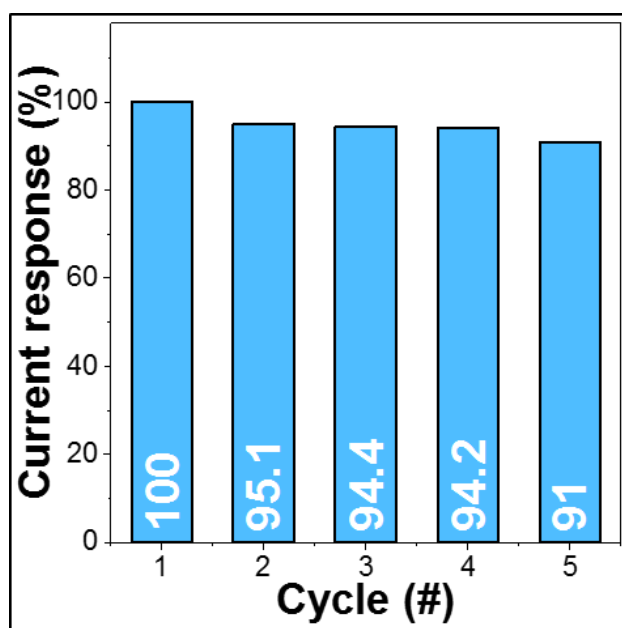


Table S1 Additions for chronoamperometric analysis of glucose in alkaline media

Figure S7 Chronoamperometric additions analysis with 3 consecutive runs in 0.5 M KOH



solution followed by the addition of 20 μM of glucose.

Figure S8 Repeatability analysis with 5 consecutive runs in 0.5 M KOH after 100 s analysis in a solution of 0.5 M KOH 10 mM glucose using the chronoamperometric technique.

Glucose addition (μM)	Current density at 5s ($\mu\text{A}\cdot\text{cm}^{-2}$)	Current density at 10s ($\mu\text{A}\cdot\text{cm}^{-2}$)	Current density at 50s ($\mu\text{A}\cdot\text{cm}^{-2}$)	Current density at 120s ($\mu\text{A}\cdot\text{cm}^{-2}$)
20	3.42	2.58	1.41	0.62
40	2.75	1.99	1.52	1.59
80	9.61	8.53	6.17	5.47
100	12.66	11.41	11.31	9.98
110	17.44	15.4	12.65	11.53
1000	22.91	20.19	15.89	15.12

Table S2 Additions for chronoamperometric analysis of glucose in synthetic saliva

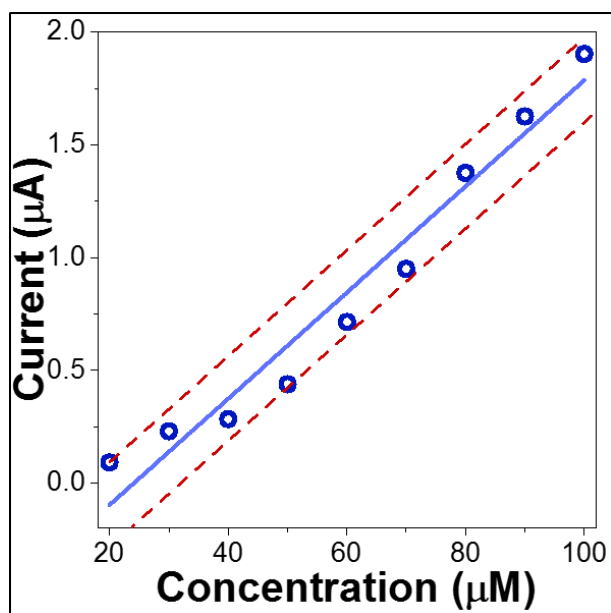


Figure S9 Calibration curve (blue) of chronoamperometric additions of glucose ranging between 20 and 100 μM . Limit lines (red) showing maximum and minimum limit ranges show the limit or error for the calibration

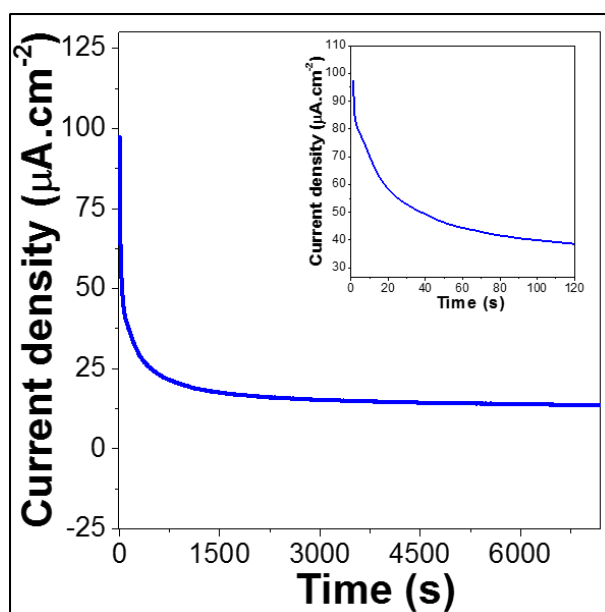


Figure S10 Stability analysis of Au/Co₃O₄ over 2 hours in synthetic saliva and 10 mM glucose solution. Inset of current response for conventional 0 – 120 s scan duration.

Number (#)	Addition (μM)	Current response ($\mu\text{A}\cdot\text{cm}^{-2}$)	Calibration curve concentration (μM)	Concentration Recovery percentage (%)	Change (%)
1	36	1.726	41.5	86.7	13.3
2	45	2.445	48.8	92.2	7.8
3	58	2.949	53.9	107.6	7.6
4	69	3.869	63.2	109.2	9.2
5	75	4.315	67.7	110.8	10.8

Table S3 Response magnitudes obtained for solutions with unknown glucose concentrations added to synthetic saliva. The percentage change in concentration output with respect to the calibration curve is presented.

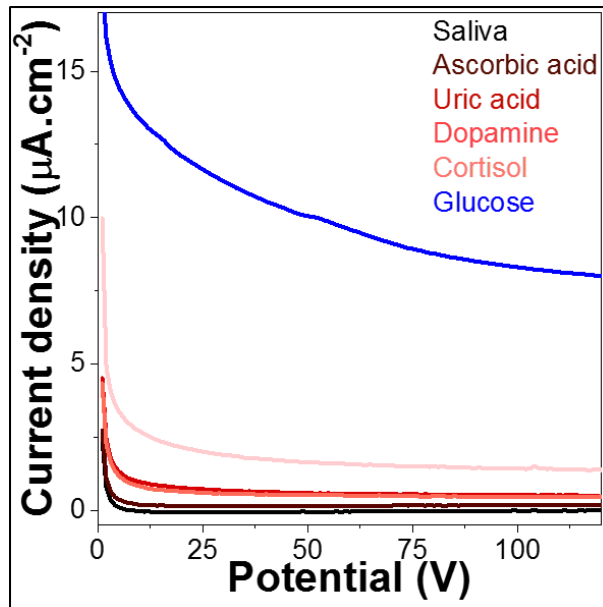


Figure S11 Chronoamperometric analysis of Au/Co₃O₄ sensor in synthetic saliva with the addition of ascorbic acid, uric acid, dopamine and cortisol followed by glucose.

CHAPTER VII:

Conclusions and Future Work

In this chapter, the summary of the work presented in this thesis is discussed and potential avenues for future work are provided

7.1 Summary of Key Findings

In this work a succession of nanostructures around the functionality of Au in different forms have been investigated for their application and modification for optimal glucose electrooxidation in the form of non-enzymatic glucose biosensors. Forms of gold studied began with the mono-metallic Au nanospikes, followed by an Au-Pt alloy using the hydrogen bubble template technique. Au nanoparticles were scattered atop Ni colloids using galvanic replacement which was then studied, finishing with a pure Au hydrogen bubble templated lattice with hydrothermally deposited Co_3O_4 nanowires. By producing various structures, the overall goal was to increase sensitivity without hindering the selectivity of Au in the presence of common physiological contaminants. The monometallic Au nanospikes provided excellent selectivity in the presence of common physiological contaminants which have consistently hindered glucose sensing, however the sensitivity ($91.8 \mu\text{A}\cdot\text{mM}^{-1}\cdot\text{cm}^{-2}$) was moderate compared to other glucose sensors. Optimal conditions of the electrodeposited nanospikes were compared to study the influence of HAuCl_4 concentration (13.6 mM optimal), Pb acetate concentration (1 mM optimal), electrodeposition time (12 mins optimal) and electrodeposition potential (+0.05 V optimal). Each of these optimal conditions were determined using cyclic voltammetry (CV) analysis for both their electrochemical surface area (ECSA) and glucose response. In this study a different method of analysing the glucose sensing response was analysed in the form of an elaborated chronoamperometric analysis method. This method showed individual extended response analysis for each glucose addition showing the stability and overall sensitivity of current responses at various response times and glucose concentrations.

To improve sensitivity the use of a Au-Pt alloy was investigated. To determine the optimum Pt concentration added to Au which produced the largest glucose sensitivity various structures were formed with varying Pt (0.5, 1, 2.5 and 5 mM) whilst maintaining the HAuCl_4 concentration. CV analysis and electrochemical surface area (ECSA) were analyzed for optimal glucose electrooxidation characteristics. Characterisation analysis (EDX, XRD and XPS) showed the surface formed was a cohesive alloyed material meaning the glucose electrooxidation was impacted by both the Pt and Au components on an even scale. Due to this a high sensitivity was detected at $109.3 \mu\text{A}\cdot\text{mM}^{-1}\cdot\text{cm}^{-2}$ with a low detection limit of 12.9 μM . Due to the presence of Au in the material, good selectivity was obtained in the presence of common physiological contaminants. The effect of Au decoration was then examined using a surface consisting of colloidal Ni monodispersed across an electrode surface with scattered Au nanoparticles across its surface using galvanic replacement reaction. Four HAuCl_4 concentrations (0.01, 0.1, 1 and 2 mM) were studied for optimising the deposition uniformity and particle size on the surface for optimal glucose electrooxidation. The optimal Au concentration was determined to be 0.1 mM by analysing the sample under cyclic voltammetry analysis in a solution of glucose. From characterisation analysis the system displayed a bimetallic functional system showing the Ni and Au components were acting as singular entities, however influencing on the other's properties for glucose sensing

optimization. Due to the bimetallic nature of the material a very large sensitivity was detected at $506 \mu\text{A}\cdot\text{mM}^{-1}\cdot\text{cm}^{-2}$ with minimal loss in selectivity in the presence of common physiological contaminants. Ni on its own had previously shown very poor selectivity however the presence of Au effected the system in a positive way by reducing the effect of contamination for Ni whilst drastically enhancing the sensitivity.

The final study performed was that of the effect of an additional material added to a large Au lattice structure. Given the numerous reports on glucose oxidation activity using Co_3O_4 , the additional material was introduced to a Au structure with a large enough surface area to support its structure. The hydrogen bubble template technique was used for the Au lattice with the metal oxide cobalt oxide (Co_3O_4) chosen due to its excellent affinity to glucose which primarily produced exceptionally large sensitivities. Studies for this dual material of Au honeycomb analysed the optimal Co_3O_4 precursor (CoCl_2) concentration (5, 10, 25, 50 and 100 mM) introduced into the system for optimal glucose electrooxidation. From CV analysis and surface cohesion for 100 mM of CoCl_2 was chosen as the optimal concentration for further studies. Initially glucose analysis was performed in alkaline media over a blood glucose range of $20 \mu\text{M} - 10 \text{mM}$. A very large sensitivity was calculated at $2014 \mu\text{A}\cdot\text{mM}^{-1}\cdot\text{cm}^{-2}$ between the glucose range of $20 - 100 \mu\text{M}$ with no effect from common physiological contaminants found within the blood concentration range. This high sensitivity at low concentrations pushed the study towards attempting non-invasive sensing analysis. Electrochemical glucose analysis was then performed in synthetic saliva media within a glucose range of $20 - 100 \mu\text{M}$. Excellent linearity was achieved using the elaborated chronoamperometric analysis method with minimal effect from common physiological contaminants found in saliva. Overall the study of Au for glucose sensing and how the form of Au used effects the glucose electrooxidation was studied comprehensively.

Comparing all the fabricated sensors in **table 1** it is clear to see that as the project progressed the quality of the sensor improved. Sensitivity improved as each new chapter project was undertaken with the Au- Co_3O_4 honeycomb sensor producing the superior sensitivity compared to all other sensors. Detection limits were similar for all the sensors with the Au-Pt honeycomb exhibiting the lowest detection limit of all the sensors mainly attributed to this sensing requiring the lowest applied potential compared to the other sensors. Unlike the Ni-Au which required a large applied potential of +0.55 V, the Au- Co_3O_4 honeycomb was able to have exhibit a very large sensitivity whilst retaining a relatively low applied potential of +0.1 V which reduced the effect of physiological contaminants.

Material	Applied Potential (V)	Sensitivity ($\mu\text{A}\cdot\text{mM}^{-1}\cdot\text{cm}^{-2}$)	Detection limit (μM)
Au nanospikes	+0.26	91.8	20
Au-Pt honeycomb	-0.01	109.3	12.9
Ni-Au colloidal crystals	+0.55	506	14.9
Au- Co_3O_4 honeycomb	+0.1	2014	20

Table 1 Comparison table of the fabricated sensors from this work

As has been shown in this thesis, the opportunity to tailor the morphology of Au structures in their pure form, alloyed form, nanoparticle form and the supporting structure with an additional material for optimal performance in glucose has been examined and studied comprehensively. Comparisons in sensitivity, selectivity, detection limit and applied potential displayed clear variances between surface structures when implementing them as glucose sensors.

7.2 Future work

From the results obtained from this study some exciting developments and research gaps have been identified in research which can provide exciting future opportunities such as:

- ❖ Device fabrication of the Au-Co₃O₄ structure mentioned in this work for a real-life saliva sensor for human trials
- ❖ Further study of other metal oxide additions to the Au structure such as TiO₂ for further optimization of the Au-based electrochemical glucose sensor
- ❖ Varying the base material of Au to other metals such as Ni, Pt and Cu to improve sensitivities whilst using similar fabrication techniques (electrodeposition, hydrothermal deposition or galvanic replacement) and determine the influence on its glucose electrooxidation capabilities compared to their Au counterpart
- ❖ Further research into other non-invasive forms of electrochemical glucose sensing using similar structures (use of Au-metal oxide composites) such as sweat, breath and tear analysis and what are the developed sensors capabilities in these different medias
- ❖ Showing other applications of the developed structures and how they could be used for various uses not just glucose sensing applications. In my other work as a collaborator Au nanospikes have been used to kill bacteria showing the possibility of the structures in multiple uses. Further studies for cortisol sensing, gas sensing and supercapacitance analysis can be performed for their viability in these areas (*refer to additional publications section*).

Overall the viability of these sensing materials and their components can be interchanged in various ways to optimally tailor a material for a specific application. These findings offer numerous possibilities for future work which can result in device production for real-life use by diabetes patients once produced.

Bibliography for published papers

Chapter 3

Au Nanospikes as a Non-enzymatic Glucose Sensor: Exploring Morphological Changes with the Elaborated Chronoamperometric Method

1. Danaei, G.; Finucane, M. M.; Lu, Y.; Singh, G. M.; Cowan, M. J.; Paciorek, C. J.; Lin, J. K.; Farzadfar, F.; Khang, Y.-H.; Stevens, G. A.; Rao, M.; Ali, M. K.; Riley, L. M.; Robinson, C. A.; Ezzati, M., *The Lancet* **378** (9785), 31-40.
2. Alwan, A.; Organization, W. H., *Global status report on noncommunicable diseases 2010*. World Health Organization: **2011**.
3. Nichols, S. P.; Koh, A.; Storm, W. L.; Shin, J. H.; Schoenfisch, M. H., *Chem. Rev.* **2013**, *113* (4), 2528-2549.
4. Shaw, K. M.; Cummings, M. H., *Diabetes and the eye*. Third ed.; John Wiley & Sons: Diabetes chronic complications, **2012**.
5. Mokdad, A. H.; Ford, E. S.; Bowman, B. A.; Dietz, W. H.; Vinicor, F.; Bales, V. S.; Marks, J. S., *Jama* **2003**, *289* (1), 76-79.
6. Clark, L. C.; Lyons, C., *Ann. N.Y. Acad. Sci.* **1962**, *102* (1), 29-45.
7. Wang, G.; He, X.; Wang, L.; Gu, A.; Huang, Y.; Fang, B.; Geng, B.; Zhang, X., *Microchim. Acta* **2013**, *180* (3-4), 161-186.
8. Ernst, S.; Heitbaum, J.; Hamann, C. H., *J. Electroanal. Chem. Interfacial Electrochem.* **1979**, *100* (1), 173-183.
9. Toghill, K. E.; Compton, R. G., *Int. J. Electrochem. Sci.* **2010**, *5* (9), 1246-1301.
10. Bai, Y.; Sun, Y.; Sun, C., *Biosens. Bioelectron.* **2008**, *24* (4), 579-585.
11. Wang, J.; Thomas, D. F.; Chen, A., *Anal. Chem.* **2008**, *80* (4), 997-1004.
12. Rong, L.-Q.; Yang, C.; Qian, Q.-Y.; Xia, X.-H., *Talanta* **2007**, *72* (2), 819-824.
13. Saha, K.; Agasti, S. S.; Kim, C.; Li, X.; Rotello, V. M., *Chem. Rev.* **2012**, *112* (5), 2739-2779.
14. Shan, C.; Yang, H.; Han, D.; Zhang, Q.; Ivaska, A.; Niu, L., *Biosens. Bioelectron.* **2010**, *25* (5), 1070-1074.
15. Xian, Y.; Hu, Y.; Liu, F.; Xian, Y.; Wang, H.; Jin, L., *Biosens. Bioelectron.* **2006**, *21* (10), 1996-2000.
16. Tian, H.; Jia, M.; Zhang, M.; Hu, J., *Electrochim. Acta* **2013**, *96*, 285-290.
17. Liu, Y.; Teng, H.; Hou, H.; You, T., *Biosens. Bioelectron.* **2009**, *24* (11), 3329-3334.
18. Zhuang, Z.; Su, X.; Yuan, H.; Sun, Q.; Xiao, D.; Choi, M. M., *Analyst* **2008**, *133* (1), 126-132.
19. Luo, J.; Jiang, S.; Zhang, H.; Jiang, J.; Liu, X., *Anal. Chim. Acta* **2012**, *709*, 47-53.
20. Ding, Y.; Wang, Y.; Su, L.; Zhang, H.; Lei, Y., *J. Mater. Chem.* **2010**, *20* (44), 9918-9926.

21. Vassilyev, Y. B.; Khazova, O.; Nikolaeva, N., *J. Electroanal. Chem. Interfacial Electrochem.* **1985**, *196* (1), 127-144.
22. Adzic, R. R.; Hsiao, M. W.; Yeager, E. B., *J. Electroanal. Chem. Interfacial Electrochem.* **1989**, *260* (2), 475-485.
23. Zhang, Y.; Chang, G.; Liu, S.; Lu, W.; Tian, J.; Sun, X., *Biosens. Bioelectron.* **2011**, *28* (1), 344-348.
24. Cheng, T.-M.; Huang, T.-K.; Lin, H.-K.; Tung, S.-P.; Chen, Y.-L.; Lee, C.-Y.; Chiu, H.-T., *ACS Appl. Mater. Interfaces* **2010**, *2* (10), 2773-2780.
25. Boisselier, E.; Astruc, D., *Chem. Soc. Rev.* **2009**, *38* (6), 1759-1782.
26. Lang, X.-Y.; Fu, H.-Y.; Hou, C.; Han, G.-F.; Yang, P.; Liu, Y.-B.; Jiang, Q., *Nat. Commun.* **2013**, *4*, 2169.
27. Schmid, G.; Corain, B., *Eur. J. Inorg. Chem.* **2003**, *2003* (17), 3081-3098.
28. Biella, S.; Prati, L.; Rossi, M., *J. Catal.* **2002**, *206* (2), 242-247.
29. Bond, G. C., *Catal. Today* **2002**, *72* (1), 5-9.
30. Sabri, Y. M.; Ippolito, S. J.; Tardio, J.; Bansal, V.; O'Mullane, A. P.; Bhargava, S. K., *Sci. Rep.* **2014**, *4*, 1-8.
31. Plowman, B.; Ippolito, S. J.; Bansal, V.; Sabri, Y. M.; O'Mullane, A. P.; Bhargava, S. K., *Chem. Commun.* **2009**, (33), 5039-5041.
32. Plowman, B. J.; Bhargava, S. K.; O'Mullane, A. P., *Analyst* **2011**, *136* (24), 5107-5119.
33. Radovan, C.; Manea, F., *Electroanalysis* **2007**, *19* (1), 91-95.
34. Cofan, C.; Radovan, C., *Sensors* **2008**, *8* (6), 3952-3969.
35. German, N.; Ramanavicius, A.; Ramanaviciene, A., *Sens. Actuator B-Chem.* **2014**, *203*, 25-34.
36. Luo, J.; Zhang, H.; Jiang, S.; Jiang, J.; Liu, X., *Microchim. Acta* **2012**, *177* (3-4), 485-490.
37. Sabri, Y. M.; Kandjani, A. E.; Ippolito, S. J.; Bhargava, S. K., *ACS Appl. Mater. Interfaces* **2015**, *7* (3), 1494.
38. Trasatti, S.; Petrii, O., *Pure Appl. Chem.* **1991**, *63* (5), 711-734.
39. Trasatti, S.; Petrii, O. A., *J. Electroanal. Chem.* **1992**, *327* (1), 353-376.
40. Kabir, K. M.; Sabri, Y. M.; Kandjani, A. E.; Matthews, G. I.; Field, M.; Jones, L. A.; Nafady, A.; Ippolito, S. J.; Bhargava, S. K., *Langmuir* **2015**, *31* (30), 8519-8529.
41. Li, Y.; Song, Y.-Y.; Yang, C.; Xia, X.-H., *Electrochem. Commun.* **2007**, *9* (5), 981-988.
42. Hsiao, M.; Adžić, R.; Yeager, E., *J. Electrochem. Soc.* **1996**, *143* (3), 759-767.
43. Pasta, M.; La Mantia, F.; Cui, Y., *Electrochim. Acta* **2010**, *55* (20), 5561-5568.
44. Makovos, E.; Liu, C., *Bioelectrochem. Bioenerg.* **1986**, *15* (2), 157-165.
45. Kirk, D.; Foulkes, F.; Graydon, W., *J. Electrochem. Soc.* **1980**, *127* (5), 1069-1076.
46. Aoun, S. B.; Dursun, Z.; Koga, T.; Bang, G. S.; Sotomura, T.; Taniguchi, I., *J. Electroanal. Chem.* **2004**, *567* (2), 175-183.
47. Burke, L., *Electrochim. Acta* **1994**, *39* (11), 1841-1848.
48. Holt-Hindle, P.; Nigro, S.; Asmussen, M.; Chen, A., *Electrochem. Commun.* **2008**, *10* (10), 1438-1441.

49. Xiao, F.; Zhao, F.; Mei, D.; Mo, Z.; Zeng, B., *Biosens. Bioelectron.* **2009**, *24* (12), 3481-3486.
50. Zhao, Z. W.; Chen, X. J.; Tay, B. K.; Chen, J. S.; Han, Z. J.; Khor, K. A., *Biosens. Bioelectron.* **2007**, *23* (1), 135-139.
51. Cho, S.; Kang, C., *Electroanalysis* **2007**, *19* (22), 2315-2320.
52. Sanz , G.; Taurino, I.; Antiochia, R.; Gorton, L.; Favero, G.; Mazzei, F.; De Micheli, G.; Carrara, S., *Bioelectrochemistry* **2016**, *112*, 125-131.
53. Qiu, C.; Wang, X.; Liu, X.; Hou, S.; Ma, H., *Electrochim. Acta* **2012**, *67*, 140-146.
54. Lee, Y.-J.; Park, J.-Y., *Sens. Actuator B-Chem.* **2011**, *155* (1), 134-139.
55. Yi, Q.; Yu, W., *J. Electroanal. Chem.* **2009**, *633* (1), 159-164.
56. Liu, X.; Hu, Q.; Wu, Q.; Zhang, W.; Fang, Z.; Xie, Q., *Colloids surf., B* **2009**, *74* (1), 154-158.
57. Guo, C.; Zhang, X.; Huo, H.; Xu, C.; Han, X., *Analyst* **2013**, *138* (22), 6727-6731.
58. Radovan, C.; Cinghit , D.; Manea, F.; Mincea, M.; Cofan, C.; Ostafe, V., *Sensors* **2008**, *8* (7), 4330-4349.
59. Tominaga, M.; Shimazoe, T.; Nagashima, M.; Taniguchi, I., *Electrochem. Commun.* **2005**, *7* (2), 189-193.
60. Bai, Y.; Yang, W.; Sun, Y.; Sun, C., *Sens. Actuator B-Chem.* **2008**, *134* (2), 471-476.
61. Chen, L.; Fujita, T.; Ding, Y.; Chen, M., *Adv. Funct. Mater.* **2010**, *20* (14), 2279-2285.
62. Habrioux, A.; Sibert, E.; Servat, K.; Vogel, W.; Kokoh, K. B.; Alonso-Vante, N., *The Journal of Physical Chemistry B* **2007**, *111* (34), 10329-10333.
63. Ren, X.; Meng, X.; Tang, F., *Sens. Actuator B-Chem.* **2005**, *110* (2), 358-363.
64. Pan, D.; Chen, J.; Yao, S.; Nie, L.; Xia, J.; Tao, W., *Sens. Actuator B-Chem.* **2005**, *104* (1), 68-74.
65. Dong, X.-C.; Xu, H.; Wang, X.-W.; Huang, Y.-X.; Chan-Park, M. B.; Zhang, H.; Wang, L.-H.; Huang, W.; Chen, P., *ACS nano* **2012**, *6* (4), 3206-3213.
66. Lin, S.-Y.; Chang, S.-J.; Hsueh, T.-J., *Appl. Phys. Lett.* **2014**, *104* (19), 193704.
67. Kabir, K. M.; Sabri, Y. M.; Matthews, G. I.; Jones, L. A.; Ippolito, S. J.; Bhargava, S. K., *Analyst* **2015**, *140* (16), 5508-5517.

Chapter 4

Hydrogen Bubble Templated Growth of Honeycomb-Like Au-Pt Alloy Films for Non-Enzymatic Glucose Sensing

1. Nichols, S. P.; Koh, A.; Storm, W. L.; Shin, J. H.; Schoenfish, M. H., *Chem. Rev.* **2013**, *113* (4), 2528-2549.
2. Wang, J., *Chem. Rev.* **2008**, *108* (2), 814-825.
3. Cryer, P.; Davis, S.; Shamoon, H., *Diab. Care* **2003**, *26* (6), 1902-1912.

4. Umpierrez, G. E.; Isaacs, S. D.; Bazargan, N.; You, X.; Thaler, L. M.; Kitabchi, A. E., *J. Clin. Endocrinol. Metab.* **2002**, *87* (3), 978-982.
5. Niu, X.; Shi, L.; Zhao, H.; Lan, M., *Analytical Methods* **2016**, *8*, 1755-1764.
6. Clark, L. C.; Lyons, C., *Ann. N.Y. Acad. Sci.* **1962**, *102* (1), 29-45.
7. Wang, G.; He, X.; Wang, L.; Gu, A.; Huang, Y.; Fang, B.; Geng, B.; Zhang, X., *Microchim. Acta* **2013**, *180* (3-4), 161-186.
8. Xu, F.; Cui, K.; Sun, Y.; Guo, C.; Liu, Z.; Zhang, Y.; Shi, Y.; Li, Z., *Talanta* **2010**, *82* (5), 1845-1852.
9. Joo, S.; Park, S.; Chung, T. D.; Kim, H. C., *Anal. Sci.* **2007**, *23* (3), 277-281.
10. Huang, H.-Y.; Chen, P.-Y., *Talanta* **2010**, *83* (2), 379-385.
11. Wang, J., *J. Pharm. Biomed. Anal.* **1999**, *19* (1-2), 47-53.
12. Toghill, K. E.; Compton, R. G., *Int. J. Electrochem. Sci.* **2010**, *5* (9), 1246-1301.
13. Sanz , G.; Taurino, I.; Antiochia, R.; Gorton, L.; Favero, G.; Mazzei, F.; De Micheli, G.; Carrara, S., *Bioelectrochemistry* **2016**, *112*, 125-131.
14. Vassilyev, Y. B.; Khazova, O. A.; Nikolaeva, N. N., *J. Electroanal. Chem. Interfacial Electrochem.* **1985**, *196* (1), 127-144.
15. Adzic, R. R.; Hsiao, M. W.; Yeager, E. B., *J. Electroanal. Chem. Interfacial Electrochem.* **1989**, *260* (2), 475-485.
16. Ernst, S.; Heitbaum, J.; Hamann, C. H., *J. Electroanal. Chem. Interfacial Electrochem.* **1979**, *100* (1), 173-183.
17. Sun, Y.; Buck, H.; Mallouk, T. E., *Anal. Chem.* **2001**, *73* (7), 1599-1604.
18. Wang, J.; Gao, H.; Sun, F.; Xu, C., *Sens. Actuator B-Chem.* **2014**, *191*, 612-618.
19. Zeng, B. Z.; Wei, S. H.; Zhao, F. Q.; Zou, Q. L., *Wuhan University Journal (Natural Science Edition)* **2005**, *2*, 7-15.
20. Ranjani, M.; Sathishkumar, Y.; Lee, Y. S.; Yoo, D. J.; Kim, A. R., *RSC Adv.* **2015**, *5* (71), 57804-57814.
21. Sun, Y.; Yang, H.; Yu, X.; Meng, H.; Xu, X., *RSC Adv.* **2015**, *5* (86), 70387-70394.
22. Mei, H.; Wu, W.; Yu, B.; Wu, H.; Wang, S.; Zhang, X.; Xia, Q., *Electroanalysis* **2015**, *28*, 671-678.
23. Jafarian, M.; Forouzandeh, F.; Danaee, I.; Gobal, F.; Mahjani, M., *J. Solid State Electrochem.* **2009**, *13* (8), 1171-1179.
24. Wang, J.; Thomas, D. F.; Chen, A., *Anal. Chem.* **2008**, *80* (4), 997-1004.
25. Cheng, T.-M.; Huang, T.-K.; Lin, H.-K.; Tung, S.-P.; Chen, Y.-L.; Lee, C.-Y.; Chiu, H.-T., *ACS Appl. Mater. Interfaces* **2010**, *2* (10), 2773-2780.
26. Plowman, B. J.; Jones, L. A.; Bhargava, S. K., *Chem. Commun.* **2015**, *51* (21), 4331-4346.
27. Cherevko, S.; Chung, C.-H., *Electrochem. Commun.* **2011**, *13* (1), 16-19.
28. Li, Y.; Jia, W.-Z.; Song, Y.-Y.; Xia, X.-H., *Chem. Mater.* **2007**, *19* (23), 5758-5764.
29. Tseng, T.-M.; Huang, R.-H.; Huang, C.-Y.; Hsueh, K.-L.; Shieu, F.-S., *J. Electrochem. Soc.* **2013**, *160* (4), A690-A696.
30. Zhou, S.; Jackson, G. S.; Eichhorn, B., *Adv. Funct. Mater.* **2007**, *17* (16), 3099-3104.
31. Yuan, L.; Yang, M.; Qu, F.; Shen, G.; Yu, R., *Electrochim. Acta* **2008**, *53* (10), 3559-3565.

32. Chang, S. C.; Leung, L. W. H.; Weaver, M. J., *J. Phys. Chem.* **1990**, *94* (15), 6013-6021.
33. Park, S.; Boo, H.; Chung, T. D., *Anal. Chim. Acta* **2006**, *556* (1), 46-57.
34. Hsiao, M.; Adžić, R.; Yeager, E., *J. Electrochem. Soc.* **1996**, *143* (3), 759-767.
35. Vassilyev, Y. B.; Khazova, O.; Nikolaeva, N., *J. Electroanal. Chem. Interfacial Electrochem.* **1985**, *196* (1), 127-144.
36. Qiu, H.; Huang, X., *J. Electroanal. Chem.* **2010**, *643* (1–2), 39-45.
37. Habrioux, A.; Sibert, E.; Servat, K.; Vogel, W.; Kokoh, K. B.; Alonso-Vante, N., *J. Phys. Chem. B* **2007**, *111* (34), 10329-10333.
38. Xiao, F.; Zhao, F.; Mei, D.; Mo, Z.; Zeng, B., *Biosens. Bioelectron.* **2009**, *24* (12), 3481-3486.
39. Ryu, J.; Kim, K.; Kim, H.-S.; Hahn, H. T.; Lashmore, D., *Biosens. Bioelectron.* **2010**, *26* (2), 602-607.
40. Kabir, K. M.; Sabri, Y. M.; Kandjani, A. E.; Matthews, G. I.; Field, M.; Jones, L. A.; Nafady, A.; Ippolito, S. J.; Bhargava, S. K., *Langmuir* **2015**, *31* (30), 8519-8529.
41. Kabir, K. M.; Sabri, Y. M.; Matthews, G. I.; Jones, L. A.; Ippolito, S. J.; Bhargava, S. K., *Analyst* **2015**, *140* (16), 5508-5517.
42. Sabri, Y. M.; Kandjani, A. E.; Ippolito, S. J.; Bhargava, S. K., *Sci. Rep.* **2016**, *6*.
43. Sabri, Y. M.; Kandjani, A. E.; Ippolito, S. J.; Bhargava, S. K., *ACS Appl. Mater. Interfaces* **2015**, *7* (3), 1491-1499.
44. Lei, H.-W.; Wu, B.; Cha, C.-S.; Kita, H., *J. Electroanal. Chem.* **1995**, *382* (1–2), 103-110.
45. Rong, L.-Q.; Yang, C.; Qian, Q.-Y.; Xia, X.-H., *Talanta* **2007**, *72* (2), 819-824.
46. Stamenkovic, V. R.; Mun, B. S.; Arenz, M.; Mayrhofer, K. J.; Lucas, C. A.; Wang, G.; Ross, P. N.; Markovic, N. M., *Nat. Mater* **2007**, *6* (3), 241-247.
47. Coyle, V. E.; Kandjani, A. E.; Sabri, Y. M.; Bhargava, S. K., *Electroanalysis* **2016**, doi: 10.1002/elan.201600138
48. Han, L.; Zhang, S.; Han, L.; Yang, D.-P.; Hou, C.; Liu, A., *Electrochim. Acta* **2014**, *138*, 109-114.
49. Lee, Y.-J.; Park, D.-J.; Park, J.-Y.; Kim, Y., *Sensors* **2008**, *8* (10), 6154-6164.
50. Niu, X.; Zhao, H.; Chen, C.; Lan, M., *ChemCatChem* **2013**, *5* (6), 1416-1425.
51. Liu, Y.; Ding, Y.; Zhang, Y.; Lei, Y., *Sens. Actuator B-Chem.* **2012**, *171*, 954-961.

Chapter 5

Nickel–gold bimetallic monolayer colloidal crystals fabricated via galvanic replacement as a highly sensitive electrochemical sensor

1. Yu, W.-Y.; Zhang, L.; Mullen, G. M.; Evans, E. J.; Henkelman, G.; Mullins, C. B., *Phys. Chem. Chem. Phys.* **2015**, *17* (32), 20588-20596.

2. He, W.; Wu, X.; Liu, J.; Hu, X.; Zhang, K.; Hou, S.; Zhou, W.; Xie, S., *Chem. Mater.* **2010**, *22* (9), 2988-2994.
3. Larki, P.; Sabri, Y. M.; Kabir, K. M.; Nafady, A.; Kandjani, A. E.; Bhargava, S. K., *RSC Adv.* **2015**, *5* (112), 92303-92311.
4. Bansal, V.; Jani, H.; Du Plessis, J.; Coloe, P. J.; Bhargava, S. K., *Adv. Mater.* **2008**, *20* (4), 717-723.
5. Jing, H.; Wang, H., *Chem. Mater.* **2015**, *27* (6), 2172-2180.
6. Zhang, W.; Yang, J.; Lu, X., *ACS Nano* **2012**, *6* (8), 7397-7405.
7. Lee, C.-L.; Tseng, C.-M., *J. Phys. Chem. C* **2008**, *112* (35), 13342-13345.
8. Lu, X.; Tuan, H.-Y.; Chen, J.; Li, Z.-Y.; Korgel, B. A.; Xia, Y., *J. Am. Chem. Soc.* **2007**, *129* (6), 1733-1742.
9. Xia, X.; Wang, Y.; Ruditskiy, A.; Xia, Y., *Adv. Mater.* **2013**, *25* (44), 6313-6333.
10. Fu, L.; Zhu, D.; Yu, A., *Spectrochim. Acta Mol. Biomol. Spectrosc.* **2015**, *149*, 396-401.
11. Lay, B.; Sabri, Y.; Ippolito, S.; Bhargava, S., *Phys. Chem. Chem. Phys.* **2014**, *16* (36), 19522-19529.
12. Lian, J.; Wang, L.; Sun, X.; Yu, Q.; Ewing, R. C., *Nano Lett.* **2006**, *6* (5), 1047-1052.
13. Hicks, E. M.; Zou, S.; Schatz, G. C.; Spears, K. G.; Van Duyne, R. P.; Gunnarsson, L.; Rindzevicius, T.; Kasemo, B.; Käll, M., *Nano Lett.* **2005**, *5* (6), 1065-1070.
14. Gan, Z.; Cao, Y.; Evans, R. A.; Gu, M., *Nat. Commun.* **2013**, *4*, 2061.
15. Retsch, M.; Zhou, Z. C.; Rivera, S.; Kappl, M.; Zhao, X. S.; Jonas, U.; Li, Q., *Macromol. Chem. Phys.* **2009**, *210* (3-4), 230-241.
16. Halpern, A. R.; Corn, R. M., *ACS Nano* **2013**, *7* (2), 1755-1762.
17. Sabri, Y. M.; Kandjani, A. E.; Ippolito, S. J.; Bhargava, S. K., *ACS Appl. Mater. Interfaces* **2015**, *7* (3), 1494.
18. Sabri, Y. M.; Kandjani, A. E.; Ippolito, S. J.; Bhargava, S. K., *Sci. Rep.* **2016**, *6*, 24625.
19. Manzke, A.; Vogel, N.; Weiss, C. K.; Ziener, U.; Plettl, A.; Landfester, K.; Ziemann, P., *Nanoscale* **2011**, *3* (6), 2523-2528.
20. Vogel, N.; Retsch, M.; Fustin, C.-A.; del Campo, A.; Jonas, U., *Chem. Rev.* **2015**, *115* (13), 6265-6311.
21. Sabri, Y. M.; Ippolito, S. J.; Atanacio, A. J.; Bansal, V.; Bhargava, S. K., *J. Mater. Chem.* **2012**, *22* (40), 21395-21404.
22. Tsvetkov, M. Y.; Khlebtsov, B. N.; Khanadeev, V. A.; Bagratashvili, V. N.; Timashev, P. S.; Samoylovich, M. I.; Khlebtsov, N. G., *Nanoscale Res. Lett.* **2013**, *8*, 250.
23. Gonzalez-Urbina, L.; Baert, K.; Kolaric, B.; Perez-Moreno, J.; Clays, K., *Chem. Rev.* **2012**, *112* (4), 2268-2285.
24. Ruminski, A. M.; Barillaro, G.; Chaffin, C.; Sailor, M. J., *Adv. Funct. Mater.* **2011**, *21* (8), 1511-1525.
25. Ye, Y. H.; Mayer, T. S.; Khoo, I. C.; Divliansky, I. B.; Abrams, N.; Mallouk, T. E., *J. Mater. Chem.* **2002**, *12* (12), 3637-3639.
26. Galisteo-Lopez, J. F.; Ibisate, M.; Sapienza, R.; Froufe-Perez, L. S.; Blanco, A.; Lopez, C., *Adv. Mater.* **2011**, *23* (1), 30-69.

27. Liu, Y.; Teng, H.; Hou, H.; You, T., *Biosens. Bioelectron.* **2009**, *24* (11), 3329-3334.
28. Ding, Y.; Wang, Y.; Su, L.; Zhang, H.; Lei, Y., *J. Mater. Chem.* **2010**, *20* (44), 9918-9926.
29. Guo, C. Y.; Wang, Y. M.; Zhao, Y. Q.; Xu, C. L., *Analytical Methods* **2013**, *5* (7), 1644-1647.
30. Coyle, V. E.; Kandjani, A. E.; Sabri, Y. M.; Bhargava, S. K., *Electroanalysis* **2017**, *29* (1), 294-304.
31. Sanz , G.; Taurino, I.; Antiochia, R.; Gorton, L.; Favero, G.; Mazzei, F.; De Micheli, G.; Carrara, S., *Bioelectrochemistry* **2016**, *112*, 125-131.
32. Xia, Y.; Huang, W.; Zheng, J.; Niu, Z.; Li, Z., *Biosens. Bioelectron.* **2011**, *26* (8), 3555-3561.
33. You, T.; Niwa, O.; Chen, Z.; Hayashi, K.; Tomita, M.; Hirono, S., *Anal. Chem.* **2003**, *75* (19), 5191-5196.
34. Cheng, X.; Zhang, S.; Zhang, H.; Wang, Q.; He, P.; Fang, Y., *Food Chem.* **2008**, *106* (2), 830-835.
35. Lu, L.-M.; Zhang, L.; Qu, F.-L.; Lu, H.-X.; Zhang, X.-B.; Wu, Z.-S.; Huan, S.-Y.; Wang, Q.-A.; Shen, G.-L.; Yu, R.-Q., *Biosens. Bioelectron.* **2009**, *25* (1), 218-223.
36. Safavi, A.; Maleki, N.; Farjami, E., *Biosens. Bioelectron.* **2009**, *24* (6), 1655-1660.
37. Xian, Y.; Hu, Y.; Liu, F.; Xian, Y.; Wang, H.; Jin, L., *Biosens. Bioelectron.* **2006**, *21* (10), 1996-2000.
38. Cheng, T.-M.; Huang, T.-K.; Lin, H.-K.; Tung, S.-P.; Chen, Y.-L.; Lee, C.-Y.; Chiu, H.-T., *ACS Appl. Mater. Interfaces* **2010**, *2* (10), 2773-2780.
39. Toolan, D. T. W.; Fujii, S.; Ebbens, S. J.; Nakamura, Y.; Howse, J. R., *Soft Matter* **2014**, *10* (44), 8804-8812.
40. Herz, A.; Wang, D.; Kups, T.; Schaaf, P., *J. Appl. Phys.* **2014**, *116* (4), 044307.
41. Hong, Y.; Jing, X.; Huang, J.; Sun, D.; Odoom-Wubah, T.; Yang, F.; Du, M.; Li, Q., *ACS Sustainable Chem. Eng.* **2014**, *2* (7), 1752-1759.
42. Luo, W.; Sankar, M.; Beale, A. M.; He, Q.; Kiely, C. J.; Bruijninx, P. C. A.; Weckhuysen, B. M., *Nat. Commun.* **2015**, *6*.
43. Grosvenor, A. P.; Biesinger, M. C.; Smart, R. S. C.; McIntyre, N. S., *Surf. Sci.* **2006**, *600* (9), 1771-1779.
44. Biesinger, M. C.; Payne, B. P.; Grosvenor, A. P.; Lau, L. W. M.; Gerson, A. R.; Smart, R. S. C., *Appl. Surf. Sci.* **2011**, *257* (7), 2717-2730.
45. Zhao, C.; Shao, C.; Li, M.; Jiao, K., *Talanta* **2007**, *71* (4), 1769-1773.
46. Luo, P. F.; Kuwana, T.; Paul, D. K.; Sherwood, P. M., *Anal. Chem.* **1996**, *68* (19), 3330-3337.
47. Vassilyev, Y.; Khazova, O.; Nikolaeva, N., *J. Electroanal. Chem. Interfacial Electrochem.* **1985**, *196* (1), 127-144.
48. Hsiao, M.; Ad i , R.; Yeager, E., *J. Electrochem. Soc.* **1996**, *143* (3), 759-767.
49. Pasta, M.; La Mantia, F.; Cui, Y., *Electrochim. Acta* **2010**, *55* (20), 5561-5568.
50. Coyle, V. E.; Oppedisano, D. K.; Jones, L. A.; Kandjani, A. E.; Sabri, Y. M.; Bhargava, S. K., *J. Electrochem. Soc.* **2016**, *163* (14), B689-B695.

51. Hsu, C.-W.; Wang, G.-J., *Biosens. Bioelectron.* **2014**, *56*, 204-209.
52. Clement, S.; Braithwaite, S. S.; Magee, M. F.; Ahmann, A.; Smith, E. P.; Schafer, R. G.; Hirsch, I. B., *Diabetes Care* **2004**, *27* (2), 553-591.
53. Anderson, J. H.; Blackard, W. G.; Goldman, J.; Rubenstein, A. H., *Am. J. Med.* **1978**, *64* (5), 868-873.
54. Kabir, K. M.; Sabri, Y. M.; Matthews, G. I.; Jones, L. A.; Ippolito, S. J.; Bhargava, S. K., *Analyst* **2015**, *140* (16), 5508-5517.
55. Li, Y.; Song, Y.-Y.; Yang, C.; Xia, X.-H., *Electrochem. Commun.* **2007**, *9* (5), 981-988.
56. Lee, S.-R.; Lee, Y.-T.; Sawada, K.; Takao, H.; Ishida, M., *Biosens. Bioelectron.* **2008**, *24* (3), 410-414.
57. Ding, Y.; Liu, Y.; Parisi, J.; Zhang, L.; Lei, Y., *Biosens. Bioelectron.* **2011**, *28* (1), 393-398.

Chapter 6

Co₃O₄ needles on Au honeycomb as a non-invasive electrochemical biosensor for glucose in saliva

1. Barry, E.; Roberts, S.; Oke, J.; Vijayaraghavan, S.; Normansell, R.; Greenhalgh, T., *BMJ* **2017**, *356*, i6538.
2. Association, A. D., *Diab. Care* **2018**, *41* (5), 917.
3. Bandodkar, A. J.; Wang, J., *Trends Biotechnol.* **2014**, *32* (7), 363-371.
4. Lankelma, J.; Nie, Z.; Carrilho, E.; Whitesides, G. M., *Anal. Chem.* **2012**, *84* (9), 4147-4152.
5. Raymundo-Pereira, P. A.; Shimizu, F. M.; Coelho, D.; Piazzeta, M. H.; Gobbi, A. L.; Machado, S. A.; Oliveira Jr, O. N., *Biosens. Bioelectron.* **2016**, *86*, 369-376.
6. Ye, D.; Liang, G.; Li, H.; Luo, J.; Zhang, S.; Chen, H.; Kong, J., *Talanta* **2013**, *116*, 223-230.
7. Anderson, K.; Poulter, B.; Dudgeon, J.; Li, S.-E.; Ma, X., *Sensors* **2017**, *17* (8), 1807.
8. Moyer, J.; Wilson, D.; Finkelshtein, I.; Wong, B.; Potts, R., *Diabetes Technol. Ther.* **2012**, *14* (5), 398-402.
9. Yao, H.; Shum, A. J.; Cowan, M.; Lähdesmäki, I.; Parviz, B. A., *Biosens. Bioelectron.* **2011**, *26* (7), 3290-3296.
10. Kownacka, A. E.; Vegelyte, D.; Joosse, M.; Anton, N.; Toebes, B. J.; Lauko, J.; Buzzacchera, I.; Lipinska, K.; Wilson, D. A.; Geelhoed-Duijvestijn, N., *Biomacromolecules* **2018**, *19* (11), 4504-4511.
11. Roberts, K.; Jaffe, A.; Verge, C.; Thomas, P. S., *J. Diabetes Sci. Technol.* **2012**, *6* (3), 659-664.
12. Wang, J., *Chem. Rev.* **2008**, *108* (2), 814-825.

13. Zhang, Y.; Chang, G.; Liu, S.; Lu, W.; Tian, J.; Sun, X., *Biosens. Bioelectron.* **2011**, *28* (1), 344-348.
14. Cheng, T.-M.; Huang, T.-K.; Lin, H.-K.; Tung, S.-P.; Chen, Y.-L.; Lee, C.-Y.; Chiu, H.-T., *ACS Appl. Mater. Interfaces* **2010**, *2* (10), 2773-2780.
15. Wang, G.; He, X.; Wang, L.; Gu, A.; Huang, Y.; Fang, B.; Geng, B.; Zhang, X., *Microchim. Acta* **2013**, *180* (3-4), 161-186.
16. Zhu, H.; Li, L.; Zhou, W.; Shao, Z.; Chen, X., *J. Mater. Chem. B* **2016**, *4* (46), 7333-7349.
17. Toghill, K. E.; Compton, R. G., *Int. J. Electrochem. Sci.* **2010**, *5* (9), 1246-1301.
18. Chakraborty, P.; Dhar, S.; Debnath, K.; Majumder, T.; Mondal, S. P., *Sens. Actuator B-Chem.* **2019**, *283*, 776-785.
19. Boisselier, E.; Astruc, D., *Chem. Soc. Rev.* **2009**, *38* (6), 1759-1782.
20. Coyle, V. E.; Oppedisano, D. K.; Jones, L. A.; Kandjani, A. E.; Sabri, Y. M.; Bhargava, S. K., *J. Electrochem. Soc.* **2016**, *163* (14), B689-B695.
21. Ding, Y.; Wang, Y.; Su, L.; Bellagamba, M.; Zhang, H.; Lei, Y., *Biosens. Bioelectron.* **2010**, *26* (2), 542-548.
22. Wang, W.; Li, Z.; Liu, L.; Zhang, H.; Zheng, W.; Wang, Y.; Huang, H.; Wang, Z.; Wang, C., *Sens. Actuator B-Chem.* **2009**, *141* (2), 404-409.
23. Tong, G.-X.; Liu, F.-T.; Wu, W.-H.; Shen, J.-P.; Hu, X.; Liang, Y., *CrystEngComm* **2012**, *14* (18), 5963-5973.
24. Solanki, P. R.; Kaushik, A.; Agrawal, V. V.; Malhotra, B. D., *NPG Asia Mater.* **2011**, *3* (1), 17.
25. Kimmel, D. W.; LeBlanc, G.; Meschievitz, M. E.; Cliffel, D. E., *Anal. Chem.* **2011**, *84* (2), 685-707.
26. Lang, X.-Y.; Fu, H.-Y.; Hou, C.; Han, G.-F.; Yang, P.; Liu, Y.-B.; Jiang, Q., *Nat. Commun.* **2013**, *4*, 2169.
27. Lay, B.; Coyle, V. E.; Kandjani, A. E.; Amin, M. H.; Sabri, Y. M.; Bhargava, S. K., *J. Mater. Chem. B* **2017**, *5* (5), 5441-5449.
28. Plowman, B. J.; O'Mullane, A. P.; Selvakannan, P.; Bhargava, S. K., *Chem. Commun.* **2010**, *46* (48), 9182-9184.
29. Plowman, B. J.; O'Mullane, A. P.; Bhargava, S. K., *Faraday Discuss.* **2011**, *152*, 43-62.
30. Dong, X.-C.; Xu, H.; Wang, X.-W.; Huang, Y.-X.; Chan-Park, M. B.; Zhang, H.; Wang, L.-H.; Huang, W.; Chen, P., *ACS nano* **2012**, *6* (4), 3206-3213.
31. Chaisiwamongkhol, K.; Batchelor-McAuley, C.; Compton, R. G., *Analyst* **2017**, *142* (15), 2828-2835.
32. Coyle, V. E.; Kandjani, A. E.; Sabri, Y. M.; Bhargava, S. K., *Electroanalysis* **2017**, *29* (1), 294-304.
33. Ibupoto, Z. H.; Elhag, S.; AlSalhi, M.; Nur, O.; Willander, M., *Electroanalysis* **2014**, *26* (8), 1773-1781.
34. Casaletto, M.; Longo, A.; Martorana, A.; Prestianni, A.; Venezia, A., *Surf. Interface Anal.* **2006**, *38* (4), 215-218.

35. Kabir, K. M.; Sabri, Y. M.; Kandjani, A. E.; Matthews, G. I.; Field, M.; Jones, L. A.; Nafady, A.; Ippolito, S. J.; Bhargava, S. K., *Langmuir* **2015**, *31* (30), 8519-8529.
36. Pearson, A.; O'Mullane, A. P.; Bansal, V.; Bhargava, S. K., *Inorg. Chem.* **2011**, *50* (5), 1705-1712.
37. Daima, H. K.; Selvakannan, P.; Shukla, R.; Bhargava, S. K.; Bansal, V., *PLoS One* **2013**, *8* (10), e79676.
38. Biesinger, M. C.; Payne, B. P.; Grosvenor, A. P.; Lau, L. W. M.; Gerson, A. R.; Smart, R. S. C., *Appl. Surf. Sci.* **2011**, *257* (7), 2717-2730.
39. Liu, X.; Chang, Z.; Luo, L.; Xu, T.; Lei, X.; Liu, J.; Sun, X., *Chem. Mater.* **2014**, *26* (5), 1889-1895.
40. Mei, W.; Huang, J.; Zhu, L.; Ye, Z.; Mai, Y.; Tu, J., *J. Mater. Chem.* **2012**, *22* (18), 9315-9321.
41. Yang, J.; Liu, H.; Martens, W. N.; Frost, R. L., *J. Phys. Chem. C* **2010**, *114* (1), 111-119.
42. Nohira, H.; Tsai, W.; Besling, W.; Young, E.; Petry, J.; Conard, T.; Vandervorst, W.; De Gendt, S.; Heyns, M.; Maes, J.; Tuominen, M., *J. Non-Cryst. Solids* **2002**, *303* (1), 83-87.
43. Bertinello, P.; Ugo, P., *Journal of the Brazilian Chemical Society* **2003**, *14* (4), 517-522.
44. Teixeira, M. F.; Bergamini, M. F.; Marques, C. M.; Bocchi, N., *Talanta* **2004**, *63* (4), 1083-1088.
45. Teixeira, M. F.; Marcolino-Júnior, L. H.; Fatibello-Filho, O.; Dockal, E. R.; Cavaleiro, É. T., *Journal of the Brazilian Chemical Society* **2004**, *15* (6), 803-808.
46. Han, L.; Zhang, S.; Han, L.; Yang, D.-P.; Hou, C.; Liu, A., *Electrochim. Acta* **2014**, *138*, 109-114.
47. Aoun, S. B.; Dursun, Z.; Koga, T.; Bang, G. S.; Sotomura, T.; Taniguchi, I., *J. Electroanal. Chem.* **2004**, *567* (2), 175-183.
48. Chen, L.; Fujita, T.; Ding, Y.; Chen, M., *Adv. Funct. Mater.* **2010**, *20* (14), 2279-2285.
49. Ding, Y.; Liu, Y.; Parisi, J.; Zhang, L.; Lei, Y., *Biosens. Bioelectron.* **2011**, *28* (1), 393-398.
50. Ramasamy, R.; Ramachandran, K.; Philip, G. G.; Ramachandran, R.; Therese, H. A.; Gnana kumar, G., *RSC Adv.* **2015**, *5* (93), 76538-76547.
51. Kung, C.-W.; Lin, C.-Y.; Lai, Y.-H.; Vittal, R.; Ho, K.-C., *Biosens. Bioelectron.* **2011**, *27* (1), 125-131.
52. Lee, I.; Loew, N.; Tsugawa, W.; Ikebukuro, K.; Sode, K., *Biosens. Bioelectron.* **2019**, *124-125*, 216-223.
53. Campos, A. M.; Raymundo-Pereira, P. A.; Mendonça, C. D.; Calegari, M. L.; Machado, S. A.; Oliveira Jr, O. N., *ACS Applied Nano Materials* **2018**, *1* (2), 654-661.

APPENDIX

-
- ❖ Abbreviations
 - ❖ Co-Author statements for the publications included in chapters III-VI
-

List of Abbreviations

AA	Ascorbic acid
AuOH	Gold hydroxide
C	carbon
CFP	Carbon nanofiber paste
CHIT	chitosan
CNT	Carbon nanotubes
CS	Biopolymer chitosan
CV	Cyclic voltammetry
ERGO	Electrochemically reduced graphene oxide
FAD	Flavin adenine dinucleotide
FESEM	Field emission scanning electron microscopy
FON	Film over nanospheres
FTO	Fluorine doped Tin oxide
GC	Glassy carbon
GCE	Glassy carbon electrode
GDH	Glucose-1-dehydrogenase
GN	Graphene nanosheets
GO	Graphene oxide
GOD	Glucose oxidase
GOH	Graphene hydro-gel
GOx	Glucose oxidase
GR	Graphene
HPT	chloroplatinic acid
IR	Infrared
ITO	Indium tin oxide
MC	Medoporous carbon
MIR	Mid-infrared
MWCNT	Multi-walled carbon nanotube
MWNR	Multi-walled carbon nanotube
NBC	Nanobiocomposite
NC	Nanocomposite
NC	Nanocubes
NIR	Near-infrared
NP	Nanoparticle
NPG	Nanoporous gold
NT	Nanotube

NW	Nanowire
NWA	Nanowire array
OH⁻	Hydroxide
ORD	Optical rotary dispersion
PAA	Polyacrylic acid
PAA	poly(allylamine)
PEC	photoelectrochemical
PET	Polyethylene terephthalate
PET	Positron emission tomography
PGE	Pencil graphite electrode
SEM	Scanning electron microscopy
SERS	Surface-enhanced raman spectroscopy
SWCNH	Single-walled carbon nanohorn
SWNT	Single-walled nanotubes
TDNT	Titania nanotube
UA	Uric acid

School of Science

Chapter Declaration for Thesis with Publications

The following declaration needs to be made for each paper included in the thesis.

Chapter 3 is represented by the following paper:

Title: Au Nanospikes as a Non-enzymatic Glucose Sensor: Exploring Morphological Changes with the Elaborated Chronoamperometric Method

Author list: Victoria E. Coyle, Ahmad E. Kandjani, Ylias M. Sabri and Suresh K. Bhargava

Journal name: Electroanalysis

Issue, volume, page numbers: 1, 29, 294-304

Year published: 2017

Declaration by candidate

I declare that I wrote the initial draft of this manuscript, and my overall contribution to this paper is detailed below:

Nature of contribution	Extent of contribution (%)
<ul style="list-style-type: none">➤ Designed the experimental protocols in collaboration with Ylias Sabri and Ahmad Kandjani➤ Performed fabrication of the electrodeposited Au nanospikes➤ Performed characterization analysis (SEM, EDX, XRD, ECSA)➤ Performed all data analysis➤ Performed electrochemical sensing analysis➤ Prepared the first draft of the manuscript➤ Edited manuscript➤ Managed the preparation of responses to reviewer comments and making amendments to facilitate publication➤ Performed additional experiments for reviewer's comments➤ Collated the amendments to proofs prepared by all authors	85

The following co-authors contributed to the work. The undersigned declare that the contributions of the candidate and co-authors are correctly attributed below.

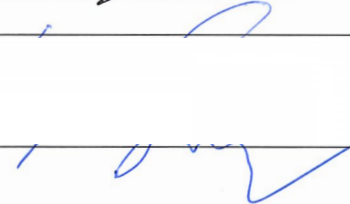
Author	Nature of contribution	Extent of contribution (%)	Signature
Ahmad E. Kandjani	<ul style="list-style-type: none"> ➤ Designed the experimental protocols in collaboration with Victoria Coyle and Ylias Sabri ➤ Edited manuscript prior to submission 	15	
Ylias M. Sabri	<ul style="list-style-type: none"> ➤ Designed the experimental protocols in collaboration with Victoria Coyle and Ahmad Kandjani ➤ Edited manuscript prior to submission 		
Suresh K. Bhargava	<ul style="list-style-type: none"> ➤ Supervision and guidance in data analysis ➤ Edited manuscript for submission 		

Candidate's Signature



Date 26/8/19

Primary Supervisor's Signature



Date 26/08/2019

School of Science

Chapter Declaration for Thesis with Publications

The following declaration needs to be made for each paper included in the thesis.

Chapter 4 is represented by the following paper:

Paper name: Hydrogen Bubble Templated Growth of Honeycomb-Like Au-Pt Alloy Films for Non-Enzymatic Glucose Sensing

Author List: Victoria E. Coyle, Daniel KJ. Oppedisano, Lathe A. Jones, Ahmad E. Kandjani, Ylias M. Sabri and Suresh K. Bhargava

Journal name: Journal of The Electrochemical Society

Volume, issue and page numbers: 163, 14, B689-B695

Year published: 2016

Declaration by candidate


I declare that I wrote the initial draft of this manuscript, and my overall contribution to this paper is detailed below:

Nature of contribution	Extent of contribution (%)
<ul style="list-style-type: none"> ➤ Designed the experimental protocols in collaboration with Ylias Sabri and Ahmad Kandjani ➤ Supervised Daniel Oppedisano during fabrication of the Au-Pt honeycomb substrates ➤ Performed characterization analysis (SEM, EDX, XRD, XPS, ECSA) ➤ Performed all data analysis ➤ Performed electrochemical sensing analysis ➤ Prepared the first draft of the manuscript ➤ Edited manuscript ➤ Managed the preparation of responses to reviewer comments and making amendments to facilitate publication ➤ Performed additional experiments for reviewer's comments ➤ Collated the amendments to proofs prepared by all authors 	80

The following co-authors contributed to the work. The undersigned declare that the contributions of the candidate and co-authors are correctly attributed below.

Author	Nature of contribution	Extent of contribution (%)	Signature
Daniel Oppedisano	<ul style="list-style-type: none"> ➤ Performed fabrication of Au-Pt honeycomb surfaces ➤ Edited manuscript prior to submission 	20	
Lathe Jones	<ul style="list-style-type: none"> ➤ Provided guidance for electrochemistry analysis ➤ Edited manuscript prior to submission 		
Ahmad Kandjani	<ul style="list-style-type: none"> ➤ Designed the experimental protocols in collaboration with Victoria Coyle and Ylias Sabri ➤ Edited manuscript prior to submission 		
Ylias Sabri	<ul style="list-style-type: none"> ➤ Designed the experimental protocols in collaboration with Victoria Coyle and Ahmad Kandjani ➤ Edited manuscript prior to submission 		
Suresh Bhargava	<ul style="list-style-type: none"> ➤ Supervision and guidance in data analysis ➤ Edited manuscript for submission 		

Candidate's Signature

 Date 26/8/19

Primary Supervisor's Signature

 Date 26/08/2019

School of Science

Chapter Declaration for Thesis with Publications

The following declaration needs to be made for each paper included in the thesis.

Chapter 5 is represented by the following paper:

Paper name: Nickel-Gold Bimetallic Monolayer Colloidal Crystal via Galvanic Replacement as a Highly Sensitive Electrochemical Sensor

Author List: Bebeto Lay (joint first), Victoria E. Coyle (joint first), Ahmad E. Kandjani, Mohamad H. Amin, Ylias M. Sabri and Suresh K. Bhargava

Journal name: Journal of Materials Chemistry B

Volume, issue and page numbers: 5, 5, 5441-5449





Year published: 2017

Declaration by candidate

I declare that I wrote the initial draft of this manuscript, and my overall contribution to this paper is detailed below:

Nature of contribution	Extent of contribution (%)
<ul style="list-style-type: none">➤ Designed the experimental protocols in collaboration with Ylias Sabri, Ahmad Kandjani and Bebeto Lay➤ Supervised Bebeto Lay during fabrication of the Ni-Au colloid substrates➤ Performed SEM analysis of the fabricated substrates➤ Performed electrochemical sensing analysis➤ Performed data analysis of chemical sensing➤ Prepared the first draft of the manuscript➤ Edited manuscript➤ Managed the preparation of responses to reviewer comments and making amendments to facilitate publication➤ Performed additional experiments for reviewer's comments➤ Collated the amendments to proofs prepared by all authors	75

The following co-authors contributed to the work. The undersigned declare that the contributions of the candidate and co-authors are correctly attributed below.

Author	Nature of contribution	Extent of contribution (%)	Signature
Bebeto Lay	<ul style="list-style-type: none"> ➤ Designed the experimental protocols in collaboration with Victoria Coyle, Ahmad Kandjani and Ylias Sabri ➤ Performed fabrication of the 		
	<ul style="list-style-type: none"> Ni-Au colloidal substrates ➤ Performed characterization analysis ➤ Worked closely with Victoria Coyle on the first draft of the manuscript ➤ Edited manuscript prior to submission 		
Ahmad Kandjani	<ul style="list-style-type: none"> ➤ Designed the experimental protocols in collaboration with Victoria Coyle and Ylias Sabri ➤ Edited manuscript prior to submission 	25	
Mohamad Amid	<ul style="list-style-type: none"> ➤ Performed HR-TEM analysis ➤ Edited manuscript prior to submission 		
Ylias Sabri	<ul style="list-style-type: none"> ➤ Designed the experimental protocols in collaboration with Victoria Coyle and Ahmad Kandjani ➤ Edited manuscript prior to submission 		
Suresh Bhargava	<ul style="list-style-type: none"> ➤ Supervision and guidance in data analysis 		

	➤ Edited manuscript for submission		
--	------------------------------------	--	--

**Candidate's
Signature**



Date
26.8.19

**Primary
Supervisor's
Signature**



Date
26/08/2019

School of Science

Chapter Declaration for Thesis with Publications

The following declaration needs to be made for each paper included in the thesis.

Chapter 6 is represented by the following paper:

Paper name: Co₃O₄ needles on Au honeycomb as a non-invasive electrochemical biosensor for glucose in saliva

Author List: Victoria E. Coyle, Ahmad E. Kandjani, Matthew R. Field, Patrick Hartley, Miao Chen, Ylias M. Sabri and Suresh K. Bhargava

Journal name: Biosensors and Bioelectronics

Volume and page number: 141, 111479

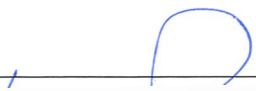

Year published: 2019

Declaration by candidate

I declare that I wrote the initial draft of this manuscript, and my overall contribution to this paper is detailed below:

Nature of contribution	Extent of contribution (%)
<ul style="list-style-type: none">➤ Designed the experimental protocols in collaboration with my supervisors➤ Performed fabrication of the Au-Co₃O₄ honeycomb substrates (electrodeposition and hydrothermal techniques used)➤ Performed characterization analysis (SEM, EDX, XRD, XPS)➤ Performed all data analysis➤ Performed electrochemical sensing analysis➤ Prepared the first draft of the manuscript➤ Edited manuscript➤ Managed the preparation of responses to reviewer comments and making amendments to facilitate publication➤ Performed additional experiments for reviewer's comments➤ Collated the amendments to proofs prepared by all authors	80

The following co-authors contributed to the work. The undersigned declare that the contributions of the candidate and co-authors are correctly attributed below.

Author	Nature of contribution	Extent of contribution (%)	Signature
Ahmad Kandjani	<ul style="list-style-type: none"> ➤ Designed the experimental protocols in collaboration with Victoria Coyle and Ylias Sabri ➤ Created schematic graphic of fabrication of Au-Co₃O₄ surfaces 	20%	
	<ul style="list-style-type: none"> ➤ Edited manuscript prior to submission 		
Matthew Field	<ul style="list-style-type: none"> ➤ Performed side-imaging SEM of the Au-Co₃O₄ substrate ➤ Edited manuscript prior to submission 		
Patrick Hartley	<ul style="list-style-type: none"> ➤ Supervision and guidance in data analysis ➤ Edited manuscript for submission 		
Miao Chen	<ul style="list-style-type: none"> ➤ Supervision and guidance in data analysis ➤ Edited manuscript for submission 		
Ylias Sabri	<ul style="list-style-type: none"> ➤ Designed the experimental protocols in collaboration with Victoria Coyle and Ahmad Kandjani ➤ Edited manuscript prior to submission 		
Suresh Bhargava	<ul style="list-style-type: none"> ➤ Supervision and guidance in data analysis ➤ Edited manuscript for submission 		

**Candidate's
Signature**

[Redacted Signature]

Date
26/8/19

**Primary
Supervisor's
Signature**

[Redacted Signature]

Date
26/08/2019